

W.A. Davis

(VA Tech)

**NATIONAL ACADEMIES OF SCIENCES AND ENGINEERING
NATIONAL RESEARCH COUNCIL
of the
UNITED STATES OF AMERICA**

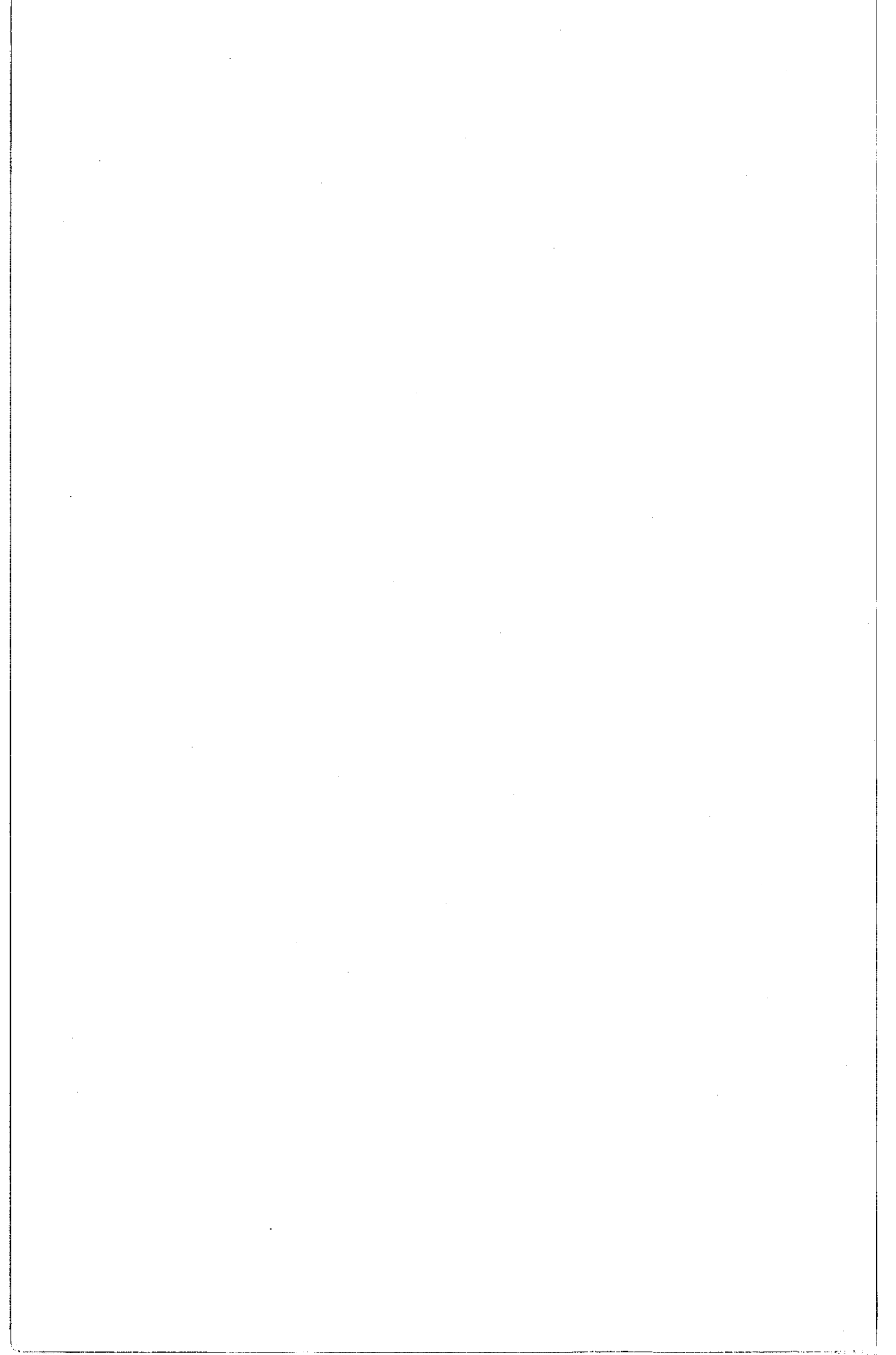
**UNITED STATES NATIONAL COMMITTEE
International Union of Radio Science**



National Radio Science Meeting
5 - 8 January 2004

Sponsored by USNC/URSI

University of Colorado at Boulder
Boulder, Colorado
USA



United States National Committee
International Union of Radio Science

ABSTRACTS

National Radio Science Meeting
5-8 January 2004

University of Colorado at Boulder

Sponsored by USNC/URSI

Table of Contents

Session	Page No.	Session	Page No.
Membership Information.....	iii	G1	185
Description of URSI	iv	G2	197
Plenary Session	vii	G3	207
A1	1	G4	219
A2	7	G5	229
B1	13	G/H1	237
B2	25	G/H2	249
B3	35	H1	259
B4	47	H2	271
B5	53	H3	279
B6	61	H4	293
C1	73	H5	305
C2	81	H6	319
D1	93	J1	329
D2	103	J2	341
D/B1	109	J3	351
E1.....	119	J4	361
F1.....	131	J5	373
F2.....	139	J6	381
F3.....	147	B/K1.....	393
F4.....	155	Index	405
F5.....	163		
F6.....	171		
F7.....	179		

Membership

United States National Committee
INTERNATIONAL UNION OF RADIO SCIENCE

Chair:	Umran S. Inan*
Secretary & Chair-Elect:	Piergiorgio L.E. Uslenghi*
Immediate Past Chair:	Gary S. Brown*

Members Representing Societies, Groups, and Institutes:

American Astronomical Society:	Thomas G. Phillips
American Geophysical Union:	Donald T. Farley
American Meteorological Society:	Dusan S. Zrnica
IEEE Antennas and Propagation Society:	Linda P.B. Katehi
IEEE Geosciences and Remote Sensing Society:	Roger Lang
IEEE Microwave Theory and Techniques Society:	Arthur A. Oliner

Members-at-Large

Amalia Barrios
J. Richard Fisher
Anthony C. Frasier-Smith
Melinda Picket-May
Ronald Pogorzelski
Michael S. Shur
Yahya Rahmit-Samii
Richard Ziolkowski

Chairs of the USNC-URSI Commissions:

Commission A	William A. Davis
Commission B	Ronald Pogorzelski
Commission C	Jeffrey Krolik
Commission D	Samir M. El Ghazaly
Commission E	Ira Kohlberg
Commission F	Kenneth Anderson
Commission G	Anthea Coster
Commission H	Gurudas Ganguli
Commission J	John Carlstrom
Commission K	Om Gandhi

Officers, Chairs and Vice Chairs of Commissions of URSI residing in the United States

URSI Honorary President	William E. Gordon
Vice Chair, URSI	Chalmers Butler
Chair, Commission A	Quirino Balzano
Chair, Commission C	A. F. Molisch
Chair, Commission H	Umran S. Inan

*Member of USNC/URSI Executive Committee

Description of the International Union of Radio Science

The International Union of Radio Science is one of the world scientific unions organized under the International Council of Scientific Unions (ICSU). It is commonly designated as URSI from its French name, Union Radio Scientifique Internationale. Its aims are (1) to promote the scientific study of radio communications, (2) to aid and organize radio research requiring cooperation on an international scale and to encourage the discussion and publication of the results, (3) to facilitate agreement upon common methods of measurement and the standardization of measuring instruments, and (4) to stimulate and to coordinate studies of the scientific aspects of telecommunications using electromagnetic waves, guided and unguided. The International Union itself is an organizational framework to aid in promoting these objectives. The actual technical work is largely done by the National Committee in the various countries.

The new officers of the International Union are:

President:	Kristian Schlegel (Germany)
Past President:	Hiroshi Matsumoto (Japan)
Vice Presidents:	Chalmers M. Butler (USA)
	François Lefevre (France)
	("URSI Exposure" Officer)
	Andrzej W. Wernik (Poland)
	(Treasurer)
	Paul H. Wittke (Canada)
Secretary-General:	Paul Lagasse (Belgium)
Assistant Secretary-General:	Frank Olyslager (Belgium)
Assistant Secretary General (Publications):	W. Ross Stone (USA)
Administrative Assistant:	Inge Heleu (Belgium)

The Secretary-General's office and the headquarters of the organization are located at Avenue Albert Lancaster, 32, B-1180 Brussels, Belgium. The Union is supported by contributions (dues) from 38 member countries. Additional funds for symposia and other scientific activities of the Union are provided by ICSU from contributions received for this purpose from UNESCO.

The International Union, as of the XXVIth General Assembly held in Maastricht, Netherlands, August 2002, has ten bodies called Commissions for centralizing studies in principal fields.

Every three years the International Union holds a meeting called the General Assembly. The next is the XXVIIth, to be held in New Dehli, India, 23–29 October, 2005. The Secretariat prepares and distributes the Proceedings of the General Assemblies. The International Union arranges international symposia on specific subjects pertaining to the work of one or several Commissions and also cooperates with other Unions in international symposia on subjects of joint interest.

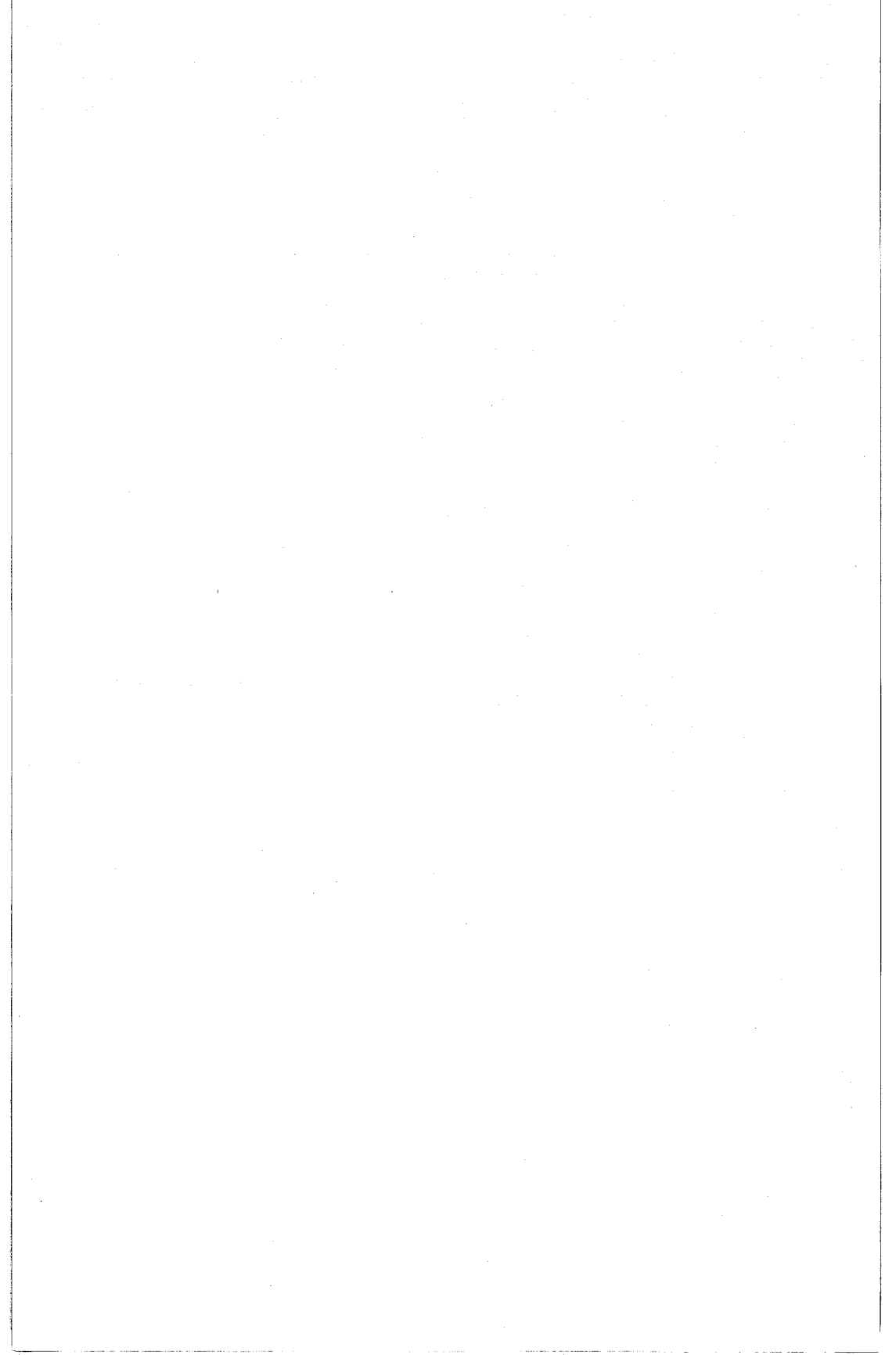
Radio is unique among the fields of scientific work in having a specific adaptability to large-scale international research programs, since many of the phenomena that must be studied are worldwide in extent and yet are in a measure subject to control by experimenters. Exploration of space and the extension of scientific observations to the space environment are dependent on radio for their research. One branch, radio astronomy, involves cosmic phenomena, URSI thus has a distinct field of usefulness in furnishing a meeting ground for the numerous workers in the manifold aspects of radio research; its meetings and committee activities furnish valuable means of promoting research through exchange of ideas.

Steering Committee:

P.L.E. Uslenghi, University of Illinois at Chicago
K. Grosland, Office of Conference Services, University of Colorado
K. Zellers, Cooperative Institute for Research in Environmental Sciences,
University of Colorado

Technical Program Committee:

U. Inan, Chair
P. Uslenghi, Secretary
S. Reising, Student Paper Competition
(A) W. Davis (F) K. Anderson
(B) R. Pogorzelski (G) A. Coster
(C) J. Krolik (H) G. Ganguli
(D) S. Ghazaly (J) J. Carlstrom
(E) I. Kohlberg (K) O. Gandhi



Plenary

Session, 9:00-Tues.

PLENARY

Chairpersons: U. Inan and S. Reising

Plenary

NANOTECHNOLOGY AND THE FUTURE OF ELECTRONICS

R. J. Trew
ECE Department
North Carolina State University
Raleigh, NC 27695

The world is experiencing rapid advancement and progress in the ability to design and fabricate mechanical and electronic structures and devices with nanoscale dimensions. This ability stems from parallel advances in materials growth technology, patterning techniques, imaging and manipulation capability, and advances in characterization and testing. When taken together, these techniques form the basis for designing and fabricating electronic devices and structures with atomic level control. Nanotechnology permits the realization of new devices and structures with performance potentially far exceeding that available from current systems and will keep electronic device performance on Moore's Law. Materials research on the nano-scale offers the potential to produce materials that do not exist in nature, and with idealized and optimum properties, while parallel effort in nano-electronics presents the opportunity to fabricate devices and circuits with orders of magnitude increase in performance compared to present devices. Recent breakthroughs provide evidence of potential success. This effort is expected to provide the basis for the next worldwide economic boom, and these advances will affect a wide variety of applications, including wireless technologies for both commercial and military systems. Current trends in nanoelectronics are discussed, attractive approaches identified, and recent advances presented.

FUTURE DETECTOR TECHNOLOGIES FOR RADIO ASTRONOMY

Jonas Zmuidzinas
Professor of Physics
G. W. Downs Laboratory
Caltech, 320-47
Pasadena CA 91125

Superconducting detectors are poised to play a key role in millimeter and submillimeter astrophysics. Superconducting devices have been used in radio astronomy for over two decades now in heterodyne receivers using SIS mixers. Such mixers offer unsurpassed sensitivity in the 100-1200 GHz frequency range, and are a key technology for the ALMA interferometer now being built in Chile as well as the HIFI instrument for the Herschel Space Observatory, to be launched in 2007. In the future, a variety of new superconducting detector technologies will be brought forward, especially for direct detection, such as Transition Edge Sensor (TES) bolometers, SQUID multiplexers, and kinetic inductance detectors. These new technologies will allow much larger detector arrays to be built, which are needed for studies of distant, high-redshift galaxies as well as for measurements of the Cosmic Microwave Background. In addition to describing the detector technologies, the presentation will discuss the astronomical motivation and science goals, and the instruments, observatories, and space missions that are being planned or built to take advantage of the new technological capabilities.

Session A1, 14:00-Tuesday

**ANTENNAS AND RADIATION
MODELING**

Chairpersons: William Davis and Everett Farr

A1

A PORTABLE AUTOMATIC TIME-DOMAIN ANTENNA RANGE: THE PATAR(TM) SYSTEM

Everett G. Farr¹, Lanney M. Atchley¹, W. Scott Bigelow¹,
Leland H. Bowen¹, Tyrone C. Tran²

¹Farr Research, Inc., 614 Paseo Del Mar, NE, Albuquerque, NM, 87123

²Air Force Research Laboratory / DE, 3550 Aberdeen Ave. SE, Kirtland AFB, NM 87117-5776

The Portable Automatic Time-domain Antenna Range, or PATAR(TM) system, provides an extremely convenient and inexpensive method of testing both narrowband and wideband antennas. This system operates well for all antennas above 900 MHz, and for non-dispersive antennas above 200 MHz. The entire system is easily stored in a small shed and can be set up outdoors and aligned in less than one hour. All measurements are made in the time domain.

The system includes a fast pulser, a fast sampling oscilloscope, a field sensor, an elevation/azimuth positioner, a computer controller, and software for data acquisition and processing. This range is more easily used outdoors than conventional frequency domain ranges, because temperature stability is less of a problem with oscilloscopes than with network analyzers. The equipment required for a time domain range is considerably less expensive than the corresponding equipment for a frequency domain range.

The antenna under test is mounted onto a custom elevation/azimuth positioner designed and manufactured by Farr Research. The positioner is extremely portable and easily positioned, leveled, and aligned. The accuracy of the positioner is better than +/-0.5 degrees in both azimuth and elevation. The antenna height is fixed at 3 meters, which we found to be the maximum height at which we could conveniently work.

The software includes everything one needs to drive the positioner, acquire the data from the oscilloscope, and process and plot the data. The system output includes antenna impulse response, gain, effective gain, return loss, and antenna pattern.

We provide here an overview of the hardware and software associated with the PATAR(TM) system. We also compare data from the PATAR(TM) system to that generated from more conventional frequency domain systems. The system is highly accurate for all antennas above 900 MHz, and for non-dispersive antennas above 200 MHz. The high end of frequency range is currently 20 GHz, but that could be extended with modest improvements.

TRANSMITTER BEAMWIDTH SIMULATION STUDY AND
VEHICULAR EFFECT ON URBAN LINE-OF-SIGHT MICRO-
CELLS AT MILLIMETER WAVE FREQUENCY 35GHZ

Goyal,A¹, Joshi,S.², Sancheti,S.³, Maheshwari,S.⁴

¹New York Institute of Technology,, Northern Boulevard,Old
Westbury, , New York, USA-11568 8000

²Engineering College, Ajmer, Rajasthan, India

³Malviya National Institute of Technology,, Jaipur,Rajasthan, In-
dia

⁴Engineering College, Ajmer, Rajasthan, India

A simulation model is developed on urban line-of-Sight microcellular environment to obtain the effect of transmitter beamwidth on the cell coverage, the power profile and delay spread. The study is performed to get a particular beamwidth on which the received power and delay spread have most significant value for particular street databases. The transmitter is assumed to be a horn antenna located at a typical lamppost height and its beamwidth variation is taken from 1-180 degrees. The receiver is assumed as a omnidirectional antenna with height 1-2m. This multiray model is developed at millimeter wave frequencies in the licensed region of 20-40GHz with 10 dBm transmitted power. In a urban city the streets have rectilinear orientation, and the building are assumed infinitely high. The surface of building walls are assumed perfectly reflecting body that means the incident ray and reflected ray have 180 degree phase shift between them. In this model only the direct ray, the ground reflected ray, the wall reflected ray component are considered, the effects of scattered component and the diffracted component are assumed negligible here. A different simulation study is performed to know the effect of vehicle on the received power profile. It is proposed that whenever a huge vehicle like a truck appears, only the wall reflected components contribute in the received power profile. The effect of scattered and diffracted ray components are considered negligible here. The appearance of a vehicle causes sudden drop in the received power because of disappearance of direct ray component and the ground reflected ray component. The studies may aid in the development of future mobile communication systems based on millimeter wave frequencies.

BAND-LIMITED ANTENNAS AND THE RELATIONSHIP TO DIFFERENTIATION IN UWB

Stanislav Licul, William Davis
Virginia Tech

The time-domain impulse response of UWB antennas generally have a doublet type of form. This "doublet" form is true for the Vivaldi, TEM horn, and bi-conic antennas. Such a response suggests that the antenna is a constant aperture antenna with $-V_o/V_i = A \cdot f$. In observing the waveform, it is found that the duration of the "doublet" corresponds to the fundamental resonant frequency of the antenna.

However, the frequency response suggests a different interpretation. The antennas appear to act as constant gain antennas. In fact, the Vivaldi and TEM horn antenna pattern measurements confirm that the antenna acts as a constant gain antenna. A constant gain antenna response, $-V_o/V_i = A/f$, is found for the response of the antenna above the fundamental resonance.

What seems to be the difference in the interpretations? If we expand the observation frequencies below the fundamental resonance the antenna, we indeed find that the antennas often act approximately like a constant aperture antenna; $-V_o/V_i = A \cdot f$. The response of these antennas can be explained by the band-limited nature of the antennas. The "doublet" type radiation that is produced by the Vivaldi and other UWB antennas is represented by a differentiation that is expected in the radiation in time-domain transmission. This differentiation is inherent to any antenna radiation mechanism. However, it is typically a result of the lower band response of the antenna where the constant aperture nature dominates. If an antenna system is band limited by filters in the system, a similar result occurs due to the band-limited nature.

Results for the Vivaldi, TEM horn, and bi-conic antennas will be presented with a comparison of a simple band-limited model for the system.

LIMITED-ANGLE-OF-INCIDENCE AND LIMITED-TIME
MAGNETIC SENSORSBaum C. E.

Air Force Research Laboratory, Directed Energy Directorate

This paper considers sensors for measurement of fast electromagnetic pulses. Instead of the time derivative of the electromagnetic wave characteristic of electrically small dipoles (electric, magnetic), these have a response proportional to the incident waveform or its time integral. However, these electrically large sensors have limitations concerning constraints on direction of incidence and polarization. Whereas previous results have concerned sensors for the incident electric field, the present paper concerns the dual case of the incident magnetic field.

A class of electric sensors, for which knowledge and control of parameters of the incident electric field, was discussed in a previous paper [C. E. Baum, Limited-Angle-of-Incidence and Limited-Time Electric Sensors, Sensor and Simulation Note 359, 1993]. There control of the direction of incidence of a uniform plane wave was used to define two types of such sensors. One had the output proportional to the time waveform of the incident field, while the second had it proportional to the time integral of the incident field. The first utilized TEM transmission lines with perfect conductors immersed in the external dielectric medium. The second had two perfectly conducting cones (of possibly general cross sections) with common apex. The price it pays, however, is that the necessary truncation of the TEM transmission line and cones (to give finite, practical size) makes the simple response functions (giving waveform or its integral) apply for only a short time related to transit times involving the signal access port, the truncation positions, and, in some cases, the direction of incidence of the wave to be measured. So these are appropriate for early-time measurements, but have problems in frequency domain.

As one might expect, the Babinet principle leading to the idea of complementary antennas plays a role here. These sensors take the forms of special linear and conical slots in a ground plane. One can use more exact expressions from which these are derived, or restrict the parameter range appropriately. Thereby, one can make the sensor response accurately calculable. There are also physical assumptions concerning the construction of such sensors. For example, the ground plane has been assumed to have negligible thickness; a thick ground plane will lower the characteristic impedances associated with the slot antennas.

Session A2, 15:40-Tuesday

**DEVICE MODELING AND
MEASUREMENTS**

Chairpersons: William Davis and Jeffery Jargon

MICROWAVE TRANSISTOR PACKAGE PARASITIC MODELLING USING COMPUTATIONAL PREDICTIONS

Bach, J.A.¹, Knudson, R.T.², Christodoulou, C.G.¹¹University of New Mexico, MSC01 1100, Dept. of EECE, Albuquerque, NM 87131²Sandia National Laboratories, P.O. Box 5800, Albuquerque, NM 87185-0537

This paper explores computer modeling of parasitics for a package that is suitable for a discrete microwave HFET device. The frequency range of interest is L-band, but the model was found to have a good match from DC to beyond 3 GHz. The package used was the StratEDGE/PTI 1616 2-lead glass flatpack. A three-dimensional structural electromagnetic model of the package was created from the manufacturer's CAD drawing using CST Microwave Studio. This model was created with consideration to the final design conditions including package dimensions, dimensions of the intended device, circuit board material, solder pad size and spacing, and via dimensions. After studying the geometry and the electromagnetic model, the form of the circuit model was determined. Both Agilent Advanced Design System and Ansoft Designer were used to automatically optimize component values to match the s-parameters of the circuit model to the electromagnetic model. Test circuits were built, packaged, and tested, and the s-parameter measurements were compared to the predictions of the computer simulations.

The model circuit topology consists of a variety of capacitors and inductors. The metals have large conductance, so series resistance is considered negligible, as well as substrate loss. The topology was determined to be similar to a distributed transmission line, except for some series capacitance. To obtain this model, the HFET device was replaced by a simple parallel-plate capacitor, since its effects on a circuit can be extracted and set as a starting point for the circuit optimization. This capacitor was chosen such that its width was the same as the transistor that would be packaged. The capacitance was calculated to be 1.3 pF, which was validated on the test boards using real parallel-plate capacitors of similar value. The computer simulations were found to be phase accurate, with amplitude variations of less than 0.5 dB at the worst-case (S₂₁ at 3GHz). Future benefits of this method of parametric extraction could include a coupled-physics model where a semiconductor device mounted in the package includes self-heating effects. A physical modeling code could then combine the electromagnetic, thermal, and semiconductor models into a unified, coupled model.

NONLINEAR TRANSMISSION MEASUREMENTS AND MODELING

William A. Davis

Virginia Tech

Current interests of many systems modeling efforts require the nonlinear characterization of a two-port, typically representing an amplifier chain. Much of this effort is being spent in the area of Volterra series. Previous work on nonlinear measurements by the author investigated a three-port model for devices, but limited the analysis to a single frequency. This paper expands the model to transmission measurements made over a range of frequencies, including two-tone measurements.

The measurements are made on a single, narrowband amplifier stage, but represent what may be expected in a typical amplifier chain. A typical amplifier chain will be dominated by a single nonlinear element as a nonlinear characteristic is approached, and often well into compression of levels more than 10dB. At higher frequencies, nonlinear capacitance effects enter at lower drive levels, but still should not modify the results substantially for regions of validity for typical Volterra series applications.

The critical observation in these measurements is the polar plot of the transmission as a function of drive level for selected frequencies. About the center frequency of the amplifier, the polar plot variation is a straight line – suggesting that a memoryless nonlinearity is present and sees a real circuit impedance. As the frequency is changed from the center frequency, the polar plot becomes a circle, still suggesting a single memoryless nonlinearity at a third port of a linear 3-port.

Two-tone tests will be displayed to demonstrate the effect of multiple frequencies in a nonlinear model. The compression occurs for a slightly lower drive level, but typically at a level corresponding to approximately one half the single output level (when the two signals are almost in phase and appear as a larger effective signal).

This paper will not address the mixer problem, but will suggest a similar approach that may be considered in the future. The method of this paper leads to a simple nonlinear model that provides flexibility and yet a simplicity desired in modeling and design.

REPEATABILITY OF HARMONIC PHASE TRANSFER STANDARDS MEASURED BY A NONLINEAR VECTOR NETWORK ANALYZER

Jeffrey A. Jargon, Donald C. DeGroot
National Institute of Standards and Technology

A class of instruments known as nonlinear vector network analyzers (NVNA) are capable of characterizing nonlinear devices under realistic, large-signal operating conditions. To do this, complex traveling waves are measured at the ports of a device not only at the stimulus frequency (or frequencies), but also at other frequencies that are part of the large-signal response. Assuming the source signals are single-frequency time-harmonic waves and the device exhibits neither sub-harmonic nor chaotic behavior, the forward and reverse waves measured at the device boundaries will be combinations of the source signals, due to the nonlinearity of the device in conjunction with impedance mismatches between the system and the device. If a single excitation frequency is present, new frequency components may appear at all harmonics of the excitation frequency, and if multiple excitation frequencies are present, new frequency components may appear at the intermodulation products as well.

To capture this type of large-signal behavior, the calibration of a commercial NVNA consists of three steps: a relative calibration that is identical to that used in a linear vector network analyzer, an amplitude calibration that makes use of a power meter, and a phase distortion calibration that makes use of a harmonic phase standard. All are performed on a frequency grid related to the source tones and the anticipated nonlinear response of the device.

The commercial harmonic phase standard, the main components of which are a power amplifier and a step recovery diode, is driven at a fundamental frequency and produces a harmonic series output signal. The harmonic phase standard, which is used as a transfer standard, is characterized by a sampling oscilloscope, which in turn is characterized by a nose-to-nose calibration. In this way we transfer the phase-dispersion calibration of an oscilloscope to knowing the phase relationship of each harmonic of the phase standard output signal.

In this paper, we present a repeatability study of commercial harmonic phase standards measured by a nonlinear vector network analyzer. Specifically, we measure two harmonic phase standards, one of which is specified to 20 GHz and the other to 50 GHz. By performing multiple calibrations and making numerous measurements at each calibration, we determine the repeatability bounds for the complex wave-variable vectors and associated phases and magnitudes of each harmonic component. We also compare our average values to those supplied by the manufacturer.

Session B1, 8:40-Monday

COMPLEX MEDIA

Chairpersons: Nader Engheta and R. Ziolkowski

FAST AND EFFICIENT APPROACH FOR N-LAYERED MICROSTRIP POLES EXTRACTION

Ying Wang, Ban Leong Ooi, Mook Seng Leong
National University of Singapore, ECE department

The precise poles locations of the Greens function are very important for the accurate evaluation of the closed-form spatial-domain Greens function for microstrip problem. The poles of the Greens function for the microstrip geometry correspond to the surface- and leaky-wave modes. In most of the analysis, the precise information on the poles locations is needed for the accurate evaluation of the residue terms used in the complex image method. In spectral-domain method, the poles also play a crucial role in the accurate evaluation of the Sommerfeld Integral.

With the introduction of new technologies such as the low-temperature cofired ceramics (LTCC), meta-materials and multilayered PCBs, it becomes increasingly necessary to look into the extraction of poles in multi-layered microstrip geometry. So far, most of the proposed techniques of poles extraction have been confined to a single-layered, dielectric microstrip geometry.

In this paper, a unified approach for fast evaluation of the poles location in multi-layered microstrip technology has been presented. For the first time, good initial values and functional expressions with quadratic convergence for multi-layered pole extraction have been derived. Numerical comparison with available methods of extraction shows that our proposed method is indeed very accurate and extremely fast in convergence.

Our earlier success in deriving fast but efficient poles extraction for single-layered dielectric microstrip problem [1] has provided a good hint on deriving a generalized approach for multilayered microstrip poles extraction. We have been able to derive novel functional expressions, which have quadratic convergence, for finding the roots of DTE and DTM [1]. In this paper, we intend to illustrate how these functional expressions, coupled with the derived initial values given in [1], can be extended to solve multi-layered microstrip problem. Instead of using the real analysis for our explanation, an algorithmic approach will be adopted in explaining the proposed method.

[1] B. L. Ooi, M. S. Leong and P. S. Kooi, A fast, accurate and efficient method for pole extraction in microstrip problems, *Microwave Opt. Technol. Lett.*, vol. 8, no. 3, pp. 132-136, Feb 1995.

METAMATERIAL REALIZATIONS OF ARTIFICIAL MAGNETIC CONDUCTORS

Erentok, A., Ziolkowski, R. W.

Department of Electrical and Computer Engineering, The University of Arizona, 1230 E. Speedway, Tucson, AZ 85721

Metamaterials are often generated by artificially fabricated, extrinsic, low dimensional inhomogeneities in some background substrate. Metamaterials that mimic known material responses or that qualitatively have new response functions that do not occur in nature have been realized. Several metamaterial designs have been conceived and modeled with both ANSOFT's High Frequency Structure Simulation (HFSS) tools (FEM based) and Finite Difference Time Domain (FDTD) simulators. They have demonstrated the possibility of realizing double negative (DNG) metamaterials with subwavelength inclusions in Rogers 5880 DUROID ($\epsilon_r = 2.2$) at X-Band frequencies. These DNG metamaterials have been fabricated and tested successfully.

The design, fabrication and measurement of a metamaterial realization of an artificial magnetic conductor (AMC) will be presented. In contrast to most current realizations of AMCs, such as the mushroom and the UC-PBG surfaces, the present design has no perfect electric conductor ground plane. The perfect magnetic conductor properties (in-phase reflection, $R = +1$) were designed with capacitively loaded loops for X-Band operation at 10 GHz. The AMC behavior occurs near where the metamaterial exhibits a large negative permeability. These elements were variations of those used to achieve the DNG metamaterial realizations. These AMC designs will be reviewed. Several of these AMC metamaterials were fabricated and tested experimentally with a free space X-Band measurement setup. The measurement methods will also be reviewed. The results of these AMC metamaterial experiments will be discussed. Very good agreement between the numerical and experimental results was achieved and these comparisons will be described. Simulations of the use of these AMC metamaterials in antenna applications will be given.

IMAGE DE-BLURRING USING DOUBLE-NEGATIVE (DNG)
OR SINGLE-NEGATIVE (SNG) METAMATERIAL LAYERSAlu, A.¹, Engheta, N.²¹University of Roma Tre, Department of Applied Electronics,
Rome, Italy²University of Pennsylvania, Department of Electrical and Sys-
tems Engineering, Philadelphia, PA, U.S.A

When an imaging system is designed for certain imaging conditions, the presence of an additional undesired transparent layer in the path of the image-forming wave can adversely affect the point-spread functions, leading to image blurring and degradation of image quality. When such a layer cannot be removed from the imaging systems, techniques to improve the image quality (or to reduce its degradation) should be used. We are interested in exploring theoretically the possibility of using double-negative (DNG) and single-negative (SNG) metamaterial slabs for reducing such image degradation. Double-negative materials are material media in which both permittivity and permeability have negative real parts in a given frequency band, while in single-negative media only one of the two parameters has a negative real part. We have recently shown that when an epsilon-negative (ENG) slab is juxtaposed with a mu-negative (MNG) slab, under certain conditions one may achieve transparency and wave tunneling [A. Alu and N. Engheta, "Pairing an epsilon-negative slab with a mu-negative slab: resonance, tunneling and transparency, *IEEE Trans. on Antennas and Propagation*, Vol. 51, No. 10, October 2003, in press]. However, here we consider a slab of DNG or SNG material that is inserted in parallel with, but at some distance away from, a conventional double-positive (DPS) layer, both of which are in the path of image forming waves. Without the DNG or SNG layer, the conventional DPS layer may affect the point-spread function of the imaging system. When the DNG layer is inserted at a distance L away from the DPS layer, the overall point-spread function of the entire system may be altered depending on the material parameters, slab thicknesses and the slab separation. We show that under certain conditions, the DNG or SNG layer can approximately remove the undesired effects of the DPS layer, which may lead to image de-blurring and enhancement of the image quality. We will present our theoretical results on this topic, and will describe physical insights behind these results.

DYNAMICAL EVOLUTION OF THE BRILLOUIN PRECURSOR IN ROCARD-POWLES-DEBYE MODEL DIELECTRICS

Oughstun, K. E.College of Engineering Mathematics, University of Vermont,
Burlington, VT 05405-0156

When an ultrawideband electromagnetic pulse penetrates into a causally dispersive dielectric, the interrelated effects of phase dispersion and frequency dependent attenuation alter the pulse in a fundamental way that results in the appearance of so-called precursor fields. For a Lorentz model dielectric that exhibits resonant dispersion these include the well-known Sommerfeld and Brillouin precursors, where the Sommerfeld precursor evolves in the high frequency region above the highest absorption band of the material while the Brillouin precursor evolves in the low frequency region below the lowest absorption band of the dielectric. For a dielectric described by the Rocard-Powles extension of the Debye model of rotational dispersion, the dynamical field evolution is dominated by the Brillouin precursor as the propagation distance typically exceeds a single absorption depth evaluated at the carrier frequency of the input ultrawideband pulse. This is because the peak amplitude in the Brillouin precursor decays only as the square root of the inverse of the propagation distance. This nonexponential decay of the Brillouin precursor makes it ideally suited for ground and foliage penetrating radar applications as well as for underwater communications and biomedical imaging. Of equal importance is the frequency structure of the Brillouin precursor. Although the instantaneous oscillation frequency is zero at the peak amplitude point of the Brillouin precursor, the actual oscillation frequency of this unique field structure is quite different, exhibiting a complicated dependence on both the material dispersion and the input pulse characteristics. Finally, a Brillouin pulse is defined and is shown to possess near optimal (if not indeed optimal) penetration into a given Rocard-Powles-Debye model dielectric.

ON THE EQUIVALENCE OF INHOMOGENEOUS INCLINED ANISOTROPIC AND BIANISOTROPIC MEDIA FOR TWO-DIMENSIONAL TM-TYPE PROPAGATION PROBLEMS

Glenn A. Wilson¹, David V. Thiel²

¹Department of Geology and Geophysics, University of Utah, Salt Lake City UT 84112 USA

²School of Microelectronic Engineering, Griffith University - Nathan Campus, Brisbane Qld 4111 Australia

Analytical and numerical solutions for the surface impedance of a horizontally inhomogeneous half-space with isotropic conductivity have been previously investigated for TM-type plane waves (D. Rankin, *Geophysics*, **27**, 666-676, 1962). With exception of the fundamental uniaxial anisotropy solution by Obukhov (*Izv. Akad. Nauk SSSR Fizika Zemli*, **4**, 106-112, 1969) and the review of d'Erceville and Kunetz's (*Geophysics*, **27**, 651-665) solution for inclined uniaxial anisotropic conductivity by Grubert (presented at *12th Workshop on Electromagnetic Induction in the Earth*, Brest, France, 8-13 Aug 1994), no significant attention has been given to the problem of exactly solving for the surface impedance above horizontally inhomogeneous media that exhibits inclined anisotropic conductivity. In this paper, we will investigate the properties of the Helmholtz equation for inclined anisotropic media. Using analytical methods, we show that for a homogeneous TM-type wave propagating in a half-space with both vertical and horizontal inhomogeneities, where the TM-type wave is aligned with one of the horizontal elements of the conductivity tensor, that the shearing term in the homogeneous Helmholtz equation for inclined anisotropic media unequivocally vanishes and solutions need only be sought to the homogeneous Helmholtz equation for biaxial media. This implies that those two-dimensional problems posed with an inclined uniaxial conductivity tensor can be identically states with a fundamental biaxial conductivity tensor, provided that the conductivity values are the reciprocals of the diagonal elements from the Euler rotation of the inclined uniaxial resistivity tensor into the fundamental plane. The consequence for numerical methods of solving arbitrary two-dimensional problems for homogeneous TM-type plane waves is that they need only to approximate the homogeneous Helmholtz equation and neglect the corresponding shearing term. The self-consistent impedance method (D.V. Thiel, R. Mittra, *Radio Sci.*, **36**, 31-43, 2001), a two-dimensional finite-difference method based on an *RC* network analogy is introduced and demonstrated to accurately solve for problems with inclined uniaxial anisotropy using the biaxial anisotropy equivalence.

PROPAGATION MODES IN IRREGULAR STRATIFIED CHIRAL MEDIA

Crittenden, P. E.^{1,2}, Bahar, E.²

¹Department of Mathematics, University of Nebraska-Lincoln

²Department of Electrical Engineering, University of Nebraska-Lincoln

The Fourier transforms of the Green's functions for the electromagnetic waves on both sides of a flat interface between two semi-infinite chiral materials are derived. These harmonic solutions are expressed in terms of the characteristic right and left circularly polarized waves. The Green's functions are converted into modal representations suitable for the complete expansion of the electromagnetic fields above and below a rough interface between two chiral materials with laterally varying material properties. The complete expansion is a sum of four branch cut integrals and two residue contributions. Using far-field approximations the physical paths associated with the various terms of the expansion are identified. The branch cut integrals are shown to be associated with direct waves from the source to the observation point and the like and cross polarized specularly reflected and transmitted waves that satisfy the generalized Snell's Law.

$$\gamma_{10} \sin \theta_{10} = \gamma_{20} \sin \theta_{20} = \gamma_{11} \sin \theta_{11} = \gamma_{21} \sin \theta_{21}, \quad (1)$$

where θ_{ij} is the angle a right ($i = 1$) or left ($i = 2$) circularly polarized wave in medium j forms with a perpendicular to the surface. The γ_{ij} are the corresponding wave numbers. In addition, there are several lateral waves associated with critical angles for total internal reflection. For example, the critical angles θ_{10}^c , for a right circularly polarized wave above the interface are obtained from the generalized Snell's Law, by setting $\theta_{ij} = \pi/2$, $(ij) \neq (10)$. These critical angles correspond to lateral waves that travel just above or below the surface. The lateral waves emerge from the surface at critical angles and can arrive at the observation point above or below the interface with either polarization. The residues are associated with surface waves that propagate upon the surface. Here too, the waves can reach the observer as either right or left circularly polarized waves. Depending on the material properties, all of the waves may be travelling or evanescent along each segment of their path. The generalized Fourier transforms can be used to obtain the generalized telegraphists equations for chiral materials. The telegraphists equations may be solved under appropriate assumptions for particular surfaces in order to obtain the diffusely scattered electromagnetic fields. The results have direct applications to possible future work using the scattered near and far fields to discriminate between chiral media and to optimize the electromagnetic characteristics of fabricated chiral materials. Chiral materials are of interest in a wide range of fields and therefore this work could have broad applications.

OPTICAL DETECTION AND CHARACTERIZATION OF
STRATIFIED CHIRAL STRUCTURES FOR ENGINEERING
AND BIOSECURITY

Bahar, E, Crittenden, P.
University of Nebraska-Lincoln

Complete modal field expansions of the electromagnetic fields scattered at rough interfaces between two chiral materials with laterally varying electromagnetic properties are derived. These complete field expansions together with exact boundary conditions are substituted into Maxwells equations to obtain the generalized telegraphists equations for irregular chiral media. The telegraphists equation are a set of coupled ordinary differential equations for the forward and backward wave amplitudes of the transverse components of the magnetic field and the electric field. The solution to these equations can be used to find the electromagnetic fields above and below the interface. This has direct applications to the detection and characterization of chiral materials, the discrimination between different chiral media and the optimization of desired electromagnetic characteristics of artificial chiral materials.

Similar sets of equations were derived using a rigorous full wave method of mode matching in irregular archival waveguides. Unlike the discrete waveguide mode spectra, the spatial wave spectra in this work are both continuous and discrete. The discrete part of the spectra is associated with surface waves and the four pairs of branch cuts (continuous spectra) are associated with lateral waves that creep just above or below the interface. To derive the generalized telegraphists equations, no assumptions are made about the characteristics of the rough interface, the frequency of the source, or the locations of the source and observation points. Therefore, they provide advantageous starting points for deriving near and far field solutions to a broad variety of physical problems. In electrical engineering, waveguides with organic chiral cores are being investigated for possible applications to integrated optic devices, including polarization transorms, modulators and directional couplers. In all these applications, sub-wavelength fluctuations in the interfaces between the media can significantly affect the physical characteristics of the chiral structures. Since biological materials possess chiral properties, this work has applications in biosecurity.

ULTRA WIDE BAND, MULTI-SCALE MULTI-PHENOMENA
THEORY, MODELLING AND SIMULATION AT THE
NANOSCALE

Bahar, E
University of Nebraska-Lincoln

Theoretical investigations to determine the electromagnetic near and far fields scattered by nanostructures due to fluctuations in the surface height and/or lateral variations in the electromagnetic medium parameters such as the complex electric permittivity, conductivity, and magnetic permeability are presented. Since the scale of the medium fluctuations of the nanostructures considered could be significantly smaller or larger than the electromagnetic wavelengths, the familiar perturbation and physical/geometrical optics solutions based on the Kirchoff approximations of the fields on the boundaries cannot be used nor is it possible to investigate sub-wavelength structures based on the far-field measurements. A rigorous full wave approach which employs complete field expansions, that include propagating and evanescent waves as well as lateral waves and surface waves are used in the analysis of the total scattered near and far fields.

The new unified full wave approach has been developed to evaluate the scatter cross sections from multiple scale composite rough surfaces. The surface is regarded as an ensemble of facets of arbitrary orientation that are superimposed on a large scale surface. The cross sections are shown to be stationary over a broad range of large scale mean square slopes. The full wave approach can be used to determine the scattered near fields as well as far fields. Both large scale and small scale (including subwavelength) fluctuations of the rough surface are accounted for in the analysis. The full wave solutions are not restricted to electromagnetic scattering by layered media which irregular interfaces. Scattering due to lateral variations in the complex electrical permittivities and magnetic permeabilities in each layer are also accounted for in the analysis.

This work is applicable to the synthesis and modification of nanostructure surfaces and contributes to the fundamental understanding of the physical analytical optical characteristics of artificially engineered surfaces with nanoscale roughness and lateral variation in the electrical and magnetic properties of the nanostructures such as quantum dots.

STOCHASTIC MODEL OF ELECTROMAGNETIC WAVE
PROPAGATION IN STRATIFIED ABSORBING MEDIA IN-
CLUSIVE A SEMITRANSSPARENT OBJECTS

V.G. Spitsyn , I.V. Fedotov , Y.R. Tsoy

Cybernetic Centre, Tomsk Polytechnic University, 84, Sovetskaya
street, Tomsk, 634034, Russia

The electromagnetic wave propagation in the stratified absorbing media bottom-poured of random discrete inhomogeneities is investigated. The media is contained the semitransparent objects in a view of sphere, cylinder, and parallelepiped. There is supposed that the typical sizes of layers and objects more large than the length of electromagnetic wave. In this paper we consider the numerical model of electromagnetic signal multiple interaction with discrete inhomogeneities chaotically disposed in the stratified media. The method of solving this problem is based on the stochastic modeling of wave interaction with random discrete media (V.G. Spitsyn, IEEE AP-S International Symposium, 1, 288-291, 2002). The oscillator of electromagnetic signal is presented as a source of photons with corresponding diagram of radiation. The type of photons interaction with discrete inhomogeneities is determined according to set cross sections of absorption and scattering. The shift of electromagnetic signal frequency conventional of photons interaction with active discrete inhomogeneities is computed (V.G. Spitsyn, Modeling of radiowave scattering on the ionospheric plasma disturbances, created of space vehicle, Tomsk: Publishing House STT, 2002). In the result of computer imitation of researched process we received the distributions in space of coordinates of energy scattering signal and energy of absorption signal into media. We received too the angular and frequency spectrums of scattering signal, going beyond of analyzed area. There is investigated the dependence of the scattering signal parameters in the receiving point from the position and forms of semitransparent objects. The genetic algorithm is applied for the solving of point-to-point propagation task (Y.R. Tsoy, Proceedings of the 7-th Korea Russia International Symposium on Science and Technology, Ulsan, Republic of Korea, 3, 181-187, 2003).

Session B2, 13:40-Monday

**MICROWAVE AND OPTICAL
CAVITIES AND NETWORKS**

Chairperson: L.W. Pearson

INVESTIGATION AND GENETIC OPTIMIZATION OF MONOPOLE ANTENNA LOADED WITH FILLED CAVITIES

Lockard, M. D., Butler, C. M., Rudbeck, J. P.
Clemson University

The effects of loading a monopole antenna with filled cavities are investigated. The monopole is loaded by means of a small cavity filled with a medium of large relative permeability, similar to those of Pisano and Butler (*IEEE Trans. Antennas Propagat.*, vol. 50, no. 4, pp.457-468, April 2002). The cavity, which is integrated into the body of the monopole, is essentially a section of coaxial guide, shorted at both ends, with a circumferential slit in its outer conductor. The exterior radius of the outer conducting wall of the cavity is the same as that of the monopole proper, causing the monopole to be of uniform radius except at the slit. The radius of the coax inner conductor may be adjusted to achieve desired properties, and the outer radius of the cavity is equal to the radius of the monopole minus the thickness of the outer conducting tube. The coaxial cavity is filled with a material of high permeability which, with proper adjustment of cavity dimensions, causes the monopole to experience an inductive load at the slit. The impedance of the inductive load presented to the monopole can be computed over a wide range of frequencies.

The input impedance of the cavity-loaded monopole is determined from the solutions of coupled integral equations. An eigenfunction expansion is used to represent the field in the cavity which is coupled to the exterior through the slit. The coupled integral equation unknowns are the electric field in the slit and the electric current on the exterior surface of the monopole. A parameter related to the impedance of the filled cavity is determined by a relatively simple calculation and, also, by a simple experiment, allowing validation of accuracy. When the parameter is found from measurements and inserted into the integral equation, the procedure can be looked upon as a hybridization of experimental and integral equation methods. The input impedance of the loaded monopole is calculated over a broad range of frequencies from the solutions of the coupled integral equations, and the effects of the filled cavity on antenna performance are examined. A genetic algorithm is utilized to optimize the performance of the antenna relative to specified performance criteria. The algorithm coerces satisfaction of the criteria imposed on the input impedance of the loaded monopole by adjusting the number of loaded cavities, the position and dimensions of each cavity, and the material in the cavities. Antennas that perform well in the optimization simulations are constructed and data obtained from the simulations are compared with those from measurements.

ANALYSIS OF TRANSMISSION OF A SIGNAL THROUGH A COMPLEX CYLINDRICAL/COAXIAL CAVITY BY TRANSMISSION LINE METHODS

Charles L. Bopp III, Chalmer M. Butler, Fred M. Tesche

Clemson University

The transmission of time-harmonic and transient signals through a complex cylindrical cavity is investigated by methods akin to microwave circuit techniques. The cavity may consist of multiple overlapping cascaded coaxial and circular cylindrical sections whose walls are perfect electric conductors. The sections may have different axial and radial dimensions and may be filled with material having different magnetic and electric properties. The first and last sections of the cavity are coaxial regions where only a TEM exists, which allow measurements to readily be performed with proper excitation and termination. The cavity sections may support both a TEM mode and additional higher order modes or may support one or the other. If two sections having a common junction and each supports only one mode, then the junction is modeled by a simple two port network. When additional modes are present, they are modeled by addition ports at the network junction. A corresponding equivalent transmission line is associated with each port at a junction. At each junction, scattering parameters are calculated and used to model the interaction of the various modes that exist. The S-parameters at each junction are determined separately by solving a simple integral equation that accounts for the structure of the junction and adjoining sections of coaxial and/or cylindrical guide. The cavity fields are, thus, associated with currents and voltages on transmission lines. A transmission line network is developed from which the input fields, fields at the cavity termination, and junction fields can be found by microwave circuit techniques or by the BLT transmission line analysis. The results from the transmission line method are compared with results calculated from a coupled integral equation analysis which has been carefully validated experimentally.

RESPONSE OF A COMPLEX CYLINDRICAL/COAXIAL CAVITY SUBJECT TO TRANSIENT EXCITATIONS

Charles L. Bopp III, Chalmer M. Butler
Clemson University

The response of a complex cylindrical/coaxial cavity is investigated. The goal is to understand the effect of a transmission path through a system of cavities on a transient signal. The effects of a particular cavity are assessed and characterized so that transmission of transient signals through a complex structure can be better understood. A coupled integral equation method is used to calculate the field in a particular cavity structure. The method is founded upon the fact that the field in a given cavity section depends on the field in the section boundaries where two or more sections may come together. The cavity may contain multiple cascaded and overlapping coaxial and circular-cylindrical regions or sections. The cavity regions may have different axial and radial dimensions and may be filled with material having different electrical and magnetic properties. The cavity walls are perfect electric conductors. In order to facilitate excitation and measurement by means of standard instrumentation, the first and last sections are coaxial cavities whose dimensions are such that higher order modes are cutoff, leaving only the TEM mode to propagate. A FFT is performed to obtain the time domain response to a specified time-domain input signal. Input signals of interest include sine bursts of various frequency modes, especially those with frequency content that coincides with a particular resonance of the cavity under investigation. Only calculated results are presented since the coupled integral equation solution technique has been validated through comparison of calculated results with results obtained from measurements on laboratory models. Conclusions are drawn from the data presented.

MODELING THERMOSET CURING IN A MICROWAVE CAVITY

Sun, R.¹, Zong, L.², Zhou, S.²
, Sgriccia, N.², Kempel, L.C.¹, Benard, A.³, Hawley, M.C.²

¹Department of Electrical and Computer Engineering, Michigan State University, East Lansing, MI 48824, USA

²Department of Chemical Engineering and Materials Science, Michigan State University, East Lansing, MI 48824, USA

³Department of Mechanical Engineering, Michigan State University, East Lansing, MI 48824, USA

Polymer processing is an important application of microwave heating in industry. Microwave assisted curing of thermosets can lead to superior materials for a variety of applications. Microwave curing has the advantage of heating the polymer precursor materials volumetrically and hence can lead to superior cure with efficiency not available with conventional convection heating. However, due to the complex interactions between the electromagnetic fields and the material, achieving the promise of microwave assisted curing is challenging. This is due to the fact that electrical properties (e.g. the complex permittivity) of the material change during the curing process. Hence, the field distribution within the cavity applicator changes as a function of the cure and local temperature of the materials being processed. It is vital in modeling the curing process that the microwave power deposition, heating, and extent of cure be coupled together.

In this work, we will briefly talk about the tightly coupled model including the electromagnetic, thermal, and kinetic effects. To illustrate the non-linear relationship between temperature, curing period, and extent of cure, the reaction kinetics for a simple epoxy resin, DGEBA/DDS was studied. The measured data agree very well with the calculated data from the kinetic model. The electric and magnetic fields within the cavity applicator, as well as within the transient material being processed, are modeled with finite element method. To demonstrate the importance of the interactions between the electromagnetic fields and the loaded sample, a cylindrical single-mode cavity loaded with a triangular polymer part has been studied. By observing the electric field distribution changes due to the location variation of the polymer, it is seen that the offset position from the center of the cavity base is not a wise choice to put the sample for TM_{012} mode to cure, since curing will not be accomplished throughout the volume of the material simultaneously. While when the same part is placed at the center of the cavity base, it will be cured much more uniformly.

MODELING OF A NOVEL MULTIMODE CYLINDRICAL CAVITY FOR MICROWAVE PROCESSING OF POLYMERS AND COMPOSITE MATERIALS

Sun, R.¹, Kempel, L.C.¹, Zhou, S.², Hawley, M.C.²

¹Department of Electrical and Computer Engineering, Michigan State University, East Lansing, MI 48824, USA

²Department of Chemical Engineering and Materials Science, Michigan State University, East Lansing, MI 48824, USA

Microwave processing of polymer and composite materials has been an increasingly important technology for the polymer industry and its customers. The advantages of microwave processing such as rapid volumetric heating leading to fine microstructure and improved mechanical properties are well recognized. Applicator design is one of the most important factors to guarantee good performance of the whole processing system. Usually it is very difficult for a single-mode applicator to provide desired temperature profiles across a sample because of the constraints of the electric field distribution for a specified mode. Sometimes the mode-switching technique, or another method with mode-stirrers is used to improve the heating uniformity. In this work, we present the modeling of a novel multi-feed multimode cylindrical cavity applicator, which is capable of accomplishing a variety of processing tasks.

Specifically, inside the cavity, a TM mode and a TE mode are excited simultaneously via two ports. The TM mode is excited through a circumferential slot, while the TE mode is excited through an axial slot. The combination of TM_{020} and TE_{211} is chosen such that we can have a bulls-eye heating pattern (by TM_{020}) at the center as well as some distributed spots (by TE_{211}) around it. With these separate TM and TE modes, we not only get desired field distribution at specific locations inside the cavity, but also have the ability to make heating direction selection, which is particularly useful when anisotropic materials are being processed. The combined electric field distribution of the two modes with different relative magnitudes of the feeds at the two ports is investigated to determine the optimal weighting factor for obtaining more uniform heating. By theoretical analysis, it is seen that with these two specific modes, we can have very low port-to-port coupling, which is very essential to get better efficiency.

NEAR-RIGOROUS THEORY OF MICRORING CAVITY RESONANCE

*Baktur, R.¹, Pearson, L. W.¹, Ballato, J. M.²¹Holcombe Department of Electrical and Computer Engineering, Clemson University, Clemson, SC 29634-0916²School of Material Science, Clemson University, Clemson, SC 29634-0922

Frolov, *et. al.* [*Appl. Phys. Lett.*, 72(22), pp. 2811-2813] have demonstrated lasing in a so-called microring created from an optically active polymer formed on a cylindrical mandrel. (Incidentally, an optical fiber was employed as the mandrel.) They provide an argument that the laser operates by virtue of a whispering gallery (WG) wave resonance. Slab waveguide modes, which also exhibit resonances, are a part of the complete field structure. Frolov, *et. al.* reason that conductor losses in the gold layer which they placed between the microring and the fiber would quench lasing in any slab waveguide mode.

In the present paper, we present a rigorous, though approximate, theoretical development for the complete electromagnetic field in the microring. The Greens dyadics developed is approximate in the sense that they are derived for a translationally invariant stratified structure excited, respectively, by electric and magnetic current line sources, thereby providing mode sets that are TE and TM to z. The resonances are observable as zeros in the denominators of the summand in the respective TE_z and TM_z expansions.

The summands in the expansion can be arranged so that a whispering gallery term appears explicitly with a residual term that combines with the WG to form a slab-guided mode that follows the circular path around the ring. As the dielectric layer is made thicker by receding the inner boundary while the outer boundary remains fixed, the residual term recedes, leaving a pure whispering gallery mode, consistent with the heuristic explanation of Frolov, *et. al.*

The resonances of the structure are examined critically and compared with published experimental data on microring lasers. Cases of non-circular structure and inhomogeneous material are discussed in terms of ray-optical asymptotic developments. Prospects for coupling of the laser mode into a fiber around which it is formed are discussed.

* a.k.a. Rehanguli Gayiti

APPLICATION OF PARTICLE SWARM OPTIMIZATION TO MICROWAVE NETWORKS

Yangyang Zhang, Chunlin Ji, Guangxing Wang

Northeastern University Mail Box: 423, Research Center of Networks and Communications, ShenYang 110004, China

This paper discusses and compares the methods of Genetic Algorithm (GA), Simulated Annealing (SA) algorithm and Particle Swarm Optimization (PSO) applied to implement the optimization of microwave networks. The PSO is operated to search minimax response objectives, which are probably the most desirable objectives in microwave network. The results indicate that the PSO is highly competitive with any of the two other algorithms.

Particle Swarm Optimization is a population-based stochastic optimization technique developed by Kennedy and Eberhart. Through cooperation and competition among the population, population-based optimization approaches often can find very good solutions efficiently and effectively. Unlike most of population based search approaches motivated by evolution as seen in nature, e.g. genetic algorithms, evolutionary strategies and genetic programming, the PSO is motivated from the simulation of social behavior.

Instead of using evolutionary operators to manipulate the individuals, like in other evolutionary computational algorithms, each individual in the PSO flies in the search space with a velocity which is dynamically adjusted according to its own flying experience and its companions experience, so that the individuals of the population can be expected to move towards better solution areas. Each individual is treated as a volume-less particle in the D-dimensional search space. The PSO has proved to be efficient at solving Global Optimization and engineering problems.

The test problems are examples of the optimization of cascaded commensurate and noncommensurate transmission lines acting as impedance transformers between resistive terminations. Previous numerical investigation found that the optimum designs were, not unexpectedly, quarter-wave Chebyshev transformers. So the results obtained by optimization may be compared with the results obtained by analytic methods. A computer program was written to calculate the reflection coefficient of a resistively terminated cascade of transmission lines at any frequency and for any section lengths and characteristic impedances.

A number of simulations were carried out to evaluate the relative performance of the PSO. Our results indicate that the PSO has many advantages over other heuristic techniques. The PSO should find immediate application to a wide range of microwave network design problems. We trust that the PSO will find most use in design problems for which exact methods are not available.

APPLICATION OF DISTRIBUTED PARTICLE SWARM OPTIMIZATION TO ANALOGUE FILTER TUNING

Yangyang Zhang, Chunlin Ji, Ping Yuan , Guangxing Wang

Northeastern University Mail Box: 423, Research Center of Networks and Communications, ShenYang 110004, China

For radio antenna transmission systems it is of great importance to transmit maximum power to the antenna to achieve maximum transmission efficiency. In many cases, for example mobile and fixed tactical applications, these systems must deal with changing load and environmental aspects. The goal of obtaining fast antenna tuning systems that are capable of offering impedance matching whilst maintaining good harmonic rejection properties has become increasingly significant. One of the most popular impedance matching configurations used is the Pi-Network, which is simple in structure, can accommodate a wide range of load impedances and offer high harmonic rejection capabilities. The Pi-Networks versatility creates problems when attempting to control it for optimal performance. When multiple objectives are considered, conflicting requirements may occur i.e. for a particular situation impedance matching may be achieved through low inductor values, while maximum harmonic rejection is achieved through maximum inductance. These conflicts between objectives compound the tuning problem by creating more complex error functions, containing greater numbers of local minima in which a search algorithm may become entrapped. Hence, efficient optimization approaches should be developed to cope with this problem.

In this work, we give a framework of a novel model of Particle Swarm Optimization (PSO), Divided Range Multi-objective Particle Swarm Optimization (DRMPSO), in multi-objective optimization for parallel processing. In the DRMPSO, the individuals are divided into sub populations by the values of their objective function. Therefore, the efficient search can be performed and the adequate local search also carried out. This model is proved to be suitable for parallel processing.

A number of simulations were carried out to evaluate the relative performance of these algorithms. Experiment results indicate that the proposed algorithm (DRMPSO) is highly competitive with the other algorithms.

To allow a fair comparison of running times, all the experiments were performed on a PC with a Pentium II processor; the simulations were carried out using MATLAB. The approximate simulation time for each of the algorithms is listed below: MOGA: approx. 60 minutes; MOSA: approx. 15 minutes; DRMPSO: approx. 2 minutes

The results indicate that the DRMPSO required much lower computational time than any of the two other algorithms tried.

Session B3, 13:40-Tuesday

ANTENNAS

Chairpersons: R. J. Pogorzelski and W. A. Imbriale

IMPROVING ANTENNA ARRAY PATTERNS IN OUTDOOR ENVIRONMENTS USING THE GENETIC ALGORITHM

Ting-Chieh Tu, Chien-Ching Chiu, Tsung-Yu Chen

Department of Electrical Engineering, , Tamkang University

In recent years, the development in the wireless communication is very quickly. In the wireless communication, capacity enhancement in limited resources becomes very important. But the heights of buildings are taller and taller in modern cities to make outdoor environments of wireless communication so complex. Due to building obstructions in outdoor environments, they will attenuate the received power and lower the speed of data transmission, even though received data error. Consequently, we need to use antenna arrays in order to produce the combination of antenna pattern for recovering the users. Otherwise, in order to make the antenna pattern with a good directivity, adopting the structure of antenna arrays is necessary. Our goal is to produce proper antenna patterns to overcome fading of complex environments. In this paper, we use four types of antenna arrays to produce better directivities and the configurations of arrays are L, Y, triangular, and circular. They consist of 8 elements that are all omnidirectional and half-wave dipoles except the triangular array, there are 9 elements in the triangular array due to the symmetric consideration. In order to produce better diversities, we adjust the excitation voltages and phases of antenna arrays. To synthesize the proposed antenna arrays, the excitation problems are reformulated as optimization problems and solved by the genetic algorithm. The current literature identifies three main types of search methods: calculus-based, enumerative and random methods, to find the extreme solution of the optimization problems. The genetic algorithm is a well-known algorithm that uses random choice to search through a coding of a parameter space. This algorithm has achieved increasing popularity as researchers have recognized the shortcomings of calculus-based and enumerative schemes. Theoretically, the genetic algorithm and enumerative method converge to the global extreme of the problem, while calculus-based method often becomes trapped in a local extreme. On the other hand, the enumerative scheme lacks efficiency compared with the other two methods. As a result, the genetic algorithm is the most robust scheme among the three methods. Then we take advantage of the 2.5 D SBR-Image method to construct the simulation environments. We combine with the genetic algorithm, simulation environments and antenna arrays together. We can get values of path loss at the running of the 2.5 D SBR-Image method to take as a fitness function of the genetic algorithm. In order to lower path loss, the genetic algorithm adjusts the excitation voltages and phases of antenna arrays to optimize antenna patterns.

ON THE BANDWIDTH OF COUPLED OSCILLATOR BASED PHASED ARRAYS

Pogorzelski, R.J.
Jet Propulsion Laboratory

Recently, several researchers have reported studies of phased array antennas in which the aperture phase distribution is derived from an array of mutually injection locked electronic oscillators. [R. A. York, IEEE Trans., MTT-41, pp.1799-1809, Oct. 1993] [P. Liao and R. A. York, IEEE Trans., MTT-41, pp. 1810-1815, Oct. 1993] [R. Ispir, S. Nogi, M. Sanagi, and K. Fukui, IECE Trans. Electron., E80-C, 1211-1220, Sept. 1997] [R. J. Pogorzelski, Microwave and Guided Wave Letters, 10, pp. 478-480, Nov. 2000] [J. Shen and L. W. Pearson, Nat. Radio Sci. Mtg, Boston, MA, July 2001] This raises the question of how the bandwidth of such an array may differ from that of a conventional phased array. (For present purposes we exclude the case of a so-called true time delay array.)

First, we distinguish between the operating bandwidth and the instantaneous bandwidth of the array. Here we deal only with the instantaneous bandwidth since the operating bandwidth is in essence that of the corresponding conventional array being determined by the operating range of the electronics and that of the radiating aperture. The instantaneous bandwidth of a conventional phased array is dependent upon the bandwidth of the radiating elements and the frequency scanning properties of the array. These are also factors determining the bandwidth of an oscillator array based antenna. However, in addition to these, the bandwidth of the oscillator-based antenna is determined by the dynamic characteristics of the oscillator array. To be sure, the dynamic behavior determines the attainable rate of scan but, more relevant to our present discussion, it also determines the rate at which the output signal can be phase or frequency modulated without undue distortion. [R. J. Pogorzelski, J. S. Acorn, and M. S. Zawadzki, Nat. Radio Sci. Mtg., Boulder, CO, Jan. 2000] The dynamic properties of the oscillator array are determined by the number of oscillators and the complex inter-oscillator coupling strength. In this paper, the factors influencing array bandwidth are evaluated in terms of their relative impact on the data rate which the antenna will support, a performance parameter which is taken to be the appropriate measure of antenna instantaneous bandwidth.

PREDICTION OF NEAR-FIELD INTENSITY FOR A RADAR PHASED ARRAY ANTENNA

Nicholas DeMinco

U.S. Department of Commerce, NTIA/ITS.E

Near-field intensities in the vicinity of a radar phased array antenna were calculated to determine if a radiation hazard condition exists. A number of different techniques were examined that would provide a fast and accurate determination of near-field intensity. Two different techniques were selected and used to perform the calculations for this paper.

The first technique consisted of modeling the phased array antenna using a method-of moments code, implemented in a computer program titled the Numerical Electromagnetics Code (NEC) Version 4 developed at Lawrence Livermore National Laboratory. This code is quite suitable for computing the near-field intensity of a phased array antenna at all locations of interest for radiation hazard determination. The key to accurate computation of the near-field intensity is the correct simulation of the phased array geometry and radiating elements, and then translating this to an acceptable NEC input file format. The analysis was performed for both an unscanned beam and a beam steered over the limits of the antenna array. The technique using this NEC software was then compared to the second technique.

The second technique required the development of a mathematical algorithm that would take into account all of the factors of a phased array antenna, and subsequently allow prediction of the near-field intensity for the radar antenna. These factors included: array factor, element factor, scan loss, grating lobes, interelement spacing, and interelement phase shift.

The two techniques were compared and good agreement was obtained. The second technique is a much faster computation technique, which is a major advantage for phased-array antennas with large numbers of radiating elements. It is also much easier and faster to change the input files for the second technique that uses the mathematical algorithm. The NEC method requires individual entry of each radiating element, but it factors in the effects of mutual impedance between elements in a more accurate manner.

WIRE ANTENNA EXPOSURE ZONE BOUNDARY ESTIMATION FROM FAR-FIELD RADIATION CHARACTERISTICS

Ebersbach, H.¹, Thiel, D.V.¹, Leckenby, M.²¹Radio Science Laboratory, Griffith University, Nathan, QLD 4111, Australia²iCOMMS Pty Ltd, Mitchelton, QLD 4053, Australia

Due to the rapid global expansion of the mobile telephone and wireless communication networks and community concerns of radiofrequency radiation exposure, there is an escalating demand for the quick and accurate determination of antenna near-field radiation characteristics to demonstrate compliance with radiation exposure limits. These computational methods must allow efficient modelling of the occupational and non-occupational radiation exposure zone boundaries measured in V/m and A/m for E- and H-fields respectively. In the Australian transmitter database maintained by the central regulatory authority, the only information stored is the antenna class (such as wire, aperture or panel antenna), gain and front to back ratio, far-field radiation patterns in both principle planes, and its maximum physical dimensions. This is insufficient for present NEC, FDTD and FEM software tools. Thus an additional pre-calculation step is required, that infers an antenna structure from the available antenna specifications.

This paper presents a method for estimating the radiation exposure zone E-field boundaries for dipole and multi-element wire antenna structures from the specified antenna gain and far-field radiation characteristics in both principle planes. These antenna characteristics are used to estimate the number of antenna elements. A suitable reference antenna with an identical number of elements and similar radiation properties to the original antenna is selected from a database. The exposure zone boundaries are calculated using the Huygens wavelets technique for Yagi-Uda and other wire antennas for a specified power level delivered to the antenna (H. Ebersbach and D.V. Thiel, *Australian Symposium on Antennas*, 8, 36, 2003).

The algorithm has been implemented in C++ and applied to several Yagi-Uda antennas with good accuracy. Results and verification against NEC near-field calculations will be presented.

MODIFICATION OF TEM-FED REFLECTOR FOR INCREASED EFFICIENCY

Baum, C.E.

Air Force Research Laboratory/DEHP

The paper explores some concepts for increasing the efficiency of a TEM-fed paraboloidal reflector. Instead of just removing sections with unfavorable polarization, one can use unconducting sheets (parallel conductors) to alter the polarization of the reflected fields so that they more effectively add to the aperture integral for the far field. For cases that the source has a not-too-large bandwidth one can also displace the reflector a quarter wave-length to change the phase (reverse the sign) of the field to make it add to the aperture integral.

The techniques discussed in this paper need not be used separately, but can be combined in various ways for each portion of the paraboloidal reflector. For example, the displacement of the reflector can be combined with the unconducting reflector. While the discussion here is in terms of a reflector, similar considerations can be used for lens-focused apertures. These are complementary. Note that in the case of a unconducting sheet the lens case involves a rotation by $\pi/2$ to give the complementary sheet for transmitting instead of reflecting the field.

For a mesoband oscillator reflector antenna (ORA) we can also revisit the feed structure. The TEM feed from focus to reflector is most appropriate for the dispersionless hyperband application as in an IRA. For hypoband application a common wave launcher toward a reflector is a microwave horn operating in some waveguide mode (not TEM). For sufficiently high frequencies such that the horn aperture is small compared to the reflector aperture, such a design is quite appropriate. As one lowers the frequency so that the reflector aperture is only a few wavelengths across, such a microwave horn may become unacceptably large. One may then prefer a TEM feed, or perhaps an offset feed from a microwave horn. Perhaps one can begin the launch as a TEM structure near the focal point, and transition to some other kind of non-TEM structure as one approaches the reflector to give some kind of hybrid.

UPDATE ON THE 6-METER BREADBOARD ANTENNA FOR THE DEEP SPACE NETWORK LARGE ARRAY

Imbriale, W. A., Weinreb, S., Feria, A. , Porter, C., Hoppe, D.

Jet Propulsion Laboratory, California Institute of Technology,
Pasadena, CA 91109

Development of very large arrays of small antennas has been proposed as a way to increase the downlink capability of the NASA Deep Space Network (DSN) by two or three orders of magnitude thereby enabling greatly increased science data from currently configured missions or enabling new mission concepts. The current concept is for an array of 400 x 12-m antennas at each of three longitudes. The DSN array will utilize radio astronomy sources for phase calibration and will have wide bandwidth correlation processing for this purpose. A development program is currently underway to develop the technology and prove the performance and cost of a very large DSN array. The program includes a 3-element interferometer to be completed by late 2004. This paper presents the current status of the low cost 6-meter breadboard antenna to be used as part of the interferometer.

The baseline breadboard antenna is a 6-meter hydroformed symmetrically shaped dual reflector system utilizing Gregorian optics. The heritage for this antenna lies in the Allen Telescope Array project plans to build 350 6m antennas specified for use up to 11 GHz. Hydroforming is the process of forming aluminum to a rigid and precise mold by using a fluid or gas under pressure. It has been highly developed for use in production of low-cost reflectors for satellite communications and thousands of antennas in the 1 to 4 meter range have been manufactured. This project improves the surface accuracy to extend the useable frequency range to 38 GHz. Three dish shells have been fabricated that have a surface accuracy of less than 0.2 mm rms. The backup structure utilizes 9 equally spaced aluminum struts connecting a center yoke to the rim of the dish. The pedestal consists of a central pipe tucked under the dish with a central bearing for azimuth motion and a jackscrew for elevation control.

The feed is a dual frequency horn covering the X (8-9 GHz) and Ka (30-38 GHz) bands. The X-band will be a coaxial waveguide fed corrugated horn and Ka-band will utilize a dielectric rod in the center of the corrugated horn.

MICROSTRIP REFLECTARRAYS WITH MULTI-LAYER GROUNDED SUBSTRATES AND SUPERSTRATES

Rengarajan, S.R.

Department of Electrical and Computer Engineering, California
State University, Northridge, CA 91330

Microstrip reflectarray antennas are becoming popular in many space applications because of their low profile and ease of deployment. An infinite uniformly spaced array of microstrip antennas consisting of identical elements and excited by a plane wave is the canonical problem of interest in the design and analysis of such antennas. The reflection coefficient obtained for this canonical problem is used as an approximation for the element reflection coefficient of a finite sized reflectarray if the element size or shape does not vary rapidly from element to element.

The infinite array of microstrip elements is usually analyzed by solving the pertinent integral equations for the induced currents in the microstrip elements. The required Green's functions appear as a Floquet series and their expressions are obtained in spectral domain by considering transmission line techniques for the TE and TM waves. The integral equations are solved by the method of moments. We have been investigating the moment method solutions for infinite arrays of different geometries such as microstrip patch arrays, crossed dipole arrays, arrays of stacked patches, and two-layer microstrip elements for dual frequency applications. In order to analyze a number of these problems we developed moment method solutions for microstrip elements with multiple layers of dielectric substrates and one or more layers of superstrates. The required Green's functions for the multi-layer problem are obtained in terms of the spectral domain TE and TM mode transmission matrices. Different choices of entire domain basis functions were studied. The reflection coefficients of infinite arrays excited by a normally incident plane wave were obtained by the finite element solver HFSS. These results compared well with our moment method results, thus validating our code.

In the symposium we will present the essential features of our moment method solutions. Numerical results for many of the structures will be presented.

VHF/UHF/L-BAND/S-BAND DEPLOYABLE ANTENNA FOR SATELLITE APPLICATIONS

Paul A. Bernhardt¹, Carl Siefring¹, Lee Atkinson², Michael Moore², Brian Whalen³, Andy Feerst³, John Burton⁴, Fred Domer³

¹Plasma Physics Division, Naval Research Laboratory, Washington, DC 20375

²Orbital Sciences Corporation, Dulles, VA

³Spacecraft Engineering Department, Naval Research Laboratory, Washington, DC 20375

⁴Commonwealth Technology Inc., Alexandria, VA 22310

A new antenna design has been developed for the Constellation Observing System for Meteorology, Ionosphere and Climate (COSMIC) satellite program. This program requires an antenna to operate simultaneously in narrow bands near 150, 400, 1067, and 2036 MHz. Satellite antennas must meet strict radio frequency and mechanical specifications. The COSMIC satellite carries a Coherent Electromagnetic Radio Tomography (CERTO) beacon that will simultaneously broadcast continuous wave signals at 150.012, 400.032, and 1066.752 MHz to ground receivers for ionospheric measurements of Total Electron Content (TEC). The requirements for the CERTO beacon antenna are (1) uniform antenna pattern to illuminate the earth from the satellite at 800 km altitude, (2) common phase center for all radiated frequencies, (3) right-hand circularly polarization, (4) no ferromagnetic properties, (5) stowage into a 60 cm x 8 cm x 8 cm volume in the satellite before launch, (6) no damage by vibration at launch, and (7) successful deployment in space. In addition an S-Band frequency near 2 GHz is used for telemetry transmissions to ground stations. The antenna uses two trapped dipoles in an orthogonal configuration for the VHF/UHF/L-Band frequencies. A quadrafilax helix for the S-Band Frequency is mounted on the end of the antenna boom just past the crossed dipoles. The CERTO beacon provides in-phase (I) and quadrature phase (Q) signals via two coax cables to the two trapped dipoles. Numerical electromagnetic modeling has been used to design the trapped elements and to account for the interactions with the S-Band antenna. Reflectors tuned to 150, 400, and 1066 2/3 MHz have been added to the antenna boom for shielding of the spacecraft and for added gain to the ground receivers. The reflections are fabricated from a nickel alloy called Elgiloy formed into curved tape-measure-like strips. The radiating elements are copper plated fiberglass tubes. These are attached to the antenna boom by spring loaded cup-cone hinges. The base of the boom is another hinge that deploys the boom. The antenna elements and reflectors fold into a small package along the boom. A matching network is located in the antenna boom to provide VSWR less than 2 in 5

A WIDEBAND CPW-FED PATCH ANTENNA WITH DEFECTIVE GROUND PLANE

Lin Xian-Chang¹, Wang Ling-Teng²

¹National Taipei University of Technology, Department of Electronic Engineering

²National Taipei University of Technology, Institute of Computer, Communication, and Control

A Wideband CPW-Fed Patch Antenna With Defective Ground Plane

CPW-fed patch antennas have been popular for various applications, because of their low cost, lightweight, and compatible with integrated circuits. However, a narrow impedance bandwidth (2The proposed antenna consists of two FR4 substrates with dielectric constant 4.6, loss tangent 0.02, and substrate thickness 1.6mm. The top layer is a traditional CPW-fed patch antenna. A square patch element with size 38x38mm is placed on topside of the substrate. The underside of the substrate is an inductive CPW-fed structure. The conventional CPW-fed line is designed with the characteristic impedance of 50 ohm. A defective ground plane consists of 49 cross-shaped elements (7x7) with dimensions of 70x70mm on underside of the bottom layer. In this work, the inductive CPW-fed structure (without patch element) with defective ground plane generates first resonant frequency and the traditional CPW-fed patch antenna (without defective ground plane) exhibits second resonant frequency. When traditional CPW-fed patch antenna with defective ground plane, the measured shows that two resonant frequencies are excited with good impedance matching. It is found that a wideband operation is obtained by making the first resonant frequency adjacent to the second resonant frequency. The impedance bandwidth of the proposed antenna could reach about 240MHz (1.6GHz-1.84GHz), which is about 13A major contribution of this antenna is impedance bandwidth enhancement. The wideband CPW-fed patch antenna can be achieved by combining with a defective ground plane. The impedance bandwidth of the antenna can reach 240MHz, which is 6.5 times that (2

Session B4, 9:00-Wednesday

**ELECTROMAGNETIC THEORY
AND NUMERICAL ANALYSIS**

Chairpersons: D. R. Wilton and F. M. Tesche

RANDOMLY-ORIENTED NONUNIFORM MULTICONDUCTOR TRANSMISSION LINES

Pincenti, J. C., Uslenghi, P. L. E.

Department of Electrical and Computer Engineering, University of Illinois at Chicago

The problem of incident field excitation of a nonuniform multiconductor transmission line is considered, in the frequency domain. In practice, the exact orientation of the transmission line is not known, hence the electromagnetic field excitation of the line is probabilistic and must be analyzed as such. Specifically, cable bundles of the type used in computer systems or mobile products such as cellular radios, or as interconnects between systems within a platform such as a vehicle or an aircraft, are considered. The cable bundle is modeled as a nonuniform multiconductor transmission line (NMTL). The orientations of different segments of the bundle are allowed to vary randomly, thus modeling the various twists and bends of a real cable.

The analysis is conducted for realizations of the bundle with various numbers of wires (both for the homogeneous and nonhomogeneous cases), various cable lengths, and various terminations. The NMTL is approximated by piecewise discretization, in which the overall line is modeled as a series of shorter uniform lines, that are analyzed via the chain parameter matrix, which relates the currents and voltages on the line. The effects due to external illumination are included in the equations by incorporating additional source terms.

In an attempt to model the twists and bends that the cable may experience as it is laid out in a practical system, the relative positions of the wires in the bundle are kept constant, while the orientation of the bundle with respect to the incident field is allowed to vary along the length of the cable. Several results are presented and discussed, including the application of a simple model to estimate the upper bound of the bundle response.

EVALUATION OF SINGULAR AND NEAR-SINGULAR POTENTIAL INTEGRALS FOR VOLUME ELEMENTS

Khayat, M.A. , Wilton, D.R.
University of Houston

Potential integrals involved in the integral equations of electromagnetics are often singular or nearly singular, and therefore require special numerical considerations for their evaluation. Quadrature rules for directly handling these singularities generally do not exist. In such situations, the singularity subtraction or singularity cancellation methods, such as the Duffy transformation, are often used.

A simple and efficient numerical procedure using a singularity cancellation method has recently been developed [D. R. Wilton and M. A. Khayat, USNC/CNC/URSI N. American Radio Sci. Meeting, Columbus, Ohio, June 2003, pp. 394.] [M. A. Khayat and D. R. Wilton, Proc. ICEAA, Torino, Italy, September 2003, pp. 83-86] for evaluating singular and near-singular potential integrals on tubular and planar elements. The procedure has been demonstrated to have several advantages over the singularity subtraction method and the singularity cancellation method utilizing the Duffy transformation. For example, the method is fully numerical, as opposed to the singularity subtraction method, and is, therefore, more suitable for use in object-oriented codes. In addition, it effectively handles near-singularities and does not introduce an angular dependence within a subtriangle as does the Duffy transformation.

In this presentation we extend the method to volume elements. In particular, we present analysis and results for tetrahedral, brick and prism elements. We find that volume elements should first be subdivided into tetrahedrons or pyramids with a vertex at the observation point. Then contributions from triangular or rectangular cross section integrations, respectively, vary linearly for the dominant static part of the potential, and thus a minimum number of cross-sectional integrals are needed. We also show that the extension to volume elements relies on two properties of the singularity cancellation method: 1) the method effectively handles near-singularities and 2) any volume element can be thought of as a superposition of triangular elements which are the base elements of the integration scheme.

ELECTROMAGNETIC SCATTERING FROM ARBITRARILY SHAPED CONDUCTING BODIES COATED WITH THIN DIELECTRIC MATERIALS

Khayat, M.A., Wilton, D.R.
University of Houston

Understanding the scattering properties of material-coated objects has become an important topic in computational electromagnetics. While considerable progress has been made in reducing the computational complexity of determining scattering by conducting bodies, efficient methods are still needed for problems that include both materials and conductors. Two examples of methods previously used are the surface-volume and surface-surface coupled integral equations. For the surface-volume integral equations the unknowns are the surface current used to represent the conductor and a volume polarization current used to represent the material. The surface integral equation is formed by requiring that the tangential component of the electric field vanish on the surface of the conductor (EFIE) while the volume integral equation is obtained by expressing the total electric field in terms of the volume polarization current. For the surface-surface coupled integral equation, the material is modeled via equivalent surface electric and magnetic currents. The EFIE is again applied to the conductor while the PMCHWT formulation is used for material interfaces.

In this work we present an alternative method for calculating scattering by conducting bodies coated with thin materials. Although the results presented concentrate on spherical scatterers, the method applies to arbitrarily shaped geometries. The thin material is modeled by a volume polarization current between two layers of surface polarization charge, where the volume current is assumed constant normal to the conductor. Using a boundary condition, the volume current is related to the surface charge, which in turn is related to the surface current on the conductor through the continuity equation. Thus, for closed bodies the conducting surface current is the only unknown.

The model has been tested using the EFIE, MFIE and CFIE formulations and good agreement with other methods has been obtained. The method requires accurate evaluation of self and near-self potential integral terms for both the surface and volume geometries. A recently introduced integration scheme [D. R. Wilton and M. A. Khayat, USNC/CNC/URSI N. American Radio Sci. Meeting, Columbus, Ohio, June 2003, pp. 394.] provides the required accuracy with good efficiency.

AN EXPRESSION FOR THE PO CURRENT FOR A THICK RESISTIVE LAYER

Dorey, S., Havrilla, M., Wood, W.
Air Force Institute of Technology

The physical optics (PO) current $\mathbf{J}_{PO} = 2\hat{n} \times \mathbf{H}^i$ (where \hat{n} is the surface normal and \mathbf{H}^i represents the incident magnetic field intensity) is frequently used to obtain a high-frequency approximation to the scattering from perfect electric conducting (PEC) structures. However, in certain applications, structures may be fabricated using imperfect conductors or resistive layers for the purpose of reducing scattering mechanisms. Under these conditions, the use of the above ideal PO current will lead to errors in the scattered-field calculation. In order to mitigate these errors, a non-PEC physical optics current expression must be developed. The purpose of this paper is to derive a physical optics current to accommodate finitely-thick resistive layers and subsequently verify the analysis via radar cross section (RCS) measurements of finitely-thick resistive strips under both horizontal and vertical polarizations.

The PO current of a finitely-thick resistive layer will be developed based upon a plane wave analysis. The derivation will assume that the layer is an infinite non-magnetic planar slab having thickness d , permittivity ϵ and conductivity σ . Next, a closed-form solution is found for the fields inside the layer using standard plane wave theory for both horizontal and vertical polarizations. A Taylor-series analysis is then performed to obtain an approximate expression for the resistive PO current \mathbf{J}_{RPO} in terms of the equivalent surface resistance $R_s = \frac{1}{\sigma}$ ($\Omega/\text{sq.}$) of the conducting slab for both polarizations, namely

$$\mathbf{J}_{RPO} = \mathbf{J}_{PO} \left(1 + 2 \frac{R_s}{Z_0} \right)^{-1}$$

where $Z_0 = \eta_0 \cos \theta_i$ for horizontal polarization, $Z_0 = \eta_0 / \cos \theta_i$ for vertical polarization and θ_i is measured relative to the surface normal. It will be shown that this expression is robust in that it remains valid to third order in the Taylor series expansion, resulting in the conclusion that this expression can be utilized in applications involving relatively thick resistive materials. It should be noted that, in the high-frequency limit, this condition will also be approximately valid in a non-planar environment so long as any curvature is small compared to wavelength.

The RCS of several resistive strips of various thicknesses will be experimentally measured and compared to RCS calculations based on the above analysis for theoretical verification. In addition, a Method-of-Moments integral equation solution based upon a resistive boundary condition will be formulated and compared to the above results to validate \mathbf{J}_{RPO} .

Session B5, 10:40-Wednesday

TIME DOMAIN ISSUES

Chairpersons: M. E. Kowalski and P. R. Hayes

ELECTROMAGNETIC FORMULATIONS AND CHARACTERISTICS OF THE FDTD TRANSPARENT SOURCE

Ching-Lieh Li, Shao-Hon Chen, Chien-Wei Liu

Department of Electrical Engineering, Tamkang University

The electromagnetic (EM) characteristics of a transparent source for the finite-difference time-domain (FDTD) method are investigated. The formulations for the corresponding electric and magnetic fields are first reported, while the associated charges and current are also demonstrated. It is shown that the magnetic field is proportional to the temporal derivative of the electric field at the source node, while the electric field is proportional to the temporal integration of the driving function at this node. Static charges may be built up to produce static E fields after the driving function has passed, which are responsible for the dc offset problem in the pulsed FDTD algorithm. The dc offset is verified for a Gaussian pulse and avoided via the use of a bipolar pulse. For the purpose of transparency, a transparent (added) source is implemented by setting the value of the E field at the source node as the sum of the driving function and the usual update equation. Unfortunately, although the transparent source can avoid the spurious scattering from the source node, the energy it couples into the grid is different from the hard source, and their EM characteristics are still not well documented. Knowing the characteristics of the source modeling is important, because their effects on the system can be quite influential. A transparent source implemented in this additive way was usually described as a field/voltage source. However, it is, in fact, an injected current source and should be labeled as a current source. In this paper, the EM characteristics of the transparent (added) source are thoroughly investigated. The driving function of the added source is shown to play the role of an infinitesimal current element (ICE). Electrical dipole charges are accumulated near the source node during the course of the driving function excitation. Static charges may be built up to produce static E fields after the driving function has passed, which are responsible for the dc offset problem in the pulsed FDTD algorithm. In addition, the accumulated charges about the source node attribute directly to the E field at the source node and result in different E field at the source node from the driving function. The formulas for the associated electric and magnetic fields are first reported, while the associated charges and current are also demonstrated.

TIME-DOMAIN CALCULATION OF GUIDED ELECTROMAGNETIC WAVE PROPAGATION ON UNSTRUCTURED GRIDS

Marc E. Kowalski, Cho-Kuen Ng, Lie-Quan Lee
, Zenghai Li, Kwok Ko

Advanced Computations Department, Stanford Linear Accelerator Center

Time-domain numerical methods offer the potential to study nonlinear and wideband phenomena. The Finite-Difference Time-Domain (FDTD) method, as the most mature and well known, enjoyed a significant increase in flexibility with the introduction of the perfectly matched layer (PML) boundary condition. However, FDTD suffers from the "staircase" boundary approximation, requiring alterations to the basic scheme near material interfaces that have high curvature, are not aligned with one of the principal axes of the Cartesian coordinate system, or present strong dielectric contrast. Moreover, the perfectly matched layer (PML) has proven difficult to apply to the computational truncation of guided-wave structures excited by wideband sources without suffering large reflection errors. If the numerical modeling of time-domain electromagnetic fields is to keep pace with the increasing sophistication of the corresponding frequency-domain techniques, methods of mitigating these difficulties must be found.

The finite-element method (FEM), employing unstructured meshes comprising elements of arbitrary type and order, inherently enjoys controllable accuracy when presented with challenging geometries without any deviation from the basic FEM scheme. The recent emergence of high-order interpolatory and hierarchical generalizations of the Whitney-type edge basis functions have enabled the frequency domain FEM scheme to more fully exploit this flexibility. However, the FEM has remained unattractive to time-domain modelers for at least two reasons. First, in unconditionally stable time-domain FEM (TDFEM) schemes, a matrix inversion is required at each time step. Second, the use of PML in TDFEM, even if easily accomplished, would still suffer the reflections that have been predicted in guided wave structures, leading to pollution of a wideband numerical solution.

In this work, we propose an approach that overcomes both of these obstacles to TDFEM modeling. First, a direct solver suitable for the sparse matrix inversion required by unconditionally stable time-stepping is described. Second, a modal boundary condition, based on the dispersive nature of guided waves in homogeneous waveguides, is applied to terminate the computational mesh with low reflection and minimal additional computation. The entire scheme is demonstrated to be easily parallelized with good scalability. Examples of studies of wakefields in linear particle accelerating structures (LINACs) are used to demonstrate the capabilities of the devised method.

TIME-DOMAIN CEM SIMULATIONS OF ELECTRICALLY LARGE STRUCTURES FOR EMI EFFECTS ANALYSIS

Paul Hayes
CEMTACH Consulting Group

Pulsed antenna systems can generate pulses in rapid succession. Provided the antenna is mobile, the pulses can expose large structures to the radiated electromagnetic fields. A mobile antenna source such as the one described provides a means to rapidly test large structures for electromagnetic interference (EMI). Physical tests provide hard insight into coupling mechanisms and full physical detail for the measurements. Simulations serve a complimentary function, providing a rigorous means for studying the EMI fields in a large structure yet do not provide all the detail involved in a physical test. A combined analysis of simulations and physical experiments provides a closed-loop analysis to more fully study the coupling mechanisms. A current challenge in computational modeling of large structures is data entry into electromagnetic modeling software. Many current computer codes envelope the entire model space with the simulation volume resulting in an unreasonably large simulation volume for electrically large structures leaving the model unable to run in a reasonable wall-clock time or unable to run on the available resources. One solution to this predicament is to partition the model space into electrically smaller pieces and simulate each separately. However, this results in unreasonably large numbers of separate data files for the codes, which are logistically challenging if changes to the original large structure are required. This work provides one solution to the data entry of electrically large structures and simulation partitioning. This facilitates large structure simulations that may then be combined with large structure physical experiments. Or, used to simulate experiments that are not practical to implement.

INTERFERENCE OF HIGH-POWER HIGH FREQUENCY PULSES ON A CMOS ADDER

Kollman, R.D., Yang, H.Y.D.

University of Illinois at Chicago, Dept. of Electrical & Computer Engineering

High-power radio-frequency electromagnetic interference to communication or control systems is becoming a serious military and civilian concern. There is increasingly renewed research interest in low-power digital circuit susceptibility to external noise. In this paper, we investigate the effects of external microwave pulses on a typical CMOS short channel circuit that is presently used in electronics industry. The results of large-scale electromagnetic scattering simulation are used here as the external noise sources at the pins to the digital circuit chip. This noise source will have linear and non-linear effects on the circuit that will affect both the data level and propagation delay and leads to a fault in the output of the circuit. In this paper, we investigate specifically the linear effects on a counter which would be built using a short channel CMOS process so that velocity saturation is taken into effect. The counter is a Finite State Machine (FSM) and so is representative and sufficiently complex to be typical of a system used in industry where combinational logic is used in conjunction with sequential circuits to achieve a result. Various pulse levels, periodicity and shapes based on what would be present at a single pin or multiple pins of the device due to an external microwave source are studied and failures for the various permutations are shown. The circuit is studied using Spice analysis and typical process parameters from MOSIS using the Berkeley Short-Channel IGFET Model version 3.1 (BSIM3v1) and an analytical insight into the causes of failure will also be given.

SCATTERING OF THE WIDEBAND SIGNALS

Yildirim, O. , Yilmaz, A.

Turkish Air Force Academy,, The Department of Electronic Engineering, Yesilyurt, Istanbul, TURKEY

As is well-known, electromagnetic forward scattering entails the prediction of the emission or the propagation of the radiation on the basis of known constitution of sources or scatterers. The backward scattering problems involves in deducing features of sources or scattering bodies from the emitted or scattered radiation that has propagated to a detection system. The process of deducing features of scattering bodies from the emitted or scattered radiation that has propagated to a detection system. The process of deducing features of scattering bodies from the emitted or scattered radiation that has propagated to a detection system. The process of deducing features of scattering bodies from radiation, namely inverse technique, has a vast domain of applications in geophysical and meteorological exploration and testing, etc.

This study involves the following steps; (1) computation of single scattering from a spheroidal scatterer at a single frequency, (2) computation of multiple scattering from a distribution of spheroidal scatters at a single frequency to simulate different rain rates, (3) extension of (2) to ultra-wideband (UWB) waveforms, such as stepped-frequency and random noise signals. (4) effect of dispersion on (3) above, (5) extension of (4) to target detection of, say, aircraft.

In this study, we extend the backscattering analysis from a volume filled with spheroidal raindrops and hailstones using physical optics (PO) and Rayleigh-Gans approximation (RGA) and check the validity of the theoretical derivation by using forward scattering theorem (FST). In order to reveal the multiple scattering effects, a model based on matrix doubling algorithm will be developed so that raindrops and hailstones are modelled as spheroidal particles under the Rayleigh approximation. The ultimate goal of this study is to show the scattering of the ultra-wideband random noise radar signals and to reveal the advantages of UWB radar in long-range target detection and the effects of inclement weather on system performance.

Session B6, 14:00-Wednesday

**VALIDATION OF NUMERICAL
METHODS BY COMPARISONS
WITH ANALYTICAL METHODS,
OTHER INDEPENDENT
NUMERICAL METHODS, OR
EXPERIMENTS**

Chairpersons: Chalmers M. Butler and
Danilo Erricolo

VALIDATION AS A PROCESS

D. R. Wilton¹, D. R. Jackson¹, W. A. Johnson²
, M. A. Khayat¹, C. Lertsirimit¹

¹University of Houston, Dept. of Electrical and Computer Engineering, Houston, TX 77204-4005

²Sandia National Laboratories, P.O. Box 5800, Albuquerque, NM 87175-1152

The development of robust, accurate, and error-free codes for solving complex electromagnetic problems of current interest requires that validation be an ongoing process during code development. While completed software must necessarily be validated by comparing computed results to applicable analytical or measured results, agreement between such results is not sufficient to guarantee code correctness. In general, validation is needed for each newly added or modified processing step in a code. Frequency domain finite and boundary element methods usually include most or all of the following major processing steps: geometry discretization, generation of basis/testing functions, generation and integration of Green's function potential integrals, testing integrations, enforcement of boundary and radiation conditions, element matrix generation and assembly, preconditioning of the system matrix, processing for fast matrix fill and matrix/vector product calculation, solution via iterative or direct methods, and postprocessing to obtain problem-dependent measurables.

A number of standard tests may be considered, including the following: satisfaction of field and potential continuity conditions, edge or interface conditions, and reciprocity; confirmation of expected convergence rates with increasing subdivision or increasing geometry or basis function order; convergence to known low- or high-frequency behavior; reduction to equivalent transmission line, circuit, canonical radiator or scattering problems; and robustness of formulation as measured by matrix conditioning and solution accuracy. Additional tests must often be devised, however, which can challenge a developer's creativity in developing novel test cases. Tests used by the authors for problems of recent interest will be provided in the presentation.

One of the last validation steps is comparison to an independent code, or to measured, analytical, or quasi-analytical solutions if they exist. In final benchmark testing, developers should test over a wide range of problem and solution parameters to determine valid ranges of code parameters.

Sandia is a multiprogram laboratory operated by Sandia Corporation, a Lockheed Martin Company, for the United States Department of Energy's National Nuclear Security Administration under contract DE-AC04-94AL85000.

ELECTROMAGNETIC BEHAVIOR OF A PARTIALLY COVERED TRENCH IN A CORNER

Erricolo, D., Uslenghi, P. L. E.

Department of Electrical and Computer Engineering, University of Illinois at Chicago

A partially covered trench located at the corner of two metallic walls perpendicular to each other is considered. The cross section of the trench is a quarter ellipse, and it is slotted from the focus to the center of the ellipse. The trench is partially covered by a thin metal strip extending outward from the focal line, as part of the metal wall under which the trench is flush-mounted. The trench is filled with a material that is isorefractive to the medium filling the quarter-space between the walls.

This boundary-value problem is solved exactly in the frequency domain, when the primary source is either a plane wave of arbitrary direction of incidence and polarization, or an electric or magnetic line source parallel to the walls and located either outside or inside the trench. The field components are expanded in infinite series of eigenfunctions that are products of radial and angular Mathieu functions, in the Stratton-Chu normalization. The modal coefficients in the expansion of the secondary fields are analytically determined by imposing the boundary conditions. The technique utilized in obtaining this new canonical solution is akin to that used for a slotted semielliptical channel (P. L. E. Uslenghi, IEEE Trans. Antennas Propagat., to be published) and has led to numerical results in excellent agreement with integral equation approaches. Some preliminary results for E-polarized plane wave incidence were reported previously (P. L. E. Uslenghi, IEEE/APS-URSI Intl. Symp., Orlando, FL, July 1999).

The canonical solutions reported here are the only ones available for a trench at the corner of two walls. This complicated boundary-value problem involves a cavity, a sharp edge and two different penetrable materials; hence, these canonical solutions constitute an important benchmark for the validation of frequency-domain computer codes.

RADIATION AND SCATTERING FOR ELLIPTIC METAL
CYLINDER BETWEEN ISOREFRACTIVE HALF-SPACESErricolo, D., Uslenghi, P. L. E.Department of Electrical and Computer Engineering, University
of Illinois at Chicago

A metal cylinder with elliptical cross section is located at the planar interface between two isorefractive half-spaces, with its cross-sectional major axis either parallel or perpendicular to the interface. The two-dimensional boundary-value problems of scattering of an incident plane wave with arbitrary polarization and direction of incidence, and of radiation from an electric or magnetic line source parallel to the cylinder axis are solved exactly, in the frequency domain.

The total electromagnetic field in the half-space containing the source is the sum of three terms: the incident field; the field reflected at the isorefractive planar interface when the cylinder is absent; the field scattered by the metallic cylinder. Each field component is written as an infinite series of eigenfunctions consisting of products of radial and angular Mathieu functions, in the Stratton-Chu notation. The incident and reflected field components are fully determined, while the expansion coefficients in the series representing the scattered field are found analytically by imposing the boundary and radiation conditions. Thus, new exact solutions to this boundary-value problem are determined. These canonical solutions are important per se, and also for the validation of frequency-domain codes. The technique utilized herein could be extended to the case when the primary source is an electric or magnetic dipole arbitrarily located and oriented; however, the solution would be cumbersome and, therefore, is not reported here.

As a particular case, the metal strip is considered in detail. The strip is either laying on the planar interface between the two isorefractive media, or is perpendicular to the interface and protrudes an equal distance into each medium. Extensive numerical results for surface currents on the elliptic cylinder and for radar cross-sections are presented and discussed.

LOW-FREQUENCY BEHAVIOR OF A SLOTTED SEMIELLIPTICAL CHANNEL

Larsen, T., Erricolo, D., Uslenghi, P. L. E.

Department of Electrical and Computer Engineering, University of Illinois at Chicago

The low-frequency analysis of penetration, radiation and scattering for a slotted semielliptical channel flush-mounted under a metallic ground plane is considered, in the frequency domain. The channel is slotted along the interfocal segment of its cross-section, and is filled with a material isorefractive to the medium occupying the half-space above the ground plane. A canonical solution to this two-dimensional boundary-value problem has been obtained recently (P. L. E. Uslenghi, IEEE Trans. Antennas Propagat., to be published), in terms of series of Mathieu functions in the Stratton-Chu normalization.

If the width of the slot connecting the channel to the half-space above it, i. e. the interfocal distance in the elliptic coordinate system, is d , then the Mathieu functions depend on the parameter $c=kd/2$, where k is the wavenumber. Low-frequency expansions of the angular and radial Mathieu functions for small values of c are obtained and compared to the exact values of the functions. Then, low-frequency expressions for the field components in the boundary-value problem under consideration are obtained and compared to the numerical evaluations of the exact expressions of the fields.

Having thus obtained reliable low-frequency results for the fields inside and outside the channel when the width of the coupling slot is small compared to the wavelength, these results are compared to the low-frequency predictions provided by the general theory developed by Hansen and Yaghjian (IEEE Trans. Antennas Propagat., vol. 40, no. 11, pp. 1389-1402, Nov. 1992). Extensive numerical results are obtained and discussed, with the goal of establishing the accuracy of the Hansen-Yaghjian low-frequency model.

VALIDATION OF INTEGRAL EQUATION METHODS: PEN-
ETRATION THROUGH A SLOT IN A CONDUCTING PLANE
BACKED BY A CHANNEL

Lockard, M. D., Butler, C. M.
Clemson University

Two types of integral equations are derived and solved for the unknowns associated with penetration of a field through a slot in a conducting plane backed by a channel. This is done for the purpose of verifying the validity and accuracy of the solutions of two types of integral equation by demonstrating the closeness of the solutions. In one case the solution of a single integral equation allows one to determine all quantities of interest, while in the other coupled integral equations are solved for two unknowns which enable one to characterize all quantities of interest. Given the fundamentally different nature of the integral equations resulting from the two formulations, one derives confidence in both methods when the data from one corroborates those from the other. In both methods, the slot electric field, or the equivalent magnetic current, is an integral equation unknown. Thus, the slot electric field, determined directly in both methods, can be compared to ascertain accuracy. No other direct comparisons can be made, but from the solutions obtained in both methods one can compute and compare the total field in the interior of the channel and outside the channel in the region above the conducting plane.

Derivations of the two types of integral equations are outlined and solution methods are mentioned. The coupled integral equation method is more general in that the configuration of the channel backing can be of arbitrary shape, but the other is more efficient since only one equation is involved. The boundary condition on the backing is enforced directly by one of the equations in the coupled equation method, while, in the single equation method, this condition is enforced by the inclusion of a backing-geometry-specific Greens function.

The total electric field in the slot, determined from the two methods, is compared for a number of cases of excitation, slot width, channel backing configuration, and material in the channel. In addition, for the same excitation and structural parameters, the field inside and outside the channel is computed by both methods. Comparisons are presented of both the slot electric field, found directly in both methods, and the indirectly-computed field near the channel-backed slot. Data obtained from the two independent methods are shown to agree to a high degree. Solutions are found and comparisons are made for the cases of a hemicylinder-backed slot, a rectangle-backed slot, and a sector-backed slot.

ALTERNATE MODELS FOR THE COUPLING OF WIRES THROUGH NARROW SLOTS IN GROUND PLANES

Keen, J.M., Butler, C.M., Tesche, F.M.

Holcombe Department of Electrical and Computer Engineering,
Clemson University, Clemson, SC 29634-0915 USA

The study of the penetration of electromagnetic fields through holes in conducting bodies has been of interest for many years, and a variety of solution techniques are available for these aperture-theory-based problems. In this paper, we examine two such techniques as they relate to penetration through narrow slots in an infinite ground plane. Specifically, wires reside on opposite sides of a ground plane in which there are two or more slots. While the wire on one side of the ground plane is excited, the resulting excitation of the other wire is considered.

One model is integral equation based. In this model, coupled integral equations are solved by standard techniques. The second model considered is based on transmission line theory. In this transmission line model, the current on one wire is calculated from standard transmission line theory for a wire over a ground plane with no slot or with the slot shorted. The field in the slot is then determined from an integral equation solution where the excitation is provided by allowing the transmission line based current to radiate onto the slot. The resulting field in the slot radiates onto the wire on the other side which is modeled as a transmission line (C. D. Taylor, R. S. Satterwhite, and C. W. Harrison, Jr., *IEEE Trans AP*, 13, 987-989, 1965). Clearly, this step-by-step computation fails to fully account for all coupling between wire(s) and slot.

Data obtained from these two models is compared and contrasted both with each other and with measured data. Though the transmission line model is tempting due to its simplicity and to the simplicity of the associated computations, it has a variety of weaknesses. Most apparent are wire-to-ground-plane separations which do not lend themselves to good transmission line approximation. However, since the transmission line model fails to obey the principles of reciprocity, the transmission line model also lacks accuracy in configurations and frequencies in which the coupling between the slot and the wires is strong. These configurations are considered and identified along with corresponding measures of inaccuracy.

VALIDATION OF TRANSFER FUNCTION MEASUREMENTS FOR ANALYZING COUPLING OF EXTERNAL ILLUMINATION TO CIRCUIT ELEMENTS WITHIN METALLIC ENCLOSURES

E. S. Siah¹, J.L. Volakis^{1,2}, V.V. Liepa¹

¹The University of Michigan, , Dept. of Electrical Engineering and Computer Science, Radiation Lab.

²The Ohio State University, Electro-Science Lab, Dept. of Electrical Engineering

The routine use of wireless devices and services generates concern associated with stray and undesired electromagnetic coupling on neighboring electronic devices. Traditionally, in EMI/EMC measurements for FCC emissions compliance, nearfield and farfield measurements are made in an anechoic chamber. Alternatively, nearfield measurements can be made in a GTEM cell. However, in these approaches, the illuminating fields are not well known at the device under test and a well compensated probe is needed for measuring the incident fields. In addition, setting up such a probe for measuring the incident field over a broad range of frequencies is both non-trivial and expensive. For example, in figure 1a, the electric field shielding is measured at the bottom of a circular cavity illuminated by an incident plane wave. The electric field shielding is defined as the ratio of the total electric field to the incident electric field at a point. Comparison of the measured data and an analysis using the method of moments accelerated by the multilevel fast multipole method shows relatively good agreement, with the measured data 10 dB lower than the analysis method at frequencies above the cutoff frequency of the reference antenna (0.35 GHz). This is primarily due to the use of a non-calibrated probe for measuring the field. In this paper, we propose the use of transfer function measurements as a validation model for numerical simulations. This obviates the need for a large measurement facility such as an anechoic chamber or a GTEM cell. A transfer function measurement is made on a circuit board housed within a cylindrical metallic enclosure. Such enclosures around circuit elements are very common. The geometry of the measurement setup is shown in figure 1b. A source probe is inserted into the cylindrical enclosure through an aperture while a microstrip filter, housed within the metallic enclosure and connected to an external port using a coaxial feedthrough through the opposite aperture, is used as the receiving element. The measured S21 shows a strong pick up of energy at 1.8 GHz where the primary resonance of the cavity and the passband of the filter coincide. The validation of this measurement and other measurements will be presented at the conference.

VERIFICATION OF THE THIN-STRUT FDTD METHOD FOR
COIL COUPLING COMPUTATIONS BY ANALYTICAL AP-
PROXIMATIONS

Stefan Schmidt, Abheek Gupta, Gianluca Lazzi

Department of Electrical and Computer Engineering, North Car-
olina State University, Raleigh, NC 27695-7914, USA

The Finite Difference Time Domain (FDTD) method extended by the thin-strut formalism is used to compute the coupling between coils for biomedical telemetry applications. The thin-strut formalism (R. Holland, L. Simpson, *IEEE Trans. Electromagn. Compat.*, **23**, 88-97, 1981) is a sub-cell model that allows embedding of linear wire elements with a specified wire radius into the FDTD grid. This method was used to compute the ratio of the current in a primary source coil and in a secondary coil. In a quasi-static approximation, the current ratio is related to the mutual and self-inductance of the coils:

$$\left| \frac{I_2}{I_1} \right| = \left| \frac{M_{12}}{L_2} \right| = \left| \frac{L_1}{M_{12}} \right| \quad (1)$$

An analytical DC approximation for the calculation of mutual and self-inductance of wire segments was developed. The analytical method is based on the Partial Inductance concept (A.E. Ruehli, *IBM J. of Res. and Develop.*, **16**, 470-481, 1972). The mutual inductance of two coils is found by partitioning each coil into a number of segments. Then the mutual inductance of each segment of one coil with each segment of the other coil is calculated. These values of partial mutual inductance form the partial inductance matrix of the coil system. The mutual inductance of the coils is simply the arithmetic sum of all the elements of the partial inductance matrix. The self-inductance of a coil is similarly found by calculating the inductance of each of its segments with every other segment of the coil, including itself. The inductance of a segment with itself is called the partial self-inductance and is given by Ruehli for the specific case of a straight conductor of a rectangular cross-section.

The coupling between a primary source coil and a smaller coaxial secondary coil is computed as a function of the coil separation and coil size. Different wire radii were considered. The results obtained from the thin-strut FDTD method are compared to numerical results from the traditional FDTD method, and the Method of Moments, and the analytical approximation.

The analytical approximation is in good agreement with results from the thin-strut FDTD method and experiments. In contrast to the traditional FDTD method, the thin-strut formalism has desired accuracy for a lower mesh resolution; hence, it can be more efficient.

SOLVING LARGE FINITE ANTENNA ARRAYS USING FEMS
- 100 MILLION UNKNOWNNS ON A SINGLE PC

Seung-Cheol Lee, Marinos Vouvakis, Jin-Fa Lee
ElectroScience Lab., Dept. of Electrical Engineering, The Ohio
State University

In this paper, the authors wish to demonstrate to the audience that applied mathematics is not only beautiful but also useful. We present a few recent breakthroughs in vector finite element method for solving Maxwell equations. Particularly, the focus is on solving large finite antenna arrays. We shall show that it is possible to solve a 100 by 100 Vivaldi array, which corresponds to roughly 100 million finite element unknowns, on a single PC with 2 GB RAM. The simulation is made possible by the combination of a few elegant applied mathematical techniques, they are: an optimal domain decomposition (ODD) method, a Mortar element technique for non-conforming finite elements, and a robust p-type Multiplicative Schwarz (pMUS) preconditioner for solving the matrix equations. First, we developed a symmetric hybrid finite element/integral equation approach. The resulting hybrid code has been employed to simulate several complex real-life array antennas and the computed results have been also validated with excellent agreement against measurements. This hybrid code can be used to simulate array problems up to couple of million unknowns. It can be useful already to solve many real-life antenna arrays. However, for many large finite antenna arrays, the total number of unknowns can easily exceed tens of millions or even hundreds of millions unknowns. Consequently, we have successfully implemented an optimal domain decomposition (ODD) method with Mortar element technique for solving large finite arrays. This time the computed results using the finite array code are compared against the hybrid FE/IE code whenever possible. In the presentation, we will not have enough time to go into details of each ingredient. We shall instead discuss what each individual technique can accomplish and how they can all fit together to provide a much-needed solution for a very important engineering problem.

Session C1, 9:00-Monday

**WIRELESS COMMUNICATIONS
CHANNEL MODELING AND
PERFORMANCE**

Chairpersons: Dev Palmer and Brian Sadler

VALIDATION OF ADAPTIVE TRANSMISSION FOR REALISTIC SINGLE- AND MULTI-CARRIER MOBILE RADIO CHANNELS

Tung-Sheng Yang¹, Alexandra Duel-Hallen¹, Hans Hallen²

¹North Carolina State University , Box 7911, Raleigh, NC 27695

²North Carolina State University , Box 8202, Raleigh, NC 27695

Reliable adaptive transmission for frequency selective mobile radio systems is addressed. In particular, we investigate adaptive channel loading for wireless Orthogonal Frequency Division Multiplexing (OFDM) systems and adaptive modulation aided by observations of another carrier (e.g. Frequency Division Duplex (FDD) channels). Adaptive transmission techniques, where the modulation size, coding rate, or other signal transmission parameters are dynamically adapted to the changing channel conditions, have recently emerged as powerful tools for increasing the spectral efficiency for wireless system. However, reliable adaptive transmission requires long-range prediction (LRP) of future channel state information (CSI) due to the variation of the wireless channel, which results in different channel conditions between the time of data transmission and the time of the channel estimation. We derive the minimum mean-square-error LRP method that utilizes the time and frequency domain correlation function of the Rayleigh fading channel. Since the channel statistics are usually unknown, reduced complexity robust prediction methods that can converge rapidly to the theoretical MMSE and do not require the knowledge of correlation functions are developed for OFDM channels and systems aided by observations of another carrier. Statistical model of the prediction error that depends on the frequency and time correlation is developed and is used in the design of reliable adaptive modulation methods. A standard sum-of-sinusoids Rayleigh fading channel model (Jakes) and a novel physical model based on the method of images augmented with diffraction are employed to test the prediction algorithm. This physical model can generate non-stationary datasets to test both the LRP and its application in adaptive transmission schemes. It is demonstrated that this physical model generates realistic datasets that closely resemble measured data, and the results of the LRP for the physical model and measured data are similar, and differ significantly from those produced for the Jakes model. We use this model to produce different scenarios to classify typical and challenging cases to test the performance of the proposed prediction algorithm. These cases are more difficult to identify with the measured data. Moreover, we examine the dependency of the correlation between two different carrier frequencies on the variation of the root mean square (rms) delay spread and investigate the limits on the adaptation rate in adaptive transmission systems aided by observations of another carrier. Thus, the physical model allows to test robustness and to determine practical constraints of the proposed adaptive transmission methods.

STATISTICAL CHANNEL MODELS FOR UWB COMMUNICATIONS

R. Michael Buehrer, Brian Donlan, Vivek Bharadwaj
Virginia Tech

Ultra-wideband (UWB) signals have been used for several years in radar applications. However, recently there has been interest within the communications community to use UWB signals for communications. This has been facilitated by the FCC which allows unlicensed UWB transmission within the 3.1-10.6GHz band. UWB is defined by the FCC as any signal which has a fractional bandwidth greater than 0.2 or an absolute bandwidth greater than 500MHz. The emergence of UWB as a potential communications signal has led to a need for channel models applicable to UWB. In this paper we present statistical channel models suitable for use in designing communication systems which utilize UWB signals.

Statistical models will be presented using both time-domain and frequency domain approaches. Both types of models are of interest since there is commercial interest in frequency domain UWB (i.e., modulation occurs in the frequency domain.) Additionally, frequency domain models can be simpler to implement with fewer parameters than time-domain models.

Statistical channel models are useful for (a) system planning and (b) receiver design. Typical system planning includes link budget determination in order to define coverage areas for a specific data rate and performance target. Such planning requires an estimate of the received signal power at a given distance. This is typically provided by a path loss model. We will discuss the application of path loss models, which were derived for narrowband communications, to UWB and propose appropriate parameters.

A second type of channel model that is required by communications engineers is a multipath model. Such models are necessary for receiver design (e.g., equalizer or Rake receiver design). The multipath phenomenon will impact the received waveshape as well as received signal energy. We will examine commonly used multipath models and discuss their applicability to UWB. We will demonstrate their accuracy (with respect to measurements) both through mean parameters such as delay spread, as well as the resulting BER for various signaling methods.

MODELING AND SIMULATION OF MOBILE-TO-MOBILE RADIO CHANNELS

Patel, C. S.¹, Stuber, G. L.¹, Pratt, T. G.²¹Dept. of Elec. & Comp. Eng., Georgia Institute of Technology, Atlanta, GA 30032²Georgia Tech Research Institute, Atlanta, GA 30332

Mobile-to-mobile communications find increasing applications in next generation communications systems such as cellular networks with user cooperation diversity, ad-hoc networks and future combat systems (FCS). The successful design and deployment of these systems require thorough understanding of the underlying wireless propagation channels. Therefore, we investigate the issues related to modeling and simulation of mobile-to-mobile wireless channels in our work, which are otherwise not addressed in the current literature .

Akki and Haber presented a theoretical model for narrowband mobile-to-mobile channels in the 80's (A. S. Akki and F. Haber, "A statistical model for mobile-to-mobile land communication channel," *IEEE Trans. on Veh. Technol.*, VT 35 , Feb. 1986), which provides channel parameters such as the Doppler spectrum, and level crossing rates, and average fade durations. We extend the analysis for this model to gain further insight into its characteristics. We specifically study the coherence time parameter for the mobile-to-mobile channels by relating it to the maximum Doppler frequency and the ratio of the speeds of the transmitter (Tx) and the receiver (Rx) through a closed form expression. This quantifies how fast mobile-to-mobile channels vary with time. Further, we modify the model by relaxing the assumption of isotropic scattering around both the Tx and the Rx to model other propagation scenarios. We employ the Geometrically Based Single Bounce Elliptical Model (GBSBEM), which is often used to model micro-cellular channels, to derive the Doppler spectrum for mobile-to-mobile channels. Since the analysis for GBSBEM tends to be mathematically intractable, we derive some typical Doppler spectra via simulations and compare them with the one predicted by Akki and Haber's model.

We further contribute by developing new methods to simulated narrowband mobile-to-mobile channels. We present a "double ring" to model the scattering environment for mobile-to-mobile channels and develop a sum-of-sinusoids based method to simulate these channels based on the "double ring" model. This work is currently being extended to develop wideband mobile-to-mobile channel models using real world results obtained by an on-going measurement campaign.

LINKING ELECTROMAGNETIC DESIGN TO SYSTEM PERFORMANCE: MEASURING BIT ERROR RATE AS A FUNCTION OF ANTENNA PROPERTIES AND MORE

Bernhard, J. T.

University of Illinois at Urbana-Champaign

Traditionally, antenna arrays have been tested using continuous wave, analog signals. This kind of evaluation helps to characterize the general behavior of arrays in terms of beamwidth, gain, scan angle, etc. When these arrays are used as components of high-speed communications links, however, BER is the one of the final metrics by which the system is judged. The complex relationship between BER and antenna array performance will become more and more critical as both data rates and array frequency bandwidth increase. Moving BER testing from final system field evaluation into a research environment promises to provide a wealth of new information about antenna design, signal processing techniques, and communication protocols.

This work describes the establishment of a state-of-the-art phased array Bit Error Rate (BER) testing system in the Electromagnetics Laboratory at the University of Illinois at Urbana-Champaign. The system can be configured for either traditional coherent continuous wave antenna testing or for bit error rate testing. System block diagrams and implementation details for both kinds of tests will be provided in the presentation. The BER testing system can implement a variety of standard or user-defined modulations, noise impairments, and propagation models with the help of specialized software from Agilent. Our first research project in this area will evaluate the BER performance of new wideband aperiodic (random) arrays and compare the results with those obtained with traditional narrowband periodic arrays. In addition to this antenna-based research, we plan for the measurement system to serve as a testbed for new modulation, coding, and interleaving schemes for wideband, multi-band, and narrowband arrays. This unique facility will enable us to apply new findings to optimize system behavior and to create entirely new avenues of research into the relationships between array characteristics, signal processing, and achievable performance.

LONG DISTANCE WAVE PROPAGATION THROUGH FORESTED ENVIRONMENTS

Wang, F., Sarabandi, K.

Radiation Laboratory, Department of Electrical Engineering and Computer Science, The University of Michigan

In recent years physics-based models for wave propagation through forested environments have attained significant prominence. However, the issue of wave propagation through a very long distance of forest is yet to be addressed. Due to lack of proper definition for phase function application, radiative transfer approach to an environment like forest which contains large scatterers (tree trunk and branches) is not possible. A promising alternative approach is based on wave theory to calculate the statistical relations of power or field between the input and output side of a truncated block of forest which has all the statistical properties of the forest. The resulting generalized ABCD matrix can be used to cascade the wave propagation block by block toward the observation point. Such technique reduces the computation intensity significantly by truncating the forest, and accounts for the multiple scattering effects by cascading the truncated blocks. Near field interactions between scatterers can also be included. In this paper, an wave propagation model based on this technique is presented.

A forest block of dimensions $h \times 10 \times 10m^3$ (h is the average height of the forest) is considered. A generalized ABCD matrix among many nodes on the input and output surfaces (both are $h \times 10m^2$) is calculated numerically. Basically the two surfaces are discretized into small cells and each is given two ports, one for horizontal and the other for vertical polarizations. For the input surface, each cell has equivalent polarized dipole source due to the tangential field distribution at this cell. The electromagnetic waves radiated by these dipoles are scattered by the forest block, and added up coherently at the center of each cell on the output surface. The tangential components of such field lead to equivalent dipole sources for the next block according to Huygens' principle. The randomness of the forest is taken into account by Monte-Carlo simulations of different forest blocks, which generates a set of ABCD matrices. Multiplying these matrices, the field or power distributions at the observation point can be obtained. The selection of cell size, the radiation pattern of the equivalent dipole sources, and the broadening effect of illumination are also carefully considered in this paper. By using the above technique to simulate the wave propagation through forest for a very long distance, e.g. 1 km, the well-known dual-slope phenomenon of the propagating wave intensity is shown. Based on the same technique, the wave propagation through discontinued forested environments can be simulated as well.

A DEMONSTRATION OF UTILIZING HIGH FIDELITY PROPAGATION MODELS FOR EMITTER LOCALIZATION IN URBAN ENVIRONMENTS

Luebbes, R.J.^{1,2}, Smith, A.¹, Fast, S.A.¹, Schuster, J.W.¹

¹Remcom Inc

²The Pennsylvania State University

High-fidelity propagation computer models make it possible to predict time-of-arrival (TOA) and angle-of-arrival (AOA) for each signal path arriving at a receiving antenna. These multipath features (TOA and AOA) can be used to form a database of multipath fingerprints for a large number of locations within an area. The location of an emitter can be estimated by comparing the received fingerprint to those in the database. This method of urban geolocation has been proven successful through a series of simulations for several small regions.

The urban propagation predictions are computed by shooting rays from a group of transmitters and propagating them through the urban environment to a receiver. For a given transmitter-receiver pair, the multipath information (the time of arrival (TOA), angle of arrival (AOA), and path loss) is computed for each ray that is traced from the transmitter to the receiver. For this application, multipath information is used to form a fingerprint database to characterize an environment, so that the source of signals received at a later time may be localized.

For an example of how the technique might be applied, consider a cellular base station (BSS) in Rosslyn, Virginia, USA. A fingerprint database for Rosslyn is formed by covering the area in a grid of closely spaced transmitters (say 5 meter spacing horizontally and vertically) and applying the ray-based propagation model to predict the channel characteristics from each transmitter to a single receiver (the BSS). If at a later time the BSS receives a 911 call, the multipath features of the channel corresponding to the location of the 911 call can be extracted from the signal, compared to the fingerprint database, and a location estimated for the emitter.

In a recent simulation of our implementation of the multipath fingerprint method, transmitters were located in Rosslyn over an area of 432 x 416 meters. Approximately 7000 transmitter locations and one receiver location were used to form the database. Then, test emitters were randomly scattered across the study area, with minimum spacing limited to roughly 40 meters. In a blind simulation of the geolocation algorithm, 19 out of 20 emitters were correctly located to within 50 meters or less. This demonstration of the accuracy available from the propagation model indicates that it could be used to improve channel capacity.

Session C2, 13:40-Monday

**RADAR REMOTE SENSING
SYSTEMS AND SIGNAL
PROCESSING**

Chairperson: V. Chandrasekar

NETRAD: NETWORK WEATHER RADAR CONCEPT

Stephen Sekelsky¹, Stephen Frasier¹, David McLaughlin¹
, Jim Kurose¹, V. Chandrasekar², Kelvin Droegemeier³
, Sandra Cruz-Pol⁴, Jose Colom⁴

¹University of Massachusetts at Amherst

²Colodaro State University

³University of Oklahoma

⁴University of Puerto Rico Mayaguez

A newly established Engineering Research Center headquartered at the University of Massachusetts at Amherst is embarking on a 10 year effort to develop new generations of sensor systems for Collaborative Adaptive Sensing of the Atmosphere (CASA). The concepts embodied in CASA represent a new paradigm in sensing of the atmosphere. For example, the current generation weather sensing network, NEXRAD, consists of approximately 100 S-band radars that blanket the United States. The NEXRAD system has performed wonderfully. However, it has certain weaknesses such as susceptibility to single point failures and the inability to detect tornadoes and other destructive weather events close to the surface due to the Earths curvature. The vision for new generations of sensing systems is a dense network of sensors that will improve coverage of the lower atmosphere and maintain a more uniform resolution and sensitivity to precipitation, humidity and other atmospheric variables versus the current system of sensors. Most importantly the new systems will collaborate to make new measurements possible.

The first generation CASA sensing system is composed of a dense network of low-cost scanning weather radars aimed at solving the Earth curvature problem facilitating significantly improved radar coverage of the lower troposphere. This initial Network Radar (NetRad) test bed will be composed of up to 9 X-band (9.5 GHz) radar nodes. NetRad will be deployed in Tornado Alley, west of Oklahoma City where direct comparisons of weather event detection can be made with the Norman, OK NEXRAD. Here we present an overview of the radar node design and network parameters. We also highlight the technical approach to developing low-cost multi-beam electronic scanning radars.

MONOPULSE RADAR SYSTEM ARCHITECTURE BASED ON COHERENT CORRELATION RECEIVER

Ram M. Narayanan¹, Yan Zhang²

¹Department of Electrical Engineering, Pennsylvania State University, University Park, PA 16802-2705, U.S.A.

²Department of Electrical Engineering, University of Nebraska, Lincoln, NE 68588-0511, U.S.A.

The correlation receiver architecture has been widely used in traditional radar and communication systems since the 1960s. In recent years, with the advances digital technology, the design gravity of receivers has been slowly shifting to a more complete digital implementation. In this paper, we explain the role of the correlation receiver in the system design of our latest radar technology research. The advantages of the time-domain correlation receiver for ultra-wideband (UWB) applications are addressed. A phase-coherent system architecture that is independent of the radar signal waveform is suggested. The main features of this configuration are analog phase coherency, true-time variable delay line implementation, monopulse beam-forming, and multi-channel I/Q digital processing.

The methodology to employ such architecture to implement functions such as radar surveillance, tracking and imaging in real-time is analyzed. We can show that the proposed architecture allows switching or paralleling of multiple radar functions. Furthermore, special emphasis is placed on the tracking function. Range/Doppler tracking is implemented by fast scanning within the moving range gate, while angle tracking is implemented through antenna scanning and monopulse processing. As an example, the correlation receiver response to constant range-speed moving targets is studied when pulsed or random noise signals are used as transmit waveforms. System simulation results and the corresponding observations are discussed.

As a more specific example, a new experimental tracking radar system based on this architecture is introduced. This radar was built primarily for detection and tracking slow-moving targets and estimation of angle-of-arrival using a wide-band random noise signal. For the phase-comparison monopulse, it is shown that the system has equivalent monopulse characteristic curve as a continuous wave (CW) single frequency monopulse radar system in the sense of statistical average. We show that the rich frequency content of the stochastic signal brings about important advantages, and the correlation receiver architecture enables continuous ambiguity-free range tracking. The basic experiment results of the system are presented and discussed.

DEVELOPMENT OF A NETWORKED PC-BASED HIGH-BANDWIDTH DIGITAL RECEIVER FOR THE CSU-CHILL RADAR

Cho, Y.G¹, Brunkow, D.A², Chandrasekar, V¹

¹Department of Electrical and Computer Engineering, Colorado State University, Fort Collins, Colorado

²Department of Atmospheric Science, Colorado State University, Fort Collins, Colorado

Essential idea of the high-bandwidth Virtual CHILL (VCHILL) is that the digitized radar signals (DRS) at the CSU-CHILL radar site are transferred to remote sites in real-time over a high-bandwidth data network. Once received over the network, parameters are estimated at remote sites and distributed to display nodes over other remote data networks. This all-digital networked approach is very useful in a multi-user environment wherein each user independently processes the same digitized output signals for various applications. Up until now, the received signals of the CHILL radar have been routinely processed by the existing digital signal processor (DRX) according to standard operating parameters. Development of this new digital receiver for CHILL combined with an innovative application protocol for the distribution of the DRS makes possible the notion of a high-bandwidth VCHILL.

The new receiver, which consists of a PC running under Linux, an Analog to Digital Conversion/Digital Downconversion signal processor, a digital I/O, and an interface circuit for Azimuth/Elevation angle conversion, is designed to operate in parallel with the existing DRX processor. The signal processor and the digital I/O card are interfaced with high-speed PCI bus. The dual-channel 10-MHz IF signals split are sampled and processed by the signal processor synchronized with DRX processor. The AZ/EL signals are read by the digital I/O and other important radar operating parameters are sent via a serial port from the antenna controller to the PC. The parallel receiver system operates as a part of the DRS server concept in the networked environment such that the DRSs are transmitted to remote sites along with radar operating conditions in a specified data format. With an overall data rate of a few hundred Mbps, the integration of all these data into a specified format in real-time requires extremely careful timing and high-speed data manipulation.

Currently, the maximum sample rate of the system is 5 MHz. The digital receiver system has been tested and calibrated with respect to the existing DRX processor over the expected receiver bandwidth and dynamic range. The entire end-to-end system architecture, including the DRS server and client, operates over a Gigabit Ethernet link in real-time. Comparison of the data show close coincidence with that of the DRX system.

PHASE COMPARISON MONOPULSE AS AN ANGLE ESTIMATOR: A GENERAL THEORY

Yan Zhang¹, Ram M. Narayanan²¹Department of Electrical Engineering, University of Nebraska, Lincoln, NE 68588-0511, U.S.A.²Department of Electrical Engineering, Pennsylvania State University, University Park, PA 16802-2705, U.S.A.

The statistical characteristics of the monopulse ratio have been an interesting topic for tracking radar researchers for a long time. The limitations of previous studies are: (i) most of the research dealt with amplitude-comparison monopulse; however, with the development of phased-array radar systems, phase comparison monopulse is gaining popularity; (ii) although the assumption that the signals in the sum and difference channels are Gaussian distributed can lead to useful conclusions, it is only valid in very limited situations, since matched filtering or correlation processing, for example, may change the signal probability distributions in receive channels; and (iii) while the monopulse angle of arrival (AOA) estimator is just one component of the angle-tracking loop, the analysis of closed-loop tracking error should also consider the factors due to servo system errors.

Motivated by above considerations, this paper develops a more general theoretical analysis of monopulse AOA estimation, while specifically addressing phase-comparison monopulse as an example. The application background is a single plane phase-comparison monopulse radar that transmits a wide-band random noise signal waveform. Some factors that affect the shape of monopulse characteristic curves are discussed. It is found out that irrespective of the actual distribution of the random monopulse vectors, for very high signal to noise ratio (SNR), the monopulse ratio is an unbiased estimator of the monopulse characteristic curve, while the variance is determined by noise power in difference channel. For more general cases, the monopulse ratio is a biased estimator and the variance is in proportional to the squared amplitude of the characteristic curve.

The monopulse angle estimator, which is denoted by its bias and variance, is then introduced into a type-I servo control loop. The total mean-square-error (MSE) of the angle-tracking loop is derived. A typical pass-course angle-tracking scenario is simulated and analyzed. The impact of characteristic curve slope, motor speed, and the open-loop gain on the total MSE are studied and presented.

RANGE-VELOCITY MITIGATION USING PHASE CODING WITH STAGGERED PRT FOR DUAL-POLARIMETRIC RADAR

Hubbert J.C.¹, Chandrasekar V.², Bharadwaj N.²

¹NCAR/ATD

²Colorado State University

The fundamental range and velocity measurement limitation of pulsed radar systems is expressed by the following equation

$$r_a v_a = c\lambda/8$$

where r_a , v_a are the unambiguous range and velocity, respectively, for wavelength λ and where c is the speed of light. Since the product $r_a v_a$ is a constant for a particular wavelength, increasing either one (r_a, v_a) necessarily decreases the other. For $\lambda = 10$ cm (S-band) and a typical pulse repetition time (PRT) of 1 ms, $r_a = 150$ km and $v_a = 25$ m/s. Weather phenomena routinely exceed both of these limits. Phase coding of the transmit pulses for single polarization radars has been shown to be an effective method for the separation of range overlaid echoes thus extending r_a without compromising v_a . Another well known technique for range-velocity mitigation is staggered PRT. Both techniques have their limitations and neither has completely solved the range-velocity problem.

Both phase coding of the transmit pulses and staggered PRT (pulse repetition time) are two techniques that have been used to mitigate the range-velocity ambiguity problem for single polarization radars. In this paper we combine these two techniques with dual polarization to greatly increase both the unambiguous range and velocity. The advent of new high speed PC based radar receivers, with the ability of real time spectral processing, makes such schemes possible for practical radars. Simulations are given which show the viability and limitations of the technique. It is shown that it is possible for radars with two transmitters to retrieve near unaliased velocities for weather targets while simultaneously having large unambiguous range.

NONLINEAR LEAST SQUARES DETERMINATION OF OPTIMA POLARIZATIONS IN TRANSMISSION

Santalla del Rio V.¹, Antar Y.M.M.²

¹Universidad de Vigo., Vigo. Spain

²Royal Military College. Kingston, Ontario. Canada

The importance of considering polarimetric covariance matrix measurements in weather radar applications has been widely discussed and already demonstrated. In order to determine the polarimetric covariance matrix elements, real systems alternately transmit two orthogonal polarizations and receive with both. Though this scheme allows determination of the scattering matrix elements, it introduces some decorrelation between the two columns of the scattering matrix since they are measured at different time instants. Because covariance matrix elements are calculated as cross-products of scattering matrix elements, the decorrelation between scattering matrix elements can seriously affect covariance matrix elements estimation. As it has been previously discussed, the described measurement scheme provides with accurate estimates of all elements of the covariance matrix in case of low temporal decorrelation, normalized spectrum width less than 0.25 approximately. For high temporal decorrelation or normalized spectrum width greater than 0.25, transmission of two orthogonal polarizations is not longer enough to obtain the complete polarimetric covariance matrix. Actually, the copolar cross-correlation term is clearly underestimated. In this case, measurement of the coherency matrix for three different polarizations alternately transmitted will provide with enough data to determine the complete polarimetric covariance matrix. In fact, with this method, twelve measured terms will be available to estimate the nine terms that completely define the polarimetric covariance matrix. In this paper the linear relationship that exists between the measured terms and the polarimetric covariance matrix terms and the linear least squares estimation of the polarimetric covariance matrix are first investigated. Then, the dependence on the polarizations used in transmission of the matrix that relates the coherency matrix measurements and the polarimetric covariance matrix and, therefore, the dependence of the minimum least squares error attainable on the transmitted polarizations are discussed. As a consequence, using of a nonlinear least squares method to determine the optima polarizations in transmission in order to minimize the least squares error is studied. Finally, statistics of the polarimetric covariance matrix estimates obtained with this method will be analyzed. Also, implications of temporal decorrelation, noise and measurement error on the statistics of the covariance matrix estimates will be discussed.

ADAPTIVE CLUTTER MITIGATION FOR OTH RADAR
WITH FAULTY RECEIVE ARRAY ELEMENTS

Ramakrishnan, D, Krolik, J.L.³
Duke University

HF over-the-horizon radar detects targets by discriminating their returns in the Doppler spectra. Separation of targets depends not only on the velocity of targets but also on the spreading of clutter return in azimuth and Doppler space. Surface clutter return is spread in Doppler space due to ionospheric motion and rough sea state environments. Azimuthal clutter spread is caused by high Transmitter sidelobes and presence of faulty sensors in the receiver array. Doppler spread of surface clutter and high azimuthal sidelobes of directional clutter produce dramatic loss in sub-clutter visibility thereby hindering the detection of weak targets. Previous approaches to clutter mitigation include spread Doppler clutter (SDC) suppression, AR based spectral enhancement techniques and adaptive elevation and azimuth nulling. SDC mitigation strategies are hampered by limited understanding of ionospheric Doppler spread mechanisms and second order sea clutter. The adaptive nulling methods are limited by the ability to estimate beamformer weights using neighboring range/Doppler bins due to inhomogeneity of clutter return. In this paper, we propose an adaptive spatial clutter mitigation method to suppress high azimuthal sidelobes of directional clutter and interference caused by faulty sensors in the receive array.

Faulty sensors in the receiver can degrade the beam pattern significantly depending on their locations in the array. Interpolation of missing sensors promises an effective solution to suppress high spatial sidelobes of the receive beamformer. The under-determined interpolation problem is solved by minimizing the noise power in the interpolated data subject to a constraint that preserves the contribution of the good sensor data. Noise power in the interpolated data is computed by projecting the data onto noise subspace eigenvectors of the spatial covariance matrix. The covariance matrix is computed separately at each range-Doppler bin without assuming homogeneity of clutter return across range-Doppler cells. Minimization of noise power produces sharper clutter features and lower spatial sidelobes while constraint on the good sensor data prevents any target cancellation. Interpolation of real OTH data collected on 12th Dec 2001 shows substantial suppression of directional clutter sidelobes and up to 10 dB improvement in sub-clutter visibility. In practice, interpolation of missing sensors followed by conventional beamforming can be implemented as a set of matrix operations on Doppler-processed pre-beamformed IQ data.

A COMPARISON OF DCT AND WAVELET BASED COMPRESSION ALGORITHMS IN SATELLITE IMAGES

Hacihaliloglu, Ilker¹, Kartal, Mesut²

¹Informatics Institute, Advanced Technologies in Engineering , Communication and Remote Sensing Graduate Program

²Istanbul Technical University, Faculty of Electrical and Electronic Engineering , Department of Electronics and Communication Engineering

Synthetic aperture radar (SAR) and SPOT images are becoming increasingly important and abundant in a variety of remote sensing and tactical applications. Thus, there is a strong interest in developing data encoding and decoding algorithms that can obtain higher compression ratios while keeping image quality to an acceptable level. This study aims to compare most of the well-known compression techniques namely discrete cosine transform and discrete wavelet transform. It investigates RADARSAT and SPOT images of different regions of different characteristics and compares its compression ratios. The performance of the compression algorithms is tested using a RADARSAT-1 fine and standard beam mode images of different regions in Istanbul. The regions, which have been investigated, were sea areas, forest areas, built environment - residential and industrial areas which define different patterns of urban land use. Because we were interested in the particular features of the data, before the compression a classification algorithm is proposed. The different regions were classified in three groups according to their pixel classification and different compression algorithms are used in the classified regions to obtain the best compression results in the total image. The studies showed that homogeneous areas like forest and sea gave better compression results compared to heterogeneous areas like industrial and environmental. For the performance criteria Mean-square-error (MSE), peak-to-peak-signal to noise ratio (PSNR) and total compression ratio (TCR) results are investigated. Different MSE results were achieved between the standard and fine beam mode images. Also the performance criterions changed due to the pixel classification of the heterogeneous and homogenous areas. A qualitative evaluation is also made with the aid of SPOT images of the same areas. An extensive study is made between the SPOT and RADARSAT images. The second purpose of this study is to compare the two compression algorithms. The discrete wavelet based algorithm gave much better results compared to the discrete cosine transform based algorithm. For the quantization process JPEG quantization matrix and uniform quantization were proposed. During the compression process the quantized coefficients were coded with run length coding. The results changed according to the quantization process. The obtained compression results were compromising

MULTISCALE SAR IMAGE SEGMENTATION USING PAIRWISE MARKOV RANDOM FIELDS

Papila, I¹, Ersoy, O. K.²

¹Istanbul Technical University, Fac. of Electrical and Electronic Eng., Elec. and Com. Dept., Maslak 34469 Istanbul Turkey

²Purdue University, School of Electrical and Computer Engineering, 465 Northwestern Ave., West Lafayette, Indiana 47907-2035

In this study supervised texture segmentation of multiscale image is introduced in Pairwise Markov Random field tree model using wavelet-domain. The essence of this tree-structured probabilistic graph is based on capturing the statistical properties of the wavelet transforms and also the intrinsic characters of textural regions of any multispectral image.

In Pairwise Markov Random Field (PMRF) model, wavelet (HAAR) coefficients are modeled with gaussian distribution using a large variance for large coefficients (edges) and small variance for small coefficients (smooth regions.). The model requires a probability mass function of each coefficient whether it is large or small and parent child state transition probability matrix which are calculated by the iterative expectation maximization (EM) algorithm. For each texture we train a PMRF model for each subband individually which covers the Up, Down, E and M step. Up step calculates the probabilities from finest scale to coarse scale, Down step calculates the probabilities from finest scale to coarse scale for all state variables. E step defines the likelihood surface, where we compute the likelihood probabilities) and M step updates the parameters. We perform texture classification according to criteria such as maximum a posterior (MAP) and maximum posterior marginal (MPM) at a range of different scales. We then fuse these multiscale classifications using a Bayesian probabilistic graph to obtain reliable segmentation directly from wavelet-compressed images.

The model performance first tested on the aerial photo and then applied to the RADARSAT data. The main difference in the algorithm for the SAR images lies in the training process. Because of the speckle noise we first determine the resolution levels which are acceptable as input. The results are found to be encouraging.

References: [1] Choi H, Baraniuk RG Multiscale image segmentation using wavelet-domain hidden Markov models IEEE TRAN. ON IMAGE PROC. 10 1309-1321 SEP 2001. [2] W. Pieczynski and A. N. Tebbache, Pairwise Markov Random Fields and segmentation of textured images, MACHINE GRAPHICS VISION vol. 9, pp. 705-718 2000 [3] R. Fjortoft, Y. Delignon, W. Pieczynski, M. Sigelli and F. Tupin Unsupervised Classification of Radar Images using hidden Markov Chains and Hidden Markov Random Fields IEEE TRAN. ON GEO. AND REMOTE SENSING vol. 41, MAR 2003.

Session D1, 13:40-Tuesday

**RF MEMS AND THEIR
APPLICATIONS**

Chairpersons: John Papapolymerou and
George Ponchak

D1

RF MEMS SWITCHES INTEGRATED ONTO POLYIMIDE
THIN FILMS FOR DEPLOYABLE ANTENNA ARRAYSPonchak, G. E., Varaljay, N. C.

NASA Glenn Research Center, Cleveland, OH 44135

The deployment of antennas in space, especially large aperture antennas, increases the satellite size and mass, which increases the launch cost. Antenna deployment has also been the cause of satellite mission failures. These problems become compounded if phased array antennas are used due to the thousands of MMIC phase shifters and the bias lines that must be integrated with the radiating elements. To solve the problem of large size and mass, antennas may be integrated onto thin film materials that may be rolled up during launch and unrolled once the satellite has reached its proper location. However, reliably integrating thousands of MMICs in a hybrid manner to a thin film polymer has not been demonstrated. Monolithically integrating phase shifters onto the thin film material may solve this problem. It may not be possible to build transistor or diode based circuits on thin film materials, but the fabrication of RF MEMS switches on a variety of materials such as GaAs, Si, quartz, and RT/Duroid has been demonstrated. In this presentation, we will demonstrate the fabrication of RF MEMS switches on a thin polyimide membrane supported by a Si wafer for ultimate integration onto a deployable antenna.

The RF MEMS switches are fabricated on top of 20 micron of PI-2611 polyimide that is spun onto a Si wafer. A Finite Ground Coplanar (FGC) waveguide is first defined on the polyimide surface, and then the MEMS cantilever is fabricated through a gold plating process. The sacrificial photoresist is removed in acetone and a critical dry release system. Note that all of these steps are standard for polyimide deposition and MEMS fabrication. Electrical testing revealed that there was some sacrificial material remaining under the cantilevers; therefore, an O₂ barrel etch was performed. This removed the material, but also etched approximately 1 micron of the polyimide.

Although the FGC line and the MEMS switch were not optimized for fabrication on a polyimide layer spun onto a Si wafer, the switch characteristics are promising. At the resonant frequency of the LC shunt switch of 36.6 GHz, the insertion loss is 0.52 dB, the return loss is 8.7 dB, and the isolation is 20 dB. Through measurements, it is determined that 0.35 dB of the insertion loss is attributed to the FGC line and not the switch. Thus, a 0.17 dB insertion loss switch is possible at Ka-Band.

TIME-DOMAIN TECHNIQUES FOR THE ANALYSIS AND DESIGN OF RF MEMS STRUCTURES

Nathan Bushyager, Manos Tentzeris

Georgia Institute of Technology, 777 Atlantic Dr., Atlanta, GA 30332

RF-MEMS device analysis and design is a difficult and challenging task. Current research efforts are focusing on both the design of RF-MEMS themselves as well as on circuits consisting of several RF-MEMS elements. As the devices themselves are under study, no firm design rules exist for their integration into circuits. Several different techniques have been employed to design these devices, with varying degrees of success. This paper suggests time-domain simulation approaches that model the entire MEMS circuit in one simulation. One popular design technique is to simulate the MEMS devices with a full-wave commercial electromagnetic simulator. These simulators can characterize MEMS structures very well, but cannot be scaled to model the entire circuit. The results of the MEMS simulation can be used in a microwave circuit simulator to determine the interaction of the microwave circuit with the MEMS device. This technique often fails to consider the parasitics and coupling effects caused by the close proximity of the elements, which may lead to simulation results that do not match measurement results. This can increase the cost and time required for designing a MEMS circuit. The finite-difference time-domain (FDTD) electromagnetic modeling technique has been shown to give very accurate simulation results for a variety of structures. However, the smallest feature of the device being modeled limits the size of structures that can be simulated in FDTD. RF-MEMS devices are built on membranes that can have very fine features. When these elements are combined into circuits containing large connecting structures, the resulting grid can grow beyond the capability of most computers. Several techniques can be applied to an FDTD implementation to reduce the grid size while maintaining required accuracy. FDTD is a robust technique that can be modified in many ways to increase computational efficiency. Three of these are parallelization, the addition of a variable grid, and the use of DSP-based spectral estimators. The simulator is still limited, however, by the need to model the small cell size of MEMS devices. The Multiresolution Time-Domain (MRTD) technique uses a wavelet discretization of Maxwells equations to provide a time- and space adaptive electromagnetic modeling scheme. The advantage of this approach is that it can use much larger cells than similar full-wave time-domain methods, such as FDTD. The number of basis functions used in each cell can be varied as a function of space and time. In this way, grids of complex structures can use high resolution cells in areas of large field variation and lower resolution cells elsewhere. As a benchmark, the above mentioned techniques are used in this paper to model a double stub 2-bit x 2-bit RF-MEMS tuner.

RF MEMS PHASE SHIFTER CIRCUITS

Jeffrey DeNatale, Robert Mihailovich
Rockwell Scientific

MEMS RF switches represent a valuable device technology with the potential for significant impacts on a broad range of communications and radar applications. These devices offer very attractive device-level characteristics, including low insertion loss, high isolation, broad bandwidth, and extremely high signal linearity. One particular application of MEMS switch technology which exploits these benefits is in phase shifter circuits for phased array antennas. Here, the MEMS switch can be used to reconfigure the circuit characteristics to controllably alter the time delay or phase delay of the transmitted signal and enable electronic scanning. A number of different MEMS-based multi-bit (2 to 6) phase shifter circuits have been developed which illustrate the performance and versatility of this technology. Two- and four-bit circuits have been demonstrated which have been optimized for low insertion loss. These circuits incorporated multi-throw switch networks and low-loss transmission lines in order to achieve loss below 0.3dB/bit at X-band (0.6dB average loss probed for a two-bit circuit and 1.2dB for a four-bit circuit). Alternate True Time Delay (TTD) circuits have used SPDT switch networks and inductive matching techniques to achieve constant time delay over extremely broad bandwidth (1-39GHz). Finally, RSC has fabricated compact two- and four-bit phase shifter circuits designed by University of Michigan which have enabled significant reductions in die size. These circuits extend the switchable transmission line architectures to include capacitive and inductive elements. The design and characterization of these MEMS-based circuits will be presented, along with brief discussion of future directions and key implementation challenges such as packaging and reliability.

DC-CONTACT RF MEMS SWITCHES FOR WIRELESS COMMUNICATIONS SYSTEMS

Dimitrios Peroulis, Linda Katehi
Purdue University, School of ECE

This paper reports on the design, fabrication and measurement of novel metal-to-metal contact RF MEMS switches for wireless communications systems. The developed MEMS switching architecture relies on electrostatic actuation because of its low-power requirements and relatively fast switching time. Unlike traditional high-frequency metal-to-metal contact switches, however, the DC-contact in the proposed design is achieved through stress-induced forces. This approach is implemented by 1) de-coupling the actuation and contact forces, and 2) constructively employing gradient stress effects. Consequently, the contact resistance is not related to the actuation force and only depends on the residual stress in the switch.

More specifically, the switch consists of two cantilever beams, namely the lower and upper beams, and an actuation pad underneath the cantilevers. The lower beam is fabricated with a high gradient-stress process that results in a significant upward deflection upon release of the structure (75 μm tip deflection for a 230 μm long cantilever beam). The upper beam, on the other hand, is a stiff cantilever suspended 3-4 μm above the lower beam. Because of the high gradient stress in the lower beam, the two cantilevers come into direct metal-to-metal contact immediately after the switch release. The switch is, therefore, fabricated in a normally-closed position (up position). The open (down) state is realized by applying a DC potential between the lower beam and the actuation pad underneath the beam. If this potential is higher than the movable beam's actuation voltage, this beam deflects and the contact points are separated.

State-of-the-art results with this switch for both its on and off states are demonstrated. The average (maximum) switch insertion loss has been measured to 0.05 (0.06) dB at 2 GHz, which corresponds to an average on-state contact resistance of 0.5 Ω . The switch average (maximum) loss remains below 0.16 (0.20) dB up to 40 GHz. Additionally, the switch provides an average (minimum) off-state isolation of 38 (35) and 14 (12) dB at 2 and 40 GHz respectively. The average extracted off-state series switch capacitance is 10 fF. These results clearly demonstrate the feasibility of employing stress-induced forces in high-frequency RF MEMS switches.

POLYIMIDE PLANARIZATION FOR RF-MEMS SWITCH ON PCB

B. Ghodsian, C. Jung, B. A. Cetiner , F. De Flaviis
University of California, Irvine

This abstract describes a new improved MEMS technology to manufacture RF-MEMS capacitive switches on laminated printed circuit board (PCB) with a higher yield. The described technology has improved the yield by more than 60-70

As RF application demands more sophisticated systems, i.e., phase arrays and re-configurable apertures antennas; then number of RF-switches to be integrated on a system chip is increased. As the number of switches increases, the issue with devices yield becomes significant. The yield of RF-MEMS switches is of major concern and is currently the subject of intense research efforts. RF-MEMS switches have come at certain stage of their development phase where they need to be looked at from the system level integration prospective. This requires addressing more important and perhaps different issues, such as yield, long and short-term reliability, packaging technologies, and their effect on yield, reliability and ultimately on production cost. For this reason we have investigated the cause of poor yield in PCB approach for manufacturing RF-MEMS switch.

One of the foremost problems of using PCB is its non-planarized surface of the substrate after the copper layer is etched. Normally, the copper layers thickness is 17m. However, some substrates can have the copper layer as thick as 70956m. These are thicker than an average metal layer used in microelectronics and MEMS technologies. The photoresist cannot be used to planarize the surface by normal spin coating method. Therefore, planarization of surface poses a unique problem and subsequently it requires a particular attention to planarize the surface for device fabrication to take place. One approach that is reported previously is based on the use of compressive molding planarization (COMP) process. The COMP process consists of placing a smooth surface (for instance a glass substrate) on PCB that has a thick spun-on photoresist layer on it. Then, through application of pressure (\approx 40psi) and high temperature (110C) the photoresist is re-flown to create a planarized photoresist mold layer over the non-planarized etched copper. The planarized photoresist will be the sacrificial layer where the switches metal membrane is subsequently deposited and patterned. Therefore, any damage to structure integrity of the photoresist results in failure of the switch. We have recently developed another process to overcome the drawbacks of COMP resulting in increased yield in the process. This technique uses polyimide as a sacrificial layer. The details of this technique will be presented at the conference.

RF MEMS CAPACITIVE SWITCHES BASED ON FLEXIBLE PRINTED CIRCUIT TECHNOLOGY: STATE-OF-THE-ART

R. Ramadoss¹, S. Lee², K.C. Gupta², V.M. Bright², Y.C. Lee²

¹Auburn University, Auburn, AL 36849-5201

²University of Colorado at Boulder, CO 80309

A novel approach for cost effective fabrication, assembly and packaging of RF MEMS capacitive switches using flexible printed circuit processing techniques will be discussed. The key feature of this approach is the use of flexible circuit film, Kapton-E polyimide film, as the flexing switch membrane. The advantages of this approach include - a) the characteristic size is in the meso-scale range and thus the required dimensional tolerance and alignment accuracy can be achieved using conventional printed circuit processing techniques, b) batch fabrication of such switches can be accomplished using existing roll-to-roll flexible printed circuit technology, and c) hundreds of such switches can be easily batch integrated with laminate circuits over large areas. These switches are compatible with the conventional printed circuit technology and are uniquely suitable for demonstration of reconfigurable antennas on laminate substrates.

The configuration of this switch can be described as follows: mechanical structure - fixed-fixed beam, actuator type - parallel plate electrostatic actuator, contact type - capacitive contact, and RF circuit configuration - shunt switch on coplanar wave guide (CPW). The switch consists of three layers - Kapton polyimide film, Duroid substrate, and Polyflon adhesive spacer film. The polyimide film, which is capable of withstanding millions of mechanical flexing cycles, is used as the flexing layer. The switch top plate is defined on the copper metallization of the polyimide film layer to form the flexing membrane. Coplanar waveguide (CPW) defined on the metallization layer of the substrate serves as the switch bottom plate. The adhesive spacer film present between the substrate and the polyimide film provides the required switch gap height. A thin Benzocyclobutene (BCB) dielectric layer present on the CPW metallization provides capacitive contact in the membrane down position.

In this presentation, design, fabrication and assembly of CPW shunt switches will be discussed. Current research effort in the development of reconfigurable antennas using these switches will also be discussed. The physical dimensions of these switches are in the meso-scale range. For example, the electrode area and the gap height of a typical shunt switch on coplanar waveguide (CPW) are 2 mm x 1 mm and 43 microns, respectively. RF performance with insertion loss less than 0.3-0.4 dB in the frequency range of 1-30 GHz and isolation value of 36 dB at 30 GHz has been demonstrated. Pull-down voltage of these switches is in the range of 90-110 Volts. Reliability testing up to 100 million operations has been carried out for this type of switches.

ADVANCED PACKAGING CONCEPTS IN SILICON SUBSTRATES

Rhonda Franklin Drayton
University of Minnesota

High-speed packaging is an essential component to the design of the next generation of highly integrated communication technologies. The use of silicon-based designs for RF-microwave applications has received significant attention in the last decade because of its potential to offer low cost solutions and leverage the use of a well-established infrastructure. In the packaging area, this material has also found significant potential from the development of circuit to system level packaging concepts for high-speed electronics. In this presentation, advanced package design concepts for optoelectronic applications will be described based on the use silicon micromachining from MEMs technology and other advanced fabrication methods. Novel interconnect designs will be described and performance capability will be shown for operation up to 50 GHz. High speed packages, based on these interconnects, will be discussed and performance metrics will be shown for a modulated laser application. In our approach, silicon micromachining is used to selectively reduce the substrate height and thereby offers scaling of 50 ohm electrical interconnects to satisfy optical array requirements, such as VCSEL devices. Traditional methods use external chips with narrow interconnect (10 micron) dimensions that result in non-50 ohm lines. Such methods present undesirable reflections in high data rate designs due to impedance mismatch between the external device and optical one. This results in performance degradation in optical system performance, especially above 40 GB/s.

Another important aspect of packaging is also high frequency integration that is needed to provide high-speed interconnection capability as well as methods for combining different design technologies. The potential for use of novel material systems on lossy substrates that may enable the integration of high performance RF passives will be highlighted.

RF MEMS TUNERS FOR HIGH EFFICIENCY MICROWAVE AMPLIFIERS

Emily Zheng¹, Srdjan Pajic², Zoya Popovic²
 , John Papapolymerou¹

¹Georgia Institute of Technology

²The University of Colorado, Boulder, CO

Low cost, low power, lightweight, compact, tunable and high efficiency RF hardware is essential for future wireless communication systems operating in multiple bands. In order to develop microwave circuits with the above characteristics, we are focusing on system-on-chip (SOC) and system-on-a-package (SOP) solutions that implement RF MEMS switches for dynamic reconfigurability. The latter are known for their low loss, low power and low distortion characteristics. One of the first circuits that we are investigating is a high efficiency, multi band, SOC or SOP X-band amplifier that utilizes RF MEMS tuners.

A double stub tuner that uses a digital capacitor bank has already been developed for frequencies between 10 and 20 GHz. The capacitances in each stub are provided by open-circuited microstrip stubs, which are selected via electrostatically activated capacitive MEMS switches. In a design with 4 capacitors per stub or a 4bitx4bit tuner, a tuning range equivalent to almost 4 quadrants of the Smith chart has been achieved at 20 GHz. Impedances with real part ranging from 1.5 Ohm to 109 Ohm and imaginary part ranging from 107 Ohm to 48 Ohm at 20 GHz, as well as impedances with real part ranging from 3 Ohm to 94 Ohm and imaginary from 260 Ohm to 91 Ohm at 10 GHz were matched to 50 Ohm with this tuner. The maximum VSWR achievable was 99, making this tuner extremely useful in amplifier matching.

In this paper, we present a monolithic X-band tuner on silicon that utilizes radial stubs for compactness and ohmic RF MEMS switches. The tuner is designed to match the output impedance of a class-E amplifier for maximum efficiency, in the range between 60 and 70% at the maximum available power from the device. Due to device variations, especially pronounced when the device is driven hard into saturation, the optimal output load circuit of the amplifier varies from device to device. A range for this variation is determined experimentally on a sample of over 30 class-E PAs fabricated with the same MESFET and using the same hybrid integration technique. The tuner provides the optimal match that covers the corresponding range of impedances. For the specific MESFET device used in this work, the tuner provides a $40+j39$ Ohm impedance at the transistor output at 10 GHz, and covers a load range from $19+j20$ Ohm to $50+j50$ Ohm. It consists of two stubs with each stub comprising of 3 radial sub-stubs that are activated via the MEMS switches (3bitx3bit tuner). The MEMS switches are of the ohmic type with a loss of 0.2 dB and an isolation better than 20 dB at 10 GHz.

Session D2, 13:40-Wednesday

RF AND OPTICAL DEVICES

Chairpersons: W. Pearson and W. Shiroma

D2

NEAR-RIGOROUS THEORY OF MICRORING CAVITY RESONANCE

*Baktur, R.¹, Pearson, L. W.¹, Ballato, J. M.²¹Holcombe Department of Electrical and Computer Engineering, Clemson University, Clemson, SC 29634-0916²School of Material Science, Clemson University, Clemson, SC 29634-0922

Frolov, *et. al.* [*Appl. Phys. Lett.*, 72(22), pp. 2811-2813] have demonstrated lasing in a so-called microring created from an optically active polymer formed on a cylindrical mandrel. (Incidentally, an optical fiber was employed as the mandrel.) They provide an argument that the laser operates by virtue of a whispering gallery (WG) wave resonance. Slab waveguide modes, which also exhibit resonances, are a part of the complete field structure. Frolov, *et. al.* reason that conductor losses in the gold layer which they placed between the microring and the fiber would quench lasing in any slab waveguide mode.

In the present paper, we present a rigorous, though approximate, theoretical development for the complete electromagnetic field in the microring. The Greens dyadics developed is approximate in the sense that they are derived for a translationally invariant stratified structure excited, respectively, by electric and magnetic current line sources, thereby providing mode sets that are TE and TM to z . The resonances are observable as zeros in the denominators of the summand in the respective TE_z and TM_z expansions.

The summands in the expansion can be arranged so that a whispering gallery term appears explicitly with a residual term that combines with the WG to form a slab-guided mode that follows the circular path around the ring. As the dielectric layer is made thicker by receding the inner boundary while the outer boundary remains fixed, the residual term recedes, leaving a pure whispering gallery mode, consistent with the heuristic explanation of Frolov, *et. al.*

The resonances of the structure are examined critically and compared with published experimental data on microring lasers. Cases of non-circular structure and inhomogeneous material are discussed in terms of ray-optical asymptotic developments. Prospects for coupling of the laser mode into a fiber around which it is formed are discussed.

* a.k.a. Rehanguli Gayiti

APPLICATIONS OF BRAGG FIBERS IN COMMUNICATIONS AND POWER TRANSMISSION

Muthitacharoen, A., Barnes, F. S.

University of Colorado at Boulder, Department of Electrical and
Computer Engineering, 425 UCB Boulder, CO 80302

The design criteria of Bragg fibers with hollow core for applications in telecommunications and optical power transmission are analyzed. Since Bragg fiber reflectivity can be sensitive to cladding thicknesses or incidence angles of lights when the index contrast of the cladding is small, we can use this property for applications in telecommunications or sensors. However, when the index contrast of the cladding layers becomes larger, Bragg fiber reflectivity seems to be more tolerant to the layer thicknesses or incidence angles. We can use this property for applications that are not concerned about light scattering or dispersion, for example, optical power transmission. In telecommunications system, the single-mode Bragg fibers are used. Single-mode Bragg fibers can be designed for large core diameters. We can show that single-mode Bragg fibers can be designed so that they have lower absorption loss, dispersion, and relative dispersion slope (RDS) than those of conventional single-mode fibers. Furthermore, multidirectional Bragg fibers are proposed for use in optical power transmission applications. The multidirectional Bragg fiber has claddings constructed by high index materials and has ability to reflect the light at any incidence angle. Both designed Bragg fibers are proved to exhibit much lower loss than conventional silicon fiber and can be made at relatively large core diameters. The loss coefficient of the fundamental TE mode in the single-mode Bragg fiber is reduced to 0.00001 dB/km when we assume that loss coefficient of high and low dielectric claddings of n_1 and n_2 are 0.15 dB/km and 0.05 dB/km, respectively. The multidirectional Bragg fiber constructed by high and low dielectric claddings of n_1 and n_2 with loss coefficients of 50 dB/km and 0.15 dB/km, respectively can reduce the loss coefficient in fundamental TE mode to 0.0003 dB/km. Both fibers are assumed to have core radius of 30 micron and operated at the wavelength of 1.55 micron.

A PROJECT-BASED UNDERGRADUATE CURRICULUM IN HIGH-FREQUENCY ELECTRONICS AND ANTENNAS

Shiroma, W.A., Murakami, B.T., Ching, K.S.

, Tamamoto, M.A., Ohta, A.T.

University of Hawaii at Manoa, 2540 Dole St., Holmes Hall 483,
Honolulu, HI 96822

The University of Hawaii has recently developed a project-based engineering curriculum in high-frequency electronics and antennas. Participating students range from the high-school sophomore through college senior levels and work in multidisciplinary, peer-mentored teams. The students write proposals to industry and government agencies to secure funding, organize themselves into engineering and management teams, and present design reviews for their sponsors.

One project is a 5-GHz RF front end for a wireless transceiver, consisting of a local oscillator, BPSK modulator, three-stage power amplifier, transmit/receive switch, microstrip patch antenna, image-reject filter, two-stage low-noise amplifier, and single-ended mixer. The ten-student team consists of three seniors, three juniors, two sophomores, with one senior serving as the overall project leader.

Another project is the CubeSat Program, the largest and most ambitious project ever undertaken by a multidisciplinary group of engineering students in our university's history: designing and constructing small satellites that are launched into low-earth orbit. Over 70 undergraduates and nine faculty advisors in civil, electrical, and mechanical engineering are participating in the project, which involves the design, manufacture, and operation of a cube-shaped satellite having a mass no greater than 1 kg and a maximum volume of 1000 cm³. The undergraduates themselves have written proposals that resulted in approximately \$200,000 in funding from NASA, the Air Force, Space Grant, and industry. Two missions are currently under development: (a) the demonstration of active quasi-optical arrays for high-speed data transmission, and (b) the use of retrodirective antenna arrays for self-steering, secure crosslinks for distributed picosatellite networks. Telemetry is carried out at amateur-band UHF frequencies to ensure worldwide coverage by radio amateurs.

Since the introduction of this engineering curriculum three years ago, two of our graduating seniors received the *Alton B. Zerby and Carl T. Koerner Award* from Eta Kappa Nu, identifying them as the nation's most outstanding electrical engineering students. Three graduating seniors have started Ph.D. programs (including one who was awarded a prestigious NSF Graduate Fellowship), and several others have pursued their M.S. degrees.

RF DISTORTION DEPENDANCE ON LASER DIODE OPERATING TEMPERATURE

Kim, E. M.¹ , Wei, Li¹¹University of San Diego, Lightwave Solutions, Inc.²Wilfrid Laurier University

This paper discusses the issues related to the use of low cost uncooled 1310 nm lasers for analog cable television (CATV) transmission. The use of low cost uncooled Distributed Feedback (DFB) lasers has given rise to increased awareness of varying RF distortion characteristics with varying operating temperatures. The many factors contributing to the temperature dependence of the laser RF distortion performance in terms of composite multi-tone distortion and its significant variation from laser to laser are summarized. The challenge becomes stabilizing and optimizing the laser over a wide frequency range (50 MHz to 870 MHz). Unfortunately, the starting laser composite second order (CSO) and composite triple beat (CTB) ratio levels are very sensitive to laser temperature, operating bias current, and optical coupling through an optical isolator. The nonlinear performance of the laser diode is dominated by variations in operating temperature. The required precision of external temperature control of these DFB lasers for given RF composite distortion are presented. Electronic predistortion methods are used to correct for the inherent distortion characteristics of the laser diode. However, these predistortion circuits must be able to compensate for the varying distortion of the laser diode at operating different temperatures. Look-up tables are commonly used to drive predistortion compensation circuits as a function of operating temperature. The laser RF distortion variation dependence on many factors renders a look-up table approach unrealistic, given the fact that wideband distortion cancellation (10 dB composite or better) is required over the full 50-870 MHz frequency range. Complicating the predistortion method for compensating for composite distortion is the varying phase of the compensating signal produced by the predistortion circuit.

Session D/B1, 8:40-Wednesday

RECONFIGURABLE ANTENNAS

Chairpersons: Jennifer Bernhard and Aly Fathy

D/B1

A RECONFIGURABLE MEMS PLANAR ANTENNA FOR FREQUENCY AND POLARIZATION DIVERSITY

Cetiner, B.A., Yoo, H.J., Grau, A.
, Ghodsian, B., De Flaviis, F.
University of California Irvine

Combination of passive radiating elements such as antenna arrays have long been devised for multifunctionality in key parameters such as frequency and polarization. We present an enabling technology of a single antenna software-defined radio solution for emerging low cost wireless appliances. Key developments in MEM actuator fabrication and pixelization schemes provide microstrip antennas much needed functional improvement and seamless integration to the transceiver block. A novel low temperature nitride process produces pixel interconnects with all reported advantages of RF MEMS.

Careful layout of pixel elements and an on-/off-state algorithm allow the antenna to reconfigure its electrical size and shape, achieving both frequency and polarization diversity. The resulting variation in antenna geometry produces the correct dimension for each desired frequency specification. The off-state of each pixel acts to produce a parasitic-loaded slot in the structure, which can then be combined with others in various geometries to produce the desired polarization. The design prototype operates in the C-band stepping up in increments as low as 600 MHz from base frequency. A reconfigurable feed that may also be incorporated into the design for compactness prevents loss of match as the antenna hops from one frequency to the next. The antenna can radiate with either x-, y-, or dual-linear polarization; the circular sense is also possible with either right hand or left hand circular polarization. Redundancy is incorporated into the design, both in hardware and algorithm, to provide robustness against fabrication yield and structural failures in the field. Characterization of radiation pattern and return loss validate the concept.

The details of the developed technology and experimental results for prototype geometries characterizing the diversity performance of the antenna for indoor mobile systems will be presented.

PLANAR CROSS-SIERPINSKI MULTIBAND ARRAY ANTENNA

Anagnostou, D.E.¹, Feldner, L.M.², Christodoulou, C.G.¹

¹Department of Electrical and Computer Engineering, , University of New Mexico, , Albuquerque, NM, 87131, USA

²Sandia National Laboratories,, Albuquerque, New Mexico, USA

Self-similar Antennas are well known for their ability to radiate similar radiation patterns at multiple frequencies. In addition, recent technological improvements have permitted the monolithic integration of antennas with other electromechanical components, such as RF-MEMS switches, resulting in re-configurable antennas capable of multiband operation, adaptive beamforming, and DoA estimation.

The Sierpinski fractal antenna is considered ideal for multifrequency applications, because its radiation pattern varies very little over its frequency bands. With the use of high-isolation, low-loss RF-MEMS switches between the individual triangular patches of the fractal antennas, we can physically reconfigure their shape and size in order to provide frequency band selection and constructive or destructive radiation pattern interference.

In this work, a novel fractal array consisting of four fractal elements, each one rotated by 90 with respect to the other, is presented. This arrangement forms a cross of fractal antennas whose radiation characteristics are expected to be similar to a planar cross-dipole antenna. Two prototype cross-Sierpinski dipole antennas that were designed to be reconfigured with mechanical switches are discussed. These antenna designs are evaluated based on their potential utility as monolithic reconfigurable antenna elements.

Prototype antennas are constructed at low microwave frequencies to evaluate the radiation and impedance characteristics of such antenna topologies. Candidate reconfigurable antenna designs will be scaled up in frequency to be fabricated monolithically with RF-MEMS switches at Sandia National Laboratories. The ultimate goal will be to demonstrate a multi-band switch reconfigurable antenna element on a single chip.

The prototype antennas were designed and simulated with the aide of Ansoft Designer software. Prototype antennas were fabricated at the University of New Mexico. Full-wave MoM simulation results will be compared to laboratory measurements.

MILLIMETER-WAVE MICROMACHINED 3-D ANTENNA
AND WAVEGUIDE SUBSYSTEM FOR BEAM FORMERSCai, Y.¹, Li, H.¹, Su, Y.C.²
, Sammoura, F.², Lin, L.², Chiao, J.C.¹¹University of Texas at Arlington²University of California at Berkeley

Millimeter systems have been increasingly drawing attention because of their shorter wavelengths for high-resolution sensors, high carrier frequencies for broadband communication capability and more environmental tolerance compared to optical systems. With the rapid progress on active devices, monolithic integrated circuits have emerged as an attractive option in the field of millimeter-wave applications. However, the front-end system integration faces some technical challenges. They are more susceptible to fabrications errors and have high series resistance or lower output powers. Many demonstration using micromachined waveguide on silicon wafers have shown significant performance improvement and great promises, compared to the conventional bulky waveguide systems. However, high cost and complex fabrication processes impose barriers for mass production.

In this work we present a new process to make a millimeter-wave antenna array with waveguide feeding networks for beam formers. This thick-layer plastic-molding process is more suitable for integrated millimeter-wave front-end systems than demonstrated thin-layer fabrication approaches. Since antennas and waveguides in millimeter wave applications have fairly large dimensions (in mm), the thick-layer process reduces the construction and alignment steps, time and costs. Multiple alignment steps, required in the thin-layer process to construct sidewalls of the horn antenna and waveguides, yield rough surfaces and introduce high losses. The proposed process could overcome these deficiencies. The process steps include plastic molding, electroplating, mechanical polishing, plastic filling, assembling and bonding. The thick electroplated metal layer could reduce the series resistance.

In the beam former fabrication processes: the first layer is the substrate and the second layer is molded to the desired dimensions as rectangular shapes for the waveguide. These layers then are bonded together. A sputtered metal seed layer is mechanically polished to smooth the surface. A third layer with molded and patterned metal is bonded to close the waveguide. A reshaped mold insert is applied to define the horn antennas. A final electroplating process coats the antennas and waveguides with thick, smooth and continuous metal layer to completes the fabrication.

The proposed micromachined beam formers are designed for W-band applications. In the presentation, we will show simulation and preliminary testing results and discuss the feasibility of the proposed system architecture.

RADIATION PATTERN RECONFIGURABLE ANTENNAS
AND ARRAYS: OPERATION AND SWITCH INTEGRATION

Bernhard, J. T. , Huff, G. H. , Feng, J. , Zhang, S.
University of Illinois at Urbana-Champaign

The idea of antenna reconfiguration is not new. Indeed, it is already more than two decades old. However, we are coming into an era where new functionality in antennas is not a novelty but rather a requirement to enable future communication and sensing systems. This work reports on the theory and measurement of individual elements and small demonstration arrays consisting of novel pattern reconfigurable antennas. The antenna being considered (G.H. Huff, J. Feng, S. Zhang, and J.T. Bernhard, IEEE Microwave and Wireless Components Letters, 2, pp. 57-59, 2003) is a single-turn Archimedean square microstrip spiral capable of both broadside and endfire radiation within a shared frequency band. Measured results from two small arrays are presented that provide insight into the array properties that are required to maintain broadside and endfire radiation. Along with factors surrounding array spacing and beamforming constraints, the spacing, orientation, and mutual coupling of the individual antenna elements are discussed.

Modifications to the pattern reconfigurable antenna that allow integration commercially-available packaged low frequency (less than 6 GHz) single pole-double throw RF MEMS switches and well as directly fabricated high frequency RF MEMS switches designed at the University of Illinois are outlined. Measured results are presented for single antennas with low frequency RF MEMS switches that illustrate the ramifications of generic switch design on antenna design and behavior. For example, the switch requires common RF and DC grounds, while the antenna requires isolated RF and DC grounds. Additionally, the characteristic impedance of the switch presents a mismatch to that of the antennas microstrip structure. These issues as well as effects of the switches pad layout are discussed in more detail. Since high frequency RF MEMS switches are not yet commercially available, several more changes to the antenna structure are necessary to enable simultaneous fabrication of the antenna and switches together. These modifications allow a standard probe fed microstrip antenna to be successfully transformed into an IC compatible structure.

MECHANICALLY ACTIVE APERTURE ANTENNAS

Washington, G.N.¹, Yoon, H.S.¹, Theunissen, W.T.²
, Burnside, W.D.²

¹Ohio State University, Intelligent Structures and Systems Laboratory

²Ohio State University, Electroscience Laboratory

Recent studies have shown that reflector surface adaptation can achieve significant performance enhancement without the complexity and cost associated with phased array technology. The work in this study develops the framework for placement and actuation of novel reconfigurable dual-offset contour beam reflector antennas (DCBRA). Based on a conventional Cassegrain dual-reflector antenna, the mechanically reconfigurable dual-reflector antenna is designed such that while the main reflector is shaped at the time of design and fixed to give a predefined beam pattern, the subreflector shape is adjusted using controlled movements in order to achieve some desired footprint on the ground. The antennas are capable of variable directivity (beam steering) and power density (beam shaping). The actuation for these antennas is employed by three different techniques: The first technique involves attaching polyvinylidene fluoride (PVDF) film to the back surface of a polymeric reflector substrate. PVDF is a lightweight piezoelectric film that is distributed in nature which leads to fully distributed control surface. The second technique involves attaching PZT (Lead Zirconate Titanate) patch actuators to a metalized polymer substrate. These actuators are more rigid and produce larger forces than their PVDF counterparts. They are semi-distributed however due the limited region associated with the patch. A voltage drop across these materials will cause the material to expand or contract. This movement causes a moment to be developed in the structure, which causes the structure to change shape. Several studies of flexible structures with PVDF films and PZT patches have shown that cylindrical antennas can achieve significant deflections and thereby offer beneficial changes to radiation patterns emanating from aperture antennas. The final technique has a number of linear point actuators perpendicularly attached on the flexible subreflector surface. When control commands are applied to the actuators, each actuator moves up and down proportionately to the input command making the subreflectors shape change. Then, the modified subreflector shape makes the radiation pattern and the beam footprint change accordingly. In this study, relatively large curved actuators are modeled and a deflection vs. force relationship is developed. This relationship is then employed in simulations where the far field radiation patterns of an aperture antenna are manipulated for a number of different countries.

RECONFIGURABLE MICROWAVE HOLOGRAPHIC ANTENNAS: MERITS AND LIMITATIONS

Aly E Fathy
The University of Tennessee

An innovative reconfigurable antenna concept based on the dynamic creation of metal-like conductive plasma channels in high resistivity silicon has been reported¹. Where the plasma channels defined along an x-y grid are precisely formed by the injection of a DC current. Surface lateral PIN [SPIN] devices has been utilized as the building block of the fully addressable grids pixels. Reconfiguring the grid allows the implementation of various antenna shapes; including microwave holographic ones.

Holographic antennas can provide multi-beam and beam-steering capabilities. Hard-wired models have been utilized to demonstrate the holographic antenna concept promise as a low cost alternative to phased arrays². The definition of the holographic fringes depends on the desired far field pattern, and the complexity of the algorithm, required to set up all the controlling currents, depends on the desired array flexibility, i.e. as a preset scan- utilizing beam lookup tables, or a real time scan and all settings are done on the fly.

However, there are some challenges to this concept, such as the required relatively high DC consumption to forward bias the SPIN devices, the complexity of the feed network -as better fringe definition means more DC feeds, the associated devices non-linearity can lead to higher noise levels in receive, and relatively high insertion loss compared to all copper- causing significant efficiency and gain drop. The required numbers of fringes are 10, and the spacing between these fringes is approximately one wavelength to provide the high resolution and contrast of the radiation patterns. This limits the operating bandwidth to 5-10

Surface wave excitation has been utilized to feed these fringes^{2,3}. Analysis of the current feed structure indicated that most of the energy of the surface wave excitation was confined to the wafer center and the excited currents were off-center, were significantly dropped. The non-uniform current distribution off caused beam broadening, and a drop in both gain and efficiency. Alternative excitation methods, device fabrication, and fringe pattern definitions have been recently investigated and will be presented at the Symposium. (A. E. Fathy, et al, IEEE Trans. Microwave Theory Tech., vol. 51, No. 6, June 2003, pp. 1650-1661)¹. (M. El Sherbiny, et al, to be published IEEE Ant. And propagation, June 2004)² (A. E. Fathy, , IEEE MTT Symposium Digest , Philadelphia, 2003, pp. 1833-1836)³.

ELECTRONICALLY TUNABLE SURFACES FOR LOW COST,
TWO-DIMENSIONAL BEAM STEERING

Sievenpiper, D.

HRL Laboratories, 3011 Malibu Canyon Road, Malibu, CA, 90265

Using a periodic resonant texture, it is possible to create metallic surfaces with new electromagnetic properties. By building capacitive and inductive regions into the periodic texture, the surface can be made to produce any desired boundary condition. For example, a textured surface can appear as an artificial magnetic conductor, an electric conductor, or any surface impedance in between.

Recently, tunable surfaces have been built by incorporating varactor diodes into the resonant texture. These tunable surfaces can be programmed to provide any reflection phase as a function of position across the surface, and can be used to steer and focus a reflected beam. This provides a very low-cost beam steering method, but it requires that the surface be illuminated by an out-of-plane feed, so antennas using this method cannot be conformal.

However, conformal antennas are possible using an alternative feed method, which retains the same low-cost steering properties. A surface wave is launched across the textured material, and it excites various modes in the complex, two-dimensional structure. By tuning the electromagnetic behavior of the surface texture, the surface wave can be made to radiate as a leaky wave. The radiation angle of this leaky wave can be electronically steered to any angle, including both forward and backward directions. In this steering method, a periodic impedance function is applied to the surface electronically. It scatters the surface wave into a particular angle within the radiation cone that depends on the wave vector of the applied impedance function. Furthermore, by using a quasi-periodic function, the surface can be programmed so that the effective aperture covers the entire surface area, regardless of radiation angle, in contrast to traditional leaky wave methods. Using this technique, a single feed is able to address many square wavelengths across a low-cost steerable aperture.

This suggests a new way of building steerable antennas, where the feed simply couples energy into multiple modes in an arbitrarily tunable surface, and that surface is programmed in such a way that the modes radiate any desired beam profile, in any direction. Because the surface handles both the beam steering and the signal distribution, this can enable significant cost reductions, leading to high-performance antennas that are simple, lightweight, and conformal.

METAMATERIALS BASED ELECTRONIC ANTENNAS

Lim, S., Caloz, C., Itoh, T.
University of California, Los Angeles

Recently, we proposed a transmission line approach of left-handed (LH) (antiparallel phase and group velocities) metamaterials and the generalized concept of composite right/left-handed (CRLH) structures, in which the physically unavoidable right-handed (RH) parasitic effects, acting in concert with LH effects, are fully taken into account. A CRLH structure is LH at lower frequencies and RH at higher frequencies with a transition at a specific frequency where the propagation constant is zero. On the basis of this new concept, a unique backfire-to-endfire leaky-wave (LW) antenna operating in its dominant mode with excellent radiation at broadside was introduced, whereas conventional LW antennas typically use higher-order modes and can not radiate efficiently at broadside.

A novel reflecto-directive system was presented as an application of the CRLH LW antenna described in the previous paragraph. This system, thanks to the backfire-to-endfire property of the CRLH LW antenna, is capable of retransmitting or 'reflecting' a signal incoming under any angle toward any desired arbitrary angle by way of tuning the LO frequency of a heterodyne mixer.

The reflecto-directive system presents, for some applications, the disadvantage that the output angle is function of frequency (frequency-scanned antenna). In the present contribution, we demonstrate theoretically and experimentally a more practical electronically-scanned version of this reflecto-director. Varactor diodes are inserted in each unit cell of the CRLH LW antenna. As the bias voltage of these varactors is varied, the capacitive loadings of the line are modified, and therefore the propagation constant is modified, which induces a variation in the scanned angle. By appropriately designing the novel structure, efficient electronic-scanning can thus be achieved at a fixed frequency.

The full-wave transmission characteristics and dispersion diagram of the structure are studied. An accurate LC parameters extraction procedure is shown, and the extracted parameters are inserted in a CRLH circuit model, from which the dispersion diagram is also computed (and compared with the full-wave one) from an analytical formula based on the transmission matrix and Floquet theorem. First the structure is demonstrated as an antenna and as a reflecto-directive system.

The device proposed may be used in several wireless applications such as WLANs and inexpensive directive antennas/reflectors replacing conventional phase-scanned arrays. The concepts presented can be potentially extended to 2D surfaces.

Session E1, 13:40-Wednesday

**ELECTROMAGNETIC NOISE AND
INTERFERENCE**

Chairpersons: Robert Gardner and Everett Far

E1

COMPACT, LOW-IMPEDANCE MAGNETIC ANTENNAS

Baum, C.E.

Air Force Research Laboratory/DEHP

In designing a damped-sinusoid electromagnetic radiator one is sometimes confronted with significant space limitations. This paper explores the design of loop antennas and associated feeds for such applications. We find that subdividing the loop can be sometimes advantageous.

If one wishes to radiate large fields from some small hypoband (pulse of approximately single frequency) source/antenna, one has a challenging engineering problem. If the source involves a resonant transformer or Marx generator charging some capacitor, one is concerned about how fast this can be switched into the load (antenna). This switching time limits how high in frequency one can make the oscillation involving the source and antenna. For a small antenna (compared to a radian wavelength) a loop type of antenna is attractive in that in the near field the ratio of electric to magnetic field can be made smaller than the wave impedance, say Z_0 , the impedance of free space (or some other dielectric medium). This in turn allows one to radiate more power for a given voltage limitation on the antenna.

Here we look at loops in low-impedance configurations in confined volumes. The object is to maximize the magnetic moment (and its time derivative) of the form $m = IA$ by maximizing the current and loop area. The reader can note that the source occupies some of the volume and thereby can reduce the loop area. Appropriate design of the source (making it somewhat "transparent" to the fields) can help in this regard.

The source also needs to be considered. In general it is not just a capacitor, but includes various other components. This also needs to fit in the volume. For symmetry, one might prefer it to be located near the center of the volume where the loop feeds, together. The source conductors can also interfere with the magnetic field produced by the loop. To the extent practical such conductors should not form closed current paths allowing currents to circulate around the z axis, thereby reducing the equivalent area of the loop.

Here we have general considerations for optimizing loop design. One could make more detailed models for the various components such as the antenna and feeds, as well as the source.

A DUAL-POLARITY IMPULSE RADIATING ANTENNA

Leland H. Bowen¹, Everett G. Farr¹, Dean I. Lawry²¹Farr Research, Inc., 614 Paseo Del Mar, NE, Albuquerque, NM, 87123²Air Force Research Laboratory / DE, 3550 Aberdeen Ave. SE, Kirtland AFB, NM 87117-5776

Dual polarity Impulse Radiating Antennas may be useful in a variety of applications, such as UWB radar, and target identification. Adding a second polarization to a single antenna essentially provides twice the information with the same aperture area. Until now, no design has been built and tested, so we report here the results of the first dual-polarity IRA.

Until now, we have not tried to construct an IRA with dual polarity, due to the difficulty of maintaining a good impedance match throughout the antenna. However, we recently built a poorly match IRA with a single unbalanced 50-ohm feed, with surprisingly good results. These results inspired us to try a dual-polarity IRA, in hopes that any mismatch at the feed point might be tolerable for those applications where reflections within the system are not of great importance.

The dual-polarity IRA described here, designated IRA-1D, is very similar to the IRA-1 developed earlier by Farr Research. For the IRA-1D we used the same feed arm configuration as used on the IRA-1, which had four feed arms spaced uniformly around the aperture, with the electrical center of the feed arms intersecting the edge of the reflector. The only difference in the IRA-1D is that each pair of opposite feed arms is connected to a separate 50-to-200-ohm balun. This produces a mismatch from 200 to 400 ohms at the focus of the reflector on each channel. In spite of this 2:1 impedance mismatch, the antenna characteristics of the IRA-1D are quite good up to at least 10 GHz. We provide here the antenna characteristics for both polarizations of the IRA-1D, and we compare these results to those of the standard IRA-1. We also compare the IRA-1D to the standard commercial version of the 18-inch IRA.

DIFFERENTIAL SWITCHED OSCILLATORS AND ASSOCIATED ANTENNAS

Baum, C.E.

Air Force Research Laboratory/DEHP

This paper extends the design options for switched-oscillator-driven paraboloidal reflector antennas to include differential systems. The switched oscillator can be differential or single-ended with a balun. The full reflector with TEM feed arms can be driven in various ways to give a variety of polarizations from the switched oscillator located at the paraboloidal focus, or on the paraboloid with a transmission line to the focus.

The oscillator reflector antenna (ORA) then has various design options. There is a single-ended version using a half reflector with ground plane. There are several differential versions using differential switched oscillators or single-ended switched oscillators with baluns. The differential versions use full reflectors with various polarizations and connections of the switched oscillator (at the focus or at the reflector) to the antenna feed arms.

Recent papers [C.E. Baum, "Antennas for the Switched-Oscillator Source", Sensor and Simulation Note 455, March 2001; C. E. Baum, "Switched Oscillators", Circuit and Electromagnetic System Design Note 45, September 2000] have considered switched oscillators and associated antennas for radiating an oscillatory waveform. The antennas considered thus far are of the single-ended variety involving a ground plane with a half-paraboloidal reflector together with feed arms as in a reflector impulse-radiating antenna (IRA). This geometry has the advantage of matching well with single-ended (e.g., coaxial) pulse-power systems and providing a place for the pulse-power equipment on the side of the ground plane (typically under) away from the antenna.

For some applications a differential source and antenna may be desired, and a half-reflector-with-ground-plane antenna may not be appropriate. Among the applications are linear-polarization diversity and circular polarization. This raises difficulties in how to feed the pulse power to the antenna.

NOISE INTERFERENCE SURVEY FOR 24 GHZ PASSIVE SENSOR BAND

Simoneau, J. B. ¹, Seetharam, V. ¹, Pearson, L. W. ¹,
Baum, C. W. ¹, Pace, Scott ², Hollansworth, J. E. ³

¹Holcombe Department of Electrical and Computer Engineering,
Clemson University, Clemson, SC 29634-0916

²Office of Space Communications, NASA Headquarters

³NASA Glenn Research Center, Cleveland, OH 44135-3191

The frequency band between 23.6 and 24.0 GHz is allocated for passive sensor applications. This band is key to weather prediction because radiometers on satellite platforms can measure noise emission from water vapor in the atmosphere in this band. This emission peaks between 22 and 23 GHz and is substantial in the 23.6-24 band. The allocation of an industrial/scientific/medical (ISM) band immediately adjacent to the passive sensor band (24.0-24.25 GHz) raises concerns that unintended emissions from ISM band devices may disrupt the long-standing weather prediction application of the passive sensor band. Furthermore, proposals to employ ultrawideband technology *in* the passive sensor band are also under consideration. Some manufacturers will soon deliver automotive radar equipment in the ISM band. It is very difficult to predict the impact of the unregulated activity on the long-term viability of critical passive sensor functions.

It is imperative that regulatory organizations have sound scientific data upon which to base decisions on further deployment around the passive sensor band. The band's utility depends on a natural phenomenon possessing a specific characteristic frequency behavior. This paper describes an activity intended to provide one component of the knowledge base needed to support regulatory decisions. We have built a receiver system that operates between 23.3 and 24.3 GHz in the form of a multi-chip module for amplification and down conversion of incoming signals to the range 0.7 to 1.7 GHz. A spectrum analyzer is used to capture the incoming spectrum over this band. Standard MMIC components are used in the amplifier/mixer chain.

The survey instrument has been used in field survey measurements in which we have scanned at 15 degree intervals in azimuth with elevations of 0, 30, and 60 degrees. Sites included in the survey include rural woodlands (Blue Ridge Parkway), a warm lake (Lake Hartwell), small and large airports (Oconee Co., SC and Atlanta Hartsfield), as well as freeway sites in urban and non-urban areas. We observe expected fluctuations in the natural noise level with variation in atmospheric water vapor. Increased water vapor content occurs, of course, over sources (lake, woodlands) as temperature increases. Measurements from urban areas have not been analyzed at the time that this abstract is written, and we are unable to comment on what has been observed. Observations of man-made signals will be reported in the presentation.

REMEDICATION OF INTERFERENCE IN DATA COMMUNICATIONS CAUSED BY MULTIPLE SCATTERING OF UNWANTED SIGNALS

Kohlberg, I.¹, Boling, R. H.²

¹Kohlberg Associates, Inc., P.O. Box 23077, Alexandria, VA 22304

²Institute for Defense Analyses, 4850 Mark Center Drive, Alexandria, VA 22311-1882

Intentional Electromagnetic Interference (IEMI), directed at electronic and communication systems, can cause serious disruption of operation by generating bit errors, causing delays in the transfer of information, loss of synchronization, or even driving the system to shutdown. Many common systems, such as those used on aircraft, LANs, and computers, may have minimal immunity to robust pulsed IEMI because they normally operate in a secure, high signal-to-noise environment.

Boling and Kohlberg recently showed (ICEAA, Turin, Sept.2003) that the effects of pulsed interference in data communications could be completely eliminated for a wide class of waveforms by properly encoding signals, using error correcting codes, or bit-interleaving (a common technique for fading dispersive communications channels). The price paid for completely error-free communications is a lower data rate and an increase in transceiver complexity. The greatest gain from message coding occurs for systems in which the interfering pulse repetition rate is significantly slower than the signaling bit rate, or where the pulse width of the interfering pulse is less than the signaling bit pulse width.

This paper extends the previous work of Boling and Kohlberg to the case where multiple scattering of the incident unwanted signal causes additional bit errors. This may, in fact, be a more realistic situation because there are usually several scattering objects in a "target" enclosure. When multiple scattering occurs, the tradeoffs between the acceptable bit error rates, IEMI pulse repetition frequency and pulse waveform, and signal pulse width can change significantly from the non-scattered case. In this case, coding to ensure error-free communications involves unique combinations of various codes combined with interleaving. Specific examples are given for selected configurations of scattering centers and pulsed IEMI waveforms.

NEURAL NETWORKS APPLIED TO THE DERIVATION OF TRENDS IN ELECTROMAGNETIC EFFECT RESEARCH

Gardner, R. L.¹, Stoudt, D. C.²¹Consultant to Naval Surface Warfare Center, 17320 Dahlgren Rd Code B20, Dahlgren, VA 22448²Naval Surface Warfare Center, 17320 Dahlgren Rd Code B20, Dahlgren, VA 22448

The prediction of electronic upset or burnout due to the illumination of a system by an electromagnetic wave begins with a description of the environment at the target and ends with a statement of the likely outcome. Traditionally, analytic techniques have been used to describe the coupling of the wave into the electronic system, to predict currents near sensitive components. The conclusion is reached using threshold analysis to describe the end state of the target. In the end, the success of these predictions is judged by their agreement with experiments. Inference directly from the empirical results forms another way of building the tools for outcome prediction in electromagnetic interference (EMI) research.

The authors [Gardner, Stoudt and Latess, of the International Conference on Electromagnetics in Advanced Applications, page 191, Turin, 2001] have previously described a multivariate statistical approach to deriving trends from empirical data taken from measured outcomes of hostile illuminations of electronic equipment. This technique is very powerful as long as there is sufficient data available. Not only can we develop a trend from this technique, but we can also easily get an idea of the quality of the fit as compared to the quality of the data itself. Multivariate fits and pattern analysis are possible as long as the parameters exercised in the data span the space being examined. The major disadvantage to this technique is that most of the fits are locally linear. There are nonlinear approaches but most of these are ad hoc transformations rather than formulas based on the character of the data.

Neural networks are much more powerful tools for finding complex patterns than traditional statistical methods but the neural net literature is far behind the statistical literature in finding goodness of fit data. We can find very complex patterns in the data using neural net techniques.

The paper uses computer failure data from the literature to demonstrate some simple feed forward networks. These are applied easily, converge quickly and show interesting patterns. We successfully fit the training data (one measure of success) and use the trained net to successfully predict data not used in training (another measure of success).

UTILIZATION OF THE LOGISTIC REGRESSION MODEL AS
A MEANS FOR IDENTIFYING HARDNESS AND CONFIGU-
RATION VARIATIONS IN A TEST BED USED IN EMI TEST-
ING

Ropiak, C.A.
Envisioneering

It has previously been demonstrated that hardness variations in test assets can have a significant impact on the outcome of susceptibility data derived from electromagnetic interference (EMI) testing. These hardness variations may be attributed to such things, as electronic component manufacturing changes or a test be comprised of different make and models of electronics. In addition to hardness variations, configuration variations such as those associated with networked computers can also impact the utility of EMI test data. It is for these reasons that we seek a means for identifying and possibly quantifying these test bed uncertainties/variations. The purpose of this paper is to investigate and quantify the impact of hardness and configuration variations in a test bed used for EMI testing. The empirical method known as multivariate logistic regression (MLR) is used to accomplish this. The parameter N, which is associated with the number of pulses in a test serves as the vehicle through which hardness and configuration variations are identified. In an ideal test bed, where all test assets are identical and there exists no impact due to configuration variations, for a sufficiently low pulse repetition frequency (PRF) one would expect each pulse to represent an independent event. However, once hardness or configuration variations are introduced, the independence is destroyed, and the probability of effect (PE) for each successive pulse changes. The degree of PE change is reflected in the coefficient for the N term in the MLR model. While this method may not lend any insight into the exact nature of the hardness or configuration variations, it does provide a means for identifying and quantifying their presence.

MODERN BUILDING CONSTRUCTION AND ITS INFLUENCE ON THE PROPAGATION OF ELECTROMAGNETIC FIELDS

Latess, J., Stoudt, D.C., Bowers, K.A.

Naval Surface Warfare Center, Attn: Code B20, 17320 Dahlgren Road, Dahlgren, Virginia, USA 22448-5100

The physical makeup of commercial office buildings continues to evolve as new construction techniques are developed by the civil engineering community. The impact of these building techniques on the propagation of electromagnetic energy is of great interest to those studying the threat of intentional electromagnetic interference (EMI) and other high power electromagnetic phenomenon. This stems from the fact that electronics equipment affected by these electromagnetic environments is often located within these buildings.

The Joint Program Office for Special Technology Countermeasures (JPO-STC) has established the Counter-Radio Frequency Program, which conducts studies to identify the susceptibility of military operations and their supporting military and civilian infrastructures based upon the potential presence of high power electromagnetic energy. From the standpoint that commercial buildings can act as barriers and significantly attenuate incident electromagnetic energy, it is important that this attenuation is quantified for specific buildings of interest. The results of this paper provides test results of an ongoing study to understand the electromagnetic response of commercial buildings and efforts to develop techniques to quickly evaluate the attenuation properties for a specific building. The electromagnetic attenuation of two large commercial buildings has been investigated. As a consequence of no noise generating devices being present (the buildings were unoccupied), ambient signals were used as the radiation source and procedures similar to those in IEC 61000-4-23. The measurements provide unique insight into the impact of the various building features on the propagation of the electromagnetic energy. This data forms the basis for a generic understanding of building attenuation based on its construction methods.

STATISTICAL CHARACTERIZATION OF VARIANCES IN
MODELING PARAMETERS FOR ELECTROMAGNETIC EF-
FECTS RESEARCH

Sessions, W.D., Baedke, W.C., Stoudt, D.C.

Naval Surface Warfare Center, Dahlgren Division, Code B20,
Dahlgren, VA

The Directed Energy Technology Office (DETO) at the Naval Surface Warfare Center Dahlgren Division (NSWCDD) is currently investigating the effects of high power microwave (HPM) / radio frequency (RF) attacks against electronic infrastructure. As part of this mission, computational and statistical models are being developed to predict the effects of such radiated fields. In order to successfully predict effects, one must attempt to quantify both numerical and experimental errors, which arise in such complex problems. In every computational model of a complex system, errors arise owing to (1) the discrete nature of the algorithm, (2) the detail of model in the simulation, and (3) the approximate values of material parameters being used in the simulation.

The first category of error can be mainly attributed to truncation error of the algorithm and sampling rates in both space and time. The second category is inherent in all complex systems since it is impossible to model every detail of every device in a complex system. Lastly, approximation must be made concerning the material properties of devices, building materials which house the electronics, and earth ground for examples.

The focus of this paper is to study the sensitivity of output from the finite-difference time-domain (FDTD) algorithm to variance in material parameters. Consideration will be given to a "generic" building of one level with concrete walls. The material properties and thickness of the concrete walls are used in the sensitivity study as variance parameters. The ranges for the properties/geometry are: (1) wall conductivity s_w (0.01 - 0.1 S/m), (2) relative wall permittivity ϵ_w (5.0 - 15.0), and (3) wall thickness L_w (+/- D_x , +/- $2D_x$).

The paper describes the sensitivity of the magnitude of the peak electric field, magnetic field, and energy density at various positions within the volume. Sensitivity of a statistical cumulative distribution function (CDF) of each of the previous quantities will also be presented for various regions of interest within the building volume and for the volume as a whole. The application of random (stochastic) process theory to the discrete time-domain functions is also investigated.

E1

Session F1, 9:00-Monday

**REMOTE SENSING OF THE
ATMOSPHERE, I**

Chairpersons: Al Gasiewski and Vallery Zavorotny

F1

ESTIMATION OF COUPLING BETWEEN MOBILE VEHICULAR RADARS AND SATELLITE RADIOMETERS

Gasiewski, A. J., Zavorotny, V. U.

NOAA Environmental Technology Laboratory, 325 Broadway MS
R/E/ET1, Boulder, Colorado, 80305 USA

It has recently been proposed by the automotive industry that wide-band vehicular collision avoidance radar be developed at a frequency centered at approximately 24 GHz. Coupling of emissions from such radar systems into passive microwave satellites can impart significant interference to earth remote sensing applications in the bands between 22 and 27 GHz, and in particular in the 23.6-24.0 band allocated on a primary basis to the passive Earth Exploration Satellite Service (EESS). One of the most obvious coupling mechanisms between mobile vehicular radar and a satellite radiometer is reflection of the main lobe of the radar by another directly-illuminated vehicle toward the main lobe of the radiometer. Since vehicular radars will commonly illuminate another close-in leading vehicle it is believed that such scattering scenarios will be commonplace.

In order to estimate the interference from a collection of such vehicular radars to a passive microwave satellite (such as the NOAA AMSU or future NPOESS ATMS and CMIS sensors) we performed both numerical simulations to determine the system coupling coefficient C_{sm} , defined as ratio of the angular power density at the radiometer for the reflected beam to the main lobe angular power density on the axis of the vehicular radar. The single reflection mechanism taken into account is that from the rear window of the leading vehicle, suspected to be the primary element that would provide interference at the angles of the radiometer receiving antenna.

The cases we consider show that reflection of radiation from vehicular radars from the rear windows of automobiles can impart a significant degree of coupling (-10 to -20 dB) with space-borne radiometers. Additional scattering can be expected from other nearby objects such as trees and the tilted roofs of buildings. Discussed will be the expected impact on satellite radiometry for weather and climate observation.

RADIOMETRIC IMAGING OF HYDROLOGICAL PARAMETERS DURING THE 2003 AMSR-E CALIBRATION AND VALIDATION FIELD CAMPAIGNS.

Klein, M.¹, Gasiewski, A.J.², Irisov, V.³,
Leuski, V.¹, Stankov, B.B.², Weber, B.W.⁴, Wick, G.A.²

¹CIRES University of Colorado, Boulder, Colorado

²NOAA Environmental Technology Laboratory, Boulder, Colorado

³Zel Technologies, Boulder, Colorado

⁴Science and Technology Corporation, Boulder, Colorado

The NOAA/ETL Polarimetric Scanning Radiometer (PSR) was recently used in several airborne experiments focused on calibration and validation of the AMSR-E sensor. AMSR-E is a Japanese passive microwave imaging radiometer on the NASA Aqua satellite, launched in May 2002. The PSR is the first airborne conically-scanned multiband polarimetric microwave imaging system. Owing to its conical scanning geometry and spectral coverage the PSR provides a unique means for polarimetric microwave imaging of water in various geophysical states (clouds/rain, sea ice, snowpack, and soil moisture).

The first experiment (Wakasa Bay, Jan-Feb 2003) occurred over the Sea of Japan and western Pacific Japanese coast with the purpose to study the impact of melting level on passive microwave rain signatures. Imaging occurred during flight lines crossing both maritime and orographic precipitation. Cases of both snow and moderate to light rain were observed with melting levels from the surface up to 8,000'. The Alaska sea ice experiment (AM-SRice03, March 2003) used two scanheads (PSR/CX and PSR/A) operating simultaneously, resulting in the first full polarimetric and spectral simulation of AMSR-E. Seven successful sea ice mapping missions were flown over a broad variety of ice classes with conditions ranging from open water to pack ice. The 2003 Cold Land Processes Experiments (CLPX03A, Feb 2003 and CLPX03B, March 2003) provided the first high spatial resolution (0.4 km) microwave imagery of snowpack in mountainous areas with observations occurring from the snowfall to melt stages. Inclusion of the PSR/CX scanhead for CLPX03B provided additional sensitivity to meltwater. The SMEX02 and SMEX03 experiments (June-July 2002 and 2003, respectively) used the PSR/CX for the first combined C- and X-band imagery of soil moisture in the presence of several types of vegetation canopies. Detailed spatial and temporal signatures of soil moisture variations were obtained on a 1-km spatial scale.

Presented will be an overview of the PSR as configured for the 2003 AMSR-E experiments and a summary of the potential of airborne microwave hydrological imaging.

PRECIPITABLE WATER VAPOR AND CLOUD LIQUID WATER RETRIEVAL FROM SCANNING MICROWAVE RADIOMETER MEASUREMENTS DURING THE 2003 CLOUDINESS INTER-COMPARISON EXPERIMENT

Mattioli, Vinia¹, Westwater, Ed R.²

¹DIEI-University of Perugia, via G. Duranti 93, 06125 Perugia, ITALY

²CIRES - University of Colorado/NOAA, 325 Broadway R/E/ET1, Boulder, CO 80305 USA

Ground-based microwave radiometers (MWR) are widely used to measure atmospheric Precipitable Water Vapor (PWV) and Cloud Liquid Water (CLW). Two dual-channel continuously scanning MWRs at 23.8 and 31.4 GHz were operated for two months (March and April 2003) during the Cloudiness Inter-Comparison Experiment (CIC IOP) at the Atmospheric Radiation Measurement (ARM) Programs Southern Great Plains site (SGP) in North-Central Oklahoma, USA. These scanning MWR measurements supplemented the operational SGP Central Facility MWR. The operational MWR scans continuously during clear conditions, but shifts to the zenith-viewing Line Of Site (LOS) mode, during cloudy conditions. One of the additional MWRs scanned continuously in the same vertical plane as that of operational unit, while the second was scanning in a direction orthogonal to the other two. The primary goal of this work is the analysis of the MWRs data to derive a spatial distribution of PWV and CLW in the atmosphere, with the aim of improving the accuracy of parameterizations describing processes involved in the formation and evolution of clouds. Data from the three radiometers were compared during clear sky condition to assess their agreement. Differences of less than 0.3 K rms were obtained. Clear conditions were determined by combined radar/lidar measurements. Two different tipping calibration algorithms were considered (the original ARM calibration algorithm and the ETL calibration method), during clear and cloudy conditions. We evaluated the two calibration methods on the brightness temperature measurements as well as on PWV and CLW retrievals. Brightness temperatures and PWV were also compared with radiosonde (RAOB) computations. The RAOBs contained the Vaisala RS90 humidity sensor, and were launched at least four times a day on the same site. PWV and CLW retrievals at each angle in presence of clouds were analyzed. We also compared the observed structures with optical and infrared cloud images, as well as ARM operational cloud boundary products.

DESIGN AND IMPLEMENTATION OF A MINIATURIZED
WATER VAPOR PROFILING RADIOMETER

Reising, S.C., Iturbide-Sanchez, F., Padmanabhan, S.

, Jackson, R.W.

Microwave Remote Sensing Lab, 113 Knowles Engineering Bldg.,
University of Massachusetts, Amherst, MA 01003 USA

In previous work we introduced the design and calibration of an innovative microwave radiometer design for profiling the water vapor density in the troposphere. At present, the vast majority of ground-based and airborne microwave remote sensing instrumentation is produced using waveguide-based or connectorized discrete microwave components. In contrast, commercially available microwave monolithic integrated circuits (MMICs) yield a higher level of integration, lower mass production costs, and generally higher reliability. The implementation of these technologies developed for the wireless communications and defense industries reduces this new radiometer's volume and weight by a factor of at least 25, and the parts cost by 5-10 times, as compared to a conventional waveguide-based radiometer. These reductions are expected to permit the deployment of a multi-station network of elevation scanning microwave radiometers for tropospheric water vapor profiling.

Currently, insufficient spatial and temporal sampling of wind, humidity and temperature observations in pre-storm environments limits improvement in forecasting precipitation and severe weather. Currently, measurements of precipitable water vapor in the troposphere are limited to twice-daily radiosonde launches, costly and limited clear weather lidar observations and networks of GPS receivers measuring wet delay to infer path-integrated water vapor. Measurements of the water vapor field at higher spatial and temporal resolutions, as well as 3-D variational assimilation into numerical weather prediction models, are needed to improve short-range forecasting. Networks of microwave radiometers for water vapor profiling, along with well-suited tomographic techniques, are needed to address these shortcomings.

This paper describes the design, testing and validation of a prototype Miniaturized Water Vapor Profiler for the 3-D measurement of tropospheric water vapor. The recently completed RF section, occupying a volume smaller than 50 cm³, and a matched antenna and IF section, are validated by viewing hot and cold reference blackbody loads in the laboratory. Then these subsystems are integrated with the data acquisition, thermal control and other electronics into a suitable outdoor enclosure. The complete radiometer will require only dc power and Ethernet external connections and have a volume one to two orders of magnitude smaller than conventional microwave radiometers. After demonstration and calibration of this prototype, several additional units will be fabricated to validate the use of a multi-station network for 3-D monitoring of the tropospheric water vapor.

THE NORTH SLOPE OF ALASKA ARCTIC WINTER RADIO-
METRIC EXPERIMENT

Westwater, Ed R.¹, Gasiewski, Albin², Klein, Marian¹
, Leuski, Vladimir¹

¹CIRES, University of Colorado/NOAA, 325 Broadway MS
R/E/ET1, Boulder, Colorado,80305 USA

²NOAA Environmental Technology Laboratory, 325 Broadway MS
R/E/ET1, Boulder, Colorado,80305 USA

Measurement of water vapor during the arctic winter is very difficult because uncertainties of radiosondes during these cold and dry conditions. Previously, at warmer locations such as the Department of Energy's Atmospheric Radiation Measurements(ARM) Program's field sites in Oklahoma and in the tropics, scaling of radiosonde measurements of water vapor profiles by microwave radiometer (MWR) precipitable water vapor measurements, has led to substantial improvements in water vapor measurements. However, due to the lack of sensitivity of conventional MWR's to low amounts of water vapor, say below 2 or 3 mm, it is difficult to achieve this scaling and/or the associated quality control checks on radiosonde data. We plan to conduct an Intensive Operating Period (IOP) at the ARM field site near Barrow, Alaska, during February-March 2004. The major goal is to demonstrate that millimeter wavelength radiometers can substantially improve water vapor observations during the Arctic winter. Secondary goals include forward model studies over a broad frequency range, demonstration of recently developed calibration techniques, the comparison of several types of in situ water vapor sensors, and the application of infrared imaging techniques. During this IOP, we plan to deploy radiometers over a broad frequency range (18 to 380 GHz), including several channels near the strong water vapor absorption line at 183.31 GHz. These radiometers will be supplemented by 4-times-a-day radiosonde observations and other in situ observations, including several "Snow White" Chilled Mirror radiosondes. The radiometers deployed will also be useful in measuring clouds during these cold conditions. Radiometers to be deployed include the Circularly Scanning Radiometer of ETL (several frequencies from 18 to 380 GHz), the MWR and Radiometric Profiler of ARM (frequencies from 22.235 to 60 GHz), a scanning 60 GHz radiometer from the Russian firm ATTEX. and an infrared imager operated by Montana State University. In addition, all of the ARM active cloud sensors (radar and lidars) will be operating.

DEVELOPMENT OF REMOTE-SENSING MICROWAVE RADIOMETER CALIBRATION METHODS AND TOOLS AT NIST

Walker, D.K.¹, Randa, J.¹, Billinger, R.L.¹, Cox, A.E.²

¹NIST RF Technology Division, Boulder, CO 80305

²NCAR Atmospheric Technology Division, and Dept. of Aerospace Engineering Sciences, U. Colorado, Boulder, CO 80307

The NIST Noise Project, in collaboration with the Antenna Theory and Applications Project, is developing tools to support cal/val requirements for existing and future microwave remote-sensing radiometers. Our emphasis is on providing fundamental measurement support based on standard antennas and primary standard noise sources. Referencing microwave remote-sensing radiometer calibrations to these standards will provide a long-term, stable basis for characterizing instrument accuracy and ensuring data integrity. Establishing traceability in remote-sensing measurements (and the uncertainty in these measurements) is a crucial component in meeting the performance specifications and goals for systems such as NPP and NPOESS. Four broad, overlapping areas of current and planned research and development are:

1. Standard radiometers, covering frequencies up to 65 GHz. The approach will combine existing NIST waveguide and coaxial radiometers, calibrated with primary noise standards, with well-characterized antennas to transform them into standard remote-sensing radiometers.
2. Portable standard calibration targets, covering frequencies up to at least 65 GHz and possibly extending up to 110 GHz. A critical component of designing and building these targets is understanding and characterizing their microwave properties as well as thermal properties.
3. Uncertainty analyses and specifications. This includes several specific topics: (a) General uncertainty analysis for total-power microwave radiometers based on the comprehensive uncertainty analyses performed on NIST's laboratory radiometers used for noise source calibrations. A representative radiometer (or class of radiometers) will be analyzed as a starting point, with extensions made to accommodate other practical instruments; (b) Measurement-based method for evaluating effect of video detector nonlinearity on measured brightness temperature (T_B) uncertainty; (c) Measurement-based method for evaluating effect of calibration target reflectivity on T_B uncertainty.
4. Standard terminology "dictionary" for microwave remote-sensing radiometry. Along with other advantages, this formalism is a necessary prerequisite to developing comprehensive, unambiguous uncertainty statements. The current list is at <http://www.boulder.nist.gov/div813/stdterms/>.

Early results from some of these efforts will be presented in the talk.

Session F2, 14:00-Monday

**REMOTE SENSING OF THE
ATMOSPHERE, II**

Chairpersons: E. Westwater and R. Doviak

SMALL-SCALE INTERMITTENCY IN THE MIXED LAYER
OBSERVED WITH A VOLUME-IMAGING UHF RADAR
WIND PROFILER

A. Muschinski¹, P. Lopez-Dekker², S. J. Frasier²
, P. B. Chilson¹

¹CIRES, University of Colorado, and NOAA Environmental Technology Laboratory, Boulder, CO

²Microwave Remote Sensing Laboratory, University of Massachusetts, Amherst, MA

For many years, it has been known that in high Reynolds number turbulent flows, the local energy dissipation rate, ε_r , varies randomly in time and space, in contrast to classical turbulence theory where random fluctuations of ε_r are ignored and the energy dissipation rate is treated as a deterministic control parameter. The randomness of ε_r , often referred to as small-scale intermittency, increases with decreasing r , the linear size of the local averaging volume. According to Kolmogorov's (1962, *J. Fluid Mech.*, **13**, 82ff.) famous hypothesis, ε_r is lognormally distributed, and the variance of the *logarithm* of ε_r increases linearly with $\ln(L/r)$,

$$\sigma_{\ln \varepsilon_r}^2 = A + \mu \ln \frac{L}{r}, \quad (1)$$

where L is the outer scale of turbulence, and the "intermittency exponent" μ is a universal constant. A may depend on the macrostructure of the flow. Later, the lognormality hypothesis was extended to local passive scalar variance dissipation rates (e.g., Antonia and VanAtta, 1975: *J. Fluid Mech.*, **67**, 273ff.) and to local turbulence structure parameters (e.g., Frehlich, 1992: *J. Atmos. Sci.*, **49**, 1494ff.). Overall, mainly on the basis of high-resolution point measurements, these lognormality hypotheses have been shown to describe small-scale intermittency quite accurately.

The University of Massachusetts' Turbulent Eddy Profiler (TEP), a unique 915-MHz, multi-receiver, interferometric boundary-layer radar wind profiler, is capable of volume-imaging ε_r and $(C_n^2)_r$ (the local refractive-index structure parameter) quasi-instantaneously (dwell time as short as 1 s) and simultaneously in as many as 144 beam directions with a "pixel" size r of about 30 m. Individual and joint statistics (probability densities, spatial structure functions, frequency spectra) of ε_r and $(C_n^2)_r$ observed with TEP in the mixed layer at altitudes between 200 m and 1000 m are presented and compared against the lognormality hypotheses.

ANGULAR INTERFEROMETRY TO SHARPEN A BEAM

Guifu Zhang¹, Tian-You Yu², Richard J. Doviak³¹National Center for Atmospheric Research, Boulder, CO 80307²University of Oklahoma, Norman, OK 73019³National Severe Storms Laboratory, Norman, OK 73069

The resolution volume of weather radars is generally determined by beam and pulse widths and the angular rotation rate of the antenna. With a focal point feed reflector antenna there is no way to decrease the beam width beyond that obtained with a uniformly illuminated reflector that is not scanning. Recently, we developed a single antenna interferometric technique to measure cross beam winds using angular interferometry and radial wind using range interferometry. Presently used interferometric measurements of cross beam winds require at least three receiving antennas. Interferometry with a single antenna cross-correlates signals from partially overlapped resolution volumes to obtain cross beam and radial wind measurements. In this paper, we apply and illustrate how angular interferometry is used to sharpen a beam.

The angular interferometry technique for beam sharpening is based on the fact that cross-correlation functions of signals from two overlapping resolution volumes are due only to echoes from scatterers within the shared volume. Therefore, all the radar measurements (e.g., Doppler velocity, reflectivity, etc.) derived from cross-correlation estimates are associated with scatterers within the shared volume rather than those within the resolution volume of the uniformly illuminated aperture. Furthermore, if the main lobe can be split, the width of each lobe is less than the width of the unsplit beam. Beam splitting can be achieved with phased array weather radars, such as that being developed at the National Severe Storms Laboratory. By displacing the pair of split beams to two angular directions so there is overlap of one beam of the pair, and cross correlating the signals received from the two directions, we obtain significant cross-correlation from only that region where the beams overlap. We illustrate the technique using wave scattering from randomly distributed scatterers and demonstrate, using simulations, the increase in angular resolution that can be achieved.

COMPARISON OF DOPPLER BEAM SWINGING AND
SPACED ANTENNA RADARS FOR WIND MEASUREMENT;
THEORY

Doviak, R. J.¹, Zhang, G.², Cohn, S. A.³, Brown, W. O. J.⁴

¹National Severe Storms Laboratory, 1313 Halley Circle, Norman,
OK 73069

²NCAR/RAP, P. O. Box 300, Boulder, CO 80516

³NCAR/ATD, P. O. Box 300, Boulder, CO 80516

⁴NCAR/ATD, P. O. Box 300, Boulder, CO 80516

The Doppler Beam Swinging (DBS) method is the most common approach to obtain vertical profiles of wind in the lower atmosphere. In this method, horizontal wind components are calculated from measurements of the Doppler shifts usually along a pair of beams sequentially pointed in the plane of the wind component (e.g., a vertical and eastward tilted beam for the easterly wind component). Spaced Antenna (SA) interferometry is an alternative method whereby vertical profiles of the wind components are obtained simultaneously along a vertically directed transmitting beam. Typically three or more spaced receiving antennas, with vertically directed beams, share the transmitting antenna aperture.

Given identical antenna size, transmitted power, and receiver performance, a theoretical comparison the accuracy of wind measurements with the DBS and SA methods is made under the condition that both have the same spatial and temporal resolution. The theory assumes that the wind is uniform within the resolution volume during the time of measurement, and that noise power from each of the receivers is white and uncorrelated. Turbulence is assumed to be uniformly distributed across the resolution volume and statistically stationary. We develop the theory to calculate the variance and covariance of the various measured parameters that are subjected to the statistical fluctuations inherent in the observations of a distribution of scatterers randomly moving within the resolution volume. We relate the accuracy of wind measurements to the accuracy with which we can measure the cross- and auto-correlation functions. It is shown that under conditions of large Signal to Noise Ratio (SNR), the SA profiler has superior performance for all levels of turbulence and wind, but under conditions of low SNR the DBS profiler can outperform the SA profiler.

GEOSYNCHRONOUS MICROWAVE (GEM)
SOUNDER/IMAGER OBSERVATION SYSTEM SIMULATION

Gasiewski, A. J.¹, Voronovich, A.¹, Weber, R. L.¹,
Stankov, B. B.¹, Klein, M.¹, Leuiski, V.², Bao, J. W.¹

¹NOAA/Environmental Technology Laboratory, 325 Broadway,
Boulder, CO USA

²University of Colorado/NOAA-CIRES, 325 Broadway, Boulder,
CO USA

Passive microwave sounding and imaging from geosynchronous orbit was first studied in the mid-1970s, although initial proposals using microwave channels at 183 GHz and lower frequencies required prohibitively large antennas. In 1992 it was proposed that submillimeter-wavelength channels could be used for many of the sounding and cloud/precipitation imaging applications that previously were believed to require the use of microwave channels. The capabilities of submillimeter-wave channels for precipitation imaging were further demonstrated in 1994 using airborne imagery of clouds at the 325 GHz water vapor band. These studies suggested that the antenna costs for geosynchronous microwave precipitation imaging and temperature and moisture sounding could be significantly reduced while retaining good spatial resolution by using key submillimeter-wavelength water vapor and oxygen bands. It was with this notion that the Geosynchronous Microwave Sounder Working Group (GMSWG) was convened to develop a model for a practical submillimeter-wave geosynchronous microwave (GEM) sounder and imager. The current GEM concept is based on a 2-3 meter center-fed reflector antenna and fast-scanning subreflector. The subreflector provides a narrow-field rapid scan capability with a wide-field scan provided by a slower motion of the entire antenna. As a result GEM will be capable of either intensively observing specific areas near severe weather or obtaining synoptic information over an extended environment. In this study we illustrate the precipitation retrieval capabilities of GEM using an observation system simulation for a landfalling hurricane event (Hurricane Bonnie, August 1998). The system simulations are based on 6-km resolution, 60-level microphysical cloud data obtained from MM5 model runs for Hurricane Bonnie using the Reisner five-phase microphysical cloud model. A unique fast forward radiative transfer model based on the discrete-ordinate (DO) method and incorporating both scattering effects and fast calculation of the Jacobian of the forward transfer model is used to compute observed brightness temperature fields and their derivatives. Discussed will be the potential accuracy of rain rate and cloud liquid and ice water content retrievals, along with the impact of numerical weather model (NWP) phase-locking on retrieval accuracy. Phase-locking of an NWP onto the atmospheric state is facilitated using GEM rapid-update microwave imagery. Results from the observation system simulations and a program of concept validation using an airborne GEM simulator will be presented.

EVALUATION OF A RADIOMETRIC PHASE RETARDATION PLATE USING PLANAR NEAR-FIELD MEASUREMENTS

Guerrieri, J. R., Mac Reynolds, K., Tamura, D. T.
National Institute of Standards and Technology

The National Polar-orbiting Operational Environmental Satellite System (NPOESS) will be the nations next-generation environmental monitoring system. Polar orbiting satellites will gather environmental information and download it to a global array of earth stations. This data will be accessible to authorized; scientists, forecasters and the military in less than 30 minutes. The NPOESS program is managed by the Integrated Program Office (IPO) a joint effort of the Department of Commerce (DoC), Department of Defense, and the National Aeronautics and Space Administration (NASA).

Currently air borne radiometers are used for remote environment sensing. Radiometers have become a very useful tool for atmospheric remote sensing. They are preferred over infrared and visible observation because of their ability to probe through optically opaque cloud cover and aerosols. They provide data on snow and ice cover, sea surface temperature and wind, soil moisture, vegetative biomass, precipitation, cloud liquid-water content, and temperature and water-vapor profiles.

Radiometers will be part of the vast number of sensors used on the NPOESS program. The National Oceanic and Atmospheric Administration (NOAA), an agency of DoC, is working to improve the measurement uncertainty of polarimetric radiometers through better calibration procedures.

Using both linearly and circularly polarized components the polarimetric radiometer can determine the speed and direction of maritime winds. A phase retardation plate is used to calibrate the polarimetric radiometer. The plate generates a predetermined phase shift ($\pi/8$) between the perpendicular field components of the transmitted waves. The plate is a lens fabricated from a slab of cross-linked polystyrene with parallel grooves machined on both sides of the lens. Verification of the phase shift is necessary to improve the polarimetric radiometer calibration procedure.

The National Institute of Standards and Technology (NIST), another agency of DoC, characterized three phase retardation plates for NOAA using the planar near-field antenna measurement technique. Plate 1 is designed to generate a phase shift of $\pi/8$ at 18.7 GHz, and Plates 2 and 3 introduce phase changes of $\pi/8$ at 10.7 GHz.

RAPID CALCULATION OF INCREMENTAL BRIGHTNESS PROFILES

Voronovich, A. G., Gasiewski, A. J., Hill, R. J. , Weber, R. L.

NOAA Environmental Technology Laboratory, 325 Broadway MS
R/E/ET1, Boulder, Colorado, 80305 USA

Assimilation of microwave radiometric data from satellite- and airborne sensors under all weather conditions is an important challenge in numerical weather prediction. Microwave radiances upwelling from the atmosphere depend strongly on frequency and carry a wealth of information on moisture and temperature profiles as well as clouds, rain, and surface parameters. Brightness temperatures generally depend on the electromagnetic scattering properties of hydrometeors through a well-described process. Statistically optimal retrieval of the environmental parameters requires accurate calculation of the derivatives of the brightness temperature with respect to all atmospheric and surface parameters. To accommodate the dense data stream from modern passive microwave satellites one requires calculations times of 0.1 msec per profile or less. In our approach the differential radiative transfer equation (RTE) for a planar stratified medium is used to model processes of emission and absorption by gases and particles as well as scattering by particles. Symmetry properties of scattering are very essential for building a fast solution, and the RTE is first cast into an explicitly symmetric form. Each layer is characterized by transmittance and reflection matrices that provide a complete description its interaction with other layers. Accurate and stable calculation of those operators for arbitrary layer parameters is a non-trivial task since the opacity and scattering coefficients vary over a wide range. Moreover, the layer can be fairly transparent at steep incident angles and opaque at grazing angles. Computationally, this problem requires inversion of ill-conditioned matrices. We solve the inversion problem by first analytically factoring the matrix to be inverted into a product of five matrices. Four of them are regular, and only one diagonal matrix remains ill-conditioned. After explicit inversion the result includes only benign matrices and works well in all cases. Once the transmittance and reflectance operators for all layers are known, the overall brightness temperature field is built using the method of slab doubling via two profile sweeps. Calculation of incremental profiles generally requires only one extra sweep. Thus, the number of operations required is directly proportional to the number of layers. This talk will present the above algorithm in the context of test data generated for a simulation of Hurricane Bonnie (1998). Methods for acceleration of the algorithm for low-albedo layers and connections between the radiative parameters of the atmosphere and prognostic variables of numerical weather models will be discussed.

Session F3, 14:00-Tuesday

**REMOTE SENSING OF THE
EARTH'S SURFACE**

Chairpersons: S. Reising and E. Bahar

REPRODUCIBLE BREAKING WAVES AND CORRELATION WITH IN-SITU FOAM MEASUREMENTS

Padmanabhan, S.¹, Reising, S.C.¹, Asher, W.E.²,
Rose, L.A.³, Gaiser, P.W.³

¹113 Knowles Engineering Bldg., Microwave Remote Sensing Laboratory, University of Massachusetts, Amherst, MA 01003, USA

²Applied Physics Laboratory, University of Washington, 1013 NE 40th Street, Seattle, WA 98105-6698, USA

³Naval Research Laboratory 7223, Washington DC 20375, USA

The principal goal of WindSat, launched on January 6, 2003, is to demonstrate reliable global retrieval of both wind speed and direction using microwave radiometric measurements. Both aircraft measurements and modeling results indicate that wind directional signals are small, on the order of 1-3 K peak-to-peak in brightness temperature. Accurate wind vector retrieval requires quantitative understanding of the dependence of ocean surface emissivity on surface roughness and foam due to breaking waves.

Our recent observations from the R/P FLIP during the Fluxes, Air-Sea Interaction and Remote Sensing (FAIRS) Experiment on the open ocean showed that the increase in brightness temperature due to wave breaking varies as the wave evolves in time, and is dependent on radiometer polarization and viewing angle. However, the inherent intermittency and relative sparseness of breaking waves makes it very difficult to perform repeatable measurements of this process on the open ocean.

Mechanically generated waves in a salt-water basin were made to break at the same location using a specially designed shoaling beach. Passive polarimetric measurements of microwave emission were performed at WindSat frequencies of 10.8, 18.7 and 36.5 GHz, at incidence angles of 45°, 53° and 60°, each at four azimuth angles from 0° to 180°. The beam fill fraction of the foam produced by the breaking waves was estimated using a video camera bore-sighted with the radiometers. Void fraction probes and an underwater camera were used to measure the amount of entrained air and the bubble size spectrum, and pressure transducers measured the surface height of the large-scale waves.

This experiment was conducted to determine the azimuthal dependence of the microwave emission due to wave breaking. Results show that the change in the measured microwave brightness temperatures was well correlated with the foam fraction in the field of view, but this strongly depends upon the azimuthal look angle, due to viewing different facets of the partially foam-covered water surface. In the future, these radiometric and in-situ foam measurements can be compared with those from breaking waves observed in the open ocean.

ACCURATE CALIBRATION OF GROUND BASED MICROWAVE RADIOMETERS USING EXTERNAL AND INTERNAL REFERENCES

M. A. Aziz, S. C. Reising, E. J. Knapp

Microwave Remote Sensing Laboratory, 113 KEB, University of Massachusetts, Amherst, MA 01003-4410, USA

To perform near ocean-surface measurements in order to obtain a better understanding of how ocean surface parameters such as surface roughness, surfactants and foam due to breaking waves affect microwave emission, a Ka-band (37 GHz) Polarimetric Radiometer (KaPR) was fabricated at the Microwave Remote Sensing Laboratory (MIRSL) at the University of Massachusetts Amherst. This paper reports a new combined external and internal calibration technique developed to calibrate radiometric measurements with high accuracy.

Microwave radiometers are typically calibrated using two reference sources at widely separated temperatures. For external calibration, an ambient load consisting of a blackbody microwave absorber is used as a hot reference source. A cold reference is obtained by viewing the sky at a series of zenith angles and extrapolating to the equivalent of zero atmospheres, often called a tipping curve or tipcurve. Two new quantitative measures of tipcurve usefulness for calibration were developed to determine the instrument temperature stability and atmospheric conditions required for high calibration accuracy.

It is often impractical to perform external calibration frequently enough to compensate for the radiometer's gain variation. To correct for short-term gain variation between external calibrations, a combined calibration technique was developed, in which an internal reference noise source and a matched load reference are used as the two reference sources for internal calibration. The noise source was determined to be stable except for temperature variations, which were measured accurately and compensated reliably. Internal calibrations were performed at a selected interval to correct system gain variations.

The Polarimetric Emissivity of Whitecaps EXperiment (POEWEX) was focused on measuring the microwave emissivity of reproducible breaking waves. Improvement in the accuracy of calm water measurements performed during POEWEX using the combined external/internal calibration technique, as compared with external calibration alone, was demonstrated by comparing these measurements with a number of calm water emission models. Recalibration of the tipcurve measurements using the new calibration technique resulted in substantially improved values of the two quantitative measures of tipcurve quality.

AIRBORNE POLARIMETRIC SCANNING RADIOMETER
(PSR) MEASUREMENTS OF SNOW COVER PROPERTIES

B. Boba Stankov¹, Albin J. Gasiewski¹, Bob L. Weber²
, Marian Klein³, Richard Kelly⁴, Don Cline⁵ , Gary A. Wick¹

¹NOAA/Environmental Technology Laboratory ,

²Science and Technology Corporation and NOAA/ETL, Boulder,
CO, USA

³NOAA/ETL - University of Colorado CIRES, Boulder, CO USA

⁴NASA/Goddard Space Flight Center Hydrological Sciences
Branch, Greenbelt, MD, USA

⁵NOAA/NWS/ National Operational Hydrologic Remote Sensing
Center, Chanhassen, MI, USA

Multispectral polarimetric microwave brightness temperature maps of snowpack in the Colorado Rocky Mountains were obtained using the NOAA Polarimetric Scanning Radiometer (PSR) during three Cold Land Processes Experiment (CLPX) missions in February 2002, February 2003, and March 2003. CLPX is NASA-funded multi-year experiment to study remote sensing of winter snow pack properties on the Colorado side of the Rocky Mountains. The PSR CLPX data offers unique high-resolution information about snow extent, polarimetric emissivity, and snow water equivalent at scales commensurate with natural inhomogeneities in terrain, vegetation cover, and precipitation patterns. The current PSR/A system includes a scanhead capable of providing imagery at most of the AMSR-E imaging bands, i.e. at 10.6-10.8, 18.6-18.8, 21.4-21.7, 36-38, and 86-92 GHz. In addition, 9.6-11.5 um IR channel is included.

During February-March, 2002 the PSR/A scanhead was flown on the NASA DC-8 aircraft (N717NA) and during the two February-March, 2003 missions the PSR/A was flown on NASA P-3 aircraft. The PSR/A was operated in conical scanning mode at low altitude (~2km AGL) to provide multi-band microwave imagery over dry mid-season snow and during the onset of snow melt in Colorado with spatial resolution of 140 and 500 m for high and low frequencies respectively.

We present multiband polarimetric snow microwave images over the three CLPX mesocell study areas (MSAs) in the AMSR-E bands. We relate the microwave brightness temperature to the physical snowpack quantities, particularly snow water equivalent (SWE). Comparisons of the PSR/A-derived SWE with the in situ measurements, gamma observations, and AMSR-E measurements are presented. In addition, we show that the brightness temperature associated microwave emissivity variations are up to 20-25%.

AIRBORNE ELECTROMAGNETICS FOR SALINITY MAPPING AND BATHYMETRY IN AUSTRALIA

James Macnae
RMIT University

Airborne electromagnetic (AEM) surveying is finding extended usage for mapping shallow conductivity associated with rising dryland salinity in Australia. Most AEM systems have been developed for 'deep' mineral exploration applications. As a result, their bandwidth is usually not high enough for sounding in the top few metres, nor is their calibration and waveform stability adequate for accurate depth and conductivity structure estimation.

Several methods exist for transformation of measured data, whether collected in time- or frequency-domain, into 2D conductivity-depth structures. These methods generally 'stitch' together 1D solutions obtained by processing on a sample by sample basis. The processing methods include inversion (Oldenburg et al., *The Leading Edge*, 17, 461, 1998) and faster approximate imaging methods (Macnae et al., *Three-Dimensional Electromagnetics*, SEG, 489-501). Inversion may take about one week of processing per day of flying on a typical workstation, and the result is strongly dependent on a-priori constraints such as starting models and the number of layers in the 1D model. The Maxwell receding image technique, first described by Macnae and Lamontagne (*Geophysics*, 52, 545-554, 1987) is about 100 times faster than stitched 1D inversions.

Research is progressing into methods to make the fast and approximate imaging methods sufficiently accurate for useful salinity mapping with standard AEM systems in the top 10 metres of the earth. To achieve the quantitative accuracy requirements, novel in-flight calibration techniques have been developed and tested; with simultaneously measuring currents induced in a known multiturn loop of wire laid out on the ground as the AEM system flies overhead. The results of improved calibration are assessed with known conductivity structures. These known structures have included sections based on borehole conductivity logs, collected as part of routine salinity assessments. However, the most extensive checks on system veracity have come from the bathymetric mapping of shallow seawater where both seawater conductivity and acoustic depth soundings were available for comparison with the predictions from AEM surveys.

SEASONAL POLARIMETRIC MEASUREMENTS OF SOIL MOISTURE USING GROUND-BASED GPS BISTATIC RADAR

Zavorotny, V.¹, Masters, D.², Gasiewski, A.¹
, Bartram, B.¹, Katzberg, S.³, Axelrad, P.², Zamora, R.¹

¹NOAA/Environmental Technology Laboratory, 325 Broadway, Boulder, CO

²CCAR/University of Colorado at Boulder, CB 431, Boulder, CO

³NASA Langley Research Center, Code 328, Hampton, VA

The results of GPS L-band (L1, 19 cm) surface reflection measurements observed using multiple polarizations and receiving antenna gains are described. The measurements were performed using the 300-m tall ETL Boulder Atmospheric Observatory (BAO) Tower during summer through fall of 2002. In this experiment the first seasonal measurements of bare soil moisture from a stationary location using bistatic reflection of signals of opportunity were studied using several receiving antennas offering various gain and polarization sensitivities. Theoretical modeling of the bistatic surface scattering process shows that the magnitude and pulse-width of the reflected waveform depends on the dielectric permittivity of the soil, vegetation cover, and the soil roughness. By observing from a fixed tower over low grass the roughness of the reflecting area remains constant, hence variations in the signal are uniquely related to changes in the dielectric permittivity and therefore, to soil moisture. Using the BAO data we demonstrate a technique to uncouple the effects of dielectric permittivity and surface roughness in soil moisture retrievals. The technique assumes the received signal to be proportional to the product of two factors: a polarization sensitive factor dependent on soil dielectric properties and a polarization insensitive factor dependent on surface roughness. The ratio of averaged signal powers received in two orthogonal polarizations thus tends to exclude the surface roughness factor (together with variations in illuminating power) while retaining the soil moisture signal. The ratio signal also rejects Rayleigh fading, thus permitting a reduction in incoherent averaging time and improvement in spatial resolution. To investigate this approach four endfire (12 dB gain) antennas with complete circular and orthogonal polarization sensitivity were used. The high-gain antennas increased the receiver dynamic range and reduced surface multipath radio wave interference. Seasonal retrievals of soil-moisture content from multi-polarization GPS reflection data will be presented and compared with in-situ soil moisture measurements. The ultimate sensitivity of the method and its implications for soil-moisture measurement using an airborne GPS bistatic system will be discussed.

POLARIZATION DEPENDENT BACKSCATTER CROSS SECTIONS OF COMPOSITE RANDOM ROUGH EARTH SURFACES USED TO DETERMINE SOIL MOISTURE CONTENT

Bahar, E

University of Nebraska-Lincoln

Polarization dependent backscatter cross sections of composite random rough surfaces, excited at normal to near grazing incidence, are analyzed. A unified full wave approach is used to express the backscatter cross sections as weighted sums of two cross sections. The first, which is associated with the larger scale rough surface height, is reduced by a factor equal to the magnitude square of the characteristic function for the smaller scale surface. The second which is associated with the smaller scale surface height, is modulated by the slopes of the larger scale surface. The sum is shown to be stationary over a wide range of slopes associated with the larger scale surface.

This work impacts on the feasibility of remotely sensing soil moisture content. In the very small height/slope perturbation limit and the high frequency physical/geometrical optics limit, the ratio of the vertically polarized and the horizontally polarized backscatter cross sections is independent of the characteristics of the surface roughness and dependent only on the incident angle and the soil permittivity. Thus for these cases, it is possible to extract the soil moisture content (related to the permittivity) from measurements of the backscatter cross sections without involving the characteristics of the rough surface. However for the general case, the characteristics of the rough surface do not factor out of the expression for the ratio of the two polarization dependent cross sections. Thus it is important to extend this work to cases in which the rough surface characteristics cannot be ignored. The unified full wave approach can be used for this purpose.

Session F4, 9:00-Wednesday

**PROPAGATION AND
SCATTERING EFFECTS OF
SURFACE VEGETATION**

Chairpersons: R. Lang and S. Saatchi

TOTAL ATTENUATION THROUGH A TWO-DIMENSIONAL TRUNK DOMINATED FOREST

Saul A. Torrico¹, Roger H. Lang²

¹Andrew Corporation, Ashburn, VA 20147

²Department of Electrical and Computer Engineering, The George Washington University, Washington, DC 20052

In this paper the attenuation of radio waves in a trunk dominated forest is studied by means of the radiative transport equation and a high frequency forward scattering approximation. The two methods are compared.

A vertically polarized plane wave is assumed normally incident on a half space of parallel lossy dielectric cylinders having random location. This model simulates propagation of radio waves through a trunk dominated forest. The radiative transport equation is solved for the specific intensity in the forest medium. The phase function appearing in the transport equation is obtained from the bistatic scattering amplitude of a dielectric cylinder and is valid for both low and high frequencies. The transport equation is solved numerically by the eigenvalue technique. The solution is used to compute both the coherent and the incoherent attenuation constants in the forest. It is shown that the total attenuation has the characteristic two-slope behavior as a function of distance in the forest. The shape of this attenuation curve is examined as a function of frequency. Also, it is shown the increase in the amount of forward scattering as the optical depth increases for a fixed frequency.

The attenuation in the forest is also found by a forward scattering approximation when the wavelength of the incident radiation is small compared to the trunk diameter. The approximation is implemented by approximating the phase function by a delta function in the forward direction. The total attenuation obtained by this technique is compared to the exact transport approach and its region of validity is determined. The absence of an attenuation curve with a two-slope behavior in the forwarding scattering result is discussed.

APPLICATION OF P-BAND SAR IN TROPICAL FORESTS:
FOLIAGE PENETRATION AND STRUCTURAL SCATTER-
ING

Sassan Saatchi

Jet Propulsion Laboratory, 4800 Oak Grove Drive, Pasadena, CA
91109

Mapping forest types and estimating their structural attributes is the first step to understanding the distribution of forest above ground biomass and carbon content in tropics. Synthetic Aperture Radar (SAR) backscatter measurements at P-band frequency over tropical forests have shown less sensitivity to structural variations in old growth forests and therefore, limitations for biomass estimation. In this study, we present a physically based model approach in simulating the foliage penetration and scattering of various forest structural components. Dominant scattering mechanisms controlling the SAR polarimetric measurements have been modeled using wave theory and ray tracing approach and structural data collected from field surveys. The forest canopy heterogeneity is included in the model by introducing analytical expressions for the crown size and shape, gap geometry, and the canopy roughness. The addition of these elements in the model will allow a more realistic simulation of radar backscatter from forest canopies. Radar data from intensely studied sites within the Amazon basin are chosen to examine the performance of the model and to analyze its behavior in terms of forest structural parameters such as basal area, height, vertical distribution of leaf area, and the above ground biomass. Once the significance of structural parameters and their contributions to dominant scattering mechanisms are determined, the model results are compared with P-band SAR measurements from AIRSAR data over three sites within the Amazon basin. Scenarios for estimation of the above ground biomass are discussed in terms of the model and measurement results and uncertainties are compared with direct ground measurement.

A COMPARISON OF VEGETATION PARAMETER EXTRACTION FOR DIFFERENT VEGETATION AND TERRAIN TYPES USING THE GEOSAR MAPPING INSTRUMENT

Scott Hensley, Ernesto Rodriguez, Paul Siqueira
Jet Propulsion Laboratory

GeoSAR is a dual frequency (X-band and P-band) interferometric mapping radar designed for mapping in vegetated regions. The system is flown on a Gulfstream II aircraft and simultaneously maps 10 km swaths on both sides of the aircraft at both frequencies with a mapping resolution better than 1 m. Using a combination of P-band signals that penetrate deeper into the canopy and X-band signals that map closer to the top of the canopy the goal of the GeoSAR system is to estimate tree height and map the ground surface beneath the vegetation. Both the X-band and P-band height measurements and vertical structure inferred from the interferometric correlation, a measure of the similarity of the returned signal received at the two antennas forming the interferometer, are used to derive vegetation parameters. Radar data along with associated ground truth data including lidar and other in situ measurements were collected for several vegetation and terrain types. Sites included coniferous forest stands in California and Arizona and deciduous vegetation at Camp Lejeune and Duke Forest on the eastern coast of the United States. This talk will present results associated with vegetation parameter estimation (in particular the tree height) for different vegetation and terrain types. Our results indicate the ability to estimate tree height for a variety of different canopy types using interferometric correlation data and that the P-band penetrates nearly to the ground surface in moderately sloped terrain. For steeper slopes the double bounce effect is lost and the P-band height measurements migrate higher into the canopy.

THE EFFECT OF LEAF CURVATURE IN ACTIVE ELECTRO-MAGNETIC MODELING OF CORN CANOPIES

Utku, C.¹, Lang, R.H.¹, O'Neill, P.², Tsegaye, T.³, Seker, S.S.⁴

¹Dept. of Electrical and Computer Engineering, George Washington University, Washington, D.C., USA

²Hydrological Sciences Branch/Code 974, NASA, GSFC, Greenbelt, MD, USA

³Dept. of Plant and Soil Sciences, AM University, Huntsville, AL, USA

⁴Dept. of Electrical and Electronics Engineering, Bogazici University, 80815, Istanbul, Turkey

This paper describes the modeling of radar backscatter from a corn canopy with curved leaves. This is an extension of a model that was previously employed where flat elliptical disks were used to represent leaves and finite cylinders were used to represent stalks. For a given polarization one can find a convenient set of canopy parameters for which the flat leaf model yields results that match with radar field measurements. However, this set of canopy parameters generally results in a data mismatch for the other polarization. Simulations have shown that the leaves play an important part in this mismatch, that is, suitable leaf configurations can be used to minimize the mismatch. This has led to the conclusion that better modeling of the leaves can yield better matching results with data for both polarizations.

The corn canopy model employed in this study incorporates the distorted Born approximation, where the particles (leaves and stalks) are assumed to be embedded in an effective medium. The leaves are assumed to have an azimuthally symmetric distribution in this medium. The effect of leaf curvature has been taken into account by dividing the leaves into facets and coherently adding the scattered field from each facet.

During the Huntsville98 experiment conducted in conjunction with the Center for Hydrology, Soil Climatology and Remote Sensing at the Alabama AM University, Huntsville, AL in June, 1998 and the OPE3 experiment between May and September, 2002 at Beltsville, MD extensive radar backscatter and ground truth data (including soil moisture and detailed plant geometry data) have been collected. The ground truth data have been used in both the flat and curved leaf models and comparisons with the actual radar backscatter data will be discussed. In addition, to reduce the complexity of the curved leaf model, the possibility of an equivalent distribution with flat leaf model yielding results close to the curved leaf model has also been investigated.

EFFECTS OF ODD-PINNATE COMPOUND LEAVES IN EM SCATTERING FROM VEGETATION

Huang, E. X., Fung, A. K.

EE Dept. Box 19016, University of Texas at Arlington, Arlington, TX 76019

Most existing EM scattering models for a vegetation medium assume that the leaves have an orientation distribution and each leaf scatters independently. For vegetations that possess compound leaves (for example leaves of a walnut tree) such an assumption is generally not valid. For this type of vegetation the leaves scatter in groups and it is each group, instead of each leaf, that scatters independently. An individual group of leaves scatters mostly coherently with a small degree of randomness in the spacing between leaves. The traditional radiative transfer approach can still be used but its phase function must be computed for a group of leaves patterned in accordance with the particular type of vegetation. To account for this group scattering effect for vegetation with odd-pinnate compound leaves we use a generalized antenna array theory. The group of leaves will be expressed as the product of a single leaf and an array factor. The corresponding power expression is averaged over the spacing between leaves which has a mean value and a random component. The vegetation medium is modeled as a half-space of randomly distributed and oriented odd-pinnate compound leaves. Theoretical analyses of the effects of the odd-pinnate compound leaves on the backscattering coefficient due to leaf size, spacing between leaves, total number of leaves in a compound and frequency are carried out. It is found that the array factor or the coherence induced by the odd-pinnate-compound leaves is important for vegetation media with a compound leaf structure, especially when the size of leaves and the average spacing between adjacent leaves in the compound are comparable to the incident wavelength. Finally, the model predication is compared with measurements from walnut trees where such a group scattering effect is expected.

Session F5, 14:00-Wednesday

PROPAGATION MEASUREMENTS

Chairpersons: K. Chamberlin and S. Burk

ESTIMATING ATMOSPHERIC EFFECTS ON RADAR PERFORMANCE IN LITTORAL REGIONS

Andrew J. Moys¹, Kenneth L. Davidson², Paul A. Frederickson²¹Fleet Numerical Meteorology and Oceanography Center, Monterey, CA²Dept. of Meteorology, Naval Postgraduate School, Monterey, CA

This study examines how well surveillance radar (S- and X-Band) performance in the littoral region can be estimated using currently available measurement technology and propagation models. The coastal zone region studied was off the US East Coast, at Wallops Island, VA, in April 2000. Propagation models from the UK (EEMS) and US (AREPS) were used to estimate S- and X-band propagation loss from near-surface METOC measurements from the Naval Postgraduate Schools flux buoy, and also from rocketsonde profiles obtained on the research vessel Sealion. Coincident propagation loss data were obtained by the Naval Surface Warfare Center, Dahlgren Division's (NSWC-DD) system, consisting of transmitters traversing up and down a tower on the R/V Sealion and a shore-based tower with fixed-level receivers. The availability of both rocketsonde profiles and surface METOC data enabled the EEMS and AREPS models to be evaluated against the propagation loss measurements in cases dominated by both evaporation ducting and surface-based ducting propagation modes.

The findings of this study demonstrated three main outcomes relative to the operational estimation of radar performance: 1) Each of the propagation model (EEMS and AREPS) configurations converged during one or more runs to an acceptable result in comparison with the measured propagation data (i.e. within 2-4dB), but they diverged far more than they converged. Each model was shown to be capable of producing accurate propagation representations when environmental conditions were relatively homogeneous and high quality METOC data were available for input. 2) The merging of evaporation duct and rocketsonde profiles varied between EEMS and AREPS, leading to different results. Even with a surface based duct the evaporation duct is vital in determining the near-surface propagation conditions, especially at X-band frequencies. 3) Under normal operational conditions there will be impacts on propagation predictions due to limited data availability. This study makes it abundantly evident that even high-quality METOC data can result in modeled propagation predictions that are significantly at odds with reality in complex littoral zone environments.

WALLOPS-2000 REFRACTIVITY STRUCTURE: A
MESOSCALE MODEL STUDY

Burk, S.D., Haack, T.
Naval Research Laboratory

During the period (April-May 2000) of a field experiment at Wallops Island, VA, measurements were taken by groups from DOD laboratories, universities, and elsewhere included low-elevation radar frequency pathloss, meteorological conditions (e.g., from buoys, rocketsondes, helicopter profiles), and radar clutter returns (an extensive description of the field campaign appears in TR-01/132 of the Naval Surface Weapons Division, Dahlgren Division by Stapleton et al.). The Delmarva or Tidewater Peninsula along which Wallops Island lies (the Chesapeake Bay to the west and the Atlantic Ocean to the east) contains complex topographic and land surface characteristics, as well as pronounced spatial SST variability, all contributing to complex BL structures (e.g., internal BLs; sea/land breezes; coastal jets). This study uses the Naval Research Laboratory's Coupled Ocean/Atmosphere Mesoscale Prediction System (COAMPS) to investigate refractive structure during selected portions of Wallops-2000. To explore the COAMPS fidelity in forecasting subtle BL and refractivity variations in this region, we nest COAMPS down to an inner grid mesh having 3 km spacing and utilize high vertical resolution in the first several hundred meters above the surface. During the field experiment, measurements were collected along radials extending SE from the coast at Wallops I. a distance of 65 km over the Atlantic. Similarity theory permits computation of evaporation duct height (EDH) based on the standard meteorological and oceanographic measurements. Model forecast EDH values may then be compared with those computed from observations. The nature of the refractivity profile above the surface layer (e.g., subrefractive, standard, superrefractive, trapping) was measured by the rocketsondes and helicopter profiles, including horizontal variations in refractive conditions along the measurement path. The ability of COAMPS to predict the correct refractive structure and its variation along the measurement path will be assessed. Time periods dominated by synoptic forcing and frontal passages, as well as periods primarily forced on the mesoscale and diurnally will be addressed. Given the difficulty of this forecasting task, model shortcomings are anticipated and will be quantified; the data set will be used to explore and test methods of improving model parameterizations, boundary conditions, etc. Upon completion of such mesoscale model refinements, propagation forecasts using model refractivity fields will be compared with measured propagation factors.

COASTAL OCEAN RADIO REFRACTIVITY DURING A SEA BREEZE CIRCULATION

Marshall, R. E.¹, Burgess, E. H., III¹, Rottier, J. R.²¹Naval Surface Warfare Center, Dahlgren Division²The Johns Hopkins University, Applied Physics Laboratory

Near surface microwave propagation in the littoral region is spatio-temporally modified by the development of a sea breeze circulation and the advection of the sea breeze front towards land (B. W. Atkinson, J. -G. Li, and R. S. Plant, *Journal of Applied Meteorology*, 40, no. 3, 586-603, 2001).

This paper will present the results of a case study that correlates the structure of a sea breeze circulation, the resulting marine internal boundary layer, and measured propagation during the Wallops 2000 Microwave Propagation Measurement Experiment (MPME).

The land and sea breeze system is one of the best examples of the interaction between land, air and sea (S. A. Hsu, *Coastal Meteorology*, Academic Press, 140-147, 1988). Early in the morning prior to the diurnal heating of the land, the adjacent water temperature is typically warmer. As the morning progresses, diurnal heating of the land surface reverses this relationship. Convective turbulence inland produces a low-level convergence zone supported by the sea-breeze front and the land breeze. At this point, a solenoidal circulation exists from tens of kilometers offshore to tens of kilometers onshore at the convergence zone. The return path is typically one kilometer above the surface seaward and produces an area of subsidence as the circulation descends towards the sea.

Synoptic or large-scale flow may be supporting offshore flow. In such a flow pattern, the offshore flow and sea breeze may co-exist (R. S. Plant and B. W. Atkinson, *Boundary-Layer Meteorology*, 104, 201-228, 2002). If the synoptically forced offshore flow is reduced to or below 6 m s⁻¹, the sea breeze front will typically reach shore (R. W. Arritt, *Journal of Applied Meteorology*, 32, 116-125, 1993).

During the MPME, a sea breeze front developed and crossed the coast during offshore propagation and boundary layer profiling measurements. Synoptic north winds in the lee of a mid latitude cyclone dropped below 6 m s⁻¹. Subsidence in the return flow produced strong low level temperature inversions and water vapor pressure discontinuities resulting in one-way X-band propagation factor values greater than 10 dB out to 65 kilometers in range.

STUDY OF DIURNAL EVOLUTION OF DUCTING IN THE
PERSIAN GULF USING HIGH FIDELITY WEATHER FORE-
CASTS

Fast, S. A., Valentine, C. G.
Remcom Inc.

It is well known that ducting has a dramatic effect on signal propagation. Recently, it has become possible to use high fidelity mesoscale weather forecasts to predict the effects of ducting on radio frequency signals. These forecasts, together with sophisticated interpolation and Monin-Obukhov theory, have allowed these forecasts to be applied to tactical problems.

This paper presents the results of a study of the Persian Gulf diurnal evolution of ducting in the littoral region. Air Force Weather Agency (AFWA) forecasts, generated using the MM5 mesoscale weather model, were used together with the Electromagnetic Propagation Integrated Resource Environment (EMPIRE) to investigate the time evolution of the ducting and consequently the radio frequency propagation morphology.

During the study, the MM5 mesoscale weather model was used by AFWA to generate meteorological forecasts for the Persian Gulf region. Two different forecasts were generated, one at 15 km resolution, the other at 45 km resolution; both were used in combination for propagation predictions. This data included humidity, pressure, and temperature at different altitudes and different points on defined grids. The data also included wind, heat, and momentum fluxes at the surface, which are needed by the Monin-Obukhov algorithm to realistically extend profiles to the surface.

An archival system, based on an XML specification for the GRIB data format published by Fleet Numerical Meteorology and Oceanography Center (FNMOC), was devised to store this data. Using this store of data, EMPIRE was used to generate propagation predictions across the Persian Gulf, concentrating on examining ducting phenomena through time. Selection of the appropriate forecast in a given calculation was automated.

DETERMINING THE LIKELIHOOD OF RADIO SIGNAL RECEPTION BASED ON PROPAGATION MODEL DATA

Albert Pelhe, Kent Chamberlin
University of New Hampshire

The objective of the work presented here is to describe an approach for determining statistical confidence intervals for actual radio reception based upon propagation model predictions. Those confidence intervals are used to predict the likelihood of radio reception at a particular location. That predicted likelihood is based upon the historical analysis of measured and modeled data over a wide range of operational conditions in addition to the model estimate at that point.

There is uncertainty in both measured and modeled signal strength data. For measured signal strength, uncertainty is introduced from a range of unpredictable effects such as multipath interference, atmospheric variations, and measurement system noise. These effects can be quite pronounced in a mobile environment, requiring repeated measurements in order to determine a mean value. Uncertainty in modeled data exists due to uncertainty in input data. For terrain-sensitive propagation models, the major source of uncertainty typically results from errors in the terrain database. The known statistics of terrain data errors is used to determine the statistics of propagation model uncertainty through a perturbational analysis.

Once the measured and modeled data statistics are known, they are used in conjunction with model validation data to estimate confidence intervals for actual signal strength based upon model predictions. Finally, a probability of reception value is determined as a function of receiver signal-to-noise threshold and background noise.

The results of this work will be used to create coverage-area maps, where color-coding techniques will be used to indicate the likelihood of radio reception. Based upon results obtained thus far, coverage area will vary with mobile radio velocity and with EMI sources near the receiver.

DUCTING EFFECTS ON SEA SURFACE CLUTTER UNDER
THE INFLUENCE OF A SLOWLY ADVECTING EAST COAST
HIGH PRESSURE RIDGE

Stapleton, J. K., Marshall, R. E.
Naval Surface Warfare Center, Dahlgren Division

Warmer air flowing over a colder littoral sea will produce a stable marine atmospheric boundary layer (MABL) capped by temperature and water vapor pressure discontinuities. The temperature and humidity of the advecting surface air is strongly influenced by the temperature and humidity characteristics of the upwind surface. The strength and height of the thermodynamic discontinuities will control the level of anomalous propagation affecting a coastal radar.

This paper will present the results of a case study that demonstrates how a seemingly benign forty-degree veering of the wind during the Wallops 2000 Microwave Propagation Measurement Experiment (MPME) resulted in two-way propagation factors in excess of 20 dB out to 55 km.

During the study day, clockwise flow around a ridge of high pressure stretched along the Atlantic coast induced a long fetch over water before air reached the MPME area. Much of this fetch was over water warmer than that in the MPME area. This produced a very stable MABL. As the high slowly moved to the northeast, the fetch was over increasingly warmer water increasing the stability and decreasing the height of the MABL. The resulting 1.5 degree C increase in the air-sea temperature difference drove the propagation environment from superrefractive to trapping over the entire MPME area.

Land based and sea based surface meteorological observations will document the slow veering of the winds and the increase in air-sea temperature difference. Range dependent MABL thermodynamic profiles and one-way propagation data will demonstrate the spatio-temporal structure of the MABL and the resulting propagation environment. Coincident clutter to noise ratio data from the NASA S-band Space Range Radar (SPANDAR) will demonstrate the dynamic evolution of the radar propagation conditions.

Session F6, 9:00-Thursday

PROPAGATION MODELING, I

Chairpersons: M. Newkirk and J. Toporkov

ATMOSPHERIC TURBULENCE MODELLING AND THE EOSTAR PROGRAM

Stephen Doss-Hammel¹, Dimitri Tsintikidis¹, Jennifer Ricklin², Eun Oh³, Charmaine Gilbreath³, Frank Eaton⁴

¹SPAWAR Systems Center, San Diego CA

²Army Research Laboratory, Adelphi MD

³Naval Research Laboratory, Washington DC

⁴Air Force Research Laboratory, Albuquerque NM

The determination of the propagation environment for surface ships can be a difficult problem. The most critical portion is the 50-meter-thick surface layer containing the ship and extending to the horizon. Extended horizontal propagation paths within this atmospheric surface layer encounter relatively dynamic refractivity conditions. For such a path near a coastal region, turbulence is usually nonhomogeneous, anisotropic, and non-stationary.

A turbulent atmosphere will cause a propagating visible or infrared beam to wander and to fluctuate in intensity (scintillation), and it will cause imagery to become distorted. Turbulence can therefore be a primary cause of signal degradation or loss of beam intensity. The single most important descriptor of the intensity of turbulent effects on beam propagation is the refractive index structure constant C_n^2 .

We will approach the modelling of turbulence effects on optical and infrared propagation in terms of the EOSTAR (Electro-Optical Signal Transmission and Ranging) model suite. The EOSTAR model is built upon a geometrical optics approach to infrared propagation: a ray is traced through the propagation environment, and path-dependent perturbations to the signal can be determined.

The atmospheric turbulence modelling effort is a development of a surface layer model that estimates C_n^2 from relatively primitive meteorological and geographical information. The goal is to retain a model that is as simple as possible while still retaining the essential elements of an accurate signature of the scintillation conditions. Part of the model development includes comparisons with other models for C_n^2 that have been developed for various environments.

We will present comparisons of the model with field data from an assortment of experimental field sites. The test sites include propagation paths over land and over water.

CORRECTIONS
TO THE MULTIPLE ATMOSPHERIC LAYER WAVEGUIDE
PROGRAM, MLAYER

Anderson, K. D.

Space and Naval Warfare Systems Center, 53560 Hull St, San
Diego CA 92152

MLAYER is an evolving research program for calculating signal levels of electromagnetic waves propagating through the troposphere over seawater or other surfaces provided the surface has a constant dielectric. It is an extension of Baumgartners XWVG program (G.B. Baumgartner, Jr., 1983: XWVG: A waveguide program for trilinear tropospheric ducts, *Naval Ocean Syst. Cen. Tech. Doc. 610*), which uses the waveguide formalism of Marcus (S.W. Marcus, 1982: A model to calculate EM fields in tropospheric duct environments at frequencies through SHF, *Radio Sci.*, 17). The assumptions of spherical symmetry and that the refractive layers can be represented by linear segments are required. Terrain effects (surface elevations) are not permitted but surface roughness, specified by the surface Fresnel reflection coefficient, is allowed.

MLAYER guarantees that all waveguide modes with attenuation rates below a user specified value will be found and is particularly useful for studies of propagation through evaporation ducts. The calculations of field strength compare favorably to experimental measurements for frequencies from 3 MHz through 94 GHz. The paper by Hitney (H.V. Hitney, et al, 1985: Tropospheric radio propagation, *Proc. of the IEEE*, 73) illustrates some of these comparisons.

MLAYER is a research tool; it is not designed for the casual user. For example, at ranges well within the horizon, the calculations fail because many modes (possibly thousands) are required to properly evaluate the fields. With this many modes, the numerical precision is inadequate. At ranges near to or beyond the horizon only a few modes are dominant and the calculations are, generally, reasonable. Depending on frequency, generally good results are obtained for ranges exceeding 0.3 times the horizon range.

Recent work with strong surface-based ducting, high winds, and high frequencies has uncovered a problem in the calculation of the height-gain function. This problem relates to a decision, based on modal attenuation rate, of how the reflection coefficient at a specified height is calculated. This presentation briefly reviews modal theory and concentrates on the fixes needed to make MLAYER more robust.

PROPAGATION OF VHF SIGNALS ACROSS ROUGH OCEANS CLOSE TO SHORE - A COMPARISON OF MODELS

Ford, C.G., Hand, G.R.

National Telecommunications and Information Administration (NTIA), Institute for Telecommunication Sciences (ITS)

Many propagation models treat the surface of the ocean as flat land, considering specular reflection only. This approximation is valid for small grazing angles; however, when the grazing angle is larger, as in the case of the path between a small boat and a shoreline antenna, the scattering is much more affected by the sea state and rms wave height. Some studies of propagation over rough seas have been done, such as The Rough Evaporation Duct (RED) Experiment, conducted by the Space and Naval Warfare System Center, which studied EM propagation models in the X-band radar frequencies over rough seas with ducting. This paper, however, presents a model comparison concentrating on the VHF bands used for public safety and maritime emergencies.

The scenario of interest involves boats with low antenna heights (about 2m) on rough seas, when relatively close to shore. Previous estimates of VHF radio coverage have assumed flat seas, but when rms wave heights are significantly higher than the antenna on the boat, emergency communications could be more affected by line-of-sight and scattering interference. Initial runs of a Longley-Rice model indicate that wave heights of only 3m can greatly affect the percentage of the flat land-modeled sea actually covered by a shoreline antenna, which can lead to loss of communications during an emergency situation.

This study compares the Irregular Terrain Model (ITM) and the Advanced Propagation Model (APM) at varying sea states for coverage of the shoreline in small boat emergency situations. ITM uses the Longley-Rice model as its core, while APM uses the parabolic wave equation method.

MODELING OF RADIO WAVE PROPAGATION OVER IRREGULAR TERRAIN USING THE MOVING WINDOW FINITE DIFFERENCE TIME DOMAIN (MWFDTD) METHOD

Wu, K., Schuster, J. W. , Luebbers, R. J.
Remcom Inc., State College, PA 16801, USA

We present a numerical method for modeling radio wave propagation over irregular terrain using a modified finite difference time domain (FDTD) approach. While physics-based propagation models have been applied successfully to many radiowave propagation problems, approximation to the physics of the problems often must be used in order to make the model computationally efficient. These approximations may result in lower accuracy for the models. Therefore, it is important that we develop high-accuracy models that can faithfully reproduce the physics of electromagnetic wave propagation. These high-accuracy models can then increase the accuracy and reliability of predictions, as well as provide benchmarks for other propagation models.

Since the FDTD method directly solves Maxwell's equations, it can include all the relevant physics of radiowave propagation. However, in conventional FDTD, the entire region of interest must be included in the computational grid, and at every time step we need to calculate the electromagnetic fields over the entire region. For propagation range long compared to the wavelength, the computational resources needed to discretize the entire propagation path and to calculate the fields are prohibitive. In this paper, we use a moving window FDTD (MWFDTD) approach. We consider the propagation of a pulse with width much less than the propagation distance so that we can limit the width of the computational grid to be on the order of the pulse width. As the pulse propagates along the irregular terrain, the computational grid moves along with the pulse. In this way we can circumvent the difficulties associated with conventional FDTD by only including a small portion of the terrain in the computational grid at every time step. In this talk we discuss the implementation of the MWFDTD method. We also compare the results of the MWFDTD calculations with measurements of path loss over irregular terrains in Colorado and show that the MWFDTD results agree closely with the measurements. We also examine propagation through foliage using the MWFDTD method.

SIMULATIONS OF RANGE-RESOLVED SEA CLUTTER AT
LOW GRAZING ANGLES

Toporkov, Jakov V. , Sletten, Mark A.
Naval Research Laboratory, Washington, DC

Many ship-borne radars and remote sensing instruments commonly operate in the low grazing angle (LGA) regime and rely on the detailed knowledge of the sea clutter properties for their successful performance. Still, despite years of effort, many important aspects of LGA sea clutter are not understood and cannot be reliably predicted by available sea clutter models. Recent advent of robust and efficient first-principles numerical scattering techniques coupled with advances in short-scale surface hydrodynamics, and the availability of high performance computers make feasible the numerical simulation approach to the problem of sea clutter characterization.

This work investigates statistical properties (probability distributions) of range-resolved LGA sea clutter. Following Monte Carlo approach, sea surface profiles are generated as realizations of Gaussian random process characterized by Pierson-Moskowitz spectrum. A non-linear transform [Creamer, JFM 1989] is further applied to each profile to account for interactions between long and short waves. Scattering from each profile is calculated using Method of Ordered Multiple Interactions (MOMI) [Kapp and Brown, IEEE TAP 1996] that solves the first-principles integral equation for the induced surface current at a particular frequency. To simulate pulse scattering, surface response is calculated at a number of frequencies, and Fourier synthesis is used. While both electromagnetic and hydro calculations are limited to a two-dimensional (2D) space, the results are readily applicable to commonly occurring 3D geometries (e.g. radar looking up/downwind).

The study is performed at X band with the synthesized pulse duration as short as 5 ns (corresponding to a 0.75 m resolution). The grazing angle is 5° , and both VV and HH polarizations are considered. From the Monte Carlo data, probability density function (pdf) and cumulative probability distribution are calculated for the normalized radar cross section. These are compared to Weibull distribution - an empirical statistical model often used for clutter characterization. The effect of using approximate scattering models (such as two-scale model by Brown [IEEE TAP, 1978]) in lieu of exact solution to scattering problem is examined. Another issue being addressed is whether and to what extent accounting for non-linear hydrodynamic interactions affects the clutter probability distributions. Attention is also given to the sensitivity of backscatter statistics to surface dielectric properties (i.e. treating surface as a lossy rather than a perfect conductor).

THE AVERAGE NORTON SURFACE WAVE ON A RANDOMLY ROUGH SURFACE

Brown, G.S.

EMIL, Bradley Department of Electrical Computer Engineering,
Virginia Polytechnic Institute and State University, Blacksburg,
VA 24061-0111

A Norton surface wave (N_{sw}) is one of the results of a dipole radiating over a flat, lossy surface. A Norton surface wave starts out close to the radiating dipole having a very complicated form but eventually morphs into a simple dependence on the radial distance from the dipole increases. This wave continues its propagation along the surface if the surface is flat and there are no changes in the electrical properties of the interface material. If the surface becomes rough, it would be highly desirable to know how this Norton surface wave changes. Based upon physical intuition, we expect that if the surface changes very gently, i.e., so that the local radius of curvature in the direction of travel is significantly greater than the electromagnetic wavelength and it does not change rapidly with distance, the Norton surface wave does not radiate. That is, the wave continues along as a pseudo-surface wave following the undulating surface. If the local radius of curvature in the direction of travel becomes comparable to the electromagnetic wavelength, we know the Norton surface wave will radiate; this situation we ignore. If the undulations are random in nature, the Norton surface wave will have an average value and a fluctuating value at any point of observation on the surface. The purpose of this presentation is to derive the mean or average value of the Norton surface wave as a function of the distance away from the dipole. The derivation is based upon the observation that the randomness imparted to the wave is a result of the wave propagating along a randomly rough surface. This implies that the distance along the planar interface should be replaced by the distance along the rough surface. Assuming that the surface roughness forms an ergodic process, we can relate integrals of the surface slope to a statistical average. If we assume that there are a sufficient number of decorrelation intervals between where the Norton surface wave assumes its wave-like form and where it is measured, the spatial integrals can then be directly related to averages. The net result of this simple analysis is that the mean or average Norton surface wave can be derived. We will present this derivation and note that the mean wave has the following characteristics. First, it is a slow wave along the planar distance as should be expected. more importantly, the mean wave has an exponential dependence upon the square of the free space wavenumber, the square of the mean squared height of the roughness, and the surface correlation length to the -3 power. This dependence clearly shows that (a) as the surface becomes flat the mean wave approaches the flat surface wave and (b) as the height of the roughness increases the mean wave attenuates due to the random distance the wave must travel.

Session F7, 13:40-Thursday

PROPAGATION MODELING, II

Chairpersons: L. Rogers and J. Krolik

POSTERIORI ESTIMATION OF LOW ALTITUDE PROPAGATION LOSS FROM RADAR SEA CLUTTER DATA

Peter Gerstoft¹, L. Ted Rogers², William S. Hodgkiss¹

¹Marine Physical Laboratory, Scripps Institution of Oceanography, University of California San Diego

²Space and Naval Warfare Systems Center, San Diego

This paper describes the estimation of propagation loss and its statistical properties based on observations of radar sea clutter data. This problem is solved by first finding an ensemble (about 10^5 models) of relevant refractivity model parameters and then using all these models to map into the propagation loss domain. In this mapping each refractivity model is weighted according to its data likelihood function.

A general weakness of all methods employed in estimating radar performance has been the lack of a means for quantifying the impact of uncertainty in the estimates of refractivity that the performance estimates are based on. This might be a particular concern when using radar clutter for the characterization.

The inverse problem is first solved using Bayes rule to compute the posterior distribution $p_p(\mathbf{m})$ of refractivity profiles \mathbf{m} . We are not interested in the environment itself but rather better estimates of the parameters in the propagation loss domain $\mathbf{u}(\mathbf{m})$. Based on the posteriori distribution $p_p(\mathbf{m})$, the distribution of $p_p(\mathbf{u}(\mathbf{m}))$ is obtained via Monte Carlo simulation. From this propagation loss distribution all relevant statistics of the propagation loss can be obtained.

This algorithm is used on radar sea clutter data. First refractivity parameters are estimated using 90,000 precomputed vectors of propagation loss versus range. Based on the probability that each of these refractivity models fits the radar sea clutter data, each model is mapped into propagation loss. This enables us to compute a full probability distribution for the propagation loss in both height and range.

RANK NORMALIZATION OF A POSTERIORI PROBABILITIES IN THE REFRACTIVITY-FROM-CLUTTER PROBLEM

Jablecki, M.¹, Rogers, L.T.², Gerstoft, P.³, Krolik, J.L.⁴

¹Science and Technology Corp., San Diego, CA 92152-7385

²Space and Naval Warfare Systems Center, San Diego, Code 2858, San Diego, CA 92152-7385

³Scripps Institution of Oceanography, La Jolla, CA 92093-0238

⁴Duke University, Dept. of Electrical and Computer Engineering, Durham, NC 27708

In the preceding talk we discussed the framework of a method to generate sample representations of the $f(\widehat{M}(r, z)|\mathbf{d}; \Theta, \epsilon)$, and $f(\widehat{p}|\mathbf{d}; \Theta, \epsilon)$, the estimated *a posteriori* probability density functions (p.d.f.'s) of modified refractivity and a parameter-of-interest p , conditioned on radar clutter \mathbf{d} . The argument Θ is a vector that governs random processes used in generating the sample representation of the joint p.d.f. $f(\widehat{M}(r, z), \mathbf{m}; \Theta)$, where \mathbf{m} is the modeled clutter. The argument ϵ affects how $f(\widehat{M}(r, z), \mathbf{d}; \Theta)$ is sampled to yield $f(\widehat{M}(r, z)|\mathbf{d}; \Theta, \epsilon)$. The central question is how do determine Θ and ϵ .

In simulation, we know the answers (i.e., the $M(r, z)$'s and q 's), so that over a large enough set of simulation runs we should be able to maximize the goodness of the *a posteriori* distribution. Because of the dimensionality of $\widehat{M}(r, z)$, we work with a scalar parameter-of-interest p — in this instance, the median propagation loss to a target at a height of 5 meters over the range of 10 to 60 km. The key insight is that the ranks of the "truth" p should be uniformly distributed within the ranks of the samples representing $f(\widehat{p}, \mathbf{d}; \Theta, \epsilon)$. We perform an optimization to yield Θ^* and ϵ^* ; the values that maximize the goodness of the *a posteriori* distributions by maximizing the uniformity of the distribution of p 's ranks.

The following point bears some consideration: Assuming Θ^* and ϵ^* are correct, measures of the width of $f(\widehat{p}|\mathbf{d}; \Theta^*, \epsilon^*)$, such as the width of the interval between the 20th and 80th percentile, are indicators of the information content arising from the inversion process.

POSTERIOR PROBABILITY DENSITY ESTIMATION
 BASED ON RADAR CLUTTER: ALGORITHM DESIGN

Rogers, L.T.¹, Jablecki, M.², Gerstoft, P.³, Krolik, J.L.⁴

¹SPAWAR Systems Center, San Diego, San Diego, CA 92152-7385

²Science and Technology Corp., San Diego, CA 92152-7385

³Scripps Institution of Oceanography, La Jolla, CA 92093-0238

⁴Duke University, Dept. Electrical and Computer Engineering,
 Durham, NC

We estimate a parameter (or parameters) of interest p (e.g., propagation loss to a low-altitude target) using radar sea clutter data \mathbf{d} over the ranges at which it is observed using the radar. The intermediate product is the atmospheric refractivity $M(r, z)$ whose map into p is (presumably) well-known. This is an inverse problem. A well known problem in inversion approaches though, is determining the certainty of estimates. In this context, it means there are problems assigning confidence levels and lower and upper bounds to p ; which we would know if we knew the true *a posteriori* probability density function. We describe difficulties in estimating the *a posteriori* arising from assumptions that are routinely used in formulating the inverse problem solution.

A new method is as follows: We construct a generator whose random draws are matched pairs of $\widehat{M}(r, z)$ and \mathbf{m} (i.e., $[\widehat{M}(r, z), \mathbf{m}]$) that, as an ensemble, represent the joint p.d.f. $f(\mathbf{m}, \widehat{M}(r, z); \Theta) = f(\widehat{M}(r, z), \mathbf{m}; \Theta)$. Θ is a parameter vector controlling the process noises that determine the ensemble behavior of the matched pairs. Correctly set, it would allow us to account for model error and signal contamination (arising from the horizontal variability of the sea clutter radar cross section). We sample the matched pairs of $[\widehat{M}(r, z), \mathbf{m}]$ in the vicinity of the observed clutter \mathbf{d} . What constitutes the "vicinity" is a function of the local density of the \mathbf{m} 's and a tuning parameter ϵ . Hence, our samples represent the p.d.f. $\widehat{f}(\widehat{M}(r, z)|\mathbf{d}; \Theta, \epsilon)$. Those samples are mapped into the parameter of interest p and represent $\widehat{f}(\widehat{p}|\mathbf{d}; \Theta, \epsilon)$.

Of course, varying Θ and ϵ will alter the sample representation of $\widehat{f}(\widehat{M}(r, z)|\mathbf{d}; \Theta, \epsilon)$ and $\widehat{f}(\widehat{p}|\mathbf{d}; \Theta, \epsilon)$. The talk that follows will describe using simulation to maximize the goodness of $\widehat{f}(\widehat{p}|\mathbf{d}; \Theta, \epsilon)$.

Session G1, 8:40-Monday

**EQUATORIAL BUBBLES AND
PLASMA DYNAMICS**

Chairperson: Erhan Kudeki

G1

IGY OBSERVATIONS OF F-REGION SCATTER IN THE FAR EAST

Smith, E. K.

ECE Department, Univ. of Colorado

An unexpected discovery just prior to and during the International Geophysical Year was an unexpected evening signal enhancement over VHF circuits from the Philippines to Okinawa. First unusual signals were recorded in October, 1956 on 36.4 MHz over the military transpacific forward-scatter link between Poro Point, P.I. and Sobe, Okinawa. The anomaly was confirmed the following year over a 49.84 MHz circuit of 1347 km operating between Poro Point and Onna, Okinawa. This second circuit was part of the US IGY program and was operated by the Central Radio Propagation Laboratory of National Bureau of Standards. It was part of a program to compare sporadic-E incidence in the Americas to that in the Far East. The anomalous signal enhancement typically began after 6 PM path midpoint time, peaked around 8 PM, and disappeared by midnight. Enhancement were 40 to 50 dB above normal on the 36 MHz circuit and 30 to 40 dB on the 50 MHz one. Range-time records were made for four nights in September, 1958 by the late James M. Watts using 50 microsecond pulses, a prf of 100/sec and with a receiver bandwidth of 120 KHz. The records for both Sept. 22 and 23, 1958 show an abrupt start of the anomalous signal at a time delay of 1200 microseconds behind the E-region pulse. They then spread in a band extending from 1000 to 3000 microseconds above the E-region trace. From simple geometrical considerations, a delay of 400 microseconds represented a midpoint height of about 300 km while 1100 microseconds corresponds to a height of 500 km. These first results were published in the April 1959 issue (pp 403-405) of the JGR and titled IGY Observations of F-Layer Scatter in the Far East, authored by R. Bateman of Page Communication Engineers, and J. W. Finney, E. K. Smith, L. V. Tveten, and J. M. Watts of CRPL. These results were also reported in the National Academy of Sciences IGY Bulletin No. 25 of August 1959 (pp 1-4). Vertical and horizontal angle-of-arrival measurements were made the following fall and showed the signals arriving from up to 150 km off path. Field-aligned irregularities seemed a logical source of the scatter. Measurements were extended to several other sites in the Far East in 1959 using the 50 MHz transmissions from the VOA sites at Poro Point and Okuma, Okinawa with mixed results.

TWO RADAR INVESTIGATIONS OF EQUATORIAL SPREAD F IN THE PACIFIC SECTOR

Tsunoda, R.T.
SRI International

Two 50 MHz radars are currently being operated routinely in the Pacific sector, one on the island of Pohnpei, Federated States of Micronesia, since June 1999, and the other on Christmas Island, Republic of Kiribati, since September 2003. Both radars were originally built by the National Oceanic and Atmospheric Administration (NOAA) as part of the wind profiler network in the Pacific region. Both use 100 m x 100 m Coco antenna arrays. The Pohnpei radar now operates with a 4 kW peak power amplifier and three antenna beams in the magnetic east-west plane. The Christmas Island radar operates with a 30 kW peak power amplifier and two antenna beams, one in the magnetic meridian and the other directed toward magnetic east. In this presentation, we describe preliminary results of equatorial spread F obtained with the two radars. The results include diurnal and seasonal dependences in occurrence frequency over Pohnpei, and a comparison of backscatter plume characteristics from the two locations. Occurrences of backscatter plumes are most frequent after sunset but prior to midnight, and during the local summer months with minimal activity during winter months. Research goals are to determine the degree to which equatorial spread F behavior is correlated over a longitudinal separation of three hours in local time, and whether the development of backscatter plumes over Pohnpei can be predicted with diagnostic measurements at Christmas Island. Observations to date indicate that there exists a promising level of correlation in the post-sunset rise of the F layer and the development of backscatter plumes.

STUDY OF THE RELATIONSHIP BETWEEN GPS L1 SCINTILLATIONS AND THE 777.4-NM RADIATIVE RECOMBINATION EMISSION

Makela, J.J.¹, Ledvina, B.M.², Kintner, P.M.², Kelley, M.C.²

¹E.O. Hulburt Center for Space Research, Naval Research Laboratory

²School of Electrical and Computer Engineering, Cornell University

Using radio and optical equipment operating on the Haleakala Volcano on Maui, Hawaii, it has been shown that intense scintillations on the L1-band signal transmitted by Global Positioning System (GPS) satellites occur as equatorial spread-F plumes pass overhead (Kelley et. al., Geophysical Research Letters, **29**, 2002). This equipment consists of an all-sky airglow imager, a narrow field (47°) imager, a GPS total electron content receiver, and a GPS-L1 scintillation monitor. The electric fields caused by equatorial spread-F map along the magnetic field lines to low- and mid-latitudes where they perturb the local ionosphere. This results in depleted regions of electron density that appear as dark regions in the 777.4-nm emission, which is proportional to n_e^2 , observed by both imagers that typically travel from west to east. As the look-direction from a collocated GPS-L1 scintillation monitor to a GPS satellite traverse these dark regions, the received signal power fluctuates, or scintillates. Although these GPS scintillations occur due to fluctuations in the electron density with scale sizes on the order of 400 meters, which is below the resolution of the imaging systems, it is well established that the spectrum of equatorial spread-F follows a power law. Thus it is reasonable to expect that a relationship exists between the intensity of the GPS scintillations and the structure at the slightly larger scale measured by the imager. We explore this by studying both the gradients and the 2D FFTs of the 777.4-nm images during times of GPS scintillations. If the relationship between these parameters and the intensity of the scintillations could be ascertained, images taken of the 777.4-nm emission could be used as a proxy for the S4 index, essentially creating a two-dimensional map of where intense scintillations should be expected.

IONOSPHERIC CONDITIONS DURING THE ONSET AND
EVOLUTION OF TEC DEPLETIONS AS SEEN WITH A
CHAIN OF GPS RECEIVERS AND A DIGISONDE

Cesar E. Valladares, R. Sheehan
Boston College

A latitudinal chain of GPS receivers extending between 5 N and 37 S (geographic latitude) has provided information on TEC depletions produced by the passage of equatorial plasma bubbles. In addition to giving the total amount of density evacuated within the plasma bubbles, the longitudinal spread of the location of the receivers serves to indicate, quite frequently, the time and the place of origin of the TEC depletions as well as their drift motion. The receivers managed by BC conduct real-time calculations of the S4 index using the L1 frequency that is recorded at 10 Hz. The latitudinal profiles of TEC measured with the GPS network can be used to infer plasma motions along the field lines and even estimate the vertical drifts across the field lines. We have also used density profiles of the F-region bottomside, measured by the Jicamarca digisonde to confirm a previous hypothesis on the development of TEC depletions and the altitude of the F-region peak. TEC depletions and scintillations develop when the altitude of the F-region peak is above 500 km. We have observed that TEC depletions and scintillations decay when the F region lowers in altitude. However, in more than 30% of the cases TEC depletions persist even when the altitude becomes as low as 300 km. We have examined the persistence of these plasma bubbles and correlated them with other parameters of the F-region such as the plasma density at the magnetic equator, the development, or intensification of the asymmetry in the anomaly. No clear correlation has been found. We suggest that the longer persistence of some TEC depletions may occur when the E-region conductivity is much lower than the field-integrated conductivity of the F-region, making the flux tube to remain unstable and favorable for the maintenance of the plasma structures.

EQUATORIAL, DAYTIME ExB DRIFT VELOCITIES INFERRED FROM GUVI 1356 A RADIANCE OBSERVATIONS

Anderson, D., Anghel, A
CIRES, Univ. of Colorado

Currently, there does not exist a way of estimating low latitude, ionospheric daytime vertical ExB drifts, day-to-day, around the globe. In this talk we present a promising, new technique that would enable us to estimate the day-to-day variability in daytime ExB drift velocities using the nighttime 1356 radiance observations from the GUVI instrument - Global UltraViolet Imager - on the TIMED satellite. It is well known that the greater the upward, daytime ExB drift velocity in the low latitude ionospheric F region, the greater the latitude separation of the crests in maximum electron density, N_{max} , known as the equatorial anomaly. At night, the observed 1356 GUVI radiance observations can be primarily attributed to the radiative recombination reaction, $O^+ + e = O^* + hv$. This means that the 1356 intensity is proportional to the height integral of Ne_2 , with most of the radiation originating near H_{max} . In this talk, we describe the procedures that have been carried out to estimate the post-sunset latitude crest separation in N_{max} inferred from GUVI 1356 observations for a significant number of nights in the low latitude Peruvian longitude sector. We then present the calculated linear relationship between crest separation and the observed strength of the daytime ExB drift velocities on these days, in this longitude sector. In addition, we have incorporated the GUVI-inferred daytime ExB drift velocities on several specific days into a theoretical ionospheric model and theoretically calculate the N_{max} and TEC crest separation values at the local times when GUVI 1356 observations are obtained. In this way, we validate that realistic ionospheric parameters can be obtained using GUVI - inferred daytime ExB drift values. We will discuss the implications of these findings to estimating daytime ExB drift velocities, on a day-to-day basis, at all longitudes.

GRAVITY AND PRESSURE TERMS IN THE ELECTRODYNAMICS OF THE LOW-LATITUDE IONOSPHERE

J. Vincent Eccles

Space Environment Corporation

The source of the plasma drift structure in the low-latitude ionosphere during magnetically quiet times is generally thought to be understood. Nearly all the quiet time electric field structure has been attributed to the neutral wind current dynamo. However, two other current generators are active in the low latitude ionosphere—a gravity-driven current and a gradient-pressure driven current. The gravity driven current is important in the development of the Rayleigh-Taylor instability and equatorial spread F (ESF), but is generally ignored along with the pressure-gradient terms in global dynamo electric field models. The flux-tube integrated electrodynamics equations presented in *Haerendel et al.* [J. Geophys. Res., 1992] have been reformulated to include pressure gradient terms. It is generally assumed that the gravity and gradient-pressure terms cancel or are small when field-line integrated. It is shown herein that the gravity and gradient pressure currents nearly cancel each other above the integrated F region peak density, but enhance each other below the density peak. The inclusion of both the gravity driven and gradient pressure driven currents in low-latitude electrodynamics equations only slightly alter the zonal drifts and significantly alter the vertical plasma drifts in the hours before sunrise and after sunset. On the important F region bottomside after sunset, the gravity and gradient pressure driven currents are reinforcing each other in the eastward direction. The inclusion of the gradient pressure terms have very important implications on the stability of the post sunset ionosphere and the development of plasma irregularities associated with Equatorial Spread F. Rayleigh-Taylor growth rates are doubled and are more strongly focused on the bottomside than those calculated using the gravity term alone. Additionally, the pressure-gradient alters the character of the plume characteristics.

EQUATORIAL SPREAD F: MACROPHYSICS, MICROPHYSICS, AND WHERE WE STAND ON THE FORECAST PROBLEM

D. L. Hysell

Earth and Atmospheric Sciences, Cornell University

Analysis of the ionospheric interchange instability implies that equatorial spread F should manifest a continuum of growth rates and intensities. In nature, however, topside spread F either develops fully after sunset or fails to occur at all. A trigger mechanism appears to be at work that may be related to thin precursor bottomside scattering layers (bottom-type) routinely observed at Jicamarca and elsewhere immediately after sunset. These layers exist in shear zones and exhibit retrograde zonal drifts. The emergence of topside plumes occurs simultaneously with the reversal of the layers.

At least four perspectives on the role of bottom-type layers have been published in the literature [1-4], and while these roles are compatible, the trigger mechanism at work has yet to be clearly identified. In this talk, new data from Jicamarca are used to help discriminate between the four theories and to elucidate the trigger mechanism. The data were taken using multiple receivers and processed using aperture synthesis imaging techniques. They give the clearest picture available of the processes at work during the initiation of spread F .

[1] Flaherty, J. P., C. E. Seyler, and L. N. Trefethen, Large-amplitude transient growth in the linear evolution of equatorial spread F with a sheared zonal flow, *J. Geophys. Res.*, 104, 10.1029/1998JA900178, 1999.

[2] Hysell, D. L., A review and synthesis of plasma irregularities in equatorial spread F , *J. Atmos. Sol. Terr. Phys.*, 62, 1037, 2000.

[3] Kudeki, E., and S. Bhattacharyya, Post-sunset vortex in equatorial F -region plasma drifts and implications for bottomside spread- F , *J. Geophys. Res.*, 28,163, 1999.

[4] Zargham, S., Numerical simulations of the ionospheric interchange instability, Ph. D. Thesis, Cornell University, Ithaca, N.Y., 1988.

SEASONAL AND DISTURBANCE VARIABILITIES OF THE
EAST-WEST EEJ BACK-SCATTER POWER ASYMMETRY
IN BRAZIL NEAR SOLAR MAXIMUM

Denardini, C. M. , Abdu, M. A., Sobral, J. H. A.
Instituto Nacional de Pesquisas Espaciais

This study is intended to demonstrate the seasonal and disturbance variabilities of the East-West asymmetry observed in the vertical power profile of the signal back-scattered by 3-m plasma irregularities of the equatorial electrojet (EEJ) in the Brazilian sector near solar maximum. We have used data collected in 2002 by the 50 MHz coherent back-scatter (RESCO) radar at the magnetic equatorial site (São Luís site, in Brazil) to obtain Range Time Intensity (RTI) maps covering the equatorial electrojet heights during daytime. The RESCO radar was operated in antenna switching mode, the beam pointing alternately (for 1-min duration) 30° West and 30° East with respect to the vertical direction. RTI maps were obtained from the East and West beams separately which showed significant asymmetry of the returned power from the two directions. We have carried out an investigation of the East-West asymmetry problem by parameterizing the electrojet irregularity power profiles in an attempt to quantify the observed asymmetry and to determine its most outstanding features. The data set was separated according to the magnetic activity and season. This analysis confirmed the presence of an East-West power asymmetry in the back-scattered radar signal strength in the Brazilian sector, as seen in other sector. The echo power received with the Westward beam was always 3 to 4 times stronger than the echo power received with the Eastward beam. Some daily and seasonal characteristics of this power asymmetry are presented. The analyzed results show also the appearance of a scattering region after sunset during magnetically quiet conditions around the southern hemisphere summer solstice.

POST-SUNSET F-REGION DYNAMICS AT THE EQUATOR
ABOVE JICAMARCA

Kudeki, Erhan¹, Chau, Jorge²

¹University of Illinois at Urbana-Champaign

²Jicamarca Radio Observatory, Lima, Peru

The *pre-reversal enhancement* in equatorial F-region drifts is a feature of a vortex-like post-sunset $\vec{E} \times \vec{B}$ flow pattern that was first observed in incoherent scatter radar drift maps produced at the Jicamarca Radio Observatory [Kudeki and Bhattacharyya, 1999]. The vortex structure is completed with eastward flow on the top and westward flow on the bottom, both associated with a post-sunset F-region zonal drift shear first reported in Valenzuela *et al.* [1980]. Bottom-type spread-F observed above Jicamarca develops in the westward flow region corresponding to the bottomside of the vortex.

The post-sunset vortex is a consequence of the charging of the bottomside F-region after sunset due to dynamo-current divergence as modeled by Eccles *et al.* [1999]. The most detailed observational data on the vortex are still the flow maps published in Kudeki and Bhattacharyya [1999] dating back from 1996-1997. The present talk will focus on Jicamarca incoherent scatter drift maps compiled since 1997 and, in particular, on solar-cycle variation of post-sunset vortex inferred from Jicamarca data. The relation between bottom-type spread-F and westward bottomside flow will also be examined.

References:

Eccles, V., N Maynard, and G. Wilson, Study of the evening plasma drift vortex in the low-latitude ionosphere using San Marco electric field measurements, *J. Geophys. Res.*, 104, 28133, 1999.

Kudeki, E., and S. Bhattacharyya, Postsunset vortex in equatorial F-region plasma drifts and implications for bottomside spread-F, *J. Geophys. Res.*, 104, 28163, 1999.

Valenzuela, A., G. Haerendel, E. Foppl, H. Kappler, R. F. Woodman, B. G. Fejer, and M. C. Kelley, Barium cloud observations of shear flow in the post sunset equatorial F layer (abstract), *Eos Trans. AGU*, 61, 315, 1980.

Session G2, 13:40-Tuesday

IONOSPHERIC IMAGING

Chairpersons: G. Bust and Farzad Kamalabadi

G2

COMPARISONS OF GUVI NIGHTSIDE IONOSPHERIC DENSITY RETRIEVALS, IONOSONDES, AND GPS OCCULTATION PROFILES

Straus, P. R.¹, DeMajistre, R.², McKenzie, D. L.¹
, Paxton, L. J.², Morrison, D.², Christensen, A. B.¹

¹The Aerospace Corporation, PO Box 92957, Los Angeles, CA 90009

²The Johns-Hopkins University Applied Physics Laboratory, 11100 Johns Hopkins Road, Laurel, MD 20723

Nightglow observations of the 135.6 nm O+ recombination emission line can provide insight into the dynamic morphology of the earth's ionosphere. The Global Ultraviolet Imager (GUVI) on the TIMED satellite has been making routine measurements of this feature since early January 2002. Limb profile data, obtained in a roughly east-west viewing geometry, can be inverted to produce profiles of F-region electron density. We present preliminary results of a comparison between these UV-derived profiles and two other ionospheric data sources: ionosondes and GPS occultations. The ionosonde data potentially provides the most direct validation of peak densities and also has the advantage that fairly routine coincidences are available during GUVI overflights. GUVI-occultation comparisons are only possible when the TIMED satellite orbit plane and the orbit plane of the satellite hosting the GPS occultation sensor are approximately co-aligned. Comparison of full F-region profiles is then possible, although consideration must be made for the differences between the generally north-south viewing geometry of the existing occultation sensors and the GUVI viewing geometry. This is so particularly in the equatorial region where east-west aligned ionospheric gradients associated with the equatorial anomaly cause greater retrieval errors for the Abel transform used to invert occultations. However, the GUVI disk-viewing data provides a measure of horizontal gradients, which can potentially be used to correct the occultation inversions, enabling better comparisons in this region. These preliminary results focus on comparisons with Ionospheric Occultation Experiment (IOX) on the PICOSat spacecraft. PICOSat/TIMED orbital conjunctions occur on a relatively infrequent basis, have a roughly month-long duration because of the similar inclinations of these satellites.

COMBINING OPTICAL AND RADIO TECHNIQUES FOR
HIGH-RESOLUTION IONOSPHERIC IMAGING

C. Coker¹, K. F. Dymond², E. J. Bennert¹, S. E. Thonnard²

¹Praxis Inc., Code 7607, Naval Research Laboratory, Washington, DC 20375

²E. O. Hulburt Center for Space Research, Code 7607, Naval Research Laboratory, Washington, DC 20375

With the proliferation of satellite-based ionospheric measurement systems, opportunities exist for high-resolution ionospheric specification. These satellite systems utilize optical and radio-based techniques. The optical techniques include UV limb scanning, UV disk scanning, and UV disk imaging. The radio techniques include, radio occultations, radio beacon tomography, and radar altimetry. While assimilative models seek to routinely ingest these data and produce global or regional specification of the ionosphere, the spatial resolution is low to moderate due to the requirement of the model to continuously specify a selected ionospheric volume. Frequently, coincident measurements from more than one technique provide opportunities to directly reconstruct the ionospheric densities with high spatial resolution. These high-resolution snapshots of the ionosphere will occur globally, routinely providing researchers insights into ionospheric dynamics in remote areas of the globe.

The concept is demonstrated using coincident UV limb scan data from LORAAS on the ARGOS satellite with radar altimetry data from TOPEX. The limb scans provide vertical resolution in the ionosphere and the altimetry data provides horizontal resolution. When combined a 2D reconstruction of the ionosphere is obtained over a large geographic region with high spatial resolution. Additional combinations of existing satellites can be used to produce high-resolution ionospheric specifications. Their advantages and disadvantages are discussed. In the future, multiple sensors on the same satellite will routinely provide opportunities for high-resolution ionospheric specification. Examples of these satellite systems include COSMIC and NPOESS. COSMIC is currently in production, with a projected launch date in 2005, while the first NPOESS launch is projected for 2008.

FAR ULTRAVIOLET IMAGING OF THE IONOSPHERE WITH
GUVI AND SSUSI

Larry Paxton¹, Hyosub Kil¹, Robert DeMajistre¹
, Daniel Morrison¹, Elsayed Talaat¹, Paul Straus²
, Andy Christensen², Geoff Crowley³, Joe Comberiate¹

¹JHU/APL

²Aerospace Corp

³SwRI

The NASA TIMED Global Ultraviolet Imager (GUVI) and the DMSP Special Sensor Ultraviolet Imager (SSUSI) have the capability to image the Earth's nightside ionosphere at unprecedented spatial and spectral resolution. GUVI was the first of the next generation of hyperspectral far ultraviolet (FUV) sensors to fly. These sensors operate from 110 to 180 nm and image, on the nightside, the recombination of O+ ions with electrons. This recombination is observed as the line of sight integral of the what is essentially the square of the electron content along the line of sight. GUVI samples all local solar times every 60 days from an altitude of 625 km. The sensor forms and horizon to horizon image with a swath width of almost 2500 km. Additionally, GUVI images the limb which provides us with height resolved information on the electron density profile. SSUSI is to fly on the DMSP F16 through F20 satellites. At the writing of this abstract F16 is planned for launch in Fall 2003. In this talk we will discuss: 1) how the technique works 2) limitations on its accuracy 3) the ability to recover spatial information 4) the current database of small and large scale structure in the ionosphere 5) ongoing validation efforts 6) comparison with physics-based models 7) comparison with climatologies 8) how we can improve our predictive capability. The GUVI observations of the nightside are only part of the picture. We will show that on the dayside limb we are able to see the signature of the F-region ionosphere. We are also able to map the column density ratio of O to N2. This ratio is a key parameter for determining the large and small scale response of the ionosphere to high latitude forcing events (geomagnetic storms) and demonstrates that the ionosphere and thermosphere are so closely coupled that a purely phenomenological approach to prescribing the F-region ionosphere will not work during disturbed conditions.

MULTI-DAY EXPERIMENTAL RUN OF IONOSPHERIC
DATA ASSIMILATION THREE DIMENSIONAL (IDA3D)

Bust, G.S., Garner, T.W., Gaussiran, T.L. II
Applied Research Laboratories, The University of Texas at Austin
(ARL:UT), 10000 Burnet , Austin Texas, 78758

A global, multi-day experimental run of the The Ionospheric Data Assimilation Three Dimensional (IDA3D) space-weather mapping algorithm was recently conducted. The experimental time frame was chosen to be during a period when there was extensive data sets available, and where both quiet and active periods were present. IDA3D is a spatial three-dimensional data assimilation algorithm based very closely on the 3DVAR objective analysis techniques developed within the meteorological community. IDA3D ingests several different data sources including ground-based GPS total electron content (TEC) data, space-based GPS TEC occultation data, ground-based regional computerized ionospheric tomography (CIT) TEC data, Ionosonde data and space-based in-situ measurements of electron density such as those obtained from DMSP. The result of the analysis is a global three-dimensional specification of ionospheric electron density.

Results will be presented from the experimental run. The data sources available for ingestion into the data assimilation algorithm include ground GPS data, GPS occultation data, ionosonde data and *in-situ* satellite measurements of electron density. The multi-day run was made on a global irregular spatial grid, with 15 minute sampling time and with the climatological model PIM used as the background electron density field. The resulting analysis from the previous time step was used to initialize the next time step through a Kalman filter. Three dimensional spatial maps of electron density will be presented, and the evolution of these maps over the course of the experimental run will be discussed. In addition, derived products from these maps such as two dimensional maps of conductances will be presented and discussed. Comparisons with background climatological models will be made, with emphasis on the space-weather features that emerge from IDA3D.

RADIO TOMOGRAPHIC IMAGING OF SPORADIC E-LAYERS DURING SEEK2

Bernhardt, P.A.¹, Selcher, C.A.², Siefiring, C.L.¹

, Wilkens, M.¹, Taylor, C.³, Yamamoto, M.⁴

, Fukao, S.⁴, Bust, G.⁵

¹Plasma Physics Division, Naval Research Laboratory, Washington, DC 20375

²Information Technology Division, Naval Research Laboratory, Washington, DC 20375

³Department of Physics, West Virginia University, Morgantown, WV

⁴Radio Science Center for Space and Atmosphere, Kyoto University, Kyoto, Japan

⁵Applied Research Laboratory, University of Texas at Austin, Austin, Texas

Sporadic E-layers are found between 100 and 120 km altitude. They have both spatially and temporal variations in electron density. The layer formation and density fluctuations have been associated with neutral wind shears. Theories on the formation of E-layer patches have involved Kelvin-Helmoltz (KH) turbulence, plasma instabilities, and gravity waves. To resolve some of the issues concerning sporadic-E occurrence, the University of Kyoto in Japan sponsored the second Sporadic-E Experiment over Kyushu (SEEK2). During the SEEK2 Rocket Campaign on 3 August 2002, a Dual Band Beacon (DBB) transmitting to Ground Receivers provided unique data on E-Region electron densities. The beacons continuously radiated unmodulated signals at 149.988 and 399.968 MHz. Information from two rocket beacons and four ground receivers provided multiple samples of E-region horizontal variations. The radio beacon measurements were made at with Coherent Ionosphere Doppler Receivers (CIDR) at four sites (Uchinoura, Taramizu, Tanagashima, Takasaki) in Japan. The two rockets (S310-31 and S310-32) were launched by the Japanese space agency with in situ instruments, a chemical release, and radio beacons. Analysis was completed for four sets of beacon data to provide electron density profiles and tomographic images of sporadic-E layers. The two-frequency beacon on the SEEK2 rockets provided TEC data that was converted into electron density measurements. Wide variations in layer structures were detected. These included horizontal Sporadic-E variations, vertical profiles of double, single, and weak layers. The radio beacon measurements were validated and with the in situ SEEK2 sensors. The first two-dimensional image of a sporadic E-layer was produced from the data. The rocket beacon technique was shown to be an excellent tool to study Sporadic-E layers because absolute TEC accuracy of 0.01 TEC Units can be easily obtained and, with proper receiver placement, electron density images can be produced using computerized ionospheric tomography with better than 1 kilometer spatial resolution.

HF PROPAGATION MODELING INCORPORATING 3-D IONOSPHERIC DATA ASSIMILATION OUTPUTS

Ryan, F.¹, Bust, G², McGraw, J³¹Maritime Surveillance Div, CODE 271, SPAWAR Systems Center, San Diego, CA 92152-5001²Applied Research Lab, Univ Texas, P.O. Box 8029, Austin, TX 78713-8029³Photon Research Associates, Inc, 1616 N. Fort Meyer Dr., Suite 1000, Arlington, VA 22209

In March–April 2003, experiments were conducted using the Wide Aperture Research Facility (WARF) HF transmitter located near Lost Hills, California and a test site at White Sands Missile Range (WSMR), New Mexico. These tests were conducted on HF frequencies near dawn local time and involved single hop ionospheric paths with skip zones of 1200–1300km range. To simulate these conditions, a parabolic wave equation propagation code was driven with a physics based synoptic ionospheric model to simulate high-fidelity propagation effects including angle-of-arrival and target doppler shift.

During the experimental period, perturbations in the bottom-side ionosphere electron density structure contributed to enhanced signal strength conditions around the local pre-dawn minimum. This perturbed ionosphere supported HF propagation paths not predicted by climatological models such as IRI. To help understand these space weather conditions, the Ionospheric Data Assimilation 3-D (IDA3D) model was used to produce synoptic electron density profiles along the propagation path. The IDA3D code assimilates data from various sources including: ionosondes, GPS ground stations, GPS satellite occultation, and Coherent Ionospheric Doppler Receivers (CIDR) ground stations to produce a full 3-D ionosphere electron density field. Comparisons between IDA3D and climatological electron density profiles between WARF and WSMR will be shown.

The propagation model used in these simulations is a full-wave (i.e. amplitude and phase) electromagnetic parabolic wave equation (PWE) code based on the split-step Fourier algorithm. The PWE code incorporates variable terrain and surface dielectrics, antenna ground plane effects, and 3-D ionosphere electron density and collision frequency models. The propagation model can accept data from both climatological (e.g. IRI) and synoptic (space weather) ionosphere models. The PWE code includes effects of the earth's magnetic field and supports both Appleton and Sen-Wyller type magnetoionic plasma models. Unlike ray-based propagation codes, this PWE model automatically includes effects due to diffraction and caustics. Comparisons of predicted and measured target Doppler shifts will be shown.

RADAR IMAGING OF E REGION PLASMA IRREGULARITIES AND QP ECHOES OVER ARECIBO

D. L. Hysell¹, M. F. Larsen²¹Earth and Atmospheric Science, Cornell University, Ithaca, New York, U.S.A.²Physics and Astronomy, Clemson University, Clemson, South Carolina, U.S.A.

A 30 MHz coherent scatter radar was deployed on St. Croix in the summer of 2002 to support sporadic *E* layer observations made with the Arecibo incoherent scatter radar. The Arecibo radar was operated in dual beam azimuth scan mode and used long coded pulses to observe sporadic *E* layers with fine spatial resolution. At times, these layers were structured and unstable and produced intense field-aligned irregularities and coherent scatter. The locus of perpendicularity from St. Croix passes directly over Arecibo, permitting common volume coherent and incoherent scatter radar experiments. Aperture synthesis imaging techniques were applied to the 30 MHz radar data, permitting the unambiguous location of the echo sources in three dimensions. Radar imaging made it possible to collocate features in the ionization detected by Arecibo with the meter-scale irregularities. In this paper, we discuss radar imaging strategies, merits, and algorithms. We then analyze image data from the evening of June 14 when an intense QP echo event exhibiting both type 1 and type 2 echoes took place. We show that the coherent backscatter sometimes arrived from localized, patchy, polarized regions of space that drifted southwestward through the radar beam, giving the radar RTI map its characteristically streaked appearance. At other times, the patches merged, forming large-scale waves or fronts that were also polarized and propagating to the southwest. In both cases, the coherent backscatter arrived mainly from altitudes between about 95 and 110 km, the altitudes of the sporadic *E* layers, although echoes from higher altitudes were sometimes received.

Session G3, 13:40-Wednesday

RADAR AND RADIO

TECHNIQUES

Chairpersons: Frank Lind and John Sahr

FUNDAMENTALS OF THE INTERACTION OF RADIO SOUNDING SIGNALS WITH IONOSPHERIC IRREGULARITIES

Zabotin, N.A.^{1,2}, Wright, J.W.^{1,2}

¹CIRES, University of Colorado

²NGDC/NOAA

Development is underway of a new dynasonde system which will extend the capabilities of ionosonde methods for the ionospheric community, especially in the field of ionospheric fine-structure diagnostics. The multiplicity of scales of ionospheric irregularities implies a broad variety of effects on the characteristics of MF/HF radio sounding signals; a corresponding diversity of diagnostic and theoretical methods may be applied to study them. Irregularities and their effects may be divided roughly into two major classes. The role of large-scale irregularities (of the order of and larger than the first Fresnel zone scale, a few kilometers) is mainly to create a multi-beam structure of the reflected signal; related effects may be described in the language of geometrical optics. Smaller-scale irregularities are responsible primarily for multiple scattering and diffraction of the wave field, which requires application of other and more sophisticated tools: radiative transfer theory, scintillation theory, etc. Some phenomena observed in ionospheric sounding are of complex character, and their explanation should involve theoretical approaches from both categories. We use ray tracing simulations and numerical calculations using the theory of multiple scattering, to study the physics of radio signal reflection from a layer of ionospheric plasma with moderate irregularity amplitude. We reproduce phenomena that are quite regularly observed in practice, by dynasonde measurements: Multi-beam reflections, characterized by significant spatial spread of echolocations, do not demonstrate noticeable spread of virtual ranges. This feature of ionospheric radio echoes results in quite well-defined ionogram traces in relatively quiet conditions, although the irregularity amplitude is sufficient to produce significant spreading of echolocations and other easily measurable effects, (by the phase structure function, for example). We apply both techniques to investigate the "Spread F" phenomenon that occurs for higher irregularity amplitude. We show that both small-scale and large-scale irregularities may contribute to it. We treat the problem of practical determination of the regular peak plasma frequency value for spread F conditions. We analyze the influence of "glint" interference on the measurable parameters of radio echoes: phase, amplitude, echolocation and polarization. We simulate vector velocity estimations using the combination of dynasonde line-of-sight Doppler and echolocation data, and confirm the validity of this procedure although with certain restrictions. We suggest a theory based on the mechanism of multiple scattering of the observed sharp decrease of echo amplitude near the F2 layer penetration frequency and successfully compare its conclusions with observations.

APPLICATION OF ARTIFICIAL NEURAL NETWORK TECHNIQUES TO E-REGION HEIGHT TREND ANALYSIS

Sikdar, P., Berkey, F.T.
Utah State University

In this paper, the results from the application of artificial neural network techniques to the trend analysis of ionospheric E region height measurements will be discussed. The motivation for this study is derived from the work carried out by Danilov and Mikhailov [1999] and Bremer [1998], who have shown that the height of the E and F layers is decreasing. The model calculations of Rishbeth [1990] predict that the height of the E layer should decrease by 2.5 km if the height of the concentration of greenhouse gases is doubled in the atmosphere, while the analysis of Bremer [1998] has shown that the height of the E layer is decreasing at a much higher rate of 0.07km/yr (ie. much greater than the predicted values).

Most of the researchers studying the height of the E and F layer trends have used the method developed by Danilov and Mikhailov [1999]. This method is based on relative foE variations and twelve month running mean values. This approach was adopted to remove the effects of strong geomagnetic activity in foF2 and HmF2 trends. E region height trends have also been related to greenhouse gas concentrations, altitude, neutral composition, and temperature perturbations.

The approach used here uses a back-propagation neural network (BPNN) which has the ability to detect complex non-linear relationships between dependent and independent variables as well as the capability to generalize the essence of a set of input data. Parameters such as day-number, solar zenith angle, Ap, and frequency of the received signal would be used as input parameters to the BPNN. The data is then propagated via a network in which every neuron is connected to every other neuron in adjacent layers. Each interconnection has associated with it a scalar weight, which acts to modify the strength of the signal. The neurons within the hidden layer (inner layers) sum the weighted inputs to the neuron and pass the resulting sum through a non-linear activation function (sigmoidal function). The output of the network would be the E region height, produced by adjusting the connection weights between the nodes. The network would be trained using the E region height information obtained from the fuzzy-clustering algorithm developed by Sikdar and Berkey [2003].

The method would be tested on data obtained from the Dynasonde located at the Bear Lake Observatory in northeastern Utah at 41.9°N, 111.4°W (L=2.5). Plots of height trends produced by this method would be presented and compared with those obtained using the running average method.

IONOSPHERIC RADIOWAVE PROPAGATION USING
PARABOLIC WAVE EQUATION METHODSRyan, F.J.Maritime Surveillance Div, CODE 271, SPAWAR Systems Center,
San Diego, CA 92152-5001

This paper describes a full-wave ionospheric radiowave propagation method using the electromagnetic parabolic wave equation (PWE) technique. The PWE model is based upon a novel implementation of the split-step Fourier algorithm incorporating variable terrain and surface dielectric properties, and full 3-D ionosphere electron density and collision frequency models. The PWE code is computationally efficient, and incorporates features to model HF antenna-ground coupling.

The PWE technique rigorously incorporates all propagation modes including surface (ground) wave, terrain diffraction, and skywave. A wide-angle PWE propagator technique is used based upon a plane-wave spectral Green's function and Huygen's principle. This wide-angle propagator supports both normal shallow angle, but also near-vertical-incidence skywave (NVIS) type HF propagation paths. Antenna-ground coupling mechanisms allow for finite conductivity and ground plane effects to be included. The code uses 3-D ionosphere electron density and collision frequency profiles, and can accept data from both climatological (e.g. IRI) and synoptic (space weather) ionosphere models. Effects of the earth's magnetic field are supported via Appleton or Sen-Wyller type magnetoionic plasma models via specification of the complex ionosphere dielectric tensor. Unlike ray-based propagation codes, this PWE model automatically includes effects due to diffraction and caustics.

Examples of MF and HF propagation will be shown for simple Chapman type electron densities and more complex ionosphere electron density models. The effect of antenna ground plane interaction and the role of surface dielectric properties will be examined. Comparisons will be made between the PWE method and a fast asymptotic coherent ray trace code to illustrate signal field enhancement at caustics.

STRUCTURE OF THE POLAR ELECTROJET ANTENNA

Riddolls, R. J., Lee, M. C.

MIT Plasma Science and Fusion Center, 167 Albany St, Cambridge, MA 02139, USA

A method is described for determining the vertical profile of ionospheric antenna current generated during an electrojet modulation experiment.

The experiment consists of transmitting an amplitude-modulated high-frequency signal into the high-latitude ionosphere, which causes periodic heating of the plasma, and thus periodic modulation of the plasma conductivity. In the region of the polar electrojet current, these conductivity changes lead to alternating "antenna" current that radiates at the modulation frequency.

During a typical experiment, the modulation frequency is swept over the range 100 Hz to 40 kHz, and the magnitude and phase of the radiated magnetic field is measured on the ground, directly underneath the modified volume of ionospheric plasma. These measurements comprise the frequency response of the so-called "polar electrojet antenna".

It is shown that when the amplitude modulation of the high-frequency signal is fast compared to the thermal response of the plasma, the vertical profile of antenna current is related to the Fourier transform of the frequency response of the polar electrojet antenna. This relation arises from the interference of radiated fields from current at different altitudes.

Experiments were performed on 10 November 2002 using the HAARP high-frequency transmitter in Gakona, Alaska to determine the frequency response of the polar electrojet antenna. The vertical profile of antenna current deduced from the frequency response shows two oppositely directed horizontal current layers separated by about 10 km in altitude. This result suggests that the dominant antenna current structure during the modulation experiment is a vertical loop. A simple analytic theory is presented which illustrates the formation of such a loop under the condition that the background plasma conductivity varies exponentially in the vertical direction.

FAST RANGE AND DOPPLER ESTIMATION ALGORITHMS FOR PASSIVE RADAR

Morabito, A N, Meyer, M G, Sahr, J D
University of Washington Electrical Engineering

Passive radars provide excellent Doppler spectral estimates for deep fluctuating targets. Because the radar illumination is unpredictable, a full lag-profile or cross ambiguity analysis must be performed to extract the scatterer power spectrum as a function of range. Direct implementations of these algorithms are computationally expensive.

When the bandwidth of the target is significantly smaller than the bandwidth of the illumination, it is possible to significantly increase the speed of the detection algorithm. We will demonstrate two techniques that may be used together to achieve speed improvements of two to three orders of magnitude for 100 MHz FM observations. Our application is the observation of auroral electrojet irregularities.

The first method is essentially a coherent integration step, which reduces the data bandwidth by a factor on the order of 50, preserving the full range resolution.

Modern desktop computers have sufficient speed to evaluate the first algorithm to provide a range-Doppler estimate from a single receiver observing FM broadcasts. However, the computational burden increases linearly with the number of different transmitters observed, and quadratically with the number of antennas used for interferometric analysis. Furthermore, even the basic algorithm run time scales quadratically with bandwidth, which creates difficulty when wider bandwidth sources are used (such as digital TV).

Therefore, we have developed a further improvement. This method works by "channelizing" the illuminating and scattered signals, splitting the spectral bandwidth by an integer factor. This technique offers a speed increase by (approximately) that integer factor, but also decreases the range resolution by the integer factor.

We will briefly present the initial coherent integration method, and then show a variety of implementations of the channelized improvements. Properly implemented with 4 or 8 channels, these methods permit additional speed increases by factors of 7 and 15 on ordinary desktop workstations. These channelized methods work nicely with transmitters whose spectral content is not white, and permit the elimination of noise power which lies strictly outside the transmitter bandwidth, as well as beyond the decimation filter bandwidth of digital receivers.

THE AMISR - CHARACTERISTICS AND CAPABILITIES

Heinselmann, C.J., Kelly, J.D., Cousins, M.D.
SRI International

The Advanced Modular Incoherent Scatter Radar (AMISR) is presently being developed and fabricated for a 2005 initial deployment at Poker Flat Rocket Range near Fairbanks, Alaska. This system is based on a UHF phased array radar design with a high degree of modularity as well as distributed monitoring and control electronics. The bulk of the design has been validated through earlier prototype efforts, in conjunction with numerical calculations and simulations. Antenna range measurements have also been conducted to validate aspects of the overall design. Finally, smaller prototype radars have been deployed in the field for operational/functional testing.

The project is actually building three separate incoherent scatter radars, and the term we use to designate each radar is a face. Each of the three faces, in turn, consists nominally of 128 panels and each panel supports 32 antenna element units (AEUs). The AEU is comprised of a solid state power amplifier, a crossed-dipole antenna, an input board, a low noise amplifier board, a delay shifter board (with two separate delay paths) and a controller board. The panels can be configured in a number of different ways, depending on the scientific objectives of a given deployment.

In this talk, we will describe the overall architecture of the AMISR system, including several of the possible face configurations. We will also describe the control architecture build into the hardware and software systems and we will discuss how this impacts the potential scientific uses of the system. Test data will be presented to illustrate the performance characteristics inherent in the design. Finally, we will discuss progress made with the development of the data acquisition system and the close ties that the system has with the radars operation (e.g., for pulse-to-pulse beam steering).

INTERPRETATION OF THE SPECTRAL FEATURES FOR
RADAR SCATTER FROM SPACE SHUTTLE BURNS IN THE
IONOSPHERE

Bernhardt, P.A.¹, Erickson, P.J.², Lind, F.D.²
, Foster, J.C.², Sulzer, M.P.³

¹Plasma Physics Division, Naval Research Laboratory, Wash-
ington, DC 20375

²Atmospheric Sciences Group, MIT Haystack Observatory, West-
ford, Massachusetts 01886

³Arecibo Observatory, Arecibo, PR 00613

The Shuttle Ionospheric Modification with Pulsed Localized Exhaust (SIMPLEX) experiments use the Space Shuttle engines to study the ion beam distributions produced in regions of large relative neutral-plasma convection. The exhaust of the space shuttle provides a high speed neutral gas that streams through the ambient plasma of the ionosphere. The exhaust molecules exchange charge with the ambient O⁺-ions in the ionosphere to give ring-beam ion distributions. The velocity distribution functions observed with ISR during SIMPLEX are similar to those observed from the high latitude F-region by the incoherent scatter radar (ISR) facilities. The SIMPLEX experiments duplicate the conditions in the high latitude ionosphere by producing a large relative motion between the neutral and plasma species. At high latitudes, convection electric fields accelerates the ionospheric plasma to high speeds where charge exchange with neutrals yields ring velocity distributions. In the SIMPLEX experiments, the ionospheric plasma is nearly at rest relative to the neutral exhaust which is injected at high speed into the plasma. The relative motion, however, between the two species is identical for the two observation conditions. These distributions are studied with ground radars using incoherent scatter of radio waves from the electrons in the ionosphere. The electrons scatter is affected by both the ion distributions and any plasma turbulence in the modified ionosphere. The effects of the ion beams are transient because the ion particle motion is damped by ion-neutral collisions, the ring-distributions are damped by instabilities, and the molecular ions created by the charge exchange eventually recombine with the electrons. The ion beams created by the high speed exhaust produce a number of additional lines in the incoherent scatter spectra. Two processes for creation of these lines are considered. First, the scatter from the electrons is modified by the non-thermal distribution of ion velocities. Second, the scatter is modified by electrostatic waves from instabilities driven by the ion velocity distribution. A general treatment of incoherent scatter from ring-beam distributions has been described by Bernhardt et al [1998]. Using this theory, the parameters for the ring-beam distribution were adjusted to produce scatter at a central peak as shown in the observations.

ANALYSIS OF ARECIBO INCOHERENT SCATTER LONG PULSE DATA USING LINEAR REGULARIZATION PRIOR TO NON-LINEAR LEAST SQUARES FITTING

Sulzer, M.P.¹, Nikoular, R.²

¹Arecibo Observatory

²University of Illinois

Extracting geo-physical parameters from incoherent scatter data requires accounting for the smearing of information from one altitude over a range of altitudes. It also involves using a model to describe the spectrum at a single altitude. The full profile technique elegantly combines the two aspects in a single application of inverse theory for which the second aspect is ideally suited. However, there are no exact models for the variations of the parameters in altitude, and so there is no best way to apply the full profile technique. We discuss an alternate technique which we are developing for the Arecibo World Day (F region) data.

Storage of the IS data as lag profiles results in a very simple presentation of the range smearing: each measured (range-smearred) lag profile is related to the ideal profile by a convolution, where the convolving function is determined by the radar pulse shape. If one considers a deconvolution process, the deconvolution of each lag profile proceeds separately. If the spatial Fourier transforms of the convolving functions contain no zeros or near zeros, the process is simple. However, the spatial Fourier transform of a rectangular pulse does contain zeros. It is necessary to use a technique, such as linear regularization, to overcome the problems of a singular or ill-conditioned matrix, or to find a way to eliminate the zeros. We discuss here a combination of the two approaches. First, we eliminate all of the zeros at spatial frequencies for which the ionospheric profile has significant energy using a pair of modulated sequences. Then we use regularization to give good stability in the solution.

The regularization does the deconvolution, but it also acts as a sort of multiple input deconvolver so that waveforms (two or possibly more) with different modulation properties, which together contain all the required information, contribute simultaneously to the resulting single deconvolved profile.

It is possible to perform the fitting one height at a time if the parameter in the regularization is adjusted to smooth the profile sufficiently. With lightly smoothed profiles it is necessary to fit across a limited range of altitudes simultaneously. These procedures gives very similar results, allowing the use of the first, which is simpler.

THE WEAVING STEP: SYNCHRONIZATION IN SOFTWARE RADAR SYSTEMS

Erickson, P. J.¹, Lind, F. D.¹, Rideout, W.¹
, Grydeland, T.², Holt, J.¹

¹Atmospheric Sciences Group, MIT Haystack Observatory, Westford, MA 01886 USA

²Department of Physics, University of Tromso, N-9037 Troms, Norway

Recent advances in computing and information technology have made the Software Radar a reality, in which the majority of control and signal processing tasks are performed entirely in the digital domain and analog to digital transformation occurs as early in the radio frequency (RF) receiver signal chain as possible. This offers several key advantages, among which are predictability and stability of receiver component transfer functions and data streams which can be consumed by many clients simultaneously to enable multiple parallel information processing chains. A Software Radar system has been successfully implemented at the Millstone Hill incoherent scatter radar facility in Massachusetts, one of several National Science Foundation Upper Atmosphere Facilities.

The underlying flexible architecture of Software Radars, combined with the explicit goal of a system which can simultaneously support more than one experiment or analysis chain, suggests an overall radar composed of hardware and software agents who perform individual tasks (such as antenna control or transmitted peak power monitoring) in an asynchronous manner. Yet, many experimental goals, such as analysis of incoherent scatter power spectra or autocorrelation functions to determine ionospheric parameters, require that received data be time integrated and furthermore that information about radar system parameters be associated in synchrony with the integrated data records.

We have identified the software pattern, called a Weaver, which resolves asynchronous radar system events into synchronized information, organized into integration periods, for record-based processing. We discuss the features a Weaver must implement, and consider what external information such an agent must obtain from the overall environment in order to successfully insulate further analysis modules from the dynamic, asynchronous nature of the radar hardware and software. We will illustrate these points with examples from Millstone Hill incoherent scatter experiments, and conclude by discussing the architectural implications of Weaving patterns on overall Software Radar designs.

PERSISTENCE MANAGEMENT FOR RADIO SCIENCE
DATA SYSTEMS

Frank D. Lind, William J. Rideout, Philip J. Erickson
, John M. Holt

MIT Haystack Observatory, Route 40, Westford, MA 01886 USA

Persistence management is the organized preservation, delivery, and manipulation of information associated with the configuration, control, and data in a software system. With the increasing complexity of modern radio science systems it is becoming necessary to have a comprehensive approach to the persistence management of information associated with experimental systems. Modern ionospheric radar systems can have complicated software systems which must be controlled with precision and whose state must be well defined at all points in time to allow proper analysis of the resulting experimental data. These systems can generate terabytes of data and many separate streams of control information all of which must be organized for processing, searching, inspection, and archival. As an additional complication the configuration of these systems can change from experiment to experiment or even dynamically as a function of operational needs.

We will discuss a framework for persistence management based on the definition of a Radio Science Object Namespace using the extensible markup language (XML). The implementation of this framework is called the System Persistence Manager and it provides the means to systematically organize data objects in a distributed Software Radar system and to refer to the objects in this Object Web using Uniform Resource Indicators (URI; W3C RFC 2396). We will describe this system and its use, demonstrate its operation with a simple example, and discuss the design of appropriate Namespaces for mono-static and multi-static radar applications. Finally we will discuss how to obtain and use the implementation of the System Persistence Manager from the Open Radar Initiative.

Session G4, 8:40-Thursday

DATA ASSIMILATION

Chairpersons: Brian Wilson and Cliff Mintner

G4

ASSIMILATION OF GPS/MET RADIO OCCULTATION DATA
FOR A COUPLED THERMOSPHERE-IONOSPHERE MODEL

Chen, M.Q.¹, Huang, C.M.¹, Chu, Y.H.¹, Richmond, A.D.²

¹Institute of Space Science, National Central University, Taiwan, ROC

²High Altitude Observatory, National Center for Atmospheric Research, Colorado, USA

We represent a four-dimensional variational data assimilation (4DVAR) for TIE-GCM (thermosphere-ionosphere electrodynamics general circulation model) by using GPS/MET radio occultation data. The NCAR/TIE-GCM global circulation model is a self-consistently electrodynamic-coupled thermosphere and ionosphere model subjected by a few parameters and boundary conditions to describe the dynamic thermosphere and ionosphere. Global Positioning System (GPS) radio occultation signals received by a low earth orbit (LEO) satellite provide precisely measurement about the total electron content (TEC) along the signal paths to GPS satellites. We consider optimal use of GPS/MET occultation total electron content data to obtain the relative accuracy parameters used in TIE-GCM by minimizing the difference between the model results and measurements. The parameters used in TIE-GCM such as solar flux, hemisphere power, cross-tail potential, tidal modes at lower boundary, ionic oxygen flux at upper boundary, and background ionization rates are assuming constant within an assimilation cycle. The cost function associated with 4DVAR is constructed as the function of the model parameters and then be minimized with respect to the parameters. In order to compare the GPS/MET occultation TEC data with the model results, we made the model observed TEC by integrating the simulated electron densities along the line of sight from GPS to LEO (Microlab-1). We will examine the 4DVAR to the weather of the ionosphere from the simulated result of TIE-GCM in the day, February 23, 1997. In this paper, we will discuss the sensitivity of the model parameters for the GPS/MET radio occultation data. The initial values of the model input parameters are typical.

GLOBAL ASSIMILATION OF IONOSPHERIC MEASUREMENTS (GAIM)

Schunk, R. W.¹, Scherliess, L.¹, Sojka, J. J.¹,
Thompson, D. C.¹, Anderson, D. N.², Codrescu, M.²,
Minter, C.², Fuller-Rowell, T. J.², Heelis, R. A.³,
Hairston, M.³, Howe, B.⁴

¹Utah State University, Center for Atmospheric and Space Sciences, Logan, UT 84322-4405

²NOAA/Space Environment Center, Department of Commerce, 325 Broadway, Boulder, CO 80303

³University of Texas at Dallas, W. B. Hanson Center for Space Sciences, PO Box 830688, Richardson, TX 75083-0688

⁴University of Washington, Applied Physics Laboratory, 1013 NE 40th Street, Seattle, WA 98105

GAIM uses a physics-based ionosphere-plasmasphere-polar wind model and a Kalman filter as a basis for assimilating a diverse set of real-time (or near real-time) measurements. Some of the data that are assimilated include in situ electron density measurements from the DMSP satellites, bottomside electron density profiles from a network of digisondes, GPS-TEC data from a network of more than 300 stations, and occultation data. GAIM provides specifications and forecasts on a spatial grid that can be global, regional, or local (25 × 25 km). The primary GAIM output is in the form of 3-dimensional electron density distributions from 90 km to the geosynchronous altitude (35,000 km). GAIM also provides auxiliary parameters ($N_m F_2$, $h_m F_2$, $N_m E$, $h_m E$, slant and vertical TEC) and global distributions of the self-consistent ionospheric drivers (neutral winds and densities, magnetospheric and dynamo electric fields, and particle precipitation patterns). In its specification mode, GAIM provides quantitative estimates for the accuracy of the reconstructed ionospheric densities. In addition to the physics-based, Kalman filter model, we have also developed a Gauss-Markov Kalman filter model and an approximate (semi-physics-based) Kalman filter model. A beta version of the Gauss-Markov model has been running continuously and autonomously since January 1, 2003. This is a regional (mainly over the U.S.), high-resolution, data assimilation model that can assimilate GPS-TEC data from up to 400 of the NOAA CORS ground-based receivers. A global Gauss-Markov Kalman Filter model has been running continuously since July 1, 2003, and this model can assimilate four data types, including Ne profiles from digisondes, in situ satellite densities, GPS-TECs from 300 stations, and occultation data. The status of the models and the relevant scientific applications will be presented.

DAILY VALIDATION OF A GLOBAL IONOSPHERIC DATA ASSIMILATION MODEL

Wilson, B.¹, Hajj, G.¹, Wang, C.²
, Mandrake, L.¹, Pi, X.¹, Rosen, I.G.²

¹JET PROPULSION LABORATORY, 4800 Oak Grove Dr.,
Pasadena, CA 91109 USA

²Dept. of Mathematics, University of Southern California, CA
90089-1113 USA

As the number of ground and space-based receivers tracking the global positioning system (GPS) steadily increases, and the quantity of other ionospheric remote sensing data such as measurements of UV airglow also increases, it is becoming possible to monitor changes in the ionosphere continuously and on a global scale with unprecedented accuracy and reliability. A fully 3-dimensional Global Assimilative Ionosphere Model (GAIM) is currently being developed by a joint University of Southern California and Jet Propulsion Laboratory team. GAIM uses a first-principles ionospheric physics model (forward model) and Kalman filtering and 4DVAR techniques to not only solve for densities on a 3D grid but also estimate key driving forces which are inputs to the theoretical model, such as the ExB drift, neutral wind, and production terms. The driving forces are estimated using an adjoint equation to compute the required partial derivatives, thereby greatly reducing the computational demands compared to other techniques. For estimation of the grid densities, GAIM uses an approximate (sparse) Kalman filter implementation in which the portions of the covariance matrix that are retained are determined by assumed but physical correlation lengths in the ionosphere. GAIM produces a snapshot of the 3D ionosphere every 12 minutes for use in space weather monitoring, forecast, and basic plasma physics research.

GAIM uses multiple datatypes and will ultimately use many data sources. To date, we have analyzed numerous case studies using the following inputs: ground GPS TEC from tens to hundreds of sites, GPS occultation data (upward and downward TEC links) from IOX, CHAMP and SAC-C, and UV radiance data from nighttime limb scans of LORAAS on ARGOS. GAIM densities are validated by comparisons to NmF2 HmF2 values or bottom-side profiles from ionosondes, in situ densities from DMSP, vertical TEC measurements from TOPEX JASON, slant TEC measurements from independent GPS sites, density profiles from ISRs, and alternative retrieval techniques. The alternative retrievals include density profiles from Abel inversions of GPS occultations and NRLs Chapman-based 2D density retrievals from LORAAS. Daily GAIM runs have been performed for more than 9 months and validated against TOPEX vertical TEC, ionosondes, and independent slant GPS TEC values. We will present accuracy statistics and validation examples from the daily GAIM runs and several case studies.

ADVANCES IN NEUTRAL ATMOSPHERIC DATA ASSIMILATION USING IMPROVED FORCING ESTIMATION TECHNIQUES

Clifton F. Minter, Timothy J. Fuller-Rowell, Mihail V. Codrescu

CIRES - University of Colorado, NOAA - Space Environment Center

Using similar data assimilation techniques developed in meteorology and oceanography, a data assimilation system has been developed to provide a time-dependent estimate of the thermospheric density, temperature, and composition. Through its application, distinct characteristics of the neutral atmosphere have become apparent. It has been long realized that, unlike the troposphere, the neutral atmosphere is more strongly driven by external forcing, which includes Joule, particle, and solar heating. It has also been understood that knowing the forcing alone, over a period of days, can allow for a fairly accurate modeling of the neutral atmospheric conditions: density, temperature, and composition. Unfortunately, the magnitude and the distribution of the forcing are difficult to observe since scalar values are typically used to describe complicated processes. The research presented here attempts to better estimate the amount and distribution of the external forcing and its effect on the neutral atmosphere from observing the neutral atmospheric conditions and the changes in these conditions spatially and temporally. Since the magnitude and distribution of the forcing cannot be observed directly, a statistical approach is used to provide the best description for this process through a Kalman filter using an ensemble of states. Each member of the ensemble of states describing the neutral atmosphere is forced using various driver definitions. The physical model propagated result of each ensemble member is scored based on a comparison of the propagated state against the most recent observations. The best ensemble member is chosen as the new state representation and should reflect the appropriate level and distribution of the external forcing.

MODELING LOW-LATITUDE IONOSPHERIC WEATHER
USING GAIM WITH A 4DVAR APPROACH

Pi, X.^{1,2}, Wang, C.², Hajj, G. A.^{1,2}, Wilson, B. D.¹, Rosen, G.²

¹Jet Propulsion Laboratory, California Institute of Technology

²University of Southern California

The 4-dimensional variational approach (4DVAR) has been developed with the global assimilative ionospheric model (GAIM). The 4DVAR technique includes the following components: (1) parameterization of selected model drivers; (2) construction of a cost function that measures the difference between ionospheric observations and model predictions; (3) computation of the gradient of the cost function with respect to the parameters using an adjoint method that significantly increases computational efficiency; (4) execution of a non-linear least-squares minimization process attempting to estimate the model drivers, such as plasma ExB drift and thermospheric winds, that are required to minimize the cost function.

Such a 4DVAR approach has been exercised with assimilation of GPS data collected from the IGS global GPS network to estimate ionospheric model drivers and to optimize modeled state. Among the major drivers, the dynamical ones (plasma drift and thermospheric winds) present complicated weather behavior and their measurements are costly to acquire in real time over all regions. In this paper we will present the 4DVAR experiments for low-latitude modeling. In the experiments, ground-based GPS measurements are used to derive TEC along satellite and receiver links, and such TEC observations from all longitudes at low latitudes (within +/- 30 degrees) are assimilated into GAIM. We will show the results of improved ionospheric state and its validation with independent TEC measurements from the TOPEX altimeter, as well as simultaneously estimated plasma drift and thermospheric winds in geomagnetic meridional planes. The experiment results indicate that GAIM with the 4DVAR technique has a great potential in predicting low-latitude ionospheric weather and its dynamical drivers that determine various ionospheric phenomena.

ESTIMATING VTEC VALUES FOR GEOMAGNETIC PERTURBED CONDITIONS USING A MULTILAYER NEURAL NETWORK

Araujo-Pradere, E.A. , Anghel, Adela
Cires-Univ. of Colorado and SEC-NOAA

Following the success of the empirical F-region STORM model (Storm Time Empirical Ionospheric Correction Model), it would be valuable to construct a similar correction model in the International reference Ionosphere (IRI) for the vertical Total Electron Content (VTEC). The ionosphere, extending in various layers from approximately 50 km to more than 1000 km above the Earth, is a dispersive medium with respect to the GPS radio signals. The dispersion, or time delay between the two frequencies, provides a measure of integral TEC along the propagation path. From this information for all GPS satellites it is possible, applying diverse methods, to obtain the vertical TEC. For a mid-latitude station, the VTEC response to geomagnetic perturbed conditions is well known. A clearly defined, short-term positive phase early in the storm periods is followed by a long-lived negative phase. The negative phase of the ionospheric storm probably results from heating effects of the neutral atmosphere, which in turn upset the normal ionospheric production-loss processes, while the mechanism behind the positive phase is more difficult to assign. In this work, a multilayer feed-forward neural network has been designed and trained to explore the quantitative relationship between the time history of a geomagnetic activity index and the VTEC response. To train the neural network, data from 3 mid-latitude GPS stations across continental USA, corresponding to three storm periods through the 2000 equinoxes, was used. We found that the neural network performed better in capturing the non-linear relationship between the input and the output values than the classical least-squares method.

ESTIMATING DAYTIME VERTICAL EXB DRIFT VELOCITIES FROM EQUATORIAL MAGNETOMETER OBSERVATIONS USING A MULTILAYER NEURAL NETWORK

Anghel, A.¹, Anderson, D.¹, Chau, J.², Veliz, O.²¹CIRES, University of Colorado²Radio Observatorio de Jicamarca, Instituto Geofisico del Peru

The daytime equatorial electrojet is a narrow band of enhanced eastward current flowing in the 100 to 120 km altitude region within +/- 2 degrees latitude of the dip equator. The strength of the electrojet varies considerably from day-to-day and has its origin in the Sq current dynamo mechanism and the penetration of electric fields from high latitudes. A unique way of determining the daytime strength of the electrojet is to observe the difference in the magnitudes of the Horizontal (H) component between a magnetometer placed directly on the magnetic equator and one displaced 6 to 9 degrees away. The difference between these measured H values provides an indirect measure of the strength of the daytime electrojet current, and in turn, the magnitude of the vertical ExB drift velocity in the ionospheric F region. This paper discusses a recent study that has quantitatively established the relationship between the vertical daytime ExB drift velocity in the ionospheric F region and the (H) values measured by two magnetometers in the South American (west coast) longitude sector. Magnetometer H component observations from Jicamarca (0.8 N. dip lat.) and Piura (6.8 N. dip lat.) in Peru and daytime, vertical ExB drift velocities measured by the Jicamarca Unattended Long-term Investigations of the Ionosphere and Atmosphere (JULIA) radar have been used to establish this relationship. The magnetometer observations and the JULIA 150 km echo drift measurements were obtained for the period between August, 2001 and August, 2003. A multilayer feed-forward neural network has been designed and trained in order to estimate the quantitative relationship between the vertical daytime ExB drift velocities in the equatorial F-region and the ground-based magnetometer observations. We found that the neural network performed better in capturing the non-linear relationship between the input and the output values than the classical least-squares method. In addition, we discuss the importance of these findings as they relate to the Global Assimilation of Ionospheric Measurements (GAIM) model.

Session G5, 13:40-Thursday

GPS AND THE IONOSPHERE

Chairperson: Attila Komjathy

SATELLITE-BASED GLOBAL TEC MONITORING

Morris B. Pongratz, David M. Suszcynsky, T. Joseph Fitzgerald
, A. R. Jacobson

Los Alamos National Laboratory, Space Atmospheric Sciences
Group, Los Alamos, NM 87545

This paper details an ongoing effort to develop a Global Positioning System (GPS) satellite-based Very-High-Frequency (VHF) total-electron-content (TEC) monitor based on the detection of VHF emissions from lightning. The proposed system would be an outgrowth of an already-funded constellation of broadband VHF receivers to be flown on the upcoming Block IIF GPS satellite constellation. The conceptual design for the system will be presented and expected system performance and capabilities will be discussed in terms of VHF data analysis results from a similar system currently being flown and operated on the FORTE low-earth-orbit satellite. Analysis of the FORTE data set will be used to show that the technique can routinely measure TECs with small uncertainties.

The TEC is measured along the line-of-sight between observed terrestrial lightning events that emit VHF electromagnetic radiation and each satellite that detects the radiation. The dispersive effects of propagation of the lightning electromagnetic wave through the ionospheric and plasmaspheric plasmas cause the higher frequency components to arrive at the satellite before lower frequency components. From the dispersed time-of-arrival at several different frequencies we can derive the TEC between the lightning event and each satellite sensor that detects the lightning. Using multi-satellite techniques we can geolocate the lightning and the ionospheric penetration point of the lightning-satellite line-of-sight quite accurately. A single ground station could provide essentially real-time regional TEC coverage. Four ground stations could provide global, real-time TEC measurements to supplement existing ground-based systems, especially over broad ocean areas that are currently difficult to monitor. The technique would produce a spatially and temporally irregular, but global and continuous near-real-time map of TEC.

GPS OCCULTATION SENSOR OBSERVATIONS OF THE IONOSPHERIC E-REGION

Straus, P. R.¹, Hajj, G. A.², Anderson, P. C.¹, Crowley, G.³

¹The Aerospace Corporation, Mail Stop M2/259, PO Box 92957, Los Angeles, CA 90009

²Jet Propulsion Laboratory, M/S 238-600, 4800 Oak Grove Drive, Pasadena, CA 91001-8099

³Southwest Research Institute, 6220 Culebra Road, San Antonio, TX 78238-5166

GPS occultation sensor measurements of the GPS L1 (1575 MHz) and L2 (1227 MHz) signal phase can be used to derive line-of-sight total electron content (TEC). The GPS TEC values are highly precise in a relative sense, with noise levels on the order of 0.01 TECu. Limb-viewing occultation profiles of vertical TEC may be converted into electron density profiles by means of the Abel transform. The high relative TEC accuracy potentially leads to very precise profiles, resulting in an ability to remotely sense density features below the $10E4/cc$ level. Thus one would expect GPS occultations to provide a new means for observing E-region features. This is particularly true because the E-region often has significant vertical refractivity gradients, to which the occultation technique is particularly sensitive. However, the absolute accuracy of these retrievals can be compromised by the presence of F-region gradients, which violate the Abel assumption of spherical symmetry. Recently, Hocke and Igarashi (Structure of the Earth's lower ionosphere observed by GPS/MET radio occultation, *J. Geophys. Res.*, 107, SAI 4-1 (DOI 10.1029/2001JA900158) (2002)) have suggested a simple analytical technique for addressing this problem. We present an initial analysis of the gradient effects on E-region retrievals and discuss the effectiveness of the proposed technique in mitigating the effects of asymmetry. Examples from simulations and actual observations from the Ionospheric Occultation Experiment (IOX) will be presented to illustrate our results. The utility of low-density E-region measurements will be discussed in the context of validation of models predicting the evolution of the structure of the post-sunset equatorial anomaly region.

ESTIMATING IONOSPHERIC TOTAL ELECTRON CONTENT USING GPS MEASUREMENTS IN A CONICAL DOMAIN

Lawrence Sparks, Attila Komjathy, Anthony Mannucci
Jet Propulsion Laboratory

The presence of the ionosphere slows the propagation of Global Positioning System (GPS) signals. From GPS measurements of ionospheric delay, the integrated electron density along raypaths between satellites and receivers can be inferred. Modeling ionospheric total electron content (TEC) is an inherently four-dimensional problem: each GPS slant delay measurement depends upon the position and orientation of its raypath. Defining the ionospheric pierce point (IPP) of a raypath to be the point where the raypath intersects a reference ionospheric height, we can, for example, treat slant TEC measurements as functions of four parameters: the sublatitude and sublongitude of the IPP and the raypath azimuth and elevation angles at the IPP. This paper presents a method by which this four-dimensional problem can be broken into a set of two-dimensional problems.

The key to our approach is to restrict each fit of GPS measurements to a spatial domain encompassing signals from only one satellite or, alternatively, only one receiver, i.e., the measurements form a cone whose vertex is the position of the satellite or receiver. Fit parameters are retrieved for a cone assuming linear deviations of the electron density from local spherical symmetry. Maps of vertical TEC over a specified region may be generated by first solving for fit parameters associated with multiple cones, each with a different receiver or satellite at its vertex. The fit for any individual cone is strictly a two-dimensional problem; only when multiple cones are fit simultaneously does the four-dimensional nature of the problem reemerge.

We present results comparing the accuracy of the conical domain approach with that achieved using the standard thin-shell model. The accuracy of each approach is assessed using a missing-measurement analysis, i.e., the value of a measurement excluded from the fit is compared to the value predicted by the model. We assess accuracy using data sets from both quiet days and days when the ionosphere is disturbed. Furthermore, we assess the dependence of accuracy on latitude by comparing results based upon data sets from networks of dual-frequency GPS receivers in Brazil and the United States.

STUDYING HIGH LATITUDE IONOSPHERIC ACTIVITY
WITH GPS AND WAAS

Anthea J. Coster¹, Susan Skone², Valerie Hoyle²
, Catherine Laurin³

¹MIT Haystack Observatory, Off Route 40, Westford, MA 01886

²University of Calgary, Dept. of Geomatics Engineering, 2500
University Drive NW, Calgary, Alberta T2N 1N4 Canada

³MIT Lincoln Laboratory, Millstone Radar, Off Route 40, West-
ford, MA 01886

The high latitude ionosphere is associated with the presence of small-scale irregularities in the electron density, frequently associated with scintillations, and with regions of spatial and temporal decorrelations in the background ionosphere, making this region hard to model. One of the sources for these effects in the high latitudes is the phenomenon known as storm enhanced density (SED). SED has been studied in detail with incoherent scatter data, satellite data, and TEC data collected from multiple GPS receivers located across the US and Canada. Analysis of the GPS TEC data shows that during geomagnetic disturbances ionospheric plasma is transported from lower latitudes to higher latitudes, redistributing plasma across latitude and local time. SED can be described as a narrow plume of greatly enhanced TEC values (100 TEC units). A typical SEC plume would extend from the New England coast across the Great Lakes region and into central Canada. This paper looks at the relationship of SED plumes in Canada to the observed scintillation levels and the WAAS ionosphere model. We focus on the tongue of ionization that forms across the polar cap as the TEC plume enters the polar region, and show its interconnection with the SED plume of plasmaspheric material observed over the continental US and into Canada. Polar tongues of ionization formed in this way constitute a strong source of high-latitude space weather effects and radio scintillation.

We study these high latitude effects using data collected from the Canadian GPS Network for Ionosphere Monitoring (CANGIM) operated by the University of Calgary. Three reference sites - in Yellowknife, Athabaska and Calgary - currently cover approximately 1500 km in the North-South direction, allowing observation of both the auroral and sub-auroral regions. The CANGIM sites are equipped with NovAtel Modulated Precision Clock (MPC) receivers. These units contain dual frequency Euro4 cards with an internal integrated PC and precise oscillator. The CANGIM receivers have specialized firmware which provides scintillation parameters extracted from 50 Hz L1 phase observations, in addition to raw GPS code and phase observations, rates of change of total electron content (TEC), absolute TEC values, and WAAS messages. Approximately one year's worth of data from the CANGIM network has been compiled and has been used for this study.

THE IGS GLOBAL TEC MAPS: PRESENT AND FUTURE

Komjathy, A.¹, Hernandez-Pajares, M.²

¹Jet Propulsion Laboratory, Pasadena, CA 91109, USA

²Technical Univ. Catalonia, gAGE/UPC, Barcelona, Spain

The International GPS Service's (IGS) Ionospheric Working Group was established in 1998 with the main focus on producing reliable global total electron content (TEC) maps. The corresponding vertical ionospheric delay maps, obtained from the combination of those independently computed by individual analysis centers (e.g., CODE, EMR, ESA, JPL and UPC), appear to achieve a quality similar to or better than the individual analysis centers' maps. We achieved this important milestone at the end of 2002, thanks to the various improvements in the combination strategies and the more advanced TEC computation algorithms of the analysis centers. As a consequence of the efforts, the IGS global TEC maps became an official product in the April 2003 IGS Governing Board meeting.

The first part of the presentation will focus on demonstrating the performance of the IGS global TEC maps during the year 2003. Comparisons with TOPEX and JASON vertical TEC measurements will be provided. Furthermore, we will show examples of describing the effects of the ionospheric products on accurate geodetic positioning. The double differences of the ionospheric observables (i.e., differences between pairs of satellites and stations) will be investigated based on different baselines lengths.

In the second part of this talk, we will discuss the status of other ongoing activities, such as the generation of rapid IGS global TEC maps (with an intended latency of less than 48 hours); other validation efforts using external sources of data, such as ENVISAT and DORIS, and additional improvements in the combination strategy and TEC map resolution, to only mention a few.

ESTIMATION OF SPATIAL AND TEMPORAL IONOSPHERIC EFFECTS ON KOREAN GEODETIC GPS NETWORKS

Lim, S.S., Hahn, J.H.

Inha University, Inha University

The Korean Geodetic GPS Networks (KGGN) provide users with medium and long distance baseline GPS measurements. Among many GPS stations, eight stations with medium baselines are selected to obtain a two-dimensional image of ionospheric electron density by applying the computerized tomography. In this paper, both spatial and temporal ionospheric density map in terms of vertical total electron content (VTEC) over the Korean peninsula has been produced and analyzed. In doing so, large variations in the ionospheric delay becomes an obstacle to determine the integer ambiguity of the phase measurements. For this, integer ambiguities and cycle slips in the phase measurements are effectively resolved by employing a newly developed fast search engine, and then the ionospheric VTEC maps are derived by using the double differenced dual-frequency pseudoranges and carrier-phase cycles from these GPS networks. For each satellite and each epoch, the VTEC is computed and interpolated with the spline method and the inverse distance weighted method. The spline method provides the VTEC with wider range, compared to the inverse distance weighted method.

Based on daily and monthly variations of ionospheric effects on the networks, a new ionospheric delay estimator is obtained. This model is compared with classical Klobuchar's model and the International Reference Ionosphere model which is available from the National Space Science Data Center. Also, this model has been used for single frequency and/or stand-alone GPS users in the region to improve their accuracy. Several field tests are performed and it was capable of recovering the ionospheric delay at decimeter-level accuracy in real time.

Session G/H1, 13:40-Monday

LIGHTNING EFFECTS

Chairperson: Steve Cummer and Victor Pasko

G/H1

LIGHTNING AND TLES: WHAT WE KNOW, WHAT WE DONT AND EMERGING OBSERVATIONAL TOOLS

Lyons, W.A.¹, Cummer, S.A.², Stanley, M.A.³¹FMA Research, Inc., Fort Collins, CO²Duke University, Durham, NC³Los Alamos National Laboratory, Los Alamos, NM

The discovery of sprites in 1989, and a host of other lightning-related transient luminous events (TLEs) in the stratosphere and mesosphere, has placed renewed emphasis on the characterization of lightning discharges. This review details how TLE research has spurred a new appreciation of the great range of values in the key metrics used to describe lightning events. For many years, visual observations, simple photography, video, spectroscopy and electric field measurements dominated lightning measurement systems. The advent of the National Lightning Detection Network (NLDN) allowed detection, location, and estimation of the peak currents and polarity of CG strokes. It soon became apparent that not only were there significant geographic variations in lightning flash density, but in other key parameters as well, including polarity, peak current and stroke multiplicity. Satellite-borne sensors, including TRMM and OTD, have mapped the marked differences between continental and maritime lightning regimes worldwide. Space Shuttle imagery visibly portrayed the complexity of lightning discharges in storm systems, often revealing exceptionally large and long-lasting illuminated regions. More recently (MEIDEX), the Shuttle has mapped both lightning and TLEs from space. ELF remote sensing utilizes intense transients associated with the TLE parent lightning to underscore the apparent necessity (though not necessarily sufficiency) of large change moment change values for sprite production, values much larger than quoted in text books of decades past. Three-dimensional lightning mapping arrays, such as New Mexico Techs LMA, reveal the horizontal and vertical extent of the cloud from which charge is removed in CG flashes. Orders of magnitude differences in the charge removal volume may be found when comparing flashes. LMA data, when combined with ELF charge moment change data, provide an estimate of the charge lowered in CGs. But many questions remain about the details of the lightning discharges which induce sprites, and in particular, the role of the continuing current. A unique set of high speed (1000 fps) images of CG discharges reveal complex patterns of optically detectable continuing currents. Often lasting hundreds of milliseconds, and occurring with both CG polarities, this new technology further illustrates the great diversity within lightning discharges. Possible approaches for using new high speed imaging techniques to investigate sprite parent +CGs, especially in combination with ELF-derived estimates of the current-moment, will be discussed.

SPRITES/TLES RESEARCHES IN TAIWAN*

Su, H.T.¹, Hsu, R.R.¹, Chen, A.B.¹, Lee, L.C.²¹National Cheng Kung University²National Space Program Office

Researches on upper atmospheric transient luminous events (TLEs) at the National Cheng Kung University, Taiwan started around 1999, when the first two authors participated in the Sprites 99 campaign led by Prof. S.B. Mende of UC-Berkeley carried out at Kitt Peak National Observatory. In the ensuing years, we have staged ground campaigns in Taiwan to look for sprites and other TLEs in this region. So far, we have successfully confirmed the existence of sprites over Asian continent and South China Sea in 2001, and found several gigantic jets in 2002. For the observed land sprites in 2001, 90 percent of them were either carrots and columniforms and 64 percent of sprites occurred in cluster. For the oceanic sprites, 89 percent of them are carrots, whereas only 22 percent were in groups. The gigantic jets established a direct optical link between a thunder-cloud (altitude ,16 km) and the ionosphere at 90 km elevation. Extremely-low-frequency radio waves in four events were detected, while likely there is no cloud-to-ground lightning to trigger these events. Our result indicates possibly that the extremely-low-frequency waves were generated by negative cloud-to-ionosphere discharges, which would reduce the electrical potential between ionosphere and ground. On the instruments, we have also added electric and magnetic elf antenna to our array of TLE monitoring tools in 2002 and 2003. With the launch of ROCSAT-2 satellite in November of 2003, we will have a set of instrument named ISUAL, which consist of a optical imager, a six-channel spectrophotometer, and a dual band array photometer, to monitor TLEs from space. In this talk, the current TLE research topics and instruments at the NCKU will be presented.

*Work supported in part by National Space Program Office under grant numbers 92-NSPO(B)-ISUAL-FA09-01 and 93-NSPO(B)-ISUAL-FA09-01.

MODELING OF AIR HEATING AND IONIZATION IN GIGANTIC JETS

V. P. Pasko

CSSL Laboratory, The Pennsylvania State University, University Park, PA 16802, USA

Recent observations of gigantic jet events emanating from thundercloud tops, exhibiting some lightning like features near the cloud tops, and then propagating upward through the altitude range typically occupied by sprites [Pasko et al., *Nature*, **416**, 152, 2002; Su et al., *Nature*, **423**, 974, 2003] represent an opportunity to study a transition from lightning-like structures at thundercloud altitudes to large scale filamentary sprite-like structures at the lower ionospheric altitudes. It is likely that this new type of transient luminous events originates from a streamer zone of conventional lightning leaders and represents a final jump stage of the leader process, when the streamer zone of a leader makes contact with the opposite electrode (i.e., ionosphere) [Pasko and George, *JGR*, **107**, doi:10.1029/2002JA009473, 2002]. The understanding of streamer-to-leader transition and scaling of this transition as a function of atmospheric pressure therefore represents a first necessary step toward understanding of complex dynamics of optical features observed in these events. In this talk we will present results of modeling studies, which allow investigation of effective time scales of the initial stage of air heating in streamer channels up to 5000 °K at which the thermal ionization becomes important. The model is zero-dimensional and accounts for time dynamics of air heating and ionization at a fixed point inside of the streamer channel. The model is derived from previous studies conducted for similar purposes at ground pressure [Lowke, *J. Phys. D: Appl. Phys.*, **25**, 202, 1992; Naidis, *J. Phys. D: Appl. Phys.*, **32**, 2649, 1999; Vidal et al., *IEEE Trans. Plasma Sci.*, **30**, 1339, 2002]. In the first part of the talk for calibration purposes we will present comparisons of our model and available laboratory data on time scales of air heating in streamer channels at ground and near ground pressures [Larsson, *J. Phys. D: Appl. Phys.*, **31**, 1998] following approach described in [Naidis, 1999]. In the second part we will present results corresponding to a range of air pressures, electric fields and electron densities representative of conditions in streamer channels in gigantic jets. The obtained transition times indicate that the re-brightening events observed by Pasko et al. [2002] and trailing jet events observed by Su et al. [2003], which terminate at altitudes around 50-60 km, likely correspond to the final section of an upward leader, which was not able to complete the next step due to a dramatic increase in air heating time scales above 50 km.

ROLE OF NEUTRAL DENSITY AND CONDUCTIVITY PERTURBATIONS IN DETERMINING SPRITE INITIATION LOCATIONS

Sao Sabbas, F.T.¹, Sentman, D.D.², Otto, A.²¹National Institute for Space Research - INPE, Brazil²University of Alaska Fairbanks, USA

Multiple sprites are often observed to occur simultaneously, laterally displaced from the underlying causative cloud-to-ground (CG) lightning discharge. The causes of this lateral displacement are presently not understood. This paper investigates the role of neutral density and conductivity perturbations in determining the locations of sprite initiation. The work was motivated by two previous studies: (1) A detailed statistical study of the temporal-spatial relationships between sprites and the associated CG was performed for July 22, 1996, showing that the distribution of sprite offsets relative to the underlying lightning had a mean of 40 km [São Sabbas et al., 2003]. (2) A follow up study for the same observations investigating the relationship of the sprites and lightning to convective activity in the underlying thunderstorm, showing that the maximum sprite and -CG production of the system were simultaneously reached at the time of maximum contiguous cloud cover of the coldest region, corresponding to the period of greatest convective activity of the system [São Sabbas and Sentman, 2003]. Thunderstorm convective activity is a potential source of gravity waves and mesospheric turbulence, which create an inhomogeneous neutral density background. For this paper computer simulations of the temporal-spatial evolution of lightning-induced electric fields in an inhomogeneous mesospheric neutral density, and therefore conductivity, were performed. The perturbations modeled in the simulations spanned the amplitude range 10% to 40% of the ambient background neutral density, with characteristic scale sizes of 2 km and 5 km, respectively. The results indicate that neutral density spatial structure facilitates electrical breakdown in isolated regions of density depletions at sprite initiation altitudes. These spatially distributed breakdown regions provide the seed electrons necessary for sprite generation, and may account for the observed sprite offsets. Furthermore, neutral density depletions may play critical role in setting the overall sprite activity level above a thunderstorm.

OPTICAL OBSERVATIONS OF CONJUGATE SPRITES AS
EVIDENCE FOR GEOMAGNETICALLY TRAPPED RELA-
TIVISTIC ELECTRON BEAMS

Robert A. Marshall, Umran S. Inan
Stanford University

Theoretical studies have predicted that large positive cloud-to-ground discharges can trigger a runaway avalanche process of relativistic electrons, forming a geomagnetically trapped electron beam. The beam undergoes pitch angle and energy scattering during its traverse, and a small percentage of electrons remain in the loss cone and precipitate in the magnetically conjugate atmosphere. In particular, N2 1P and N2+ 1N optical emissions are expected to be observable. The remaining beam electrons are predicted to constitute a significant source of radiation belt electrons. In July and August 2003, an attempt was made to detect these optical emissions, called conjugate sprites, and thus evidence of geomagnetically trapped electron beams, and correlate them to sprite observations in Europe near $L \sim 1.8$. In the northern region, two remote-controlled low-light CCD cameras were installed at the Observatoire Midi-Pyrenes (OMP) in France to observe sprites in southern France and northern Spain. Additionally, VLF receivers were installed in Europe to detect causative sferics and ionospheric disturbances associated with sprites. In the southern region, the Wide-angle Array for Sprite Photometry (WASP) was set up to observe conjugate sprites near Sutherland, South Africa, with a field-of-view magnetically conjugate to the northern observing region. A VLF receiver was also set up at SAAO to detect ionospheric disturbances of VLF transmitter paths caused by relativistic electron beams. The team at OMP has observed over 100 sprites. Further analysis is required to determine whether conjugate sprites have been observed. We present initial analysis of optical data recorded at SAAO as well as charge-moment analysis of causative sferics to determine the likelihood of the conjugate events.

COMPARISON OF PHOTOMETRIC MEASUREMENTS AND
CHARGE MOMENT ESTIMATIONS IN TWO SPRITE-
PRODUCING STORMSGerken, E.A.¹, Inan, U.S.²¹Cornell University²STAR Laboratory, Stanford University

Hundreds of sprites have been observed by the Stanford University telescopic imager [Gerken *et al.*, 2002]. This imaging system includes a telescopic ($\sim 1^\circ$) photometer and a wide field of view ($\sim 3.3^\circ$ by 6.6°) photometer. Electromagnetic signatures of causative lightning discharges, known as sferics, are recorded simultaneously using crossed-loop magnetic antennas and ELF/VLF receivers located at Stanford and in Colorado. The photometer tubes are Hamamatsu HC-124-01 PMTs and have photocathodes that are sensitive to photons between 185 nm and 800 nm wavelength. The wide FOV PMT is longpass filtered with a cutoff of ~ 650 nm in order to provide a better signal-to-noise ratio for the observation of excitation in sprites, namely the N2 first positive band around 700 nm. The electrical signal output from a single PMT is low-pass filtered to frequencies below 25 kHz. Results of a two-storm case study suggest that storm properties such as the spatial extent and flash rate can play a significant role in determining the properties of sprites. In one relatively small storm on July 2, 2000, 276 sprites were observed between 04:00-07:00 UT. These sprites were largely confined to 70-85 km altitude, were relatively faint and diffuse, were typically associated with very high peak currents and short time duration, and exhibited little or no associated ELF generation. The second storm, on July 4, 2000, had a much larger spatial extent and 27 sprites were observed between 04:00-07:00 UT in a wide range of shapes and time scales spanning 40-90 km altitude. These sprites were produced by 20-120 kA CG's, had complex optical signatures, and were frequently associated with observed ELF radiation. These observations lead to the hypothesis that relatively small storms mainly produce sprites in the form of diffuse glow whereas larger storms with higher cloud tops can initiate streamer discharges leading to more spectacular sprites. Examination of optical decay time constants suggests that it may be possible to distinguish between diffuse glow and streamer mechanisms on the basis of photometric measurements.

INTERACTION OF SPRITE STREAMERS WITH THE LOWER IONOSPHERE

N. Liu, V. P. Pasko

CSSL Laboratory, The Pennsylvania State University, University Park, PA 16802, USA

Sprites are large luminous discharges, which appear in the altitude range of ~40 to 90 km above large thunderstorms [e.g., Sentman et al., *GRL*, **22**, 1205, 1995]. Recent telescopic imaging of sprites revealed that sprites commonly consist of large numbers of needle-shaped filaments of ionization, called streamers [e.g., Gerken and Inan, *JASTP*, **65**, 567, 2003]. Also recently, it has been demonstrated that sprites often exhibit a sharp altitude transition between their upper region, which has appearance of a diffuse glow, and the lower highly structured region dominated by streamers [e.g., Pasko and Stenbaek-Nielsen, *GRL*, **29**, 10.1029/2001GL014241, 2002; Gerken and Inan, 2003, and references cited therein]. A new two-dimensional model has recently been developed at Penn State for studies of sprite streamers [Liu et al., *Eos. Trans. AGU, Fall Meet. Suppl.*, **83**, F137, 2002]. The model accounts for effects of photoionization on dynamics of streamers in air at different pressures and allows studies of streamers initiated by single electron avalanches in large applied electric fields exceeding the conventional breakdown threshold defined by the equality of the ionization and dissociative attachment coefficients in air [Raizer, *Gas Discharge Physics*, 1991, p. 135]. The physical mechanisms of initiation of sprite streamers are poorly understood at present [Moudry et al., *JASTP*, **65**, 509-518, 2003], especially in those sprites, which are created by relatively weak lightning discharges not capable of generating electric fields exceeding the conventional breakdown threshold at the mesospheric/lower ionospheric altitudes [Hu et al., *GRL*, **29**, 10.1029/2001GL014593, 2002]. It has recently been speculated that an enhancement of the electric field at the bottom of sprite halo may create favorable conditions for subsequent streamer breakdown [Barrington-Leigh et al., *JGR*, **107**, 1065, 2001]. In this talk we will discuss the vertical structuring of optical luminosity in sprites and existing mechanisms of initiation of sprite streamers, including a possible role of sprite halo in this process. We will also provide related results of numerical simulations of interaction of sprite streamers with the lower ionosphere in the streamer-to-diffuse glow transition region of sprites using a modified version of Liu et al. [2002] model.

SPRITE LIGHT IN A BOTTLE

Earle Williams¹, Michael Valente², Robert Golka³

¹Massachusetts Institute of Technology, Parsons Laboratory 48-211, Cambridge, MA 02139

²East Coast Induction, Inc., Brockton, MA 02305-2039

³Golka Associates, P.O. Box 676, Brockton, MA 02303-0676

A large (diameter 2 ft; length 6 ft) air-filled glow discharge tube operating at pressures typical of the atmospheric altitude range 50-80 km is being used to interpret ground-based observations of red sprites. The larger-than-usual tube size has been used with the aim of minimizing wall and electrode effects on the internal glow discharge. Absolute radiance measurements (watts/m²/sr/nm) in a band from 380-780 nm have been obtained with a PR-650 photometer (Photo Research). The absolute radiances are converted to Rayleighs (R) for quantitative comparison with published field observations. Current and voltage measurements during DC excitation have been used to compute volume power dissipation (watts/m³). Consistent with measurements on sprites, the dominant spectral features in the positive column of the discharge tube are the first positive (N₂1P) bands from molecular nitrogen, and are remarkably well matched with published observations of spectra on red sprites (e.g., Hampton et al, 1996). Similar spectra (and similar luminous efficiencies of order one percent) are obtained over three orders of magnitude of power dissipation and current density in the tube. Traditional glow discharge tube measurements reported in the literature have been carried out with current densities of order 10 amp/m² and with dissipation rates of kilowatts/m³. When the present tube is operated under these conditions, the measured radiances are in the gigaRayleigh range. To duplicate the smaller radiance values (100 kR-several MR) in telescopic imagery of sprites (Gerken et al, 2000), the tube must be operated up the negative differential resistance characteristic to higher voltage (1 kilovolt), lower current density (10-2 amp/m), and lower power dissipation (watts/m³). The laboratory measurements relating radiance in Rayleighs and the tube current density can then be used in conjunction with calibrated telescope imagery to infer the current in observed sprite filaments. On this basis, a sprite filament 100 meters in diameter (Gerken et al, 2000) is inferred to carry a current of the order of 100 amperes. Further analysis on the tube luminous efficiency and the plasma electron density and electrical conductivity, over a wide range of pressure and current density, will be discussed.

FULL-WAVE SOLUTION OF PROPAGATION OF TRANSIENT SIGNALS IN WAVE-GUIDES

Ferencz, O. E.

Space Research Group, Eotvos University, Geophys. Dept.

The investigation of (short) impulse propagation in wave-guides is important research topic. The known solutions are based upon the well-known monochromatic approaches, examining the different frequencies separately or building the model and the theory on a fundamentally monochromatic starting point (e.g. permittivity tensor, which is defined originally by assuming an $\exp(j\omega t)$ type solution form).

In this paper a new theoretical model and solving method will be presented for a square cross-sectioned wave-guide filled by vacuum or magnetised anisotropic plasma, excited by an arbitrarily formed transient electromagnetic signal (Dirac, or real, even short impulse). This method avoids the application of the former assumptions regarding the sinusoidal waveforms. The theoretical basis of the solving method can be found in [1] for transient plane waves. The obtained closed-formed solution leads back to the ones known for monochromatic excitation, by using a sinusoidal excitation with a given frequency. The generally directed exciting current density is

$$\vec{J}_1 = J_{1x} \cdot \vec{i} + J_{1y} \cdot \vec{j} + J_{1z} \cdot \vec{k} \quad (1)$$

$$|J_1| = \delta(t) \cdot \delta(x) \cdot B_1(y) \cdot B_2(z) \quad (2)$$

where $B_1(y)$ and $B_2(z)$ are envelope functions containing the boundary conditions

$$B_1(0) = B_1(a) \equiv 0 \quad B_2(0) = B_2(b) \equiv 0 \quad (3)$$

Applying the presented solving method for Dirac excitation, the transfer function of the wave-guide filled by vacuum or magnetized plasma can be described. This result opens the way for investigation of real (short) impulse propagation in wave-guides and the transient propagation phenomena. As a possible application of the new result, a geophysical example will be presented for the Earth-ionosphere wave-guide. By the application of this solution it became possible to monitor the bottom of the ionosphere continuously. It is not necessary to use the averaging of many observed spherics for the estimation of the height of the D layer, because the new model makes it possible to use each individual observed spheric separately. The distance of the lightning source can be estimated from the dispersion fitting of the measured and calculated signals. The direction of incidence is well determinable from the ratio of H_x and H_y components.

Reference: [1] Ferencz Cs., Ferencz O.E., Hamar D. and Lichtenberger J: Whistler Phenomena, Short Impulse Propagation; Kluwer Academic Publishers, Astrophysics and Space Science Library, Dordrecht, 2001.

CURRENT AND CHARGE MOMENT IN SPRITE-PRODUCING AND NON-SPRITE-PRODUCING LIGHTNING

Cummer, S.A.¹, Lyons, W.A.²¹Electrical and Computer Engineering Department, Duke University, Durham, NC 27708 USA²FMA Research, Inc., Fort Collins, CO 80254 USA

Ongoing measurements have shown that the relationship between lightning and sprites is be complicated. Lightning discharges with large charge moment changes, which create relatively strong electric fields at mesospheric altitudes, do preferentially generate sprites. However, it is known experimentally that exceptionally few sprites are created by negative cloud-to-ground (CG) lightning, despite measurements showing similar occurrence rates between large +CG and -CG lightning in many circumstances [e.g., Huang et al., JGR, 1999]. This polarity asymmetry is not well-understood. Moreover, a preliminary analysis of charge moment changes in many North American sprite-producing discharges during the summer of 2000 has indicated that similar discharges sometimes do and sometimes do not make sprites [Hu and Cummer, GRL, 2002], suggesting at a minimum some day-to-day variability in the ability of lightning to generate sprites. We will present a systematic study of the lightning in individual thunderstorms to determine the differences between lightning that does and does not generate sprites. Local video and remote extremely low frequency (ELF) magnetic field measurements were made during the Severe Thunderstorm Electrification and Precipitation Study (STEPS) in the summer of 2000. These measurements are a relatively complete set of sprite occurrences and lightning charge moment changes spanning many days and individual storms. Specific issues that will be addressed include a comparison in individual storms of charge moment changes in positive cloud-to-ground (CG) lightning that did and did not generate sprites, and a determination of the distribution and limits of charge moment changes in negative CG lightning throughout the entire campaign period. An improved understanding of why some lightning discharges do generate sprites and others do not should expand our knowledge of sprites processes and their global implications.

Session G/H2, 8:40 Wednesday

METEORS

Chairperson: Sigrid Close

G/H2

THE APPLICATION OF PLASMA CONCEPTS TO RADAR
METEOR ISSUES

John D Mathews
Penn State University

Recent observations of head-echoes, anomalous trail-echoes, and "classical" trail-echoes at frequencies ranging from HF through about 1 GHz has raised radio science issues concerning the origins of the observed radar scattering cross-sections. In particular, the role of under- versus over-dense (relative to plasma frequency) scattering has been widely discussed. We review the relationship between dielectric permittivity and the concept of "plasma frequency" and how standard concepts such as scattering, reflection, multiple-scattering, phase velocity, and group velocity arise in "plasmas" without DC B-fields. In particular, the need for "Fresnel areas"—the analog for Fresnel-zones along a meteor trail—is demonstrated in terms of building a multi-scattering outcome that comprises reflection of a wave of frequency below the plasma frequency. The volume—and total enclosed electrons—from which forward scattering, observed from a point within a plasma, develops determines the incumbent phase and group speeds. This volume can be made progressively smaller for equal effects as the number of enclosed electrons increases. A small-volume plasma can only exhibit over-dense scattering behavior if the local plasma frequency is well above the frequency of the incident wave. This limit underscores the transition from plasma to metal behaviors. When this condition is violated—that is, when coherent multiple-scattering does not occur—then net scattering can be simply determined by coherently adding the scattering contributions from individual electrons in what is essentially under-dense scattering that includes the possibility of incoherent scattering if a suitable description of electron location and motion is included. Possible over-dense scattering from meteor trails is also discussed from the point of view of the development of multiple scattering and the validity of plasma frequency as a measure of the scattering properties of trails.

LARGE, SHOCK-LIKE LUMINOUS STRUCTURES OBSERVED IN LEONID METEORS

Stenbaek-Nielsen, H.C.Geophysical Institute, Univ of Alaska

A 1000 frames per second intensified CCD camera with a 6.4x6.4 degree field of view was used to record Leonid meteors during the November 2001 and 2002 meteor showers. The 2001 observations were made from Poker Flat research range, Alaska, while the 2003 observations were from the NASA DC-8 flying over the Atlantic as part of the 2002 Leonid Multi-instrument Aircraft Campaign. A total of 63 meteors were recorded in 2002 and 4 in 2001 (the weather in 2001 was not cooperating). Of these 43 have tracks consistent with the known Leonid radiant and hence are likely Leonids. The altitudes of the tracks ranged from 142 km to 89 km as determined assuming an entry velocity and that this velocity is not affected by ablation. The height-luminosity curves varied considerably between events, and there were a number of sudden brightness changes in individual events possibly indicating breakup of the meteor body. A bright (estimated mag -3) Leonid in the 2001 shower displayed a spectacular, shock-like luminous front around the meteor with a scale size of several 100 m. The structure started to develop at an altitude of 111 km and was fully developed at an altitude of 105 km. This single observation was very surprising, and hence, a major goal for the 2002 mission was to confirm the 2001 observation. While no similarly spectacular event was recorded, there were two meteors with indications of a shock-like structures, but observations were only made at altitudes below that of the 2001 event. The cause of the shock-like structure is uncertain. The size is too large for a classical fluid shock. Possible plasma and photo-chemical processes are being investigated.

THE APPLICATION OF AN AUTOMATED SEARCHING ROUTINE TO SPORADIC METEOR OBSERVATIONS

Briczinski, S.J., Mathews, J.D.

The Pennsylvania State University, Communications and Space Sciences Laboratory

The micrometeor observations performed using the 430 MHz Arecibo Observatory radar have proven to be crucial for the understanding of meteoric effects on the aeronomy of the upper atmosphere. Previous techniques using the Arecibo radar have required manual confirmation of each event, followed by direct measurements of the parameters (i.e. altitudes, velocities and decelerations). Observations of sporadic (non-shower) meteors during February of 2001 have been analyzed with an FFT periodic search algorithm that automatically detects meteor events between altitudes of 85 and 125 km. We present the new technique used to detect meteors as well as the measured parameters obtained from this method. The results of the new automated technique are compared with previous results. This new technique shows an improvement over traditional searching routines by increasing the event rate by as much as 30 percent. In some cases meteor events are observed that appear to catastrophically destruct within the beam. These events appear to undergo minor ablation of their volatile components before annihilation—the terminal event—that occurs in under 1 ms. As with essentially all observed meteoroids, the meteoroids that disappear in a terminal event appear to experience linear decelerations before their abrupt disappearance. This non-ablative mass deposition process may play an important role in the composition of the upper atmosphere as it apparently produces sub-micron sized particles. We present the meteor parameters obtained from an automatic FFT meteor searching routine and consider the terminal-event destruction of meteoroids and resultant mass deposition as an important factor in the aeronomy of the meteor zone. We also present the first results on the altitude, speed, and mass distributions of terminal event meteoroids yielding some clues on the physics of the terminal-event.

USING METEOR CASE STUDIES TO DETERMINE HEAD ECHO AND

Lars Dyrud, Sigrid Close, Meers Oppenheim
Center for Space Physics, Boston University

Recent observations demonstrate that sensitive radars, such as Altair, Arecibo, EISCAT, Jicamarca and MU, are capable of detecting non-traditional meteor phenomena. These large aperture radars detect plasma generated from direct meteor entry (head echos) which are often followed by non-specular trail reflections over an extended range. We present case studies of simultaneous head echos and non-specular trails that present us with the unique opportunity of determining some of the radio scattering properties of both head echos and non-specular trails. An understanding of head echo and non-specular trail scattering properties is critical for using these radar phenomena to derive the properties of the meteor that generated them.

The case studies we present are examples where head echo reflections and trail radio scatter were generated from a single meteor but the reflections do not necessarily occur at the same altitude. Such examples include cases where non-specular trail scatter occurs at lower altitudes than the head echo. These examples allow us to analyze two aspects of head scattering properties. The first is that the head echo SNR decreases rapidly - falling to noise levels over the course of only a few range gates. Without the trail echo one would likely determine that the meteoroid has been completely ablated at the altitude where the head echo disappears. Yet, the trail scatter below this point indicates that the meteor plasma has merely rapidly fallen beneath the head echo scattering threshold, not disappeared. Second, using models of both meteor ablation and head scattering we can use these cases to derive the minimum line density required for a head reflection at various altitudes.

These cases also allow us to understand the how non-specular trails and head echos vary when generated by meteors of different velocities as discussed in Dyrud et al. [GRL, 2002].

MICROMETEOR OBSERVATIONS WITH THE ARECIBO AND JICAMARCA RADARS

Janches, D.¹, Nolan, M.C.¹, Chau, J.L.²,
Woodman, R.F.², Mathews, J.D.³, Meisel, D.D.⁴

¹Arecibo Observatory

²Radio Observatorio de Jicamarca, Instituto Geofisico del Peru

³Communication and Space Sciences Lab, Department of Electrical Engineering, Penn State University

⁴Department of Physics and Astronomy, SUNY-Geneseo

We present and discuss statistical results from recent observations of meteor-head echoes obtained with the high power-aperture Jicamarca 50 MHz and Arecibo 430 MHz dual-beam radars. These radars detect decelerating micron size particles for which precise altitude; instantaneous Doppler velocity (rms errors of the order of 10-100 m/sec) and (constant) deceleration are obtained. This provides a tool for the study of a mass-region of the interplanetary dust distribution and its influence to the mesopause that was previously inaccessible to ground-based instruments and helps bridge the gap between spacecraft dust measurements and traditional meteor radar capabilities. The meteor rate detected inside the Arecibo 305 m-diameter radar beam (~ 4 0 events per minute at sunrise) and the distribution of meteor radians obtained with interferometric techniques at Jicamarca show that the micrometeor influx comes from the Apex (direction of the Earth's motion around the Sun). This flux is present every day and is not due to shower activity. We find the meteor flux rate as well as the geocentric velocity distribution to be strongly dependent on the topocentric declination implying a function with radiant ecliptic latitude. In addition, we present estimations of the total micrometeor dynamical mass (i.e. derived from meteor decelerations) flux from both radars derived from these observations, resulting in ~ 2000 tons of meteoric material deposited over the whole earth each year in the 80-120 km altitude region. Preliminary results also show that the mass flux peaks in June (i.e. a function of ecliptic longitude) along with mesosphere metallic densities derived from lidar observations.

RECENT UHF METEOR HEAD ECHO OBSERVATIONS AT
MILLSTONE HILL

Erickson, P. J.¹, Frazier, K.², Durand, D.³, Coster, A. J.¹

¹Atmospheric Sciences Group, MIT Haystack Observatory, Westford, MA 01886

²Cornell University, Ithaca, NY 14853

³MIT Lincoln Laboratory, Lincoln Space Surveillance Complex, Lexington, MA 02420-9108

We present recent observations of short duration meteor head echoes at UHF frequencies utilizing the Millstone Hill 440 MHz incoherent scatter radar. Millstone Hill's 2.5 megawatt transmitter combined with 46 meter steerable and 68 meter fixed zenith antennas allows observation of incoming micrometeoroids as they ablate in the 95 - 115 km altitude range, with typical radar cross section (RCS) values of $10^{-4} - 10^{-5}m^2$ and masses of 70 micrograms. Using the MIDAS-W Software Radar system, we are able to examine voltage-level information from each returned radar echo, and the transmitted waveform repetition rate allows multiple observations during a single micrometeor event. We further analyze MIDAS-W voltage level data using a robust meteor processor code developed by Lincoln Laboratory for use with ALTAIR multi-frequency observations. The code performs automatic meteor identification, assembly of individual echoes into single meteor streaks, and analysis of range rate information and correlation statistics to determine line of sight velocity and meteor track coherence.

We focus on initial observations of several sporadic meteor shower datasets from 2002 and 2003. In particular, significant numbers of observed meteor head echoes have unexpected range signatures with multiple peaks, although mean altitudes, range rates, and time durations are consistent with statistical averages produced with other radars and with earlier Millstone Hill work. We review experimental work designed to examine this phenomenon more closely using multiple interleaved waveforms. Finally, we present summary statistics for recent sporadic observations and discuss future plans for greatly enhanced dynamically adjustable observational programs which are made possible by the architectural flexibility of Software Radar platforms.

METEOR HEAD ECHOE MEASUREMENTS AT SONDRERSTROM

Heinselman, C.J.¹, Jordan, C.², Jorgensen, J.¹¹SRI International²MIT

The Sondrestrom incoherent scatter radar (ISR) regularly characterizes the high-latitude ionosphere in terms of the bulk plasma parameters electron number density (Ne), electron temperature (Te), ion temperature (Ti), ion velocity (Vi), and ion composition. Its primary purpose is to enable ionospheric and upper atmospheric research of the solar UV produced photoionization, the auroral impact ionization, and the ionized component of the products of meteoroid ablation (sporadic E). Because of several advancements in the data acquisition software, it can now also routinely and simultaneously measure the signals scattered from the ionization around the heads of ablating meteoroids. Analysis of the temporal evolution of the returns also, in conjunction with background atmospheric parameters provided by empirical models such as MSIS, allows the extraction of a number of characteristics of the ablating meteoroid material. This capability now exists at all incoherent scatter radars. What makes Sondrestrom somewhat unique is the relatively high frequency at which it operates and, as a result, its relatively small k-vector.

Recent measurements with the Sondrestrom ISR suggest a number of differences between the characteristics of meteor head echoes made with that instrument and those made with other ISRs. In particular, the altitude distributions appear to be somewhat lower and the velocity distributions somewhat broader. It appears that both of these effects might be explained in terms of a simple model of meteoroid ablation, ionization, and scattering of RF waves. In this report, we will discuss a simple modeling effort and interpret our experimental results in terms of that model. We find that the trends suggested by the model are reasonable, but that significant disparities remain between the quantitative model predictions and the actual measurements.

DETERMINING METEOROID PLASMA DENSITIES,
MASSES AND ORBITS USING ALTAIR TWO-FREQUENCY
HEAD ECHO DATA

Close, S.^{1,3}, Hunt, S.^{1,3}, Brown, P.²
, Drew, K.², Durand, D.¹, Oppenheim, M.³
, Dyrud, L.³, Coster, A.¹

¹MIT Lincoln Laboratory

²University of Western Ontario

³Boston University

This presentation contains the results from a multi-level analysis applied to ALTAIR head echo data that were collected simultaneously at VHF and UHF during the Leonid 1998 and 1999 showers. Specifically, we have 1) developed a spherical full-wave scattering model, 2) applied our scattering model to ALTAIR data to determine meteoroid plasma densities and masses, and 3) utilized the 3D position and velocity measurements to determine meteoroid orbits, radii and densities. We then correlate all of the meteoroid parameters in order to categorize the meteoroid population detected by ALTAIR.

We model meteor head echoes as spherically distributed plasmas with densities that decrease with distance from the meteoroid and radii that scale with the atmospheric mean-free-path. We then solve for the interaction of a radar wave with head echo plasma without assumptions relating to wavelength or plasma density, which is referred to as the full-wave scattering method. The measured ALTAIR RCS are input into this full-wave model in order to determine plasma density and meteoroid mass. Concurrently, we utilize the measured 3D velocity and 3D deceleration data to determine meteoroid radius*density products and orbital parameters. Finally, we combine all of these results to fully characterize the meteoroids. Our results indicate that the maximum head echo plasma density associated with a single meteoroid increases as altitude decreases, and also that head echo detection altitude is strongly dependent upon meteoroid mass and velocity. We also find that a small percentage of our detected meteoroids have eccentricities greater than one, and that these interstellar meteoroids tend to have fairly low masses and create head echoes at very high altitudes.

H1

Session H1, 8:40-Monday

DUSTY PLASMA

Chairperson: Marlene Rosenberg

AEROSOL CHARGING IN THE MESOSPHERE

M. Horanyi^{1,2}, S. Robertson², Z. Sternovsky², B. Smiley¹

¹LASP, U. of Colorado

²Department of Physics, U. of Colorado

Small grains immersed in low density plasmas and UV radiation can significantly alter the density, energy distribution and the composition of their plasma environments, by continuously collecting and releasing electrons and ions.

Noctilucent clouds (NLCs) and polar mesospheric summer echoes (PMSEs) are good candidates, where plasma depletion due to the presence of small aerosol particles is thought to explain unusually large radar echoes.

We will briefly summarize the most important charging processes that apply in the Mesosphere, and discuss the need for possible extensions of the traditional orbit limited charging calculations to account for electron-neutral and ion-neutral collisions in this partially ionized plasma environment. We will consider electron and ion collection currents and UV induced photoelectron production during average conditions. During high auroral activity periods, high energy electron beams can reach down to 80-85 km altitude region, altering the background plasma conditions and the expected charge state of the aerosols.

We will discuss how charging can influence the condensation and coagulation processes that control the growth rates of the aerosols. We discuss the possible build up of large scale electric fields due to differential settling of various sized and/or composition dust particles and its possible effects on forming vertically structured aerosol layers. We will also consider high aerosol density regions, where grain-grain interaction might become important and possibly lead to collective behavior.

The theoretical models will be compared with available in situ and remote observations and suggestions will be made for further in situ observations and laboratory experiments. In addition, we will close by describing a dust experiment on-board the upcoming Aeronomy of Ice in the Mesosphere (AIM) SMEX mission, that will monitor the dust influx in the Mesosphere.

ROCKET-BORNE PROBES FOR CHARGED IONOSPHERIC
AEROSOL PARTICLES

Robertson, S.¹, Horanyi, M.^{1,2}, Smiley, B.^{1,2}, Sternovsky, Z.¹

¹Department of Physics, University of Colorado, Boulder, CO 80309-0390

²Laboratory for Atmospheric and Space Physics, University of Colorado, Boulder, CO 80309-0392

A series of rocket-borne probes are described for detecting charged aerosol particles in the ionosphere. The probes are flat charge-collecting surfaces on the skin of rockets. The collection surfaces have behind them permanent magnets that shield the probe from electrons. Some of the probes have been electrically biased to repel light, positive ions. The current that is recorded is thus from heavier charged aerosol particles. This heavy charge carrier current is converted to a charge number density.

A probe launched from White Sands in November 1998 detected a narrow layer at 86 km consistent with sporadic E layer of metallic ions. Two launches were made from the Andoya Rocket Range (Norway) during the MIDAS SOLSTICE campaign in the summer of 2001. Layers of positively and negatively charged aerosol particles were detected on both flights, but inadvertent positive ion collection complicated the analysis. The final experiment using only magnetic shielding was launched aboard the Hygrosonde 2 into non-NLC conditions in January 2002 from Esrange, Sweden, carrying an array of five probes with differing magnetic field strengths. This flight allowed comparisons revealing the degree of positive ion rejection. Subsequent payloads included a probe with a positive bias potential to improve positive ion rejection. Three launches were made from Andoya during the MIDAS MacWAVE campaign in July 2003 with this dual-probe package. Within PMSE, the probes measured an aerosol particle distribution, clearly resolving small positive, small negative, and large negative particles. Data are currently being analyzed from three launches made from Svalbard in June and July of 2003.

A new probe is being developed in which electric fields alone deflect charged particles to determine their mass. This probe takes advantage of the reduced density behind the shock front to increase the mean free path within the instrument so that a vacuum pump is not required.

TRANSPORT IN IONOSPHERIC DUSTY PLASMAS_iBR_i

Gelinas, L.J.¹, Lynch, K.A.², Collins, R.³, Kelley, M.C.¹

¹Cornell University

²Dartmouth College

³University of Alaska Fairbanks

Evidence from recent rocket launches indicates that there may be a connection between charged, nanometer-sized dust particles and neutral atomic metals in the Earth's mesosphere. An earlier rocket flight had also indicated that this may be possible (Gelinas et al., 1998). The rocket launches being considered here occurred in March 2002 at the Poker Flat Research Range. The goal of the experiment was to characterize the relationship between charged dust, plasma, and atomic neutral metals (sodium and iron) with multiple launches over the course of one night. Neutral metal densities were monitored by ground-based sodium and iron lidars. Charged dust and plasma profiles were determined by three separate in-situ measurements on the night of March 15, 2002.

A surprising correlation of the charged dust layer profile and the neutral iron profile was observed in the 80-95 km altitude range. A negatively charged, 100/cc charged dust layer was observed in this altitude range. Anti-correlation between the charged dust layer and the atomic sodium was also observed. The in-situ plasma profile was not well-correlated with the neutral metals at lower altitudes, though some features in the charged dust profile appear to be related to the local plasma density. The strong correlations in the neutral iron and charged dust data lead us to consider whether the two are related by chemistry or by transport. The mesospheric and ionospheric conditions on the night of the launch were quiet and well-behaved, with no auroral activity. In this paper we consider the dust charging rate and transport of the various species, as determined by the multiple launches on the night in question. The goal is to determine to what extent the behavior of the charged dust, plasma and neutral metals can be accounted for by simple transport and charging, and whether this dust population may influence mesospheric chemistry.

NONLINEAR DEVELOPMENT OF A LOW-FREQUENCY
HALL CURRENT INSTABILITY IN A DUSTY PLASMAScales, W.¹, Chen, C.¹, Wang, J.²¹Department of Electrical and Computer Engineering, Virginia
Tech, Blacksburg, Virginia²Department of Aerospace and Ocean Engineering, Virginia Tech,
Blacksburg, Virginia

The nonlinear evolution of dust waves generated by a low-frequency Hall current instability in a collisional dusty plasma is investigated with theory and nonlinear numerical simulations. The instability is driven by an electron $\vec{E} \times \vec{B}$ current and is an analog of the well-known Farley-Buneman instability in the dust acoustic type wave regime. This instability is believed to have broad applications to irregularity production in regions where dust is present in the earth's ionosphere such as noctilucent clouds and meteor trails. A two-dimensional hybrid simulation model has been developed to study the nonlinear evolution of plasma irregularities produced by this mechanism. A three species plasma is considered which consists of fluid electrons and ions and collisional dust which is modeled with the Particle-In-Cell PIC method. A two-dimensional plane is considered that is perpendicular to the background magnetic field. At early times during the evolution, the results of linear plasma instability theory agree well with the nonlinear simulations. However, at later times, the numerical results clearly show that the nonlinear effects are crucial in ultimately determining the characteristics of the steady state. The results indicate that the instability nonlinearly saturates with dust heating and the production of secondary waves that propagate in a direction perpendicular to the primary dust acoustic type waves. Results of the investigation also indicate that dust-neutral collisions increase the amplitude of the unstable dust waves after nonlinear saturation which is contradictory to the predictions of linear plasma instability theory. Possible mechanisms for the production of the secondary waves as well as implications of these waves are discussed. Predictions of radar signatures produced by these irregularities are also made.

COMPLEX (DUSTY) PLASMAS UNDER MICROGRAVITY
CONDITIONS ON THE INTERNATIONAL SPACE STATION

Thomas, H.M.¹, Morfill, G.E.¹, Nefedov, A.P.²
, Fortov, V.E.², Annaratone, B.M.¹, Ivlev, A.¹
, Klumov, B.¹, Konopka, U.¹, Kretschmer, M.¹
, Rothermel, H.¹, Yaroshenko, V.¹, Molotkov, V.I.²
, Petrov, O.F.², Lipaev, A.I.², Ivanov, A.³, Rubin-Zuzic, M.⁴

¹Centre for Interdisciplinary Plasma Science, Max-Planck Institut
fr extraterrestrische Physik, D-85741 Garching, Germany

²Institute for High Energy Densities, Izhorskaya13/19, Moscow,
127412, Russia

³RSC Energia, Korolev, Russia

⁴Department of Physics, Faculty of Science, University of Troms,
9037 Troms, Norway

The plasma crystal experiment PKE-Nefedov, the first basic science experiment on the International Space Station (ISS), was installed in February 2001. It is designed for long-term investigations of complex (dusty) plasmas under microgravity conditions. Since the first experiments in March 2001 we continuously performed experiments ? about three missions with three experiments of 90 minutes per year.

Complex plasmas are of special interest, because they can form liquid and crystalline states and are observable at the kinetic level. In experiments on Earth the microparticles are usually suspended against gravity in strong electric fields. This creates asymmetries, stresses and pseudo-equilibrium states with sufficient free energy to readily become unstable. Under microgravity conditions the microparticles move into the bulk of the plasma, experiencing much weaker volume forces than on Earth. This allows investigations of the thermodynamics of strongly coupled plasma states under substantially stress-free conditions.

In this presentation we will give an overview of the structure and dynamics of complex plasmas under microgravity conditions. Special topics will be highlighted, like (1) the formation and closure of the void in the centre of the complex plasma, a special feature observed under different experimental conditions and one of the major topics of recent theoretical research, (2) wave propagation through a complex plasma cloud, formed by external excitation, (3) the coalescence of two complex plasma droplets, showing interesting plasma boundary effects and (4) the investigation of the discharging of a complex plasma after the plasma is switched off - a measurement, which can only be performed under microgravity conditions. The experiments are compared with theoretical estimates and numerical simulations.

Acknowledgements: This microgravity research was funded by DLR (FKZ 50WB9852), Rosavia-Cosmos and RKK-Energia.

ELECTROSTATIC DISCHARGING OF DUST IN LOW-PRESSURE ATMOSPHERES

Krauss, C.E.¹, Horanyi, M.^{1,2}, Robertson, S.²¹Laboratory for Atmospheric and Space Physics, University of Colorado, Boulder, CO 80309²Department of Physics, University of Colorado, Boulder, CO 80309

Dust devils and large dust storms provide an environment in which the natural interactions within a dusty plasma can be studied. The turbulent motions of particles within a dust cloud cause individual dust particles to collide. This contact allows charge to be transferred between the grains. Wind driven dust studies (Stow, 1969) show that when particles with identical compositions collide, the particle with the larger radius in the collision preferentially becomes positively charged. The upwinds within a dust cloud can then carry the lighter, negatively-charged particles to higher altitudes. The stratification of particle sizes causes an electric dipole to form. If the electric potential within the cloud exceeds the breakdown voltage of the surrounding atmosphere, a discharge occurs.

We have conducted laboratory experiments to examine the creation of electric fields and the subsequent discharges due to vertical charge separation in a low-pressure Earth atmosphere and a simulated Martian environment. The range of pressures and the amount of mass loading required to produce discharges have been examined. When a regolith simulant is vertically dropped in a low-pressure atmosphere, electrical discharges are both visually and electronically detected. Measurements of the frequency and intensity of these discharges show that they can occur under conditions expected on the Martian surface.

Additionally, we have created a simple theoretical model to examine the creation of discharges in a dust storm. The effects of pressure, dust density, and particle size are presented. These model results are compared to our laboratory experiments.

This work is supported by NASA Space Science GSRP, NGT5-50345.

FIRST REPORT ON MEASUREMENTS OF MICROPARTICLE TRANSPORT USING STEREOSCOPIC PARTICLE IMAGE VELOCIMETRY

Edward Thomas, Jr., Jeremiah Williams, Jennifer Silver

Physics Department, Auburn University

A dusty (or complex) plasma is a four-component system composed of ions, electrons, neutral particles and charged microparticles. The presence of the microparticles (*i.e.*, dust) component alters the plasma environment, giving rise to a wide variety of new plasma phenomena. Observations in dusty plasmas range from the identification of strongly coupled states, e.g., plasma crystals [H. Thomas and G. Morfill, *Nature*, 379, 29 (1996)] and plasma clusters [M. Klindworth, *et. al.*, *Phys. Rev. B*, 61, 8404 (2000)], to measurements of new dust-driven collective modes, e.g., dust acoustic waves [A. Barkan, *et. al.*, *Phys. Plasmas*, 2, 3563 (1995)].

Over the past several years, the Auburn Plasma Sciences Laboratory (PSL) has applied particle image velocimetry (PIV) [E. Thomas, *Phys. Plasmas*, 6, 2672 (1999)] techniques to make real-time measurements of particle transport in dusty plasmas. In PIV, a pair of laser pulses expanded into a sheet by a cylindrical lens and separated by a time interval dt are used to illuminate the microparticles. A CCD camera oriented perpendicularly to the light sheet and synchronized to the firing of the laser pulses is used to capture the light scattered by the particles. From the displacement of the microparticles between the two images, the two-dimensional motion of the particles in the plane of the light sheet can be reconstructed. In spite of the new insights into microparticle transport and dusty plasma particle dynamics that have been obtained using 2D-PIV techniques, it is clear that information on the third dimension of motion is required to fully understand this complex system.

The PSL has recently acquired and installed a stereoscopic PIV (3D-PIV) diagnostic tool for dusty plasma investigations. It employs a synchronized dual-laser, dual-camera system for measuring particle transport in three dimensions. This talk will present the first results of dusty plasma measurements using 3D-PIV.

This work is supported by National Science Foundation awards PHY-0096254 and PHY-0216421.

ROTATION WAVES AND STRONG TURBULENCE IN A
 MULTI-COMPONENT PLASMA*

 Ganguli, G.¹, Rudakov, L.²
¹Plasma Physics Division, Naval Research Laboratory, Washington DC 20375

²Berkeley Scholars Inc., P.O. Box, 852, Springfield VA 22150

We show that in a three-component plasma, e.g., electrons, ions, and negatively charged dust, such that $n_d \ll n_i \sim n_e$, the light components (electrons and ions) can rotate rigidly with a frequency, $\Omega_r = Zn_d\Omega_i/n_e$, where $n_{i,e,d}$ are ion, electron, and dust densities, Z is the dust charge state, and Ω_i is the ion gyro-frequency. The origin of this rotation is shown to be due to $n_i \neq n_e$, so that there is a current perpendicular to the magnetic field due to ion and electron $\mathbf{E} \times \mathbf{B}$ drift, which induces an electric field in the direction of the current. Hence the plasma is subject to electric forces simultaneously in the two orthogonal directions perpendicular to the magnetic field resulting in a rotation. A new low-frequency resonance at $\omega = \Omega_r$ appears in the MHD limit and affects the dispersion character of the electromagnetic waves. The magnetosonic dispersion relation [$\omega^2 = \Omega_r^2 + k^2(V_A^2 + C_s^2)$, where V_A and C_s are the Alfvén and ion sound speeds] is modified and becomes isomorphic to the electrostatic Langmuir wave dispersion relation. We find that the interaction of the fast rotation time-scale with the slow magnetosonic time-scale can be achieved via ponderomotive force and this could lead to a nonlinear Schrödinger equation for the magnetosonic branch. We also find that it is possible to develop nonlinear structures at very large MHD scales with scale-size $L \sim V_A/\Omega_{r0} \sim (c/\omega_{pi})(n_e/Zn_d)(n_i/n_e)^{1/2}$, where ω_{pi} is the ion plasma frequency, which could be comparable to astrophysical dimensions. Linear stability and nonlinear structures that could arise in the frequency regime $\omega \sim \Omega_r$ will be discussed along with some space and laboratory applications.

*Work supported by NASA and ONR.

OBSERVATION OF MICROPARTICLE GYROMOTION IN A
MAGNETIZED DC GLOW DISCHARGE DUSTY PLASMA*W. E. Amatucci¹, D. N. Walker¹, G. Gatling², E. E. Scime³¹Plasma Physics Division, Naval Research Laboratory, Washington, DC 20375²Advanced Technology Division, SFA Incorporated, Largo, MD 20774³Department of Physics, West Virginia University, Morgantown, WV 26506

Laboratory observations of the motion of charged microparticles have been made in an argon dc glow discharge plasma created within a strong dc magnetic field. The experimental configuration consists of an anode-cathode pair centered between a pair of neodymium iron boride permanent magnets. The cylindrical axis of the resulting plasma column is directed vertically (i.e., along the direction of the gravitational force). Depending upon the orientation of the magnets, the magnetic field can be directed either upward or downward, with a field strength of approximately 2.5 kG. A pair of Helmholtz magnetic field coils external to the vacuum chamber allows the magnetic field to be varied by approximately $\pm 75G$ in the experimental region.

Alumina microparticles ($\sim 1.2\mu\text{m}$) placed directly on the grounded cathode provide the source of charged dust in the plasma. Individual dust grains suspended in the plasma can be observed to move in an oscillatory fashion in a plane perpendicular to the direction of the magnetic field. Measurements of the oscillation frequency, orbital radius, and rotation direction have been made. By using an additional field produced by the Helmholtz coils, the scaling of the oscillation frequency with magnetic field strength was tested. The frequency is found to scale linearly with magnetic field strength and the slope of the data is found to be consistent with independent determinations of the charge-to-mass ratio. The scaling of orbital radius with tangential velocity has been tested by analyzing the motion of individual particles within a group of orbiting dust grains. These data show that the radius scales linearly with velocity and the reciprocal of the slope is consistent with the measurement of the oscillation frequency. The measurements are consistent with the gyromotion of magnetized dust grains under the ambient plasma conditions. The data are shown to provide an effective method for the noninvasive determination of the dust grain charge.

*Work supported by ONR.

DRIFT INSTABILITIES IN COLLISIONAL DUSTY PLASMAS:
APPLICATIONS TO SPACE AND THE LABORATORYRosenberg, M.

Dept. of Physics, University of San Diego, San Diego, CA 92110

Charged dust or aerosols may occur in certain regions of the Earth's ionosphere, including for example, polar mesosphere summer echo (PMSE) regions or dusty meteor trails. In such regions, the plasma is weakly ionized, there is a background magnetic field, and there can be electric fields. If, in addition, there are local spatial gradients in the dust charge density which lead to associated electron and/or ion density gradients, there arises the possibility of drift instabilities driven by diamagnetic and $\mathbf{E} \times \mathbf{B}$ drifts. In this talk, some recent work on drift instabilities in collisional dusty plasmas will be summarized. Though the focus will be on instabilities that may be relevant to dusty plasmas in the Earth's ionosphere, conditions for observing such instabilities in laboratory dusty plasmas will also be explored.

First, we consider the effect of charged dust on the gradient drift instability with frequency \gg the dust plasma frequency. This was previously considered with application to dusty regions of the mesosphere (M. Rosenberg and P. K. Shukla, *Planet. Space Sci.*, **51**, 1, 2003). Here we explore applications to magnetized dusty plasmas in the laboratory.

Next, we consider drift instabilities in a much lower frequency regime associated with the dust dynamics. A dust-acoustic drift instability was previously considered with application to dusty meteor trails (M. Rosenberg and P. K. Shukla, *J. Geophys. Res.*, **107**, 1492, 2002). Here, we extend that work to consider the effect of magnetized ions. We discuss applications to possible dusty plasmas in space shuttle exhaust plumes (P. A. Bernhardt et al., *J. Geophys. Res.*, **100**, 23811, 1995) and to laboratory dusty plasmas with strong magnetic fields.

Session H2, 14:00-Monday

ACTIVE SENSING OF SPACE

PLASMAS

Chairpersons: Bob Bension and Paul Bernhardt

**STRONG PULSED ELECTROMAGNETIC INTERACTIONS
WITH SPACE PLASMAS**Alfred Y. Wong

Dept of Physics and Astronomy, UCLA

The concentration of electromagnetic energy into pulses of high peak power(oscillating electric field pressure of the order of plasma pressure)is described in order to achieve enhanced interactions with space plasmas. This concept is realizable with present heating facilities without increase in average power. Laboratory experiments (1) using high power pulses at UHF, microwave and laser frequencies have demonstrated that the pressure from self-consistent oscillating field can become comparable to the plasma pressure. Such strong excitation is expected to impact both the high and low frequency response of the ionosphere, e.g. in the reflection of high frequency waves and the generation of low frequency waves. It was found that the self-consistent electric field of these ES waves rises linearly with time with a coefficient that is proportional to the peak power. The energy of electrons accelerated by these plasma waves also increases as a function of the peak power of incident EM waves. This pulsed excitation allows the heating of a local volume rapidly in a time scale faster than the heat transport rate at the boundary. The local electron temperature can undergo a rapid increase and a corresponding large change in the conductivity. The excitation of low frequency EM wave (ULF/ELF/VLF) might be more efficient by concentrating the available ground-based energy into pulses of high frequency EM waves. In the F region the short pulse excitation will generate intense plasma waves propagating along the earths magnetic field lines. These waves will scatter field-aligned electrons and might cause changes in the electrojet in the E region, thereby affecting the excitation of low frequency EM waves. By sweeping the frequency of the excitation EM wave (2), a field-aligned current can be driven and sustained by wave-particle interactions. The ponderomotive force from this pulsed excitation is expected to produce an ambipolar potential and ion energy ~ 1 KTe. Both laboratory and theoretical analyses support the use of pulsed power for greater efficiency of utilizing HF heating facilities. The use of pulsed excitation combined with arrays of antennas spaced at large distances might result in active sensing of space plasmas with improved temporal and spatial resolutions. This research is supported by the International Foundation for Science, Health and Environment. I.B.S. Bauer, A.Y. Wong, V.K. Decyk and G. Rosenthal, Experimental Observation of Superstrong Electron Plasma Waves and Wave Breaking, Phys. Rev. Lett v. 68, 3706 (1992); Wong, A.Y.,

RAY-TRACING AND IN-SITU OBSERVATIONS OF Z-MODE WAVES DURING AN HF HEATING EXPERIMENT AT ARECIBO

Mishin, E. V.¹, Starks, M.², Gelinias, L. J.³, Kelley, M. C.³¹Boston College Institute for Scientific Research, Chestnut Hill, MA, USA²Air Force Research Laboratory, Space Vehicles Directorate, Hanscom AFB, MA, USA³Cornell University, Ithaca, NY, USA

On March 11, 1998 the Langmuir Turbulence sounding rocket was launched through the Arecibo heater beam during an experiment to measure electric fields and plasma densities in the heater interaction region. The rocket data has provided evidence of Z mode waves a few km above the O mode reflection height H_O (Gelinias et al, *JGR*, 2003, accepted). As the rocket trajectory was to the north of Arecibo, the classical $O \rightarrow Z$ conversion at the Spitzke angle cannot contribute to the observed perturbations near the Z mode reflection height H_Z .

On the other hand, Z mode waves can be generated between the upper hybrid resonance height H_{UH} and H_O due to resonant scattering of the heating wave on small-scale field-aligned density irregularities (FAIs) generated by heater waves. Ray paths of the generated Z mode waves are computed using the Power Tracing Code, operated by the Space Weather Center of Excellence in the Air Force Research Laboratory's Space Vehicles Directorate. The density profile is chosen to be the Chapman layer fitted to the observed profile. Z mode waves are injected in the magnetic meridian plane between H_{UH} and 0, H_O with different angles off vertical. The ray-tracing results show that the region occupied by Z mode waves is rather wide with a dominant portion to the north of the heater. This may explain the observations near H_Z .

These results give credence to the theory that Z mode wave interactions with field-aligned striations may be, in part, responsible for some of the features of the reflected HF spectrum observed in heating experiments.

MEASURING WHISTLER MODE SIGNALS IN THE MAGNETOSPHERE ORIGINATING FROM GROUND-BASED VLF TRANSMITTERS USING THE IMAGE/RPI SATELLITE

Sales, G., Paznukhov, V., Song, P. , Reinisch, B., Khmyrov, G.

Center for Atmospheric Research, 600 Suffolk St, Lowell MA 01854

Whistler-mode signals propagating upward through the ionosphere from ground-based VLF transmitters were measured in the magnetosphere using the RPI receiver onboard the IMAGE satellite. These observations were limited to times when the satellite was on L-shells between 1.5 and 5 and where the distances along the magnetic field from the ground to the satellite varied from approximately 1 Re to 6 Re. In the Dynamic Spectrum mode, RPI steps across the VLF band in frequency steps that varies between 300 and 400 Hz every 3 to 4 minutes. When the satellite footprint, that is, where the magnetic field line through the satellite intersects the ground is in the vicinity of the transmitter, then signals leaking out of the ionosphere-ground waveguide are received at the satellite via a whistler mode. The spatial and temporal distribution of these received signals from the strongest transmitters (500 kW to 1 MW), in the band from 18 to 28 kHz, are presented as a function of latitude and longitude over a two year period (2001-2002). The latitude/longitudinal region on the ground from where VLF signals were observed was significantly smaller during the daytime compared to when the region around the VLF transmitter is in darkness. We also present the range and azimuthal characteristics along the ground of the received VLF signal amplitude from several of the VLF transmitting stations. Saturation effects caused by the strong VLF transmitters during the routine RPI operation, made it necessary to up load special mprograms where the receivers are set to lower gain in order to determine the actual field strengths associated with these whistler modes.

Detail comparisons are made with the VLF ray tracing results (B. Small and M. Starks) using modeled ionosphere-magnetosphere electron densities and VLF waveguide and ionospheric penetration losses.

RELATING MAGNETOSPHERIC UPPER-
HYBRID BAND ENHANCEMENTS ON PASSIVE DYNAMIC
SPECTRA TO CHARACTERISTIC PLASMA FREQUENCIES
DETERMINED FROM ACTIVE RPI SOUNDING ON IMAGE

Benson, R. F.¹, Webb, P. A.², Green, J. L.¹, Reinisch, B. W.³

¹NASA/Goddard Space Flight Center, Greenbelt, Maryland

²USRA/Goddard Space Flight Center, Greenbelt, Maryland

³University of Massachusetts, Lowell, Lowell, Massachusetts

Plasma emissions in the frequency region between the greater of the electron plasma frequency f_{pe} or the electron cyclotron frequency f_{ce} and the upper-hybrid frequency f_{uh} , which is related to f_{pe} and f_{ce} by the expression $f_{uh}^2 = f_{pe}^2 + f_{ce}^2$, have been observed in the ionosphere during rocket experiments since the mid 1960's. These Z-mode emissions are often referred to as the upper-hybrid band. Observations of similar emissions in the magnetosphere by Imp 6 have been interpreted in terms of providing a diagnostic tool for determining the electron density N_e since $f_{pe} \text{ (kHz)}^2 \approx 80.6 N_e \text{ (cm}^{-3}\text{)}$ (S. R. Mosier et al., *J. Geophys. Res.*, **78**, 1673-1679, 1973; Shaw and Gurnett, *J. Geophys. Res.*, **80**, 4259-4271, 1975). When $f_{pe} > f_{ce}$, the resulting magnetospheric emission line is often called the "plasma line" or, more often, the "upper-hybrid" line. In the ionosphere, however, a comparison of active and passive ISIS-2 topside-sounder records indicated that emissions at f_{uh} were not as common as those at f_{pe} and that the peak emission was more often between f_{pe} and f_{uh} (R. F. Benson, *AGU Monograph*, **80**, 267-274, 1993).

Here we present active/passive comparisons of these emissions in the magnetosphere based on data from the Radio Plasma Imager (RPI) on the Imager for Magnetopause-to-Aurora Global Exploration (IMAGE) satellite. Plasma resonances and wave cutoffs stimulated by RPI active soundings during several plasmopause crossings, and one case with extended operations near the $L = 4$ field line, were used to make accurate (within a few percent) determinations of f_{pe} and f_{uh} . These values were then related to the observed emission enhancements in the same frequency region as observed on the dynamic spectra obtained during passive RPI operations (interspersed among the active soundings). Comparisons were made between the plasma resonance f_{pe} and f_{uh} determinations, interpolated to the time of an intermediate dynamic spectrum enhancement, and the leading and trailing edges of the enhancement as well as the peak value over a range of ambient f_{pe}/f_{ce} values (approximately 1 to 4). Most of the comparisons indicated that the peak was between f_{pe} and f_{uh} . The leading and trailing edges of the enhancement often, though not always, coincided with the interpolated values for f_{pe} and f_{uh} , respectively. Some of the results appeared to be significantly influenced by interpolation uncertainties introduced by N_e gradients.

ARTIFICIAL DISTURBANCES OF THE IONOSPHERE OVER
THE MILLSTONE HILL RADAR DURING DEDICATED
BURNS OF THE SPACE SHUTTLE OMS ENGINES

Bernhardt, P.A.¹, Erickson, P.J.², Lind, F.D.², Reinisch, B³

¹Plasma Physics Division, Naval Research Laboratory, Washington, DC 20375

²Atmospheric Sciences Group, MIT Haystack Observatory, Westford, Massachusetts 01886

³Center for Atmospheric Research, University of Massachusetts Lowell, Lowell, MA 01854

The Shuttle Ionospheric Modification with Pulsed Localized Exhaust (SIMPLEX) series of experiments has been conducted by the Naval Research Laboratory for the past 6 years. The experiments use the Space Shuttle OMS engines to inject exhaust over ground radar sites. The radar detects the changes in the ionosphere with incoherent scatter. SIMPLEX I was conducted over the Jicamarca Radio Observatory in Peru during STS-86 [Bernhardt et al., 2001]. This experiment monitored the recovery of ionosphere by field aligned transport of plasma. The SIMPLEX II experiment was conducted over the Arecibo Observatory in Puerto Rico during STS-93 [Bernhardt et al., 2003]. For SIMPLEX II, the ion-beams from the exhaust produced non-thermal spectra with the incoherent scatter radar. The SIMPLEX III and IV experiments over the Millstone Hill radar in Massachusetts are reported here. The experiments used 10 second burns of the dual Orbital Maneuver Subsystem (OMS) engines to produce the injection of high speed molecules in the ionosphere near 380 km altitude. Charge exchange between the high speed exhaust molecules and the ambient oxygen ions yield molecular ion beams that disturb the natural state of the ionosphere. Radar scatter measurements are used to measure the ion velocity distributions that result from the ion beam interactions. Ground based observations with the University of Lowell Digisonde recorded the ionospheric density depressions resulting from recombination of the molecular ions with electrons. Prompt signatures of a non-equilibrium ion distribution in the OMS engine plume are seen in the data taken during Space Shuttle Flights STS-108 and STS-110 show. The presence of the stimulation of plasma turbulence is seen in the short-time measurements with the ISR for about 30 seconds duration and large scale irregularities are detected by the Digisonde for up to 20 minutes after the engine burn. The SIMPLEX experiments provide localized simulations of naturally occurring disturbances in the ionosphere that can be studied under controlled conditions. The experiment conditions are similar to the strong convection seen with high-latitude plasma during geomagnetically disturbed times.

Session H3, 13:40 Tuesday

WAVES IN SPACE PLASMAS

Chairpersons: Jim Green and Roger Anderson

IRREGULARITY FORMATION AT CACHIMBO ON THE
MAGNETIC EQUATOR AFTER SUNSET DURING THE
COPEX CAMPAIGN IN BRAZIL

Sales, G¹, Reinisch, B¹, Abdu, M.², Batista, I.²

¹University of Massachusetts Lowell, Center for Atmospheric Research, 600 Suffolk St Lowell MA 01854 USA

²Instituto Nacional de Pesquisas Espaciais, feAve dos Astronautas 1758, 12202-970 Sao Jose dos Campos, SP BRAZIL

Three digital ionospheric sounders operated continuously on a five-minute schedule during the COPEX campaign that lasted from October 3 through December 9, 2002. Using these soundings it was possible to closely follow the earliest stages of irregularity formation at Cachimbo, the sounder lying very close to the magnetic equator. The other two sounders, one at Boa Vista (BV), Brazil and the other at Campo Grande (CG), Brazil were located north and south of Cachimbo, respectively, at the foot of the geomagnetic field line passing over the magnetic equator (Cachimbo) at 600 km. Besides producing routine ionograms and electron density profiles, the sounders were operated in the drift mode in between the ionograms and measured the horizontal and vertical drift velocity variations during the campaign. Particular emphasis is placed here on the changes in the ionospheric structure beginning at around 2100 UT. F-layer sunset during the COPEX campaign at Cachimbo varied from 2135 to 2145 UT and the pre-reversal peak vertical velocity occurred on the average around 2110 UT. The peak vertical velocity varied from 30 to 80 m/s with a median value of 52 m/s. On most days (61 out of 68 days of operation), spread-F appeared, where the earliest onset time was 2215 UT with a median onset time of 2250 UT. With the closely spaced ionograms it was possible to identify a precursor to the onset of bottom-side spread-F. On all nights, before the onset of spread-F, a bottom side deformation of the F-layer appeared as satellite traces, sometimes at several locations. This rippling of the layer has been modeled and using orthogonality condition to locate reflections, the results agree with the ionosonde observations. These ripples spaced several 100s of kilometers apart and growing and drifting are the likely precursors of the equatorial bubbles. An intensive examination of sporadic-E occurrence at the outlying sites (BV and CG) at the foot of the magnetic field line during the F-layer rise and spread-F formation periods showed no correlation with the foEs values.

THE OBSERVATION OF ULF WAVES IN SUPERDARN DATA

Ponomarenko, P. V.², Menk, F. W.^{1,2}, Waters, C. L.^{1,2}
, Fraser, B. J.^{1,2}

¹CRC for Satellite Systems, University of Newcastle NSW 2308, Australia

²School of Mathematical and Physical Sciences, University of Newcastle NSW 2308, Australia

Measurements of ionospheric ExB drifts obtained with HF radars from the SuperDARN (Super Dual Auroral Radar) Network sometimes show signatures of ultra-low frequency (ULF) waves. We will show a new data display technique that facilitates the detection of ULF waves in both ground and sea scatter returns. The detection of low velocity wave-like variations in SuperDARN data is greatly improved by removing low frequency trends and using a compressed dynamic range. Data is from the SuperDARN TIGER radar in Tasmania, Australia, where the FOV covers lower magnetic and geographic latitudes than most other SuperDARN radars, in particular the sub-auroral regions where a variety of ULF wave features may be observed. Analysis of 43 days of data revealed an abundance of ULF wave signatures in the mHz frequency range. These were observed for 4-5 hrs/day on average. Statistical study of high time resolution data confirmed that ULF wave signatures occur on an everyday basis with ground scatter accounting for about 60% of the wave events. About half of these events exhibit high coherence across large spatial distances and are associated with ULF pulsations recorded by a ground magnetometer at Macquarie Island. These are typically low wave number Pc5 waves which exhibit high coherence over large azimuthal distances. Other wave-like features observed were more local and are likely to be associated with different types of ULF wave sources and modes. These include band-limited daytime Pc3-4 pulsations which probably represent upstream waves, and nighttime Pc4 oscillations which may be signatures of local field line resonances. Overall the results show that SuperDARN radars may be used to routinely monitor ULF waves in the high latitude ionosphere.

FULLY KINETIC SIMULATIONS AND LINEAR THEORY OF
THERMALLY MODIFIED E-REGION INSTABILITIES

Oppenheim, M. M., Dimant, Y.
Boston University

We present new results of our continuing efforts to simulate and understand turbulent E-region plasma driven by a strong ambient DC electric field. Such processes, including the Farley-Buneman (FB) and gradient drift instabilities, have been studied experimentally and theoretically for four decades. In the last decade, two new thermally driven instabilities have been described along with some supporting observational evidence. In this talk, we will show the significant role played by ion thermal effects in fully kinetic, 2-D, simulations. Further, we will discuss the linear theory of thermal waves based on simplified kinetic and fluid models. These models predict that ion thermal effects play an important role at higher altitudes, electron thermal effects should prove important in the lower E/upper D region. Our new results show that the ion and electron thermal driving mechanisms strongly modify the linear behavior of the FB instability in a homogeneous plasma.

Taking advantage of modern, massively parallel, supercomputers, we can represent both electron and ion dynamics using a fully kinetic PIC algorithm. This allows us to correctly simulate electron and ion temperature variations and other kinetic effects. The resulting simulations demonstrate that thermal effects become especially pronounced when driven by a large DC electric field, well above the threshold of the FB instability. Even at more moderate driving electric fields, the 2-D, saturated, turbulent, waves show some modifications due to thermal effects. Therefore, thermal effects should have consequences for the saturated behavior of the waves and, hence, for radar and rocket observations and electrojet conductivities.

MODELING OF SPACECRAFT EXHAUST JET - IONOSPHERIC PLASMA INTERACTION

V.G. Spitsyn

Cybernetic Centre, Tomsk Polytechnic University , 84, Sovetskaya street, Tomsk, 634034, Russia

We consider the disturbances of ionospheric plasma, created of spacecraft moving on the altitudes 100 300 km from the earth surface. The stochastic method of modeling of ionospheric plasma interaction with spacecraft exhaust jet is applied (V.G. Spitsyn, Modeling of radiowave scattering on the ionospheric plasma disturbances, created of space vehicle, Tomsk: Publishing House STT, 2002). The process of ion ionospheric plasma diffusion in the exhaust jet of spacecraft is analyzed (V.G. Spitsyn, IEEE AP-S International Symposium, 2, 750, 2002). The results of computation are shown that the maximum of relative number of ionospheric ions disturbances is disposed in the area of near boundary of jet and consist of the value 5. The effect of ion accumulation in this area is explained of ions braking in the gas jet. The size of space disturbance is increased with decreasing of ratio of mass ionospheric ion to mass of exhaust jet neutral particle. This result is take place because the light ions in duration of more long time keep the energy under collisions with massive neutral particles. The increasing of concentration of exhaust jet neutral particle is reduced to increasing of collisions number of ions with exhaust jet neutral particles and to the augmentation of maximum value of relative disturbance of ion concentration. The influence of earth magnetic field on the forming of disturbances of charged particles concentration created by shock wave is substantially on the altitudes 130 300 km from the earth surface. The assessments of amplitudes disturbances of electron concentration and the typical sizes of areas of low and high electron concentration are produced. The models of disturbances of ionospheric plasma by spacecraft exhaust jet in dependence of altitude from earth surface are offered.

RECENT ADVANCES IN THE PLASMA IMPEDANCE
PROBE MEASUREMENT TECHNIQUE

Chad G. Carlson¹, Charles M. Swenson¹, Chad Fish²
, Jeff D. Ward¹

¹Department of Electrical and Computer Engineering, Utah State
University

²Space Dynamics Laboratory, Utah State University

The electrical impedance of an antenna exposed to the space environment is dependent upon the parameters of the space plasma in which it is immersed. This property was first observed by J. E. Jackson (*J. Geophys. Res.*, 64(8), 1074-1075, 1959). For nearly four decades, Utah State University (USU) has been developing instruments based upon this effect for *in situ* measurements of plasma parameters on sounding rocket and satellite platforms. The latest USU designed instrument is the plasma impedance probe (PIP). The PIP is an integrated suite of instruments for observing relative and absolute electron densities, magnetic field strength, and electron-neutral collision frequency. The suite consists of a plasma frequency probe, a swept impedance probe, a Q probe, an experimental ion impedance probe, and a DC Langmuir probe. The first four instrument diagnostics are based on the impedance characteristics of an antenna immersed in plasma. This antenna impedance measurement technique has a significant advantage over Langmuir methods in that it is insensitive to vehicle potential and probe surface contamination.

Recently, four USU PIP instruments were flown as a part of NASA's Sequential Rocket Study of Descending Layers in the E-Region (E-Winds) from Wallops Island, Virginia. Spaced over a period of approximately 4 hours, the mission investigated the dynamics of descending intermediate layers in the nighttime D and E-regions. The four PIP instruments were thoroughly tested and calibrated to ensure accuracy. Preliminary flight data shows a considerable amount of sensitivity in all of the instruments that should allow for absolute electron density measurement in the 1 to 10 per cc range and comparable accuracy in electron neutral collision frequency. Additionally, data collected from the impedance probe measurements demonstrates plasma dynamics that are not evident in the DC Langmuir probe measurements, possibly due to vehicle charging or probe contamination. Two nearly identical instruments with swept Langmuir probes are scheduled to be launched from Kwajalein atoll in 2004 to study equatorial spread-F anomalies. These flights will provide further validation of the instrument, its sensitivity, and vehicle-instrument interactions. This paper presents a review of the instrumentation techniques, calibration techniques and results, and initial flight results.

REVIEW OF RECENT ROCKET OBSERVATIONS OF HIGH
FREQUENCY PLASMA WAVES

LaBelle, J., Samara, M.
Dartmouth College

Three recent NASA-sponsored sounding rocket experiments included electric field waveform receivers covering frequencies up to 5 MHz: Sounding the Ion Energization Region and Resolving Ambiguities (SIERRA), Rocket Auroral Correlator Experiment (RACE), and High Bandwidth Auroral Rocket (HIBAR). All were launched from Poker Flat Research Range in 2002 or 2003. Initial data analysis reveals at least two significant results: First, the SIERRA experiment detected structured whistler mode signals at 100-500 kHz, the kilometric wavelength range, lasting over 200 s, corresponding to more than 200 km in spatial extent along the rocket trajectory below 750 km altitude. The whistler mode signals do not appear locally generated since no electron signatures coincide with them. Previous experiments in this altitude range detected hints of such signals lasting at most a few seconds. These structured whistler mode signals may originate as X- or O-mode AKR generated at high altitudes and converted to whistler mode, or they may be generated directly in the whistler mode. Second, the HIBAR experiment encountered source regions of the electromagnetic electron cyclotron harmonic waves known as "auroral roar." These source regions are characterized by intense upper hybrid waves where the upper hybrid frequency matches twice the electron cyclotron frequency. The measured upper hybrid wave amplitudes allow the wave conversion efficiency to be estimated. The waves exhibit banded structure which may support recent theoretical work explaining the fine structure of auroral roar as signatures of eigenmodes of upper hybrid waves generated in an inhomogeneous ionosphere. These recent results, and others, will be reviewed in the context of previous experimental and theoretical work.

PLASMA WAVE MAPS OF THE MAGNETOSPHERE

J. L. Green¹, S. Boardsen², S. Fung¹
, L. Garcia³, B. W. Reinisch⁴

¹NASA Goddard Space Flight Center, Greenbelt, MD

²L3 Communications, Largo, MD

³Raytheon, ITSS, Landover, MD

⁴Center for Atmospheric Research, UMass Lowell, MA

The Earth's magnetosphere supports a rich variety of plasma waves. Two of the most important aspects about plasma waves in space are their source locations and emission mechanisms. Three decades of space plasma wave research have shown that it is sometimes difficult to pinpoint plasma wave source regions. Rarely do we know the exact site of wave generation, yet this is the region where knowledge of a complete particle distribution is needed to identify the free energy source and the wave generation mechanism. Part of particle-wave comparison problems stem from the fact that there are many types of plasma waves and these waves can propagate to large distances from their source regions. We now have the opportunity to globally analyze plasma waves in a quantitative and systematic fashion. Very high quality plasma wave measurements from a variety of instruments are now in the NASA National Space Science Data Center archive. When properly combined into a 3-D database, plasma wave measurements from missions such as Hawkeye, Dynamics Explorer-1, Polar, and IMAGE, can be used to construct wave maps that would statistically yield important source region information that may be impossible to recognize previously. Plasma wave maps will allow us to look for "hot spots" in the wave intensities, thereby identifying either the source regions or sites of plasma wave amplification. In addition, plasma wave maps can easily characterize an emissions radiation pattern allowing for the identification of a source location. Examples of wave maps from magnetospheric emissions such as plasmaspheric hiss, non-thermal continuum, and auroral kilometric radiation will be discussed.

THE NONLINEAR COUPLING OF ALFVN AND LOWER HYBRID WAVES IN SPACE PLASMA

George V. Khazanov

National Space Science and Technology Center, NASA Marshall Space Flight Center

Space plasmas support a wide variety of waves, and wave-particle interactions as well as wave-wave interactions which are of crucial importance to magnetospheric and ionospheric plasma behavior. The excitation of lower hybrid waves (LHWs), in particular, is a widely discussed mechanism of interaction between plasma species in space and is one of the unresolved questions of magnetospheric multi-ion plasmas. It is demonstrated that large-amplitude Alfvén waves may generate LHWs in the auroral zone and ring current region and in some cases (particularly in the inner magnetosphere) this serves as the Alfvén wave saturation mechanism. We present several examples of observational data which illustrate that the proposed mechanism is a plausible candidate to explain certain classes of LHW generation events in the ionosphere and magnetosphere and demonstrate electron and ion energization involving these processes. We discuss the morphology, dynamics, and level of LHW activity generated by electromagnetic ion cyclotron (EMIC) waves during the May 2-7, 1998 storm period on the global scale. The LHWs were calculated based on a newly developed self-consistent model (Khazanov et. al., 2002) that couples the system of two kinetic equations: one equation describes the ring current (RC) ion dynamic, and another equation describes the evolution of EMIC waves. It is found that the LHWs are excited by helium ions due to their mass dependent drift in the electric field of EMIC waves. The level of LHW activity is calculated assuming that the induced scattering process is the main saturation mechanism for these waves. The calculated LHWs electric fields are consistent with the observational data.

INJECTION OF VLF WAVES USING ELECTRIC DIPOLE ANTENNAS IN THE MAGNETOSPHERE

Chevalier, T.W., Bell, T.F., Inan, U.S.
Stanford Univeristy

The ion sheath surrounding an electric dipole antenna in plasma significantly impacts terminal and radiation properties at VLF (Very Low Frequencies). In addition, the refractive index in the plasmasphere can become very large compared to free space. These two factors make it very difficult in determining the radiation pattern and impedance of antennas operating within this type of environment. In this paper we have developed both a warm and cold plasma model, which includes both electrostatic and electromagnetic effects in order to calculate the properties of electric dipole antennas operating in the earth's inner radiation belts.

In this paper we consider having peak-to-peak operating voltages of up to 10,000 Volts. Thus, the sheath region will have length scales anywhere from a debye length up to a few meters. In this region, thermal and bulk motions of the particle are affected by the presence of strong electrostatic fields. Immediately outside of the sheath, up to a few hundred meters, particle motion is heavily influenced by the electromagnetic fields generated by the antenna. Because of this, a warm plasma treatment is needed in these two regions. The warm plasma model uses the first three moments of the Boltzmann equation for electrons and one species of ions (hydrogen) in addition to Maxwell's equations to form a fully electromagnetic two fluid model. From this model, properties of the antenna such as impedance and current distribution can be found.

Outside of this warm plasma region, particle energization is negligible and electrostatic waves are virtually non-existent. Therefore a cold plasma treatment is appropriate. Using the currents at the edge of the simulation space calculated with the warm plasma model as sources in the cold plasma region, the antenna pattern can be calculated. This model solves Maxwell's equations along with a simplified momentum equation, which neglects the bulk motion of particles.

Simulation results are presented along with comparisons with predictions of warm and cold plasma theory.

NASCAP2K SIMULATION OF A VLF ANTENNA PLASMA SHEATH IN THE PLASMASPHERE

David L. Cooke¹ , Myron J. Mandell²

¹AF Res. Lab / VSBX, Hanscom AFB, MA, 01731

²SAIC, San Diego CA

NASCAP2K is a 3D spacecraft plasma interaction code being developed by SIAC for the Air Force Research Laboratory and NASA's Space Environment Effects (SEE) program. It supersedes the older codes charging interaction codes, NASCAP/GEO, NASCAP/LEO, POLAR, and DynaPAC. In addition to the steady state algorithms used for most spacecraft charging calculations, NASCAP2K can also be used as a Particle-In-Cell simulation to capture plasma dynamic effects, such as the dynamic sheath surrounding a low frequency antenna. NASCAP2K has a number of advanced features that make it uniquely suitable for this application including: 3D nonlinear finite elements for strictly continuous electric fields, smooth object geometry that can represent both the antenna and spacecraft, multiple nested grids that can resolve fine object features while spanning the problem space with a reasonable number of grid nodes, a variable time step orbit averaged particle mover that allows for a smooth transition from steady state simulation to finite time steps, and a charge stabilized implicit Poisson solution that provides stable solutions in regions where the grid size significantly exceeds the local Debye length. Although our investigation is just beginning, preliminary results indicate that although the dynamic sheath is rich in structure, the overall size of the sheath, current collection, and thus charging is similar to steady state estimates. In addition to the 3D NASCAP2K models, we have conducted 1D simulations that indicate that a square pulse rather than a sinusoidal wave form can drive ringing oscillations at the electron plasma frequency. Because NASCAP2K can model the spacecraft and its charging, it can also provide guidance concerning the placement and sizing of plasma diagnostics by computing the expected fluxes and direction of the charged particles seen at the spacecraft.

ION HEATING BY HEAT FLUX GENERATED ION CYCLOTRON WAVES IN SOLAR CORONAL HOLES

Markovskii, S. A., Hollweg, J. V.
University of New Hampshire

The recent observational data from UVCS/SOHO strongly suggest that the ions in solar coronal holes are heated by the waves in the ion cyclotron frequency range. However, the origin of these waves still remains unknown. We suggest that the ion cyclotron waves generated by intermittent heat flux. We postulate that small-scale reconnection events (microflares) at the coronal base launch the heat flux up into the corona where it excites plasma microinstabilities. We demonstrate that coupling of the unstable electrostatic and shear Alfvén waves results in a very strong resonance with protons and provides efficient heating of the solar wind. We also argue that the waves propagate from the generation site toward the Sun. Closer to the Sun, the waves become resonant with heavier ions and can thus heat them. We have developed a simple method of calculating the heating in each burst of the intermittent heat flux. We have shown that particles interacting with electrostatic ion cyclotron waves diffuse along finite-length one-dimensional curves in the phase space and form a quasi-plateau. This fact allows us to determine the final distribution function, which results from the heating of the initial distribution, using geometrical reasoning, without actually solving the diffusion equations. The diffusion paths of the particles are simply overlaid in the initial distribution and then the particle density is evened out along these paths. Our calculations based on this method demonstrate that the intermittent mechanism is efficient enough to account for the heating and acceleration of the fast solar wind suggested by the observations.

Session H4, 8:40-Wednesday

NUMERICAL METHODS

Chairperson: Dave Newman

NUMERICAL CALCULATION OF FORCE EQUILIBRIA IN
THE EARTH'S MAGNETOSPHERE;BRj

Lemon, C.¹, Toffoletto, F.¹, Hesse, M.³, Birn, J.²

¹Rice Space Institute, Rice University, 6100 Main St./MS 108,
Houston, TX 77005, USA

²Space Plasma Physics Group, Los Alamos National Laboratory,
MS D466, Los Alamos, NM 87545, USA

³Laboratory for Extraterrestrial Physics, NASA/GSFC, Code 696,
Greenbelt, MD 20771, USA

A numerical technique for computing three-dimensional force equilibria in the Earth's magnetosphere will be described. Plasma force equilibrium is the state in which the magnetic force ($\vec{J} \times \vec{B}$) balances the pressure gradient force (∇p) on every plasma fluid element. The method we use employs the equations of ideal magnetohydrodynamics (MHD), with a small modification: in the momentum equation, we include an additional force term which is directed against the motion of the plasma fluid ($\vec{F}_f = -\alpha \vec{v}$). This frictional term constitutes an energy sink that removes excess kinetic energy from the system until it approaches a minimum potential energy equilibrium state with zero velocity. In order to improve the convergence rate using this technique, the friction term coefficient α is kept to a minimum value while the system is approaching equilibrium and is enhanced only when the system is moving away from equilibrium. Oscillations about equilibrium are thereby damped more rapidly than with a static friction term. Results which illustrate the application of this technique to space weather modeling will be presented.

The equations are solved on a nonuniform cartesian grid, using a 3rd-order Adams-Bashforth numerical scheme for the timestepper. Several other numerical schemes were tested, and the 3rd-order Adams-Bashforth method was chosen for its relative lack of unfavorable properties, as well as its computational efficiency. Multi-step numerical schemes (including the family of Adams-Bashforth schemes) have spurious computational modes that may grow exponentially unless the timestep is sufficiently small. This restriction can often be more limiting than the well known Courant-Friedrichs-Lewy restriction. Problems such as the conservation of magnetic flux ($\nabla \cdot \vec{B} = 0$), and the prevention of grid scale fluctuations of the grid variables were also addressed. These properties, as well as the numerical theory that lead us to choose the 3rd-order Adams-Bashforth scheme over the many others that are available, will be discussed.

GLOBAL MHD SIMULATION OF OBSERVED MAGNETOPAUSE WAVES

Slinker, S.P.¹, Fedder, J.A.², Sibeck, D.G.³,
Lyon, J.G.⁴, Frank, L.A.⁵, Mukai, T.⁶

¹Naval Research Laboratory

²George Mason University

³NASA Goddard Space Flight Center

⁴Dartmouth College

⁵University of Iowa

⁶Institute of Space and Astronautical Sciences, Kanagawa, Japan

On January 9, 1996, the Geotail spacecraft observed a series of oscillations in plasma parameters from 0100-0300 UT. Geotail was located inside the magnetosphere near the magnetopause on the dusk flank. The oscillations occurred most strikingly in the plasma density and the plasma bulk velocity. The period was about 8 minutes and it appears that the spacecraft crosses into the magnetopause boundary region for a few minutes each cycle.

Using a global, 3D, ideal MHD simulation model of the magnetosphere, we simulated this period. The model was driven by solar wind and interplanetary magnetic field data measured by the Wind spacecraft. Wave-like behavior similar to that recorded by Geotail was reproduced in the simulation. We discuss our analysis of the event and various numerical experiments we performed. The results lead us to the conclusion that the observed oscillations were likely caused by the Kelvin-Helmholtz instability at the magnetopause.

In the simulation, a disturbance first appears near the magnetopause at about 1400 magnetic local time. It is seen as a perturbation in the plasma density and a counter clockwise vortex in the plasma flow as seen from above the north pole. The flow vortex propagates down the magnetopause in the antisunward direction at around 100 km/s, somewhat less than the magnetosheath flow speed. The size grows as it propagates tailward reaching a radius of about 2 R_E when it reaches the terminator near the Geotail position. For this event, vortices appear only on one flank of the magnetosphere, although other simulated events show them on both sides. The results from this study have appeared in Slinker et al., *Geophys. Res. Lett.*, **30**(11), 1569, doi:10.1029/2003GL017063, 2003.

NUMERICAL MODELING OF SMALL-SCALE ELECTRO-
MAGNETIC STRUCTURES IN DOWNWARD AURORAL
CURRENT CHANNELS

Anatoly V. Streltsov
Dartmouth College

Small-scale, intense electric fields and currents with transverse wavelengths less than 10 km are frequently observed by low-altitude satellites and sounding rockets above the nightside ionosphere in the vicinity of bright, discrete auroral arcs. Despite intensive investigation during the last thirty years, the origin of these low-altitude, quasi-electrostatic structures and their connection with auroral arcs remains poorly understood. The main hypothesis investigated in this study is that these structures can be interpreted as small-scale, intense Alfvén waves generated by the development of the ionospheric feedback instability inside the resonant cavity formed by the ionospheric E-layer and an auroral acceleration region (AAR). The acceleration region is induced in the model self-consistently by the current-driven, electrostatic ion-cyclotron (EIC) instability. The major factor regulating feedback unstable dynamics is the downward current channel of a large-scale, slowly evolving auroral current system interacting with the ionosphere. The downward current lowers the instability threshold by depleting the E-region plasma density and conductivity, thereby allowing the development of a large perpendicular electric field in the E-layer. The downward field-aligned current also produces a collisionless resistive layer/AAR in the lower magnetosphere where the parallel drift speed of current-carrying electrons exceeds a critical threshold for onset of microinstability. This resistive layer provides a highly reflective upper boundary for the resonant cavity confining small-scale Alfvén waves generated at the ionosphere by the feedback mechanism. The quality of the ionospheric resonator without the turbulent upper boundary is shown to be very poor for resonator modes with transverse wavelengths of order 10 km. The paper emphasizes the role on numerical simulations in studying of dynamics of generation and propagation of ULF waves in strongly inhomogeneous plasma. Application of the numerical results to the interpretation of satellite measurements of small-scale electromagnetic structures in the auroral zone is discussed.

INSTABILITY OF INERTIAL ALFVÉN WAVES IN TRANSVERSE SHEARED FLOW

Wu, K.¹, Seyler, C. E.²¹Remcom Inc, State College, PA USA²School of Electrical and Computer Engineering, Cornell University, Ithaca, NY USA

We study the stability of dispersive Alfvénic structures with transverse scales near the electron inertial length c/ω_{pe} . In particular, we examine instabilities in the presence of inhomogeneous currents and flows. Interest in this problem is driven by spacecraft observations of waves in the auroral region. For example, strong, localized inhomogeneous electric and magnetic fields associated with dispersive Alfvénic structures have often been observed by the Freja satellite. These inhomogeneous fields can give rise to parallel current sheets, as well as transverse sheared flow due to $\mathbf{E} \times \mathbf{B}$ drift.

The parallel current sheets drive an interchange instability which can excite localized, small-scale structures. Physically, this instability is due to the interchange of plasmas with different current densities, leading to a build up of electric fields which feed back on the instability. However, we show that the addition of the transverse sheared flow decreases the growth rate of the instability. In addition, we show that the sheared flow itself can drive the plasma unstable. Owing to a resonance between the sheared flow velocity and the phase velocity of the Alfvén wave, energy can be transferred from the sheared flow to the wave, driving the plasma unstable. This sheared-flow driven instability can be illustrated as a wave over-reflection process. A small-scale inertial Alfvén wave which incidents on a sheared flow layer is scattered and reflected by the sheared flow. Over-reflection occurs when the reflected wave has a greater amplitude than the incident wave due to the transfer of energy from the sheared flow to the incident wave. In this way, small-scale Alfvén waves are amplified by the sheared flow, giving rise to instabilities. We present numerical and analytical study of the instabilities. The result of this study shows how inertial Alfvén waves can be generated in the auroral region, and may explain the origin of broadband extremely low-frequency (BBELF) waves associated with Alfvénic structures.

MOMENTUM COUPLING IN THE ION KINETIC LIMIT: HYBRID CODE APPLICATIONS

P. A. Delamere, F. Bagenal

Laboratory for Atmospheric and Space Physics, University of Colorado

The coupling of energy and momentum between spatially separate but magnetically linked plasma populations is a general problem in space plasma physics. Several obvious examples include the transport of energy and momentum between the solar wind and such small obstacles as weak comets, magnetized asteroids, Mars, and Pluto. Other examples include magnetosphere-ionosphere coupling, a classic example being the Io-Jupiter interaction. In many of these cases ideal magnetohydrodynamic (MHD) treatments are not valid due to finite ion gyroradius effects. A hybrid code technique provides a reasonable solution for the cases where ion kinetic effects are important while the fluid treatment of massless electrons is valid. Our three-dimensional hybrid codes includes three components: a kinetic treatment of ions, a fluid treatment of massless electrons, and an optional (seamless) interface with a cold ion fluid population. The fluid treatment of ions can provide considerable computational savings for systems that contain regions where the fluid treatment is valid (i.e. dense, cold ionosphere). The electric fields are determined by the electron momentum equation and the magnetic fields are updated with Faraday's law. The code assumes quasi-neutrality and is non-radiative. We will present hybrid code results from several "Pluto-like" simulations where the size of the obstacle (mass loading region), L , varies from less than to greater than the upstream ion inertial length (c/ω_{pi}). Through this transition, the interaction is mediated by a) whistler waves (with minimal momentum transfer) for L less than the upstream ion inertial length and b) magnetohydrodynamic modes for L greater than the upstream ion inertial length.

WAVE GENERATION AND WAVE-PARTICLE INTERACTIONS IN INHOMOGENEOUS AND NON-MAXWELLIAN PLASMAS

Schriver, D., Ashour-Abdalla, M., Convery, P.
IGPP- UCLA

At various locations in and around Earth's magnetosphere, space plasmas can be inhomogeneous and the velocity distribution functions can have non-Maxwellian characteristics. In this study the generation of plasma waves and ensuing wave-particle interactions are examined for such conditions using kinetic particle simulations. In the upstream electron foreshock region, electrostatic and electromagnetic electron plasma oscillations (and their harmonics) are observed. To understand the generation of these observed waves, beam generated electron plasma oscillations are examined in the presence of density gradients using particle in cell simulations. In particular linear mode conversion of electrostatic plasma frequency oscillations to electromagnetic plasma waves is examined for various types of density gradients. The generation of plasma oscillation harmonics and the effects of the waves on the background plasma that contains the gradient are examined. To study the effects of non-Maxwellian velocity distribution functions, wave generation due to non-gyrotropic features in transverse velocity space is examined for the Earth's plasma sheet, where such distributions can be formed when ion motion through the magnetotail is non-adiabatic. Using hybrid simulations, waves generated by different types of non-gyrotropic distribution functions are examined. The waves excited by these distributions occur at frequencies of the order of the proton gyrofrequency. The resulting wave modes and maximum wave energy are compared to instabilities driven by a gyrotropic ring distribution. The effects of the waves on the non-gyrotropic distribution functions are examined including the time scales over which the non-gyrotropic feature stabilizes and disappears. In the different spatial regions (upstream and magnetotail), results from the simulations are compared with analytic theory and observations.

SIMULATING PERPENDICULAR SHOCKS WITH PIC:
FULLY ELECTROMAGNETIC VERSUS DARWIN
SIMULATION RESULTS

Muschietti, L.¹, Lembege, B.²

¹Space Sciences Laboratory, UC Berkeley, CA

²CETP-CNRS-UVSQ, 78140 Velizy, France

We compare two particle-in-cell simulation models of a fast magnetosonic shock. While both models treat electrons and ions as macroparticles and are 1D3V, they differ on the electromagnetic field equations used. One integrates the full Maxwell equations. The other implements the Darwin approximation, which neglects retardation effects and hence radiation. A perpendicular geometry is considered, where x points into the shock and the electromagnetic field structure is $\mathbf{E} = (E_x, E_y, 0)$ and $\mathbf{B} = (0, 0, B_z)$. We assume moderately supercritical shocks with Mach number $M_a \sim 2-4$ and low upstream $\beta_i \sim 0.01$, a parameter choice which favors the process of cyclic shock reformation associated with the reflected ions accumulating in the foot.

The simulation techniques used are discussed and the results obtained by the two codes compared. A critical issue in these simulations is the large discrepancy between the ion cyclotron period, which characterizes the shock reformation time, and a time step small enough to follow the electron physics. In the fully electromagnetic code the Courant condition based on the velocity of light imposes: $dt \Omega_{ci} < \delta(\beta_e/2)^{1/2}(\Omega_{ce}/\omega_{pe})^2(m/M)$ where δ is the size of a grid cell in Debye length, Ω_{ce}/ω_{pe} is the gyro-to-plasma frequency ratio for the electrons, and m/M is the electron-to-ion mass ratio. Both ratios are very small in the solar terrestrial environment, resulting in a prohibitive RHS of $10^{-7}\delta$. The situation is less dire for the Darwin code, which only requires $dt \Omega_{ci} \approx 0.25(\Omega_{ce}/\omega_{pe})(m/M)$, namely a value an order of magnitude less small. Advantages and limitations of either code are examined in terms of computing efficiency and compromising via unrealistic plasma parameters.

DYNAMICALLY EVOLVING DOUBLE LAYERS AND DENSITY DEPLETIONS

Singh, N., Khazanov, I.
University of Alabama in Huntsville

Electric fields parallel to an ambient magnetic field in collisionless plasmas are most likely localized in double layers. Using 1-D Vlasov and particle-in-cell (PIC) codes we study the localization processes for double layers in the return current region of the auroral plasma. Simulations include large-scale density gradients. The PIC simulations include mirror force as well. Plasma is driven by an applied potential drop. In the presence of a preexisting density cavity in the plasma, a double layer forms in the cavity localizing the entire potential drop. If there is no preexisting localized density cavity in the plasma, cavities are created by plasma instabilities localizing the parallel electric fields in them. When the current density in the plasma developing in response to the applied potential becomes sufficiently large, even a slight density depletion becomes the site for double layer formation; a cavitational instability occurs and deepens the depletion. When the current reduces, the deepened cavity refills weakening the double layer and causing redistribution of the potential drop. The cavitational instability and associated formation of a double layer generate a rich variety of plasma processes, including generation of counterstreaming electrons on the high potential side of the double layer, electron-electron two-stream instability, and phase-space vortices as electron holes. The localized current disruptions associated with the electron holes are used to estimate the perturbations in magnetic fields. Simulations show that the recurring deepening and refilling of a cavity depending on the time history of the current in the plasma and associated recurring formation of double layers greatly contribute to the complexity of the plasma turbulence and fluctuations in the electron fluxes accelerated by the double layers. Relevance of results from the simulations to satellite observations is discussed.

EFFECTS ON THE PERPENDICULAR TEMPERATURE OF
 H^+ AND O^+ IONS DUE TO AN OBLIQUE DOUBLE LAYER
AT THE TRANSITION REGION OF THE AURORAL CAVITY

Main, D. S., Ergun, R. E., Andersson, L.

Laboratory for Atmospheric and Space Physics, University of Colorado, Boulder

The observed upward current region in the auroral oval is either potential or current driven, creating earthward travelling electrons that maintain the current. To maintain the current between the magnetosphere and ionosphere along a magnetic field line, changes in particle populations' densities and temperatures are required. The change in plasma conditions results in particle acceleration in the region between .5 - 3 R_e . From observations (Reiff, et al., *JGR*, **93**, 7441, 1988) and simulations (Ergun, et al., *GRL*, **27**, 4053-4056, 2000) this acceleration mainly takes place in two transition regions, where the region between the transition layers has low densities and is usually referred to as the auroral cavity. In the upward current region, the transition layers accelerate electrons earthward and the ions are accelerated anti-earthward. From observations (Ergun et al., *Physics of Plasmas*, **9**, 3685, 2002) the lower transition region is extended over a small spatial region ($\sim 1-3$ km) and can be modeled as an oblique double layer (Raadu, *Physics Reports*, 25-97, 1989). Often already heated ions in the form of ion conics are accelerated anti-earthward through this lower transition region. In the auroral cavity these ions are observed as a beam which consists mainly of H^+ and O^+ .

In this presentation, a test particle simulation of the ion motion through the lower transition region of the auroral acceleration region will be described. At the lower transition region, the O^+ is weakly magnetized and the H^+ is moderately magnetized. The transition region is simulated as an oblique double layer and represented by a monotonic potential shape. The initial ion distributions are represented as a cold maxwellian ($\sim 10-20$ eV) and resulting energized distributions will be compared to observations. The simulation investigates the effects of changing the thickness and obliqueness of the double layer on the final perpendicular energies of H^+ and O^+ . Because the O^+ ion gyro radius is on the same order as the observed double layer width, the O^+ distribution undergoes significant perpendicular heating. Therefore, the first adiabatic moment is not conserved for O^+ ions. However, the thickness of the double layer is much greater than the H^+ ion gyro radius. Therefore, the first adiabatic moment is conserved and H^+ experiences nearly zero perpendicular heating. This difference in perpendicular temperature has been observed by Kaufmann et al (*JGR*, **91**, 10080-10096, 1986). The authors attributed this perpendicular heating of O^+ to two stream instability. However, our results indicated that the heating may be due to an oblique double layer.

VLASOV SIMULATIONS OF TRANSITION LAYERS IN THE
AURORAL REGION: INFLUENCE OF BACKGROUND ELECTRON
POPULATIONS

Newman, D.L.¹, Andersson, L.², Goldman, M.G.¹,
Ergun, R.E.²

¹Center for Integrated Plasma Studies, University of Colorado,
390 UCB, Boulder, Colorado 80309-0390

²Laboratory for Atmospheric and Space Physics, University of
Colorado, 392 UCB, Boulder, Colorado 80309-0392

One-dimensional adaptive-open-boundary Vlasov simulations of *transition layers* in the downward-current region of the auroral ionosphere (D. L. Newman et al., *Phys. Rev. Lett.*, **87**, 255001, 2001) have shown how large potential jumps can form in an initially field-free current-carrying plasma seeded with a small charge-neutral density depression. Such transition layers, can be either turbulent or laminar. In the latter case the potential structure is that of a classical *double layer*. In both regimes, the transition-layer electric field accelerates electrons originating on the low-potential side of the layer. These accelerated electrons then interact with a background population on the high-potential side, resulting in a two-stream instability that saturates via trapping and electron phase-space hole formation. During the laminar phase, the shape of the accelerating electric field is in good agreement with FAST satellite observations (R. E. Ergun, et al., *Phys. Rev. Lett.*, **87**, 045003, 2001).

In the aforementioned simulations, the (laminar) double-layer state is relatively short-lived because it is susceptible to disruption by Buneman-like instabilities (M. V. Goldman et al., *Nonlin. Proc. Geophys.*, **10**, 37, 2003). Subsequent 1-D simulations indicate that the stability of laminar double layers is enhanced by the inclusion of a low-density hot *halo* electron population. Such halos not only suppresses disruptions, but also facilitate the formation strong (laminar) double layers. Interestingly, subsequent FAST observations also suggest a relationship between double layers in the downward current region and halo electrons. A comparison of simulations with and without halo electrons will be presented in the context of satellite observations.

The results of 1-D simulations seeded by two independent density depressions will also be presented. These simulations provide some insight into the possible interaction of two transition layers along the same magnetic field line. Depending on the relative depths of the seed density depressions, either of the two transition layers may ultimately be disrupted due to outflow from the other. Possible differences in higher dimensions will be discussed.

Session H5, 13:40-Wednesday

RADIATION BELT DYNAMICS

Chairpersons: G. Ganguli and G. Ginot

PITCH ANGLE SCATTERING AND PRECIPITATION OF
PRECIPITATION OF ENERGETIC ELECTRONS BY VLF
WHISTLER-MODE WAVES

Umran S. Inan
Stanford University

While it has long been known that the lifetimes of energetic radiation belt electrons in the inner magnetosphere are largely determined by their resonant interactions with whistler-mode waves, the particular contributions of waves from different sources have long been a source of scientific debate. Different methodologies have been employed for quantitative estimation of wave-induced pitch angle scattering, including diffusion type treatments appropriate for incoherent waves versus test particle formulations tailored for interactions invoking discrete and coherent waves. While initial work on wave-driven loss of energetic particles was incumbered by the sparse availability of data on the spectrum and type of waves, a wealth of new information is now available on the wave distributions. Furthermore, experimental observations of electron precipitation bursts produced by individual discrete wave packets allow quantitative comparison of theoretical predictions with observations. Ground- and space-based observations of various types of lightning-induced electron precipitation effects have been particularly useful in providing the data base with which we can assess and improve our theoretical models. We present a historical overview of the development of our understanding of wave-induced precipitation of energetic radiation belt electrons and also assess our current state of understanding of the role of different type of waves in determining the loss rates of energetic electrons in the inner radiation belts. With highly evolved quantitative models, it has recently been possible to quantify the relationship between wave power levels and particle lifetimes on a global basis. Using these types of estimates, we also comment on the possibility of active control of particle fluxes by artificial injection of VLF waves from space-based sources.

ON THE PHYSICS OF ARTIFICIALLY STIMULATED EMISSIONS

K. Papadopoulos
University of Maryland

Artificially Stimulated Emissions (ASE) also known as triggered emissions are a unique complex, nonlinear plasma phenomenon, that involves coherent wave-particle interactions followed by ballistic wave emission and amplification of a radically different nature from the well studied linear, quasilinear and nonlinear interaction of whistler waves with anisotropic particle distributions in the random phase approximation. The complex nonlinear features described by Helliwell as triggering, suppression, entrainment, mode locking and combination of the above represent a most serious challenge to our understanding of nonlinear plasma physics. Furthermore, ASE is a unique nonlinear plasma effect that has only been observed in space, predominantly using the Siple station and has yet to be reproduced in the laboratory. The paper will review first the experimental results and the status of understanding of the plasma physics underlying ASE. The theoretical review will include both analytic theories and computer simulations. Issues associated with the triggering threshold, the phase space bunching and the connection of ASE, to the Kennel-Petcheck theory of radiation belt control and to the gyrotron emission as observed in the laboratory and space will be discussed. Suggestions for proof-of-principle experiments in space and laboratory plasma chambers will be presented. Particular emphasis will be placed in experiments involving injection of VLF waves generated by modulating the auroral electrojet using the ionospheric heater of the High Frequency Active Auroral Research Program (HAARP) located in Gakona, Alaska, including the possibility of VLF injection into artificial ducts supported by F-region HF heating. Novel schemes for space based ELF and VLF generation using permanent or superconducting magnets and their potential for triggering ASE will be examined. The paper will conclude with suggestions for laboratory experiments in large plasma chambers.

PARTICLE TRANSPORT IN RADIATION BELTS: PRINCIPLES AND APPLICATIONS

Schulz, M.

Lockheed Martin ATC (Dept L9-42), 3251 Hanover Street (Bldg 255), Palo Alto, CA 94304 (U.S.A.)

Particle radiation environments are usually determined empirically by measuring the differential particle flux j (number of particles per unit energy, per unit solid angle, per unit area of detector, per unit time) as a function of energy E , local pitch angle α , L value, local magnetic-field intensity B , magnetic local time (MLT) ϕ , and universal time (UT) t . From a theoretical standpoint, however, the relevant quantity is the phase-space density $f (= j/p^2$, where p is the scalar momentum) as a function of the three adiabatic invariants, their three conjugate phases, and UT. The adiabatic invariants M , J , and Φ are respectively proportional to the canonical action integrals associated with gyration, bounce motion, and azimuthal drift. Any dependence of f on the conjugate phases can be interesting from the standpoint of radiation-belt microphysics but is usually unimportant for specifying the environment to which a spacecraft is exposed. Thus, it is common to analyze the temporal evolution of \bar{f} , which denotes the average of f over the various conjugate phases. For dynamical processes that satisfy Hamiltonian mechanics, the evolution of \bar{f} commonly satisfies a diffusion equation with respect to phase-space coordinates specified by the canonical action integrals. Whereas f itself would satisfy Liouville's theorem under the influence of such processes, the quantity \bar{f} satisfies a diffusion equation instead. Either way, it is usually necessary to specify boundary conditions on the problem, typically that f go to zero on any adiabatic trajectory that intersects the dense atmosphere, and that the phase-space density match an appropriate boundary spectrum at the interface between closed and open adiabatic drift paths. (Open drift paths typically are those that intersect the magnetopause and/or the nightside neutral line.) Dynamical processes of a "frictional" character (e.g., synchrotron loss, Coulomb drag) do not satisfy Hamiltonian mechanics and typically require the addition of first-order Fokker-Planck terms to the diffusion equation for their description. Other non-Hamiltonian processes such as charge exchange require the addition of source and/or loss terms to the basic diffusion equation for each particle species of interest. Processes such as wave-particle interactions commonly lead to pitch-angle diffusion and consequent loss of particles into the atmosphere. It is often profitable to adopt an eigenmode formulation for such processes, in which case the corresponding eigenvalue λ appears as a loss rate (reciprocal lifetime) in the corresponding radial-diffusion equation. Such an eigenmode formulation typically reduces the number of dimensions in which the diffusion equation needs to be solved (e.g., to the quasi-spatial variable $1/L$ alone in the case of a radial-diffusion equation).

INTENSITY DISTRIBUTION OF WHISTLER MODE EMISSIONS IN THE PLASMASPHERE: COMPARISONS WITH THE RADIATION BELTS

J. L. Green¹, S. Boardsen², S. Fung¹
, L. Garcia³, B. W. Reinisch⁴

¹NASA Goddard Space Flight Center, Greenbelt, MD 20771

²L3 Communications, Largo, MD

³Raytheon, ITSS, Landover, MD

⁴Center for Atmospheric Research, UMass Lowell

Five years of plasma wave observations from the Dynamics Explorer-1 spacecraft and three years from the Imager for Magnetopause-to-Aurora Global Exploration (IMAGE) spacecraft are used to construct plasma wave intensity maps. These intensity maps show the potential source locations or sites of wave amplification due to particle-wave interactions of whistler mode emissions in the plasmasphere. The plasmaspheric hiss spectrum can be viewed as having low (10-300 Hz) and high (300 Hz-3.3 kHz) components. Observations of plasmaspheric hiss in the low frequency portion of the spectrum show that the most intense region is in or near the magnetic equator in the afternoon sector and that during times of negative B_z that maximum intensity moves from L values of 3 to less than 2. These observations are consistent with particle-wave interactions in or near the magnetic equator in the slot region of the electron radiation belts. The high-frequency portion of the hiss spectrum shows intensity enhancements at high latitudes ($L=4$) and in the magnetic equator near over L values from 2 to 3. The longitudinal distribution of the hiss intensity is similar to the distribution of lightning with the peak intensity near late afternoon and the minimum near early morning local times in addition to particle-wave interactions in the magnetic equator. At frequencies above 3.3 kHz whistler mode emissions from ground-based transmitters are observed. For these emissions the maximum intensity shifts almost exclusively to the local evening with enhancements all along L shells from 1.8 to 3. Indications are that the cyclotron resonance also operates in this frequency range.

OBSERVATIONS OF THE INNER MAGNETOSPHERIC AND
RADIATION BELT PROCESSES BY RADIO PLASMA IM-
AGER ON IMAGE

Reinisch, B¹, Song, P¹, Huang, X.¹, Green, J²

¹Center for Atmospheric Research, 600 Suffolk St, Lowell MA
01854 USA

²NASA, Goddard Space Flight Ctr, Greenbelt MD 20771 USA

Using the sounding measurements from the radio plasma imager on IM-AGE, and a plasma density inversion algorithm, we derive the plasma density profiles along the magnetic field from one hemisphere to the other in less than 2 minutes. In each satellite orbit, several such measurements are possible, providing a tool to measure two-dimensional plasma density distributions in a meridian plane. From these measurements, we derived a functional form for field-aligned density distribution as well as the radial cross-field distribution. When the satellite revisits the same region in different orbits, the temporal variations of the density in this plane can be measured. We are using such measurements to develop the plasma density distribution models and to study the depletion, refilling, and other dynamical processes. In a case study of a magnetic storm event, the plasmopause was moved from $L = 4$ to about $L = 2.3$ during the storm. Namely, the background plasma conditions within $L=2.3$ were essentially unchanged during the storm while the plasma between $L = 2.3$ was evacuated during the storm. We think that these dynamical changes in the plasma conditions may affect the lifetime of the radiation belt. Passive plasma wave measurements are also made by the same instrument. We have conducted a comprehensive survey of the whistler wave observed in the magnetosphere. Enhanced wave power is observed in good correlation with the magnetic footprint and the operating frequencies of ground VLF transmitters. These waves appear to have substantial effects on the lifetime of the radiation belt particles. The amplitude and the effective area of the transmitters will be evaluated.

LABORATORY INVESTIGATION OF THE PROPAGATION AND DUCTING OF WHISTLER-WAVES*

W. E. Amatucci¹, G. Ganguli¹, D. N. Walker¹, G. Gatling²¹Plasma Physics Division, Code 6755, Naval Research Laboratory, Washington, DC 20375²Advanced Technology Division, SFA, Incorporated, Largo, MD 20774

There have been a number of interesting in situ and laboratory observations of whistler wave propagation and stimulated emissions over the past few decades. For example, Stenzel [1975] reported on the self-ducting of large amplitude whistler waves in a laboratory plasma. Those experiments showed that with increasing amplitude, the radiation pattern from a small dipole antenna becomes increasingly narrow, and ultimately forms a duct with diameter of the order of the parallel wavelength. The ducted waves were observed to propagate virtually undamped along the length of the plasma column. In the space environment, observations of artificially stimulated VLF emissions triggered in the magnetosphere by whistler modes from VLF transmitters have been reported by Stiles and Helliwell [1975]. Emission radiation is assumed to come from the transverse currents formed by counterstreaming electrons that have been temporarily phase bunched by the constant frequency triggering signal.

These observations have prompted a new NRL Space Physics Simulation Chamber investigation of whistler wave dynamics in a simulated radiation belt environment. The ultimate goals of these experiments are to understand and quantify ducting, self-focusing, and amplification of whistler waves, to investigate nonlinear whistler-plasma interactions, and to study the secondary emission of whistler waves. The initial experiments will concentrate on the ducting of whistler waves in pre-existing density depletions and enhancements. Density structures with controllable scale size and depth will be created using methods previously developed for a Space Chamber investigation of the dynamics of magnetospheric boundary layers [Amatucci et al., 2003].

*This work supported by ONR and USAF/HAARP.

Amatucci, W. E. et al., *Phys. Plasmas*, **10**, 1963 (2003).

Stenzel, R. L., *Phys. Rev. Lett.*, **35**, 574 (1975).

Stiles, G. S. and R. A. Helliwell, *J. Geophys. Res.*, **80**, 608 (1975).

GENERATION AND PROPAGATION OF WHISTLER MODES IN A LABORATORY PLASMA

Reiner L. Stenzel, J. Manuel Urrutia, Kyle D. Strohmaier

Department of Physics and Astronomy, University of California,
Los Angeles, CA, , 90095-1547

Whistler-mode waves in laboratory plasmas are usually excited with antennas. The radiation pattern of loop antennas has been studied, showing that loops small compared to the wavelength radiate predominantly along the resonance cone, $\cos\theta \simeq \omega/\omega_c$ for $\omega_p \gg \omega_c$. Large loops aligned along the guide field, \mathbf{B}_0 , generate spatial wavepackets whose fields, $\delta\mathbf{B}$, have the topologies of vortices. In each half cycle $\delta\mathbf{B}$ can be decomposed into linked toroidal and poloidal field components. The linkage is right-handed for propagation along \mathbf{B}_0 , left-handed for opposite propagation. Helicity injection from linked or knotted antennas produces unidirectional radiation of whistler vortices. By reciprocity, such antennas can be used to determine the direction of wave propagation, e.g., of whistler-mode noise. The radiation resistance of loop antennas has been studied. In order to excite strong whistlers, large near-zone fields are required. This can lead to nonlinear effects, i.e., modifications of those parameters which determine the wave propagation. First, electron heating has been observed to produce a field-aligned density depression which efficiently guides the wave. Since the guide radius can be smaller than the wavelength, the ducting is not by wave refraction but by a new eigenmode of the perturbed density profile. Second, for large time-varying fields which exceed the guide magnetic field, the wave propagation becomes instantaneously nonlinear. Magnetic null points are formed when the loop field is opposite to, and larger than, \mathbf{B}_0 . In this case, the vortex cannot propagate through the null point and the wave energy nearly stagnates. For the opposite polarity, the wave energy convects rapidly. For oscillating fields, this asymmetry produces dc fields and harmonics. The evolution of a stagnating whistler vortex has been studied in detail. Such a field-reversed configuration decays by magnetic field annihilation in the toroidal current sheet. The dissipation is anomalously fast, which may be associated with the observed current-driven ion sound turbulence in the neutral sheet. Magnetic energy is converted into electron heat. The configuration has also been observed to become unstable to tilting of the current ring. The tilted field precesses around an axis defined by \mathbf{B}_0 . The toroidal null line degenerates into two spiral null points. The energy is partly convected, partly dissipated. Finally, the emission of whistler modes from moving sources will be addressed, which has various applications to space plasmas.

Work supported by NSF PHY.

LIFETIME ESTIMATES OF ENERGETIC RADIATION BELT
ELECTRONS DRIVEN BY LIGHTNING-GENERATED MAG-
NETOSPHERICALLY REFLECTING WHISTLER WAVES

Bortnik, J., Inan, U. S., Bell, T. F.

Stanford University, David Packard Building, 350 Serra Mall, Palo
Alto, CA. 94305

We estimate the lifetimes of energetic radiation-belt electrons in the inner magnetosphere by combining data on magnitude and occurrence of lightning with our model predictions of electron precipitation driven by magnetospherically reflecting (MR) whistler waves generated by lightning sources at a variety of latitudes.

The model we use consists of four stages: (i) an extensive ray tracing and interpolation technique is used to compute the frequency-time ($f - t$) signature of an MR whistler wave at 1° latitude intervals along a given L -shell in the magnetosphere including the effects of spatial spreading and Landau damping, (ii) this information is used as an approximation to the MR whistler wave structure along the particular L -shell, and the equations of motion for a population of test particles are integrated to obtain overall pitch angle changes. The pitch angle changes of a broad range of resonant electron velocities are computed for harmonic resonances ranging from $m = -5$ to $+5$ including the longitudinal or "Landau" resonance. (iii) The pitch-angle change data obtained in (ii) is convolved with a realistic model of the electron distribution (AE8 with a typical loss-cone distribution) to yield precipitated electron flux. (iv) Step (iii) is repeated for L -shells in the range 1.3 to 5.5 in order to simulate the entire inner magnetosphere. Results from our calculations are presented in terms of the percentage reduction in the flux of a given energy of electrons due to a single lightning discharge at a certain latitude, and only require a lightning rate to determine the overall lifetimes of energetic electrons at any L -shell.

NON-LINEAR COUPLING OF THUNDERSTORM GENERATED RELATIVISTIC ELECTRON BEAMS WITH THE MAGNETOSPHERE

Michael W. Chevalier, Umran S. Inan, Timothy F. Bell

Stanford University

Gamma ray observations from the BATSE experiment on the Compton Gamma Ray Observatory indicate that some gamma ray bursts originate in the Earth's atmosphere near large scale thunderstorm systems. It is believed that these gamma ray bursts consist of bremsstrahlung from relativistic electrons accelerated to MeV energies by the intense quasi-static electric fields which temporarily exist above thunderclouds after intense positive cloud to ground discharges. If so, most of these relativistic electrons would escape the atmosphere and enter the Earth's radiation belts without much loss of energy. In the radiation belts the relativistic electron beam will interact with the cold background plasma through the two-stream instability, and some of the relativistic electrons may become trapped in the radiation belts. In the present paper we carry out a theoretical analysis of how these relativistic electron beams can couple to the magnetosphere. The motivation for this study is to assess the contribution of this phenomenon to the relativistic electron population in the inner radiation belts. The interaction of the beam and the cold magnetoplasma results in changes in the beam's pitch-angle distribution. We use 1D and 2D electromagnetic, particle-in-cell (PIC) simulators to calculate the evolution of the beam's pitch-angle distributions. We first study the 1D electrostatic interactions between the beam and the background magnetospheric plasma along a given L shell. We then assess the importance of other electromagnetic beam/plasma interactions with our 2D model. On the basis of these interaction models, we estimate the fraction of the original relativistic electron beam which can be trapped in the radiation belts. Our analysis is carried out for a range of initial beam densities and L shell values.

MODELING VLF PROPAGATION FROM GROUND TRANSMITTERS TO THE MAGNETOSPHERE

Small, B. L.¹, Starks, M. J.¹, Sales, G. S.²¹Space Weather Center of Excellence, Space Vehicles Directorate, Air Force Research Laboratory²Center for Atmospheric Research, UMass Lowell

A new VLF wave propagation code is being created to calculate the VLF wave power reaching the magnetosphere from ground transmitters. The code comprises three components to model the following processes: (a) ground/ionospheric wave-guide propagation, (b) ionospheric penetration and (c) magnetospheric propagation. The ground/ionospheric wave-guide component uses a short dipole model to calculate near-field radiation for ground transmitters and a simple attenuation model for VLF waves traveling along the earth-ionosphere waveguide. The ionospheric penetration component accounts for VLF leakage from the waveguide and absorption as the waves travel through the 60 to 1500km altitude range. Ionospheric penetration is computed as a function of season, GMT, and geomagnetic latitude. This penetration component is coupled with a ray-tracer that models the VLF from the topside of the ionosphere out to the magnetosphere where waves are guided as rays along magnetic field lines.

Details of the modeling will be discussed and results from the code will be compared with VLF receiver data from the IMAGE spacecraft (see Ground-based VLF transmissions received in the magnetosphere by the IMAGE/RPI satellite by G.S. Sales, et al., this session.) These results will show the correlation between VLF propagation predicted by the code and signal measurements from space of U.S. Navy transmitters such as the one on Lualualei, Hawaii.

This code also integrates with a larger set of codes that calculate the decay of trapped electrons in the radiation belts due to VLF wave-particle interaction. This is a relevant tool for investigating methods of reducing energetic particles that damage spacecraft.

MODELING A RADIATION BELT REMEDIATION SYSTEM

Starks, M.J.

Air Force Research Laboratory, Space Vehicles Directorate,
Hanscom AFB, MA

The ability to rapidly reduce the charged particle population in radiation belts is of interest in order to ensure safe spacecraft system operations. One actively explored method utilizes very low frequency (VLF) radio waves to scatter particles into the loss cone. An end-to-end computer simulation of depopulation by VLF comprises a major component of our investigation.

For ground-based scenarios, a VLF penetration model provides input to the central power tracing system, which propagates individual rays throughout the plasmasphere. For space-based approaches, far-field models of antennae on orbiting platforms provide the initial conditions. The AFRL Space Weather Center of Excellences Next Generation Power Tracing Code tracks the input energy as it expands outward into the plasmasphere, using models of ionospheric and plasmaspheric particle densities and the geomagnetic field. A Volumetric Power Aggregator maps these results into a three-dimensional database of the aggregate power flux at any point in space.

Using the resulting pictures of power flux, a Diffusion Coefficient Algorithm computes the effects on energetic particles making up an artificial radiation belt. By exploring the parameter space of transmitter frequencies and locations, and radiation belt populations and locations, an effective practical system for radiation belt remediation can be conceived.

Results from initial studies show the benefits of coupling these models, and their promise for designing systems that favorably impact the space environment. These simulations also create opportunities for comparisons with radio environment data obtained by satellites such as IMAGE, and with the results of ground-based experiments in VLF propagation into the plasmasphere. The modularity of the system allows easy extension to a host of propagation problems, including subionospheric HF and ducted VLF.

H6

Session H6, 8:40-Thursday

LABORATORY PLASMAS

Chairperson: Bill Amatucci

DISPERSIVE ALFVÉN WAVES: LAB VERIFICATION OF DEPENDENCE ON FINITE PERPENDICULAR WAVE NUMBER

Kletzing, C. A.¹, Bounds, S. R.¹, Skiff, F.¹,
Gekelman, W.², Vincena, S.²

¹Department of Physics and Astronomy, The University of Iowa

²Department of Physics and Astronomy, University of California, Los Angeles

Shear Alfvén waves are thought to play a significant role in several regions of near-Earth space including the plasma sheet, magnetopause, and auroral zone. The interesting physics occurs when the waves have narrow perpendicular structure such that the perpendicular scale is of the order of the ion acoustic gyroradius or the electron skin depth. Despite the importance of these waves, there are few experimental tests of the basic theory of the Alfvén wave for conditions for which finite k_{\perp} is important. We present the results of a series of laboratory measurements of the shear Alfvén wave dispersion relation for waves in the inertial ($V_{th} \ll V_A$) and kinetic regimes ($V_{th} \gg V_A$) as well as for when the waves are in the regime which is in-between inertial and kinetic ($V_{th} \approx V_A$). The measurements were performed at the Large Plasma Device at UCLA using the University of Iowa Arbitrary Spatial Waveform antenna. This antenna allows us to probe the dispersive nature of these waves for non-negligible k_{\perp} . Examples of the kinds of waveforms which can be generated are shown to demonstrate the flexibility of the system. By comparing the arrival times of the waves at spatially separated points, the wave phase velocity is determined which is then compared to the theoretical dispersion relation. The dispersion relation shows the expected response in parallel phase velocity with increasing perpendicular wave number. We compare two-fluid and kinetic descriptions of the dispersion and find that the best agreement between theory and experiment occurs for the warm plasma dispersion relation including collisional damping.

A STUDY OF NONLINEAR INTERACTIONS BETWEEN
SHEAR ALFVEN WAVES IN A LABORATORY PLASMA

Carter, T.A.¹, Brugman, B.¹, Pribyl, P.¹
, Dorland, W.², Quataert, E.³

¹Dept. of Physics and Astronomy, UCLA

²Physics Department, Univ. of Maryland

³Astronomy Department, UC Berkeley

Electromagnetic turbulence is thought to play an important role in plasmas in astrophysical settings (e.g. interstellar medium, solar wind, and accretion disks) and in the laboratory (e.g. transport in magnetic fusion devices). In Alfvénic turbulence, nonlinear interactions between counter-propagating shear Alfvén waves are fundamental to the turbulent energy cascade. Under ideal, incompressible MHD, analytic theory and simulations show that these interactions lead to a Kolmogorov inertial range and to anisotropy in the wavenumber spectrum, with a preference for cascade in the perpendicular direction. We will describe a new experimental effort to test these predictions in the Large Plasma Device (LAPD) at UCLA. In these experiments, a large scale shear Alfvén wave is driven using either an antenna or an instability driven Alfvén wave MASER in the plasma source region^a. A counter-propagating spectrum of shear waves is established using reflecting boundary conditions or a second antenna source. The wavenumber spectra of the waves are measured by magnetic pick-up probes and cross-correlation techniques, making use of the high repetition rate of the LAPD plasma for gathering statistics. I will discuss the requirements (launch wave amplitude, T_e , etc.) for successfully observing a cascade initiated by the large scale “stirring” wave in LAPD as well as the physics issues which may be addressed through such an experiment (inertial range spectrum, dissipation, non-ideal effects, parametric decay, etc). The discussion will be supported by theory and gyrokinetic simulation of the planned experiments. Gyrokinetic simulation is well suited for studying the anisotropic kinetic Alfvén wave cascade; simulations will be performed using the electromagnetic GS2^b code. Preliminary experimental results will be presented including observations of nonlinear interaction between the MASER source wave and a low frequency wave during the initial experiments with reflecting boundary conditions.

^aJ.E. Maggs and G. Morales, PRL 91, 035004 (2003)

^b<http://gs2.sourceforge.net>

SPONTANEOUS DOUBLE LAYER FORMATION IN A HIGH-DENSITY PLASMA

Scime, E.E., Sun, X., Biloiu, C. , McGeehan, B.
West Virginia University

Spontaneous formation of a strong, current-free, electric double layer (DL) with $e(\phi)/kTe \approx 3$, based on axially resolved plasma potential measurements, was recently observed in an expanding helicon plasma source after the neutral pressure was decreased to less than 0.5mTorr [1]. Laser-induced fluorescence (LIF) measurements in the MNX helicon plasma source indicate that an energetic ion beam with parallel kinetic energy $\approx 30\text{eV}$ spontaneously appears in the expansion region at low neutral pressures $\approx 0.6\text{mTorr}$ - consistent with the spontaneous formation of a DL [2]. Pulsed plasma experiments have also reported the spontaneous formation of a double layer as the plasma expands into a vacuum region [3]. In this work, LIF measurements of the ion flow speed at three different places along the axis of the steady state, magnetized, high-density, HELIX helicon plasma source and in the expansion region at the end of the source indicate large ion acceleration towards the expansion region and decreasing parallel ion flow speeds beyond the expansion region. The parallel ion acceleration in HELIX is a strong function of neutral pressure below 2.5 mTorr. Estimates of the electric field in HELIX based on multiple Langmuir probe measurements are comparable to the field magnitudes reported in Ref. [1]. We will discuss the similarities and differences between these different laboratory observations of spontaneous double layer formation and comment on the possible relevance to double layer formation in space. [1] C. Charles and R. Boswell, Applied Phys. Letters 82, 1356 (2003) [2] S.A. Cohen, N.Siefert, S.Stange, R.Boivin E. E. Scime, et al. Phys. Plasmas 10, 2593 (2003) [3] G. Hairapetian and R.L. Stenzel, Phys. Rev. Lett. 65, 175 (1990)

PROPOSED EXPERIMENT ON MEASURING PAYLOAD POTENTIALS OF SOUNDING ROCKETS WITH EMISSIVE PROBES

Sternovsky, Z., Knapmiller, S., Robertson, S. , Horanyi, M.

Physics Department, University of Colorado, Boulder, CO 80309-0390

Charging of spacecrafts to large potentials in the magnetosphere and interplanetary space has been long recognized as a nuisance and possible hazard and its mitigation has been undertaken in several ways. Sounding rockets, launched to the mesosphere and lower ionosphere, are exposed to the ionospheric plasma. The charging is due to collection of plasma electrons and ions and photoemission, respectively. Due to the high thermal motion of free electrons, negative payload potential is probable. The structure of the plasma sheath surrounding the rocket is a function of the local plasma density, temperature and the rockets speed. The charging of sounding rockets is not as severe as for spacecrafts; however, the nonzero payload potential affects the performance of many on-board instruments. Moreover, narrow layered structures with depleted free electron densities are known to exist near the mesopause region that may cause sudden changes in the payload potential. Langmuir probes or retarding potential analyzers can be used to measure the payload potential. These techniques require sweeping of potentials for a full measurement and thus has limited time resolution. An in-situ experiment, using an emissive probe, is proposed to measure the rockets potential and the structure of the surrounding plasma sheath. The emissive probe is a short filament heated to incandescence, which emits electrons. The heating circuit of the probe is electrically floating and thus the probe self-biases to a potential of the immediate ambient space, thus allowing a fast, direct measurement of space potentials. An emissive probe is constructed that can withstand the mechanical strain during launch. The probe is mounted on a linear moving stage and is swept back and forth from the rockets surface out to a distance that is comparable to the rockets diameter.

GROWTH AND SUPPRESSION OF LOW FREQUENCY INSTABILITIES IN A MAGNETIZED PLASMA COLUMN

Edward Thomas, Jr., Jon David Jackson, Edwynn Wallace

Physics Department, Auburn University

Low frequency instabilities have long been investigated in plasma physics. Nonetheless, through careful theoretical and experimental investigations new types of instabilities continue to be predicted and observed in plasmas. One particular class of plasma instabilities that has been the subject of recent studies are flow shear driven instabilities both parallel and transverse to the background magnetic field.

The role of transverse sheared flows is important in a wide variety of plasma phenomena. For example, in fusion plasmas, transverse flow shear at the plasma edge is often associated with internal transport barriers, the transition to enhanced confinement regimes, and a general reduction in the level of plasma instabilities. By contrast, in the study of magnetospheric plasmas, both transverse and parallel flow shears are believed to be important mechanisms for particle acceleration and the generation of ion acoustic and ion cyclotron instabilities. Although these plasma environments have vastly different parameters, the underlying physical mechanism of particle flows driven by crossed electric and magnetic fields remains the same. Our experimental investigations focus on understanding the role of transverse flow shear in the stabilization and destabilization of plasma instabilities in the ion cyclotron regime.

Experiments are performed on the ALEXIS (Auburn Linear Experiment for Instability Studies) device; a 180 cm long, 10 cm diameter, magnetized plasma column. Helium plasmas are generated in ALEXIS using heated tungsten filaments. Sheared flows in the plasma are established using an array of four concentric ring electrodes placed at the opposite end of the chamber from the filaments. Earlier studies on ALEXIS have shown the formation of instabilities driven by transverse shear flow [E. Thomas, Jr., *et. al.*, Phys. Plasmas, **10**, 1191, (2003)]. This presentation will discuss observations of shear flow driven instabilities, the transition to current driven modes, and initial observations of an asymmetric plasma response to applied transverse electric fields.

This work is supported by Department of Energy Grant No. DE-FG02-00ER54476.

THE FLOATING POTENTIAL MEASUREMENT UNIT (FPMU) CALIBRATION AND LABORATORY PLASMA VALIDATION

Charles M. Swenson¹, Don Thompson², Chad Fish³, William Amatucci⁴

¹Department of Electrical and Computer Engineering, Utah State University

²Center for Atmospheric and Space Science, Utah State University

³Space Dynamics Laboratory, Utah State University

⁴Naval Research Laboratory

NASA has set a priority on validating the vehicle charging physics and charge control system on the International Space Station (ISS). Vehicle charging is a function of the local electron density and temperature and involves a complex interaction of exposed potentials on solar panels, photoelectrons, surface properties, vehicle wake effects, and secondary electron emission. Excessive vehicle charging has been identified as a risk to astronauts working outside of the station as well as accelerating the degradation of the space station surface properties. A fully redundant set of plasma contactors are used to control the charging of the space station.

The Floating Potential Measurement Unit (FPMU) has been developed to assess how well ISS plasma contactors are working. The FPMU is being built by the Space Dynamics Lab at Utah State University and consists of two sweeping Langmuir probes, a floating potential probe, and a combination impedance / plasma frequency probe. This suite of instruments will directly measure the floating potential of the space station over a +20 to -80 volt range at 100 Hz. The local electron density will be measured at 400 Hz over the range of 10^3 to 10^7 per cubic centimeter using ion ram currents, electron currents and the plasma frequency measurements. The electron temperature will be determined from Langmuir sweeps at a 1Hz rate and will provide temperature in the range of 500 to 4800 K. The FPMU instruments are fully redundant in the determination of the required parameters of floating potential, density, and temperature. The FPMU will be operational for 3 years and is expected to be launched on the next shuttle mission.

There have been a total of four identical flight FPMU systems developed for this program. One of the units has been tested in the Naval Research Laboratory plasma chamber. As such, FPMU presents an interesting opportunity to correlate Langmuir and impedance probe techniques for plasma diagnostics both in space and laboratory conditions. This paper presents a review of the calibration techniques, the calibration results, and plasma chamber testing results at NRL for the FPMU.

CHARGED DUST AND PLASMA MEASUREMENTS IN
IONOSPHERIC AND LABORATORY DUSTY PLASMAS

Gelinas, L.J.¹, Amatucci, W.E.², Lynch, K.A.³, Kelley, M.C.¹

¹Cornell University

²Naval Research Laboratory

³Dartmouth College

Measurements of charged species in dusty plasmas, both in the laboratory and in space, are complicated by the response of the charged dust population to disturbances. Understanding how dust influences these measurements is becoming more important as interest in in-situ mesospheric dust and ice particle measurements increases. The accuracy of in-situ charged dust measurements depends on many factors, including detector geometry, motion of the payload and sensor through the medium, payload electric potential, dust charge and size, neutral density, plasma density, as well as geophysical effects. The presence of a charged dust population may also influence other in-situ measurements, such as plasma densities and electric fields, due to the dust response to payload charging and dynamics.

A set of rocket launches from Poker Flat Research Range in March 2002 made in-situ measurements of charged dust, plasma densities and electric fields. The electric field and plasma density measurements show wake effects which appear to intensify when the payload is inside the charged dust layer. While it is possible to estimate the configuration of the wake potential structure using multiple probes on the payload, interpreting these type of measurements can be difficult if the response of the dust population is unknown. Laboratory dusty plasmas can fill in some details of how dust responds to different perturbations, and may eventually help in interpreting the in-situ dusty plasmas. In this paper we present in-situ data from the March 2002 rocket launches showing dust-related wake effects. We also describe ongoing laboratory dusty plasma experiments which we hope to use in determining how charged dust effects can be accounted for in in-situ data.

Session J1, 13:40-Monday

**NEW SCIENCE AND TECHNICAL
DEVELOPMENTS FROM THE
GREEN BANK TELESCOPE**

Chairperson: Phil Jewell

THE CURRENT STATUS OF THE GREEN BANK TELESCOPE

Balsler, D., Ghigo, F., Jewell, P.R.
, Langston, G., Maddalena, R.J., Minter, A. , O'Neil, K.

National Radio Astronomy Observatory, PO Box 2, Green Bank,
WV 24944

The Robert C. Byrd Green Bank Telescope (GBT), the world's largest, fully steerable, single-dish radio telescope, is now in routine use by astronomers. The GBT was formally dedicated in August 2000 and the first scientific observations took place in April 2001. Commissioning is successfully completed up to an observing frequency of 25 GHz. We plan to commission the GBT to 50 GHz by January 2004 and 100 GHz in two years.

The GBT is an advanced telescope designed for a wide range of projects. Novel features of the GBT include an unblocked aperture with a projected diameter of 100 m, an active surface for removing gravitational deformations, and a precision control system that includes various laser metrology and ranging systems. The GBT's performance is as good or better than that stated in the original specifications.

Current instrumentation includes a large suite of receivers that almost completely covers from 0.3 to 50 GHz. Bolometer and heterodyne array receivers for 68-98 GHz observing are either in construction or are being designed. Observers can pick from a wide suite of backends. The GBT Spectrometer is a quarter-million channel autocorrelation spectrometer with up to 16 samplers, each having bandwidths from 12.5 to 800 MHz. We support a 16-channel, wide-bandwidth digital continuum receiver and various pulsar backends. Observers frequently supply their own backends for experiments like bi-static radar and pulsar observations.

About 50-60% of the time the telescope is used for astronomical observing with the rest going to expanding the telescope's capabilities or maintenance items such as painting and system tests. We are investigating upgrades to the telescope's azimuth track which is experiencing premature wear, though none of these problems are affecting the astronomical performance of the instrument. We expect the percentage of time devoted to observing will substantially increase over the coming months.

FIRST RESULTS FROM GBT STUDIES OF THE 21CM HYDROGEN LINE

Lockman, F.J.

National Radio Astronomy Observatory, Green Bank, WV USA

The Green Bank Telescope (GBT) is exceptionally well-suited for studying the 21 cm line of HI in the Milky Way and nearby galaxies because of its good sky coverage and angular resolution, low-noise receivers, and freedom from aperture blockage. In this presentation I will discuss some discoveries that have resulted from 21cm observations at the GBT in its first two years of operation.

With the GBT it has been possible to resolve much of the HI in the lower Galactic halo — far from the thin gaseous disk yet still bound to its rotation — into discrete clouds. These clouds are orders of magnitude denser than their surroundings and are unlikely to be in static equilibrium against the gravity of the disk. They may be the return products of a galactic fountain: cool clouds which have condensed out of a hot galactic halo and are now bringing material enriched by supernova ejecta back into the disk. They might also be material flung out of the disk by energetic events like multiple supernovae. The halo clouds are being used as probes of the dynamics of the interstellar medium, its physical conditions, and chemical evolution.

Observations with the GBT have also shed new light on a prominent high-velocity HI cloud which appears in GBT 21cm spectra to show significant interaction with the outskirts of the Milky Way. These data support a model in which the cloud is a satellite of the Galaxy in the process of being accreted into the disk. The GBT data constrain models for its orbit and mass loss.

Observations of HI in nearby galaxies with the GBT suggest that they too may contain a constellation of high-velocity clouds surrounding them. Here the sensitivity of the GBT to low surface brightness emission was a key factor in the experiments' success. One implication of these early results is that the high-velocity cloud phenomenon seen in our own Galaxy might be a reflection of ongoing processes of galaxy formation, and an expected feature of many galactic systems.

Finally, work is near completion on a survey of 21cm HI in the first quadrant of the Galactic plane, using the VLA for high angular resolution and the GBT for the low spatial frequencies, which will give HI maps containing complete information to the 1-arcmin resolution limit of the survey. Already these data are showing interesting features that are revising our understanding of the atomic phase of the interstellar medium.

PULSAR RESULTS WITH THE GREEN BANK TELESCOPE

Camilo, F.

Columbia University

I will summarize some of the pulsar work done at the Green Bank Telescope during the past two years. Among the projects are the search for and (sometimes) discovery of weak pulsars — e.g., young pulsars in supernova remnants and EGRET sources (Camilo et al.), millisecond pulsars in globular clusters (Ransom et al., Jacoby et al.), and nearby X-ray bright, but apparently radio weak/silent, neutron stars (Ransom et al.). Also, regular timing programs have been established for a number of young, binary, and/or millisecond pulsars resulting in, e.g., measurement of secular changes in the binary parameters of PSR J1740-3052 due to the mass quadrupole of its main-sequence companion star (Stairs et al.); improvement in the mass determination of the double neutron star binary PSR J1518+4904 via measurement of relativistic effects (Nice et al.); an improved experimental constraint on the existence of dipolar gravitational radiation through timing of the binary pulsar B0655+64 (Arzoumanian et al.); observations of the eclipsing binary PSR B1744-24A showing orbital evolution with both signs of period derivative, and large levels of timing noise (Nice et al.); measurement of the radio-X-ray pulse phase offset and radio spectrum for the young and energetic pulsar J2229+6114 (Camilo et al.); observations of some tight binary systems showing that the pulsars are not, in fact, eclipsed, even at relatively long wavelengths (Nice et al.). These observations have used instrumentation developed by Berkeley/Caltech (BCPM; Backer et al.) and NRAO (Spectral Processor). By the time of the meeting the “spigot card” (Kaplan et al.), developed by Caltech/NRAO, should also be routinely available.

PLANETARY RADAR RESULTS FROM THE GBT

Margot, J. L.

California Institute of Technology

The Green Bank Telescope (GBT) offers new capabilities with considerable promise for solar system studies. Some of the exciting developments involve the use of the GBT in conjunction with the powerful planetary radars at Arecibo and Goldstone.

The Arecibo-GBT baseline is of convenient length and orientation for the measurement of Venus topography by radar interferometry at 12.6 cm wavelength. The ~ 2 km fringe spacing at Venus implies that 100-200 m height resolution can be obtained in high SNR regions. A preliminary interferogram over Maxwell is being used to study the relationship between altitude and surface emissivity/reflectivity and to evaluate surface slopes [1].

Several near-Earth asteroids (NEAs) have been observed with the GBT configured as a radar receiver. The advantage of this configuration is to allow continuous recording for long periods of time and therefore high spectral resolution of the Doppler-broadened echoes. The Arecibo-GBT configuration has been used to identify and characterize an end-member NEA, 2001 EC16, with a small size (~ 150 m) and a very long spin period (~ 6 days) [2]. This asteroid is most likely tumbling, which is of great interest because the damping timescale is related to asteroid mechanical properties. High resolution images of another NEA demonstrate that it is a slowly-rotating contact binary [3].

The GBT is also being used to probe the interior of Mercury and the atmospheric dynamics at Venus. A technique derived from the laser speckle literature [4] has been successfully implemented with the Goldstone-GBT baseline to measure planetary rotations with 10^{-5} fractional uncertainty. Those observations reveal minute oscillations in the spin rate of Mercury resulting from the 88-day forced librations in longitude [5]. Measuring the amplitude of the librations was suggested by Peale [6] as a way to distinguish between a liquid and solid core at Mercury, because the amplitude is expected to be twice as large if the mantle is decoupled from the core. Long-term monitoring of the spin of Venus with the same technique is expected to reveal seasonal changes. A 1% change in atmospheric angular momentum affects the rotation of the solid planet in a measurable way, hence the Venus observations will probe its atmospheric dynamics and climatic variations.

- [1] L. M. Carter, D. B. Campbell, B. A. Campbell, J. L. Margot. *LPSC*, **34**.
- [2] J. L. Margot *et al.*, 2001 EC16, in preparation.
- [3] S. J. Ostro *et al.*, 1993 OM7, in preparation.
- [4] I. V. Holin. *IVUZ, Radiofizika*, **31**, 515 (1988).
- [5] J. L. Margot, S. J. Peale, R. F. Jurgens, M. A. Slade, I. V. Holin, in prep.
- [6] S. J. Peale. *Nature*, **262**, 75 (1976).

GBT OBSERVATIONS OF WATER MASERS IN AGN

Braatz, J.¹, Henkel, C.², Greenhill, L.³
, Moran, J.³, Wilson, A.⁴

¹NRAO, PO Box 2, Green Bank, WV 24944 USA

²MPIfR, Auf dem Hugel 69, D-53121, Bonn, Germany

³Harvard-Smithsonian Center for Astrophysics, 60 Garden St.,
Cambridge, MA 02138 USA

⁴Department of Astronomy, University of Maryland, College Park,
MD 20742 USA

We are using the Green Bank Telescope (GBT) to study the nuclear gas in active galaxies through observations of the 22 GHz water maser line. The sensitivity of the GBT at K-band and its capability of observing over large bandwidths with high spectral resolution have enabled advances on two fronts: monitoring the maser spectra in known sources, and searching for new water maser systems. Monitoring observations are used to trace gas dynamics. In cases where the maser exists in an edge-on, circumnuclear disk in the AGN, such observations reveal the rotational velocity and the centripetal acceleration of gas in that disk, and are used to estimate the mass of the central black hole in the AGN. We will show observations of several sources, including NGC 1386, IC 2560, and Mrk 1419 taken over 1.5 years.

We are also using the GBT to search for maser emission in a sample of nearby ($v < 10000 \text{ km s}^{-1}$) galaxies with type 2 AGNs. The principal goal is to identify additional examples of disk masers similar to the one known in NGC 4258. Several new sources have been discovered with the GBT, including masers in the nuclei of NGC 6323, NGC 5728, and NGC 4388. Each of these has a maser spectrum which includes features near the systemic velocity of the galaxy in addition to features at large velocity offsets (up to 600 km s^{-1}), suggesting the presence of a nuclear disk. The maser spectrum in NGC 6323 in particular has a classic profile showing three distinct groups of maser features which we interpret to derive from distinct loci in the edge-on disk. We will describe how future observations of the maser in NGC 6323 might lead to an accurate geometric measurement of the distance to this galaxy. Such a measurement would provide an important data point in studies of the extragalactic distance scale.

POLARIZATION MEASUREMENTS AT THE GBT: TECHNIQUES, CALIBRATION, AND SIDELOBES

Heiles, C.¹, Robishaw, T.¹, Troland, T.H.²¹Astronomy Department, University of California, Berkeley²Department of Physics and Astronomy, University of Kentucky

Our scientific interests require measuring circular polarization of spectral lines, which we accomplish with cross-correlation of linear polarizations using the Green Bank Spectral Processor. Calibration issues are extremely important. The cornerstone of our calibration technique is using a correlated noise source as the reference. We develop the Mueller matrix for the system with respect to the deflection of this noise source. We derive its elements from physical models of the voltage transfer functions in the feed and the coupling of the noise source to the system. We then express its elements in terms of the parallactic angle dependence of the system response to a linearly polarized astronomical calibration source such as 3C286. We follow the parallactic angle dependence of the calibrator, compared with a correlated noise source, using repetitive "spider scans".

These scans are fast and also provide complete beam maps, including the first sidelobe. The derived parameters include pointing offsets, beamwidth, beam ellipticity, beam coma, and system temperature, and also the first sidelobe parameters expressed in a Fourier series around beam center, in all four Stokes parameters. This allows us to also derive the variation of polarization within the primary antenna beam, popularly known as "beam squint" and "beam squash", for all Stokes parameters.

We examine the sidelobe response within about 8 degrees from beam center by mapping Cas A, which is a very strong continuum source. In addition, we examine the far-out sidelobe response out to 25 degrees from beam center from a very sparsely-sampled map of the Sun; these distant sidelobes are very weak and are not clearly related to spillover from the illumination of the secondary.

THE GBT: PROBING MAGNETIC FIELDS WITH ZEEMAN SPLITTING OF THE 21-CM LINE

Robishaw, T.¹, Heiles, C.¹, Troland, T.H.²¹Astronomy Department, University of California at Berkeley²Department of Physics and Astronomy, University of Kentucky

The extremely low sidelobe response and unblocked aperture of the GBT make it a unique instrument for inspecting the nature and origin of magnetic fields using Zeeman splitting of the 21-cm hydrogen line. We accomplish this by obtaining the Stokes V spectrum from the Green Bank Spectral Processor, which cross-correlates linear polarizations. Having characterized the L-band polarization response of the GBT, we observed a suite of sources using in-band frequency switching. Our targets are of three types: (1) in the Galactic plane, to derive the large-scale Galactic field; (2) at selected high-latitude positions, to derive field strengths in the Warm Neutral Medium and assess instrumental effects; and (3) in external galaxies, specifically M31.

Our Galactic-plane targets include positions where the Zeeman effect might be seen in emission at the tangent points (G32.30+0.15, G38.15-0.15, G43.75-0.10, G52.20-0.05, G112.7-0.60, G139.1+0.70) and in absorption against continuum sources (W3, W43, W49A, W49B, W51). At high latitudes we pointed to four positions (G135.3+40.8, G135.5+39.5, G142.5+41.0, G142.6+38.4, and the North Celestial Pole). In M31, we observed at two positions where the rotation curve is flat and the emission is completely separated in velocity from that of the Milky Way.

We discuss our observing method and results for each source. We also discuss instrumental effects that are produced by polarization within the main beam and also the near-in and far-out sidelobes. These effects manifest themselves not only in the Stokes V spectra, but also in the Stokes I spectra. We discuss the locations and magnitude of these sidelobes based on measurements in both the continuum and the 21-cm line.

This work was supported by the NSF through a GBT Student Support Program award to the author.

THE GBT PRECISION TELESCOPE CONTROL SYSTEM

Prestage, R.M.¹, Constantikes, K. T.¹, Balser, D.S.¹
, Condon, J.J.²

¹National Radio Astronomy Observatory, P.O. Box 2, Green Bank,
WV 24944, USA

²National Radio Astronomy Observatory, 520 Edgemont Road,
Charlottesville, VA 22903, USA

The Green Bank Telescope (GBT) is a 100m diameter advanced single dish radio telescope designed for a wide range of astronomical projects with special emphasis on precision imaging. The GBT is a massive structure weighing approximately 7700 metric tons, but is expected to deliver extraordinarily precise performance, in order to allow effective operation at observing frequencies up to 115GHz. The ultimate performance goals are two dimensional tracking error $\sigma_2 < 1.5''$ and surface accuracy $\epsilon < 0.2\text{mm}$.

The key to delivering this performance is the Precision Telescope Control System (PTCS) project, which was formally launched in November 2002, and is expected to run through Winter 2005/6. The project has two major areas of activity. One aspect is the continued development and implementation of the Precision Telescope Control System itself. This consists of an extensive metrology system, including temperature sensors, accelerometers, laser rangefinders and other devices; the existing precision servo systems (for primary, secondary and active surface) and a control system architecture which will allow us to harness these measurement and control capabilities to deliver a wide variety of observing modes with the precision necessary for 3mm operation.

The second main aspect of the PTCS project is the performance of a series of astronomical and engineering experiments to identify, understand and correct the residual pointing and surface accuracy errors which need to be controlled to achieve 3mm operation. These errors can have multiple causes, many of which depend on variable environmental conditions. For example, thermal gradients in the antenna are responsible for the largest currently uncompensated pointing and focus tracking errors.

In this paper, we will present the results of recent commissioning activities, which will highlight the physical processes which must be mitigated in order to achieve precise operation of a 100m telescope. We will also present an overview of the control system which will be used to alleviate these effects, allowing effective operation of the GBT at frequencies up to 115GHz.

FUTURE HIGH FREQUENCY INSTRUMENTATION WITH THE GBT

Mason, B.S.

National Radio Astronomy Observatory, Green Bank, WV

NRAO has made significant progress commissioning high-frequency instrumentation on the Green Bank Telescope, with the result that the GBT is a premier astronomical facility at frequencies up to 40 GHz. Key assets include the world's largest collecting area at frequencies above 40 GHz, a clean beam, an existing 4 GHz correlator, and a clear aperture. In the near future 3mm operations with the GBT will be possible. We briefly review the science which this groundbreaking capability will enable. The GBT can be expected to have a significant impact on studies of high-redshift galaxies, Galactic star formation, astrochemistry, extragalactic masers, and the SZE to name but a few. NRAO has an active high frequency instrumentation development program underway. With funds from NRAO's Universities Instrumentation program, the University of Pennsylvania, Goddard Space Flight Center, and NIST are building a 64 pixel 3mm bolometer array for the GBT. When initially constructed this instrument will have an 8 GHz bandwidth centered at 90 GHz, although a future filterwheel upgrade could allow the bandwidth to be increased under good conditions. We are also building two pseudo-correlation receivers, one for each of Ka and W bands. With funding from the Universities Instrumentation program Caltech is building a fast-switching continuum backend for the pseudo correlation receivers. With the current antenna performance this backend should yield a continuum sensitivity of $\sim 0.3 \text{ mJy } \sqrt{\text{sec}}$ at 1cm. We are investigating the funding of a wideband spectrometer. This spectrometer would be intended for wideband radio redshift searches, and would notionally be used at wavelengths from $\sim 1 \text{ cm}$ to 3mm.

Session J2, 13:40-Tuesday

**ADVANCES IN LARGE FOCAL
PLANE ARRAYS I: BOLOMETRIC
DETECTORS**

Chairperson: Kent Irwin

LARGE FORMAT BOLOMETER ARRAYS FOR ASTROPHYSICS

Moseley, H., Benford, D.

Goddard Space Flight Center, Greenbelt, Md. 20782

Some of the most compelling questions in modern astronomy are best addressed with submillimeter and millimeter observations. The question of the role of inflation in the early evolution of the universe is best addressed with large sensitive arrays of millimeter polarimeters. The study of the first generations of galaxies requires sensitive submillimeter imaging, which can help us to understand the history of energy release and nucleosynthesis in the universe,

Our ability to address these questions is dramatically increasing, driven by dramatic steps in the sensitivity and size of available detector arrays. While the MIPS instrument on the SIRTIF mission will revolutionize far infrared astronomy with its 1024-element array of photoconductors, thermal detectors remain the dominant technology for submillimeter and millimeter imaging and polarimetry. The last decade has seen the deployment of increasingly large arrays of bolometers, ranging from the 48 element arrays deployed on the KAO in the late 1980s, to the SHARC and SCUBA arrays in the 1990s. The past years have seen the deployment of a new generation of larger detector arrays in SHARC II (384 channels) and Bolocam. (144 channels). These detectors are in operation and are beginning to make significant impacts on the field. Arrays of sensitive submillimeter bolometers on the SPIRE instrument on Herschel will allow the first large areas surveys of the sky, providing important insight into the evolution of galaxies. The next generation of detectors, led by SCUBA II, will increase the focal scale of these instruments by an order of magnitude.

Two major missions are being planned by NASA for which further development of long wavelength detectors is essential. The SAFIR mission, a 10-m class telescope with large arrays of background limited detectors, will extend our reach into the epoch of initial galaxy formation. A major goal of modern cosmology is to test the inflationary paradigm in the early evolution of the universe. To this end, a mission is planned to detect the imprint of inflation on the CMB by precision measurement of its polarization. This work requires very large arrays of sensitive detectors which can provide unprecedented control of a wide range of systematic errors, given the small amplitude of the signal of interest.

We will describe the current state of large format detector arrays, the performance requirements set by the new missions, and the different approaches being developed in the community to meet these requirements. We are confident that within a decade, these developments will lead to dramatic advances in our understanding of the evolution of the universe.

BOLOCAM: A MILLIMETER-WAVE CAMERA FOR COSMOLOGY

Glenn, J.¹, Ade, P.A.R.², Aguirre, J.¹
 , Bock, J.J.^{3,4}, Edgington, S.F.³, Goldin, A.⁴
 , Golwala, S.³, Haig, J.², Lange, A.E.³
 , Laurent, G.¹, Maloney, P.¹, Maukopf, P.²
 , Nguyen, H.⁴, Rossinot, P.³, Sayers, J.³
 , Stover, P.¹, Wilson, G.⁵

¹University of Colorado

²University of Wales

³California Institute of Technology

⁴Jet Propulsion Lab

⁵University of Massachusetts

Bolocam is a millimeter-wave bolometer array camera built for observations from the Caltech Submillimeter Observatory. It has been optimized for sensitive cosmological observations, however its excellent sensitivity, three bands (1.1 mm, 1.4 mm, and 2.1 mm), and rapid mapping speed enable a broad range of astronomical observations. The 1.1 mm band is optimum for detecting submillimeter galaxies in extragalactic fields and thermal dust emission from Galactic star formation regions. The 2.1 mm band is optimum for observations of the thermal Sunyaev-Zeldovich effect to detect galaxy clusters and measure secondary cosmic microwave background anisotropies. These provide sensitive probes of our cosmological model. Combined with the other two bands, the 1.4 mm band could enable measurements of the peculiar velocities of galaxy clusters and hence measure the matter density of the Universe.

The heart of Bolocam is an array of 120 neutron-transmutation-doped silicon nitride micromesh, feedhorn-coupled bolometers on a single silicon wafer. The metallized meshes facilitate efficient absorption of millimeter-waves, low heat capacity, and small cross section (5%) to cosmic rays. The bolometers are cooled to 260 mK with a triple-stage helium (⁴He/³He/³He) sorption refrigerator. Cold (140 K) JFET amplifiers near the bolometers amplify the signals before they are processed by room-temperature electronics. Three modes have been implemented for observations: drift scans, raster scans, and slow-raster scans plus chopping by the CSO subreflector. Rapid raster scans modulate astrophysical signals above atmospheric 1/f noise. Slow-raster scans provide high observing efficiency for small fields (less than approximately a square degree). Custom software has been developed to reduce and analyze the data, and to simulate observations to quantify uncertainties and systematic effects.

THE SHARC II AND HAWC 12X32 POP-UP BOLOMETER ARRAYS

Dowell, C. Darren¹, Allen, C. A.², Babu, S.²
, Chuss, D. T.², Dotson, J. L.³, Harper, D. A.⁴
, Jhabvala, M. D.², Moseley, Jr., S. H.², Silverberg, R.²
, Voellmer, G.², Wollack, E. J.²

¹Jet Propulsion Laboratory, 4800 Oak Grove Dr., Mail Stop 169-506, Pasadena, CA 91109

²NASA-Goddard Space Flight Center, Greenbelt, MD 20771

³NASA-Ames Research Center, MS 245-6, Moffet Field, CA 94035

⁴Yerkes Observatory, University of Chicago, Williams Bay, WI 53191

We describe the two 12×32 ‘pop-up’ filled bolometer arrays built at NASA/Goddard. The first array was completed in 2002 and is in service in the SHARC II 350 μm / 450 μm camera at the Caltech Submillimeter Observatory (CSO). The second array will be used in HAWC, the 50–200 μm facility camera for SOFIA. The bolometers are micromachined 1 μm silicon membrane with ion-implanted thermistors and have continuous bismuth (SHARC II) or gold (HAWC) absorbing films. The four thermally-isolating legs of the bolometers are 16 μm wide \times 420 μm long and are shaped to allow their folding behind the plane of the bolometers. In the case of SHARC II, the bolometers are located in front of a reflective backshort to give resonant absorption approaching unity at $\sim 400\mu\text{m}$. The HAWC bolometers are placed in front of an absorptive stop to provide frequency-independent $\sim 50\%$ absorption. The cold readout circuitry consists of custom chromium silicide load resistors and commercial silicon JFETs. All components are located in a single 4 K housing with thermal isolation of the bolometers and JFETs. Wiring is accomplished with micromachined wires for thermal isolation and rigid circuit boards. With the readout electronics powered up, the bolometer stage experiences a load of only 4 μW from the 4 K stage. The 120 K JFETs dissipate 83 mW into the 4 K stage, a load which is managed with copper straps and bus bars. The SHARC II array has a quantum efficiency in excess of 75% and background-limited performance in a post-detection band from 25 Hz to 0.05 Hz; this band is well suited for scanned observing modes at the CSO without a chopping mirror.

SQUID MULTIPLEXERS FOR LARGE BOLOMETER ARRAYS

K. D. Irwin¹, K. W. Lehnert², S. Deiker¹
, W. B. Doriese¹, G.C. Hilton¹, C.D. Reintsema¹
, J.N. Ullom¹, L.R. Vale¹

¹National Institute of Standards and Technology, Boulder, CO 80305

²JILA, National Institute of Standards and Technology, Boulder, CO 80309

Both submillimeter and CMB astronomers require a new generation of large bolometer arrays. Technologies used in presently deployed instruments cannot be scaled to the larger formats now required without the introduction of cryogenic multiplexers. These multiplexers must combine the information from many bolometers into a single output channel. For the larger arrays, it must be possible to integrate the multiplexers into the focal plane.

We are developing time-division multiplexers based on SQUID amplifiers for a variety of bolometer arrays including SAFIRE and SCUBA-2, which will have more than 10,000 pixels. In these multiplexers, a SQUID is connected to each TES detector. The bandwidth of the signal is limited by a one-pole low-pass L/R filter formed by the inductance of the SQUID loop and the resistance of the TES. The SQUIDS in a column of detectors are turned on one at a time. The signals for a column of SQUIDS are summed in one output SQUID. The off SQUIDS are left in the superconducting state, contributing no noise and no signal. One row of SQUIDS is turned on at a time with a common address signal, and one output channel is used for each column. In this way a kilopixel array can be implemented using 32 address lines (one for each row of a 32 x 32 array) and 32 output channels (one for each column). We have developed a full set of custom room-temperature electronics to address and read out the multiplexer. We will describe the performance of the multiplexer, which is sufficient to instrument the next generation of bolometer arrays.

We are also developing higher performance multiplexers based on ultra-low-power SQUID amplifiers operated at microwave frequencies. In this approach, the outputs of many SQUID amplifiers are frequency-division multiplexed in high-Q resonant circuits into a single HEMT amplifier channel. Microwave SQUID multiplexers may make it possible to read out thousands of pixels of bolometers in a single HEMT amplifier channel without loss of sensitivity. The microwave SQUID multiplexer will be useful for most detector technologies that can be read out with low-noise SQUIDS. These include transition-edge sensors, magnetic calorimeters, superconductor-insulator-superconductor tunnel junction detectors, and normal-insulator-superconductor tunnel junction detectors, all of which have been successfully demonstrated with SQUID readout.

THE SCUBA-2 CAMERA FOR THE JAMES CLERK MAXWELL TELESCOPE

William David Duncan¹, The SCUBA-2 Collaboration²

¹UK Astronomy Technology Centre, Royal Observatory, Edinburgh, Blackford Hill, Edinburgh, EH9 3HJ

²UK Astronomy Technology Centre, The Canadian SCUBA-2 Consortium, The University of Edinburgh, the National Institute of Standards and Technology, Cardiff University

SCUBA-2 is wide-field camera for the James Clerk Maxwell Telescope in Hawaii. It is designed to obtain sensitive maps of the submillimeter-emitting Universe at wavelengths of 850 and 450 microns. With a much larger field-of-view and sky-background limited sensitivity, SCUBA-2 will map large areas of sky up to 1000 times faster than the current SCUBA camera. The instrument is expected to be fully operational in 2006.

The SCUBA-2 detectors are based on superconducting transition-edge sensor bolometers cooled to 100mK. To fully instrument the field of view of the JCMT, a total of 10,000 detectors are needed with a 1 mm pixel size. To achieve this pixel count, it is necessary to multiplex the bolometer signals in the focal plane. Thus, the TES bolometer array is bump bonded to an in-focal-plane superconducting quantum interference device (SQUID) multiplexer circuit.

We describe some of the science that the instrument will do and detail the current state of the development of the TES bolometers and SQUID based multiplexers and pre-amplifiers selected for the detector technology. We also describe some of the focal plane engineering challenges that have been met. We include measurements of single pixel noise-equivalent powers, as well as the noise performance and bandwidth of the in-focal-plane SQUID multiplexers. We also describe the mounting and interconnects between the array at 100 mK and the second-stage SQUID electronics at 1K. SCUBA-2 will be one of the first bolometer cameras with multiplexed arrays and to provide unparalleled amounts of astronomical data about the submm Universe.

LARGE FORMAT BOLOMETER ARRAY SYSTEMS FOR MICROWAVE OBSERVATIONS

Dobbs, M.¹, Cho, H.M.², Clarke, J.^{2,3}
, Holzapfel, W.², Lanting, T.M.², Lee, A.T.^{1,2}
, Lueker, M.², Richards, P.², Spieler, H.G.¹

¹Physics Division, Lawrence Berkeley National Lab

²Dept of Physics, University of California, Berkeley

³Materials Science, Lawrence Berkeley National Lab

The next generation of Cosmic Microwave Background (CMB) observations will require large format arrays with 100-1000's of sensors to achieve their science goals. The APEX-SZ receiver, scheduled for deployment in fall 2004, will discover and catalog thousands of galaxy clusters using the CMB signature of the Sunyaev Zel'dovich (SZ) effect. The South Pole Telescope (2006), being a dedicated survey with a factor three more sensors, will augment the catalog with an order of magnitude more galaxy clusters. The POLARBEAR experiment (2005) will provide a detailed map of the CMB polarization, including the signatures of gravitational lensing and possibly inflationary gravity waves. The performance and status of the instrumentation being developed for these receivers is described.

The general structure of the detector and readout system is as follows. An array of 300 - 1000 Transition Edge Sensor bolometers are manufactured photolithographically and arranged on 6 pie shaped wedges. The SZ survey sensors use horn-coupled Silicon Nitride spider web bolometers, while the polarization sensitive bolometers are coupled to a pair of polarization sensitive dipole slot antennae. The bolometers are voltage biased with an AC carrier from a programmable Direct Digital Synthesizer. The sky signal amplitude modulates the carrier. The AC bias renders the system insensitive to low frequency noise upstream of the bolometers. The larger arrays will employ frequency domain multiplexing, greatly reducing the complexity of the cold wiring, while reducing the heat load due to wiring between the warm and cold electronics. The bolometer signal currents are amplified with a series array SQUID ammeter operating in shunt feedback mode to provide large dynamic range with a very low input impedance. The SQUID controller electronics are housed on fully programmable multichannel boards. The signal is mixed down to base-band using custom demodulator electronics, before being sampled and digitized. System tests involving complete readout channels are currently underway.

THE MBAC CAMERA FOR ACT: 3000 BOLOMETERS, 500
SQUIDS, AND A BIG DISH IN THE DESERT

Suzanne Staggs¹, The ACT Collaboration¹

¹Princeton University

²Princeton, Penn, Rutgers, GSFC, NIST, Colorado, Columbia,
CUNY, Catolica

The Atacama Cosmology Telescope (ACT) Collaboration is building the Millimeter Bolometric Anisotropy Camera (MBAC) to make high-fidelity maps of the cosmic microwave background (CMB) at high angular resolution (2.7 arcminutes). MBAC features pop-up transition-edge sensor (TES) detectors fabricated by Goddard Space Flight Center, operating near 300 mK, and read out with time-domain muxing, using NIST mux chips.

The recent technological breakthroughs in detector development and muxing capabilities have arrived just as CMB experiments in this decade (most notably WMAP, but also Boomerang, Archeops, Maxima, DASI, and soon Planck) have provided exhaustive measurements of the CMB temperature anisotropy at large and medium scales (multipole moment less than 1000). At finer angular resolution, the primordial CMB anisotropy is small and requires high sensitivity to detect. A host of secondary effects, including lensing of the CMB by dark matter, and upscattering of photons off electrons in overdense regions, imprint the fine-scale CMB, leaving evidence of the structure and composition of the universe between here and the surface of last scattering. The Sunyaev-Zel'dovich effect of upscattering of CMB radiation as it traverses the hot gas of clusters leaves a spectral signal which may be decoded by use of measurements in multiple frequency bands. The MBAC includes filled arrays of 1024 TES detectors at each of three such bands, providing excellent sensitivity and the requisite spectral discrimination.

The ACT MBAC arrays will be described and progress noted. Some mention of the design considerations for the experiment will be given; the need to control systematic errors dominates the optical and thermal design, the scan strategy, and the site selection.

LARGE FORMAT POLARIZATION SENSITIVE BOLOMETER ARRAYS FOR THE CMB

Brian G. Keating¹²¹University of California, San Diego, 9500 Gilman Dr., La Jolla, CA 92093-0424²Caltech, 1200 E. California Blvd - Mail Stop 59-33, Pasadena, CA 91125

Recent progress in polarization sensitive bolometric focal plane architecture and sensitivity has been astounding. Bolometers currently offer sensitivities near theoretical limits over a decade in frequency coverage, with rapid detector response times. These detectors are being deployed in ever larger numbers on ground, balloon, and spaced-based platforms. Future missions require not only raw sensitivity on a pixel-by-pixel basis, but also the capability to combine large numbers of detectors with minimal efficiency degradation. As a contemporary example of a large format bolometric array polarimeter, we describe the design and performance of BICEP (Background Imaging of Cosmic Extragalactic Polarization) which will observe the polarization of the cosmic microwave background from the United States South Pole Station, Antarctica. BICEP will measure polarized signals over a $\simeq 15$ degree field of view with better than 1 degree resolution using an array of 96 polarization sensitive bolometers operating in two frequency bands : 80-110 GHz and 125-165 GHz. BICEP is optimized to detect the faint signature imprinted by a stochastic background of primordial gravitational waves – which is a generic prediction of inflationary cosmologies. NASA has recognized the richness of CMB polarization cosmology and has allocated an Einstein Probe mission opportunity – the “Inflation Probe – CMBPOL”. To accomplish its goals, CMBPOL requires ~ 30 times the polarization sensitivity of Planck and ~ 300 times that of WMAP. The mission requirements for CMBPOL are quite daunting and will most certainly require an array of thousands of background limited detectors operating from ~ 50 to 500 GHz. We discuss the implications of CMBPOL for both short and long-term bolometric focal plane architectures.

Session J3, 9:00-Wednesday

**EXPERIMENTAL CHALLENGES
FOR CMB POLARIZATION
MEASUREMENTS**

Chairperson: Stephan Meyer

CMB POLARIMETRY BY DESIGN: THE IDEAL AND THE REAL IN THE CAPMAP EXPERIMENT

Suzanne Staggs¹, The CAPMAP Collaboration

¹Princeton University

²Chicago, JPL, Miami, Princeton

Inflation, reionization, and dark-matter-driven oscillations of the primordial plasma polarize the cosmic microwave background (CMB) radiation slightly. Initial detections of small polarization anisotropies in the CMB agree with theoretical predictions. Just as the recent fabulous published results from the WMAP satellite on the anisotropy of the intensity of the CMB bring great insights into the latter two processes, further study of (and search for) the patterns of polarization anisotropy offers its own bounty. However, polarization experiments grapple with distinct systematic effects from those confronted and conquered by temperature anisotropy measurements in the last decade. Typical polarization anisotropies (measured in microKelvin) are more than ten times smaller than temperature anisotropies at similar scales, and the B-modes which might be imprinted by gravity waves are at least an order of magnitude smaller still.

The high-resolution CAPMAP experiment was designed to mitigate risk from systematic errors as much as possible. We confront the design goals with reality, and detail how data from the first season of data from the 4-element prototype lead to certain design improvements for the second season. CAPMAP comprises a 16-element correlation polarimeter array operating at 40-90 GHz, the sweet spot in the foreground spectrum. One dozen of the receivers have bandwidths 84-100 GHz, while the final four have bandwidths 35-46 GHz. These disproportionate numbers allow for equal sensitivity in each frequency band and thus substantial discrimination against foregrounds. The polarimeter array illuminates a 7m off-axis Cassegrain antenna in Holmdel, NJ (owned by Lucent Technologies.) The CAPMAP instrument will be described in detail, with discussion of the data collected from the first season of the 4-element prototype and preliminary results from the ongoing campaign of the full-up system. Future directions for large arrays of correlation polarimeters will also be indicated.

CMB POLARIZATION : LOOKING FORWARD FROM BOOMERANG

John Ruhl

Case Western Reserve University

CMB polarization measurements promise to be challenging in both the sensitivity and systematic arenas. In January 2003, we flew the Boomerang instrument on a stratospheric balloon around Antarctica to measure polarization in the CMB. Boomerang is a polarization-sensitive bolometric array receiver coupled to a 1.3m telescope. The focal plane uses two detector technologies. Four single mode corrugated feed structures are coupled to 150GHz polarization sensitive bolometer pairs developed at Caltech and JPL. An additional four single mode corrugated feed structures are coupled to an overmoded lightpipe, where a dichroic beam splitter is used to direct radiation to two detectors, one at 240GHz, the other at 340GHz. In this two-color photometer, the polarization selectivity is done with a polarization placed at the front of the input corrugated feed horn. Analysis of the Boomerang data is currently underway. In this talk I will describe the Boomerang instrument in some detail, explain our approach to measuring CMB polarization, and described lessons learned both from our efforts to characterize the instrument prior to flight, and those learned so far from analyzing the flight data.

Future measurements of CMB polarization will require more powerful multi-color focal plane arrays. I will discuss one possible approach to this technology challenge, the Polarization and Frequency Selective Bolometer (PFSB). This approach, currently in the early stages of development, will enable wide bandwidth multi-frequency coverage at each position in the focal plane. It can also be configured to reduce the number of detectors in a focal plane while retaining total focalplane sensitivity, at the expense of angular resolution.

POLARIZATION MEASUREMENTS WITH WMAP

Lyman Page

Princeton University, Dept. of Physics

The Wilkinson Microwave Anisotropy Probe (WMAP) has mapped the entire sky in five frequency bands between 22 and 94 GHz with polarization sensitive radiometers. Twenty radiometers are distributed among the bands yielding roughly comparable sensitivity per band. Each of the radiometers is a type of correlation receiver based on NRAO HEMT amplifiers. The radiometers are fed by corrugated horns illuminated by back-to-back offset shaped Gregorian telescopes with optical axes separated by approximately 140 degrees. Each horn supports two orthogonal polarizations. As a result, in one radiometer WMAP measures the power difference between linearly polarized modes from different directions. Each pair of horns measures two polarization differences using two independent radiometers. The polarization signal is derived from the difference in the outputs of the two radiometers associated with each pair of feeds.

WMAP observes from the second Earth-Sun Lagrange point (L2). The full sky coverage is achieved with a compound spin and precession in addition to the annual rotation of L2 around the Sun. In effect, every pixel is observed with multiple spacecraft orientations, allowing us to produce separate Stokes I, Q, and U maps.

We use WMAP as an example of a method for measuring the polarization of the cosmic microwave background. Though the most recent WAMP results will be reviewed, the emphasis of the talk will be on the general lessons we have learned about making polarization measurements. In particular, we discuss the control and identification of systematic errors.

This talk will complement related talks at the conference by Gary Hinshaw and Al Kogut.

QUAD: A SOUTH-POLE CMB POLARIZATION EXPERIMENT

Sarah Church

Stanford University, 382, Via Pueblo Mall, Stanford, CA 94305-4060

QUEST at DASI (QUaD) is a ground-based high-sensitivity, high-resolution ($l_{max} \sim 2500$) Cosmic Microwave Background (CMB) polarization experiment designed to measure the power spectra from E -modes due to density fluctuations in the early universe, B -modes from gravitational lensing of the CMB, and B -modes from primordial gravitational waves. The experiment comprises a 2.6m Cassegrain optical system, equipped with an array of 62 polarization-sensitive bolometers (PSBs), that will be located at the South Pole. QUEST on DASI will observe at 100 and 150 GHz and will commence operation in early 2005. The instrument is designed to minimize systematic effects; design features include an on-axis telescope to minimize instrumental polarization, careful design of the optics and feedhorns to minimize the effects of spillover and sidelobes, differencing of pairs of orthogonal PSBs within a single feed in software, an achromatic sapphire waveplate that will be used to rotate the plane of polarization of the sky with respect to each PSB, and axisymmetric rotatable optics. In addition the South Pole location will allow both repeatable and highly-controlled observations.

Polarization measurements require not only a significant increases in raw sensitivity over temperature measurements, but also comparable improvements in the control of systematic errors. I will describe the design of QUaD, with particular attention to steps that have been taken to minimize systematic effects, especially from instrumental polarization, and from the atmosphere. QUaD is designed not only to minimize expected systematics, but also to allow them to be thoroughly characterized to allow their impact to be assessed and removed. I will also briefly mention the expected science from this experiment.

BOLOMETER-BASED TECHNIQUES FOR MEASURING
CMB POLARIZATION

Lee, A.T.^{1,2}, Dobbs, M², Engargiola, G³
, Holzapfel, W¹, Kermish, Z¹, Lanting, T¹
, Myers, M¹, O'brient, R¹, Richards, P.L.¹
, Spieler, H.¹, Tran, H^{1,4}

¹Dept. of Physics, U.C. Berkeley

²Lawrence Berkeley National Laboratory

³Dept. of Astronomy, U.C. Berkeley

⁴Miller Fellow, Miller Institute

CMB polarization measurements promise to probe the inflationary era, measure large scale structure via lensing of the CMB, and to improve measurements of cosmological parameters. There are many challenges to fully characterize the polarization of the CMB, however. The signals are extremely faint and they have to be measured in face of large interfering signals including the CMB itself. Therefore, the design of the experiments simultaneously require high sensitivity and high rejection of systematic errors.

First, the optical system of a CMB polarization experiment has to be designed to give low spurious polarization. Two effects that must be minimized are instrumental polarization (turns intensity to polarization), cross-polarization (rotates polarization), and depolarization (turns polarization into intensity). We will discuss an example of a system with low-spurious effects.

Second, the detector system including the coupling optics must separate polarizations cleanly and be free of cross polarization. We will discuss the development of antenna-coupled bolometer systems that will give large arrays of detectors with good optical properties.

Finally, we will discuss polarization modulation techniques, such as the use of a rotating half-wave, and sky scanning strategies. We will discuss the POLARBEAR experiment, which is in the planning stages, as an example of the implementation of these ideas. POLARBEAR will be based on a 2m diameter off-axis telescope and a bolometer array receiver. The bolometers will use superconducting transition-edge sensors (TES) and SQUID readouts. A rotating half-wave plate will be used between the telescope and the bolometer array. The receiver will use a mechanical pulse-tube cooler, which eliminates the need for liquid cryogens.

SUPERCONDUCTING FOCAL PLANE TECHNOLOGY DEVELOPMENT

Zmuidzinas, J.¹, Bock, J.², Day, P.K.²
, Goldin, A.², Hunt, C.¹, Lange, A.¹
, LeDuc, H.G.², Mazin, B.A.¹, Vayonakis, A.¹, Yun, M.²

¹California Institute of Technology, Division of Physics, Mathematics, and Astronomy, Pasadena, CA 91125

²Jet Propulsion Laboratory, 4800 Oak Grove Drive, Pasadena, CA 91109

Future CMB polarization experiments will require order of magnitude increases in focal plane array size, to roughly 10^3 pixels, in order to achieve the sensitivity goals. However, a simple scaling of existing CMB array technology appears to be prohibitive in terms of the size, mass, wiring, and cost of the resulting array. One promising solution is the use of superconducting thin-film technology to produce a highly integrated monolithic detector array. In many cases, concepts and designs previously developed for superconducting tunnel junction (SIS) mixers may be adapted for this use. The superconducting components under development for CMB detection include: high-directivity phased-array planar antennas to replace the corrugated feed-horns; low-loss microstrip transmission lines for transporting mm-wave signals across the chip, from the antenna to the detector; on-chip high-performance lumped-element superconducting filters for defining multiple spectral channels; microstrip-coupled superconducting detectors; and perhaps even on-chip polarization modulators. Several types of microstrip-coupled detectors may be used, including TES bolometers as well as kinetic inductance devices. These components are now under development at Caltech/JPL. The design considerations as well as the test methods and results achieved with prototype devices will be described. Several of the prototype devices incorporate tunnel junction detectors to allow simple measurements at helium (4 K) temperatures. The results to date include measurements of the millimeter-wave properties of superconducting microstrip lines, including their characteristic impedance, phase velocity, and loss; beam pattern measurements of the new phased-array antennas; demonstration and characterization of a microstrip-coupled TES bolometer using a twin-slot antenna; and the demonstration of a novel kinetic inductance detector with a multiplexable microwave readout.

CALIBRATION OF BOLOMETRIC CMB POLARIMETERS

Lange, A.E.

Caltech, Pasadena, California

Bolometric detectors can provide both the broad frequency coverage and the high sensitivity necessary for an orbital mission dedicated to polarimetry of the Cosmic Microwave Background (CMB). The goal of such a mission will be to accurately measure the spatial distribution of polarization to an extremely low level of fractional polarization and over a wide range of angular scales. The calibration of any instrument designed to achieve this goal will be a challenge.

There is little experience to date in the use of bolometric polarimeters at millimeter wavelengths. Polarization-sensitive bolometers (PSBs) made of crossed, free-standing absorbers embedded in circular waveguide have been used in balloon-borne experiments (BOOMERanG) and are planned to be used in the near future in ground-based experiments (BICEP and QUEST) and, ultimately, on the High Frequency Instrument (HFI) on Planck. These detector systems provide high rejection of many common-mode signals that would otherwise confound attempts to measure small fractional polarization. The challenges to proper calibration of these detector systems differ significantly from those of HEMT-based systems, and the calibration strategies and system requirements are correspondingly different.

Antenna-coupled bolometric systems are currently envisioned for a post-Planck mission. The calibration of these systems will be similar in many respects to that of the PSB-based systems now in use. Experience gained over the next 2 to 3 years in calibration of ground-based and balloon-borne experiments will be crucial to understanding the proper design of a post-Planck orbital mission dedicated to CMB polarimetry.

EXPERIMENTAL ISSUES FOR THE EINSTEIN INFLATION PROBE

Gary Hinshaw

Code 685, NASA Goddard Space Flight Center, Greenbelt, MD
20771

NASA Headquarters' Office of Space Science has put out a call for mission concept studies for a planned "Einstein Inflation Probe". The goal of this mission would be to search for primordial gravity waves generated during a period of inflationary expansion in the early universe. Gravity waves from inflation produce a faint but characteristic pattern in the polarization of the cosmic microwave background (CMB) radiation. Thus a sensitive CMB polarization experiment might be the only way to probe physics at the grand-unified theory (GUT) scale, exceeding by 12 orders of magnitude the energies studied at the Large Hadron Collider. A detection of gravity waves would represent a remarkable confirmation of the inflationary paradigm and set the energy scale at which inflation occurred when the universe was a fraction of a second old. Even a strong upper limit to the gravity wave amplitude would be significant, ruling out many common models of inflation, and pointing to inflation occurring at much lower energy, the supersymmetry or electroweak-symmetry breaking scales, if at all.

In this talk I will present an overview of the scientific case for the Einstein Inflation Probe and highlight some of the experimental challenges the mission poses. Some of the open experimental questions that need to be addressed are 1) The degree to which astrophysical foregrounds, including polarized Galactic emission and gravitational lensing, will compromise the detection of gravity waves. 2) The degree to which systematic errors can and must be controlled and verified to reach the required measurement accuracy. 3) The choice of detector, polarimeter, and other experimental technologies required to meet sensitivity, systematic error and calibration budgets.

Session J4, 13:40-Wednesday

**RADIO ASTRONOMY BEYOND
THE EPOCH OF REIONIZATION**

Chairperson: Chris Carilli

REIONIZATION OF THE UNIVERSE

Nick Gnedin

University of Colorado

Cosmological reionization, the process of ionization of the bulk of cosmic gas by ultra-violet radiation from primeval galaxies, is by far the most dramatic event that occurred in the recent history of the universe. I will overview recent observational and theoretical progress in our understanding of a general process of reionization, its stages, sources of ionizing radiation, and time-scales. I will present the latest numerical simulations of reionization and will highlight their limitations and successes. I will then describe the theoretical progress that will be achieved in the nearest future as next generation numerical tools are being developed. I will emphasize the role and importance of the observational data from the recent discoveries of high redshift quasars by the Sloan Digital Sky Survey, and the measurement of large optical depth for Thompson scattering in the polarization component of the Cosmic Microwave Background by the Wilkinson Microwave Anisotropy Probe satellite.

I will also discuss the observational opportunities for studying reionization that are going to open to us with the development of the next generation radio telescopes, LOFAR and later SKA, in this and the next decade. I will describe studies of the redshifted 21 cm emission and absorption from neutral hydrogen, currently considered to be the main observational approach to mapping the distribution of neutral and ionized gas in the early universe. I will mention possible observational strategies that can be attempted with LOFAR and SKA within the next decade, the role of galactic and extra-galactic foregrounds, and approaches for substructuring them.

WMAP DETECTION OF EARLY REIONIZATION

Alan Kogut
NASA's GSFC

The Wilkinson Microwave Anisotropy Probe (WMAP) has mapped the full sky in Stokes I, Q, and U parameters at frequencies 23, 33, 41, 61, and 94 GHz. We detect correlations between the temperature and polarization maps significant at more than 10 standard deviations. The correlations are inconsistent with instrument noise and are significantly larger than the upper limits established for potential systematic errors. The correlations are present in all WMAP frequency bands with similar amplitude from 23 to 94 GHz, and are consistent with a superposition of a CMB signal with a weak foreground. The fitted CMB component is robust against different data combinations and fitting techniques. On small angular scales the WMAP data show the temperature-polarization correlation expected from adiabatic density perturbations. The data for $\ell > 20$ agree well with the signal predicted solely from the temperature power spectra, with no additional free parameters. The existence of correlations on super-horizon scales provides significant support for inflationary cosmologies. We detect excess power on large angular scales compared to predictions based on the temperature power spectra alone. The excess power is well described by reionization at redshift $11 < z < 30$ at 95% confidence. A model-independent fit to reionization optical depth yields results consistent with the best-fit Λ CDM model, with best fit value $\tau = 0.17 \pm 0.04$ at 68% confidence, including systematic and foreground uncertainties. This value is larger than expected given the detection of a Gunn-Peterson trough in the absorption spectra of distant quasars, and implies that the universe has a complex ionization history. I will discuss the WMAP data and its implications for reionization in the early universe.

PROBING THE REIONIZATION HISTORY OF THE UNIVERSE

Haiman, Z.
Columbia University

The recent discovery of a high optical depth τ to Thomson scattering from the Wilkinson Microwave Anisotropy Probe (*WMAP*) data implies that significant reionization took place at redshifts $z > 6$. This discovery has important implications for the sources of reionization, and allows, for the first time, constraints to be placed on physical reionization scenarios out to redshift $z \sim 20$. Using a new suite of semi-analytic reionization models, we show that the high value of τ requires a surprisingly high efficiency ϵ of the first generation of UV sources for injecting ionizing photons into the intergalactic medium. We find that no simple reionization model can be consistent with the combination of the *WMAP* result with data from the $z \sim 6$ universe. Satisfying both constraints requires either of the following: (i) H_2 molecules form efficiently at $z \sim 20$, survive feedback processes, and allow UV sources in halos with virial temperatures $T_{\text{vir}} < 10^4\text{K}$ to contribute substantially to reionization, or (ii) the efficiency ϵ in halos with $T_{\text{vir}} > 10^4\text{K}$ decreased by a factor of 30 between $z \sim 20$ and $z \sim 6$. We discuss the relevant physical issues to produce either scenario, and argue that both options are puzzling from a theoretical point of view, although they are allowed by current data. In detailed models of the reionization history, we find that the evolution of the ionized fractions in the two scenarios have distinctive features that Planck can distinguish at 3σ significance. At the high *WMAP* value for τ , Planck will also be able to provide tight statistical constraints on reionization model parameters, and elucidate much of the physics at the end of the Dark Ages. The sources responsible for the high optical depth discovered by *WMAP* should be directly detectable out to $z \sim 15$ by the *James Webb Space Telescope*.

COSMOLOGICAL REIONIZATION

Renyue Cen
Princeton University

Cosmological reionization process is likely to be very complex. Cosmological and perhaps equally importantly astrophysical processes related to galaxy formation come to play. Therefore, probing the reionization process is potentially extremely rewarding scientifically in terms of understanding cosmology and galaxy at high redshift. In fact, recent Wilkinson Microwave Anisotropy Probe (WMAP) has already produced very exciting results, indicating that the universe was reionized at an epoch much earlier than indicated by the quasar absorption spectrum observations by the Sloan Digital Sky Survey (SDSS). However, the SDSS observations appear to firmly point to a picture where the universe experienced a dramatic change in its ionization state at $z \approx 6$, mostly likely being a transition from a significantly neutral state to a highly ionized state of the intergalactic medium in a very brief period of time, normally termed the completion of the reionization (i.e., the relatively short overlapping period of HII regions). This suggests that the universe may have experienced more than one reionization, as recently suggested (Cen 2003). The actual evolution of the intergalactic medium from $z \approx 30$ to $z \approx 6$ may be even more complex than the double reionization picture. It is therefore extremely useful to find direct probes for the reionization process. While ongoing CMB experiments such as WMAP will continue to firm up the results and future CMB experiments such as PLANCK surveyor will provide more accurate results, radio observations afford a unique window to the high redshift universe. Specifically, properties of the intergalactic medium and small galaxies at high redshift are expected to show dramatic differences under different reionization histories. Therefore, direct radio observations such as through hydrogen 21 cm lines may hold a key to unlock the mystery.

21-CM LINES FROM MINIHALOS BEFORE AND DURING
COSMIC REIONIZATIONShapiro, P.R.

Dept. of Astronomy, University of Texas

In the standard Cold Dark Matter (CDM) theory of structure formation, virialized minihalos (with virial temperatures up to 10,000K) form in abundance at high redshift ($z \gtrsim 6$) during the cosmic "dark ages." The hydrogen in these minihalos, the first nonlinear baryonic structure to form in the universe, was mostly neutral and sufficiently hot and dense to emit significantly at the 21-cm line. We have calculated the emission from individual minihalos and the radiation background contributed by their combined effect. Minihalos create a "21-cm forest" of emission lines. We predict that the angular fluctuations in this 21-cm background may be detectable with the planned LOFAR and SKA radio arrays, thus providing a direct probe of structure formation during the "dark ages." Such a detection will serve to confirm the basic CDM paradigm while constraining the background cosmology parameters, the shape of the power spectrum of primordial density fluctuations, the onset and duration of the reionization epoch, and the conditions which led to the first stars and quasars. The minihalos which emit this 21-cm background will also cause a "21-cm forest" of absorption lines, as well, in the spectrum of radio continuum sources at high redshift, if the latter came into existence before the end of the reionization epoch. Reionization exerted a strong feedback effect on the minihalos, when the ionization fronts which photoionized the intergalactic medium encountered individual minihalos, which trapped the I-fronts and were photoevaporated by them. We have studied this process in detail, including the first gasdynamical simulations of minihalo photoevaporation which include radiative transfer. Recent observations by WMAP of polarization of the cosmic microwave background which fluctuates on large angular scales imply that reionization was already well underway by redshift $z = 15$, while observations of the Gunn-Peterson effect and the Lyman alpha forest at lower redshift imply that reionization did not end until about $z = 6$. We will discuss the implications of these observations for the predictions of minihalo 21-cm lines and the role and fate of minihalos during reionization.

FOREGROUNDS FOR 21CM OBSERVATIONS OF NEUTRAL GAS AT HIGH REDSHIFT

S. Peng Oh¹, Katherine Mack²¹Dept. of Physics, UC Santa Barbara²Theoretical Astrophysics, Caltech

We investigate a number of potential foregrounds for an ambitious goal of future radio telescopes such as the Square Kilometer Array (SKA) and Low Frequency Array (LOFAR): spatial tomography of neutral gas at high redshift in 21cm emission. While the expected temperature fluctuations due to unresolved radio point sources is highly uncertain, we point out that free-free emission from the ionizing halos that reionized the universe should define a minimal bound. This emission is likely to swamp the expected brightness temperature fluctuations, making proposed detections of the angular patchwork of 21cm emission across the sky unlikely to be viable. H α observations with JWST could place an upper bound on the contribution of high-redshift sources to the free-free background. An alternative approach is to discern the topology of reionization from spectral features due to 21cm emission along a pencil-beam slice. This requires tight control of the frequency-dependence of the beam in order to prevent foreground sources from contributing excessive variance. We also investigate potential contamination by galactic and extragalactic radio recombination lines (RRLs). These are unlikely to be show-stoppers, although little is known about the distribution of RRLs away from the Galactic plane. The mini-halo emission signal is always less than that of the IGM, making mini-halos unlikely to be detectable. If they are seen, it will be only in the very earliest stages of structure formation at high redshift, when the spin temperature of the IGM has not yet decoupled from the CMB. We also discuss the effects of early reionization (as suggested by WMAP observations) on proposed 21cm observations. Early reionization produces an entropy floor which suppresses small-scale structure such as mini-halos, but also results in a warm, partially neutral IGM which is ideal for 21cm observations.

THE 21 CM FOREST AND REIONIZATION

Steven Furlanetto
California Institute of Technology

Recent observations of the cosmic microwave background and high-redshift quasars suggest a significantly more complicated reionization history than had previously been supposed. It now appears that an early ionized phase may have stalled or even recombined before a second generation of sources could fully reionize the universe. We describe one potential method to distinguish the different reionization scenarios that have been proposed: measuring the amount of small scale structure in the intergalactic medium (IGM) through the "21 cm forest." When the line of sight to a high redshift radio source intersects "minihalos" (i.e., gas clumps too cool to form stars) or proto-filaments in the IGM, the neutral hydrogen in these objects creates weak absorption features that are potentially observable by the next generation of radio telescopes. "Standard" structure formation models predict that a substantial fraction of baryons are locked up in these objects, but the heat and entropy injected by an early ionization episode suppresses small scale structure and eliminates the absorption signal. The abundance of absorbers in a patch of the IGM therefore constrains the ionization history of that patch. In addition, the mean-density IGM provides a small optical depth that depends on both its current temperature and the radiation background; the mean level of absorption therefore provides a measure of the instantaneous state of the IGM. We describe the characteristics of the expected absorption signatures, including their number density, optical depth, and equivalent width, and how these quantities depend on the radiation background and IGM properties. We conclude by discussing their observability with instruments such as the Low Frequency Array and the Square Kilometer Array.

LOW FREQUENCY RADIO TELESCOPES

Neb Duric

University of New Mexico

The region of the electromagnetic spectrum below 250 MHz remains largely unexplored despite the fact that low frequency radio astronomy was born at these frequencies. Using the Very Large Array (VLA) as a benchmark, meaningful exploration of this region of the spectrum requires angular resolution of order 1 second of arc and sensitivity approaching 1 mJy/beam for integrations of a few minutes in duration. The technical challenge associated with detecting and processing signals that have passed through the ionosphere and have been polluted by radio frequency interference has kept this branch of radio astronomy instrumentation from developing to the level of a VLA-type instrument.

The Low-Frequency Array (LOFAR) is an instrument that is being designed to perform at sensitivities and resolution comparable to the VLA. I describe the planned operating characteristics of LOFAR and the proposed solutions for correcting ionospheric-based phase errors and excising radio frequency interference that will allow for imaging performance rivaling that of the VLA.

A major science driver for LOFAR is the potential ability to detect radiation from the Epoch of Re-Ionization. Other science topics that LOFAR will address include The Origin of Cosmic Rays, Space Weather, The Search for Extrasolar Planets and Probing Fundamental Constants. The ability of LOFAR to maximally impact these science topics, will depend on the layout of the instrument, the manner in which the instrument is scheduled and used and the degree to which it can be made virtual (digitized and buffered for time-reversed observations). I will discuss the various schemes that have been proposed to allow LOFAR to overcome the technical challenges of processing data at low frequencies and achieving the broadest possible science productivity.

MOLECULAR GAS AT THE END OF COSMIC REIONIZATION

Walter, F.

NRAO, P.O. Box 0, Socorro, NM 87801

The highest redshift quasar currently known so far (J1148+5251 at a redshift of $z=6.4$) is only one of the few sources which show a complete Gunn Peterson trough in optical spectra, indicative of a significantly neutral ($>1\%$) universe at these look-back times. Likewise, recent WMAP measurements suggest that the Epoch of Reionization had a fairly complex history, extending from $z \sim 6$ to 15. Our recent detection of carbon monoxide (CO) emission in the quasar J1148+5251 using the Very Large Array and the Plateau de Bure Interferometer shows that massive reservoirs of molecular gas, the fuel for star formation, are already present in systems ~ 850 Myr after the Big Bang (i.e. when the universe was only $1/16$ of its current age). The detection of CO also implies a relatively enriched cold interstellar medium and puts constraints on the metal production of the earliest population of stars in the universe. Observations of molecular gas in objects located in the Epoch of Reionization also give the best estimate for the redshift of the host galaxy which is difficult to determine from optical spectra. A careful inspection of optical and radio spectra enable us to derive the extent of the ionizing sphere around the quasars which contribute to the reionization of the universe (cosmological Stromgren spheres). Future instruments such as ALMA will be instrumental in resolving the molecular gas disks of quasar host galaxies in the Epoch of Reionization. Such studies will help to constrain the dynamical masses of some of the first luminous structures in the universe.

SUBMILLIMETER GALAXIES

Glenn, J.
University of Colorado

A cosmic far-infrared background radiation, with integrated flux approximately equal to the integrated optical and ultraviolet extragalactic starlight, was discovered by COBE. This radiation arises from interstellar dust heated by star formation and active galactic nuclei. It has been partially resolved into galaxies by deep surveys with the SCUBA camera on the James Clerk Maxwell Telescope at $\lambda = 850\mu\text{m}$, and the MAMBO camera on the IRAM 30-meter telescope at $\lambda = 1.3\text{ mm}$. Several hundred sources have been detected with characteristic brightnesses of several mJy. The sources appear to have a mean redshift of approximately 2.5, luminosities in excess of 10^{12} solar luminosities, and star formation rates of 100 to 1000 solar masses per year. Because of these very large star formation rates, it has been proposed that these submillimeter sources are elliptical galaxies or spiral galaxy bulges in formation.

Two new instruments have come on line at the Caltech Submillimeter Observatory, Bolocam and SHARC II, that will enable surveys for extremely rare, bright sources, and submillimeter photometry of the galaxies. Bolocam is a feedhorn-coupled, millimeter-wave bolometer camera with a large field-of-view (8 arcminutes) and SHARC II is a submillimeter camera with a fully-sampled focal plane array of bolometers.

Because they are so dusty and the submillimeter beams are large, it has been very difficult to identify optical counterparts of these galaxies to measure their properties and correlate them with known populations of galaxies. Photometric techniques have been used to estimate redshifts, however, recent progress has been made in determining redshifts spectroscopically. Galaxies are first detected by their radio emission then their submillimeter brightnesses are measured. The interferometric radio astrometry enables optical spectroscopy. In addition, a new generation of spectrometers is under construction that will enable redshifts to be measured directly from rotation CO lines.

Session J5, 9:00-Thursday

**ADVANCES IN LARGE FOCAL
PLANE ARRAYS II: COHERENT
DETECTORS**

Chairperson: Todd Gaier

COHERENT FOCAL PLANE ARRAYS FOR THE BEAST TELESCOPES AT WHITE MOUNTAIN.

Williams, B., Meinhold, P., Lubin, P. M
, Levy, A., Stebor, N., Childers, J., O'Neill, H., Marvil, J.

Physics Department, University of California, Santa Barbara

HEMT focal plane arrays offer significant advantages for ground based experiments and below 100 GHz are the most sensitive detectors to date when operated within the earth's atmosphere. We will show some comparisons between HEMT based and bolometer based detectors when used for similar systems.

The Background Emission Anisotropy Scanning Telescope (BEAST) is a large low background telescope designed for Cosmic Microwave Background (CMB) measurements. The telescope is optimized for large focal plane arrays and minimum cross polar contamination. The first focal plane instrument for the telescope was a mixed Ka and Q band HEMT array. To date, the system has flown on two suborbital balloon flights and operated for an extended period of time at the UC WMRS high altitude (13000') site on White Mountain in the Eastern Sierra. We will discuss and present data from these observations. We are currently fielding a second set of the optics with a Q and W band polarization sensitive array to the same site. We will describe the radiometer and results obtained as of the conference.

Our future plans call for a much larger HEMT array in Q and eventually Wband (more than 50 elements), to be fielded on the BEAST optics at WMRS or possibly South Pole. In addition to the array we will describe a novel polarization modulator appropriate for large arrays. The modulator is optically coupled (free space), low loss, and can be used over a very wide range of frequencies. We will briefly describe this concept and present some test data. The modulator concept could enhance many planned polarization instrument designs.

A 32 ELEMENT FOCAL PLANE ARRAY FOR 85-115 GHZ USING MMIC PREAMPLIFIERS

Neal Erickson¹, Ronald Grosslein¹, Sander Weinreb²,
Ronna Erickson¹, John Wielgus¹, Vern Fath¹, Karen Werner¹

¹University of Massachusetts, Amherst, MA

²Jet Propulsion Lab, Pasadena, CA

A 32 pixel focal plane array has been built for radio astronomy use in the 85-115 GHz range. The array uses cryogenic InP MMIC preamplifiers, and has an overall receiver noise temperature of 40-80K. With an IF bandwidth of 15 GHz, the entire signal band may be covered with single sideband response using just two fixed LO's. The array consists of two nearly identical 16 element sub-arrays in opposite polarizations, combined with a polarizing grid.

The input amplifiers are the best wideband MMIC low-noise devices made to date and were fabricated using InP technology at TRW. At 20 K their typical noise is 35-55 K from 85-115 GHz. These chips deliver a wideband gain (cold) of 20 dB, at best low-noise bias. They are housed in a compact block with WR10 waveguide ports. A second stage amplifier has higher noise but flatter gain. The two MMIC's cascaded produce 40 dB gain.

Two isolators are needed in the system, one on the input and the other between the two MMIC stages to ensure stability. A very compact isolator has been developed for this application with an insertion loss of 0.4-0.6 dB. The isolators have a well-shielded magnetic field to permit close packing with minimal interactions.

The input feeds are square corrugated horns, with an aperture 25 mm square. Square horns are most easily packed in an array, and with corrugated E-plane walls, they achieve symmetric low side-lobe patterns. The aperture and most of the horn at room temperature. Toward the waveguide end there is a 0.2 mm gap in the wall, and the remainder of the horn is at 20 K. The gap is a very effective thermal insulator and has choke grooves in the walls to minimize signal loss. The horns require a correcting lens made from grooved teflon, which also serves as the vacuum window.

The cryogenic subharmonic mixer uses commercial beam-lead antiparallel-pair diodes, and has a conversion loss of 10-15 dB across the band with an LO power of only 8 mW. The mixer operates single sideband through the use of effective LO frequencies above and below the signal band. LO is provided at 40 and 60 GHz by four 220 mW power amplifiers driven by a multiplier chains, which are each diplexed and split 16 ways.

CAPMAP: A 16 ELEMENT ARRAY FOR MEASURING THE
POLARIZATION OF THE CMB

Hedman, Matthew¹, CAPMAP Collaboration²

¹U of Chicago

²Princeton, U. Chicago, U. Miami, JPL

The polarization of the Cosmic Microwave Background (CMB) provides important information about the dynamics of the hot, dense phase of the early universe, and if it can be measured sufficiently accurately, it can probe the growth of structure and even the primordial gravity wave content of the universe. However, this polarized signal is extremely faint (one part in 100,000) so accurate measurements are a significant experimental challenge, requiring specialized instruments.

This presentation will describe the CAPMAP experiment, which is an effort to measure the polarization of the CMB using correlation polarimeters and a 7-meter off axis telescope. During early 2003, we had our first observing season with an array of 4 polarimeters. This winter we will have an array of 16 polarimeters, 12 operating in W-Band (84-100 GHz) and 4 in Q-Band (35-45 GHz).

Each polarimeter in the array is a heterodyne system with low-noise HEMT RF amplifiers and 2-18 GHz analog correlators. In order to extract the tiny polarized signal from largely unpolarized radiation, these polarimeters include phase switches which modulate the polarized signal at 4 kHz, well above the 1/f knee of the amplifiers and the atmosphere. Each polarimeter views the sky through a separate feed horn and lens system, which is located in the focal plane of the 7-meter telescope.

In order to perform optimally, the two arms of each polarimeter must be adjusted so that they have the same effective phase lengths at all frequencies. We have devised methods for measuring the phase difference between these arms in a non-invasive way, using appropriately polarized signals injected into the radiometers. Furthermore, we have developed methods for calibrating these polarimeters using metal plates to inject calculable polarized signals into the radiometers. These techniques will have useful applications for future large coherent arrays.

FOCAL PLANE ARRAYS FOR THE VLA?

Walter BriskenNational Radio Astronomy Observatory, PO Box O, Socorro, NM
87801

The NRAO Very Large Array (VLA) is currently undergoing a first set of upgrades which will allow for much greater observing bandwidths and complete tuning capabilities over the 1.2 to 50 GHz frequency range. A second set of upgrades will add new antennas and antenna pads to allow greater and lower resolutions respectively. This upgrade also includes adding UHF observing capabilities to all of the antennas, which would provide complete coverage over the 0.24 to 1.2 GHz range. Vivaldi element focal plane arrays are being investigated as a possible wide-band solution which would cover part or all of the UHF band.

Although Vivaldi arrays have been built to operate over 5:1 bandwidth ratios, arrays with smaller bandwidth ratios are more appealing for radio astronomy focal plane applications because they can be optimized for a better match over the operational band and fewer elements are required to adequately tile the focal spot. A possible plan for the VLA upgrade is to use a 2m by 2m dual-polarized array containing about 100 elements for the 0.24 to 0.44 GHz portion of the band, a scaled down version of this for the 0.44 to 0.8 GHz range, and a cooled, high performance horn feed for above 0.8 GHz.

Many aspects of the Vivaldi arrays still need to be investigated. These include array phasing over large bandwidths, cancellation of spillover, mutual coupling of the elements, manufacturability, and others. This talk will focus on the beam forming aspects of Vivaldi arrays when used in a prime-focus system. The potential for synthesizing multiple beams will be discussed.

TECHNOLOGIES FOR VERY LARGE MMIC BASED FOCAL PLANE ARRAYS

Charles Lawrence, Michael Seiffert, Todd Gaier
Jet Propulsion Laboratory

We describe a new technology which enables very large focal plane arrays using MMIC HEMT amplifier technology. The technique involves the integration of all high frequency components in a single compact hybrid package. The standard package is modified for waveguide inputs on the lid. No connectors are needed as the modules are DIP-style plug-in assemblies. The open bottom carrier lends itself to automation and thus mass production. In the focal plane array the modules are mounted on a "motherboard" for bias and signal distribution. The motherboard and all of its components operate at 20 K for optimal noise performance. Bias control circuits and readouts are located on nearby circuit boards, mechanically coupled, but thermally isolated from the motherboard, comprising a complete receiver "stack". We will describe how this technology is being developed into the 90 GHz QUIET polarimeter array for CMB observations. The array elements are each pseudocorrelation polarimeters with 15-20 GHz bandwidth. Each polarimeter is fed with the output of a left-right circularly polarized orthomode transducer. Each receiver has DC outputs carrying the Stokes Q and U parameters of the incoming signal. Bias controls are provided by a separate printed circuit board located in the stack, but at 300K. The bias controls are remotely programmable through an addressed serial bus. Readout electronics including low noise video preamplifiers and signal demodulation and data multiplexers are also located on a different board in the stack and are connected to a control and acquisition computer. via a single cable with less than 100 leads. This technology is being developed initially into a 91 element array for CMB observations, but is completely scalable to arrays as large as 1000 elements. We will also describe how this technology can be used for millimeter-wave heterodyne array receivers, particularly with narrow IF.

HETERODYNE ARRAY RECEIVERS FOR THE FAR- INFRARED

Walker, C.¹, Groppi, C.¹, Kulesa, C.¹
 , Golish, D.¹, Hedden, A.¹, Kooi, J.²
 , Lichtenberger, A.³, Chin, G.⁴, Narayanan, G.⁵
 , Weinreb, S.², Prober, D.⁶

¹University of Arizona

²California Institute of Technology

³University of Virginia

⁴Goddard Spaceflight Center

⁵University of Massachusetts

⁶Yale University

In the wavelength regime between 300 and 60 microns there are a number of atomic and molecular emission lines that are key diagnostic probes of the interstellar medium. These include transitions of [CII], [NII], [OI], HD, H₂D⁺, OH, CO, and H₂O. In Giant Molecular Clouds (GMCs), evolved star envelopes, and planetary nebulae, these emission lines can be extended over many arc minutes and possess complicated line profiles that can only be disentangled using high resolution ($R = \lambda/\Delta\lambda > 10^6$) spectroscopy. Observations of these lines are crucial to understanding the delicate interplay between the interstellar medium and the stars that form from it. The only instruments capable of realistically providing the required spectral resolution and spatial coverage for these studies are heterodyne array receivers. While the possibility of large format (≥ 10) array receivers has been discussed for more than two decades, only recently have advances in mixer and local oscillator (LO) technology, device fabrication, micromachining, digital signal processing, and telescope design made the construction of such an instrument tractable. In our talk we will discuss how recent advances in these technologies can be implemented to develop integrated, far-infrared heterodyne arrays. For frequencies ≤ 1 THz the arrays will utilize SIS devices and solid-state LO sources. Above ~ 1 THz the arrays will use HEB mixing devices and either laser LOs (for large format arrays) or solid-state LOs (for modest size arrays). Efficient, compact waveguide mixer mounts can now be fabricated well into the THz range. The new generation of MMIC amplifiers can provide both the low-noise performance and low-power consumption required by THz imaging arrays. The IF output of each array pixel can be processed by commercially available single-chip, auto-correlator spectrometers.

Large format array receivers could be deployed on a number of existing and planned observatories, with the potential of increasing their mapping speed by more than an order of magnitude. In our presentation we will present the detailed design of a 1.5 THz array for the AST/RO telescope at the South Pole.

Session J6, 13:40-Thursday

**CORRELATORS FOR RADIO
ASTRONOMY**

Chairperson: Andrew Harris

THE COBRA CORRELATOR SYSTEM

Hawkins, D. W.
Caltech-OVRO

The COBRA Correlator System is an FPGA (field programmable gate array) based correlator system used to implement both wide bandwidth continuum and narrow bandwidth spectral line correlator systems. The system consists of three major components; downconverters, digitizer boards, and correlator boards. The downconverters produce output bandwidths of 500MHz, 250MHz, 125MHz, 62.5MHz. Bandwidths lower than 62.5MHz are implemented using FIR filters in the digitizer board FPGAs. The correlator is implemented as a lag correlator, with a frequency-channel count that depends on bandwidth as; 16-channels at 500MHz, 32-channels at 250MHz, and 64-channels for lower bandwidths. The change in channel count (which is half the number of lags) is due to the parallelism required in the correlator logic at wider bandwidths.

The first application of the COBRA Correlator System hardware is the implementation of the Owens Valley Radio Observatory's (OVRO's) 10m diameter, six telescope interferometer, 4GHz bandwidth, COBRA Wideband Correlator. The 4GHz bandwidth is processed by the correlator as eight 500MHz bands. A detailed description of the correlator, and results from this system will be presented.

The COBRA hardware will also be used to implement the University of Chicago SZA and the CARMA correlator systems. Both of these arrays will be located in the Owens Valley (or on a mountain peak nearby). The SZA array consists of eight 3.5m telescopes and will have an IF bandwidth of 8GHz. CARMA will consist of the six 10m OVRO antennas plus nine 6m antennas from the BIMA array. The CARMA array will initially process 4GHz of bandwidth. This 4GHz will be processed using eight COBRA subsystems; providing for 4GHz of continuum, or a mixture of continuum and spectral line bands over the 4GHz IF. Detailed descriptions and results for the correlators for these arrays will be presented.

One significant issue in digital correlator design, whether the correlator be lag (XF), or frequency (FX) based, is the distribution of data between the digitizer and the correlation hardware. The CARMA system expects to be able to operate several sub-arrays containing a variable number of telescopes, and will eventually contain focal-plane arrays on the larger telescopes. Options for implementing a correlator system with flexible (dynamically reconfigurable) interconnects will be discussed.

THE ATA IMAGER UPDATE

Urry, W. L.

University of California - Berkeley

The Allen Telescope Array will be a unique instrument in its ability to conduct several experiments at once. It will have the ability to observe in several independent directions within the primary beam of the individual antennas. Four 100 MHz dual polarization IFs can be independently tuned to anywhere within the .5 to 11.2 GHz RF band of the front end. SETI searches, pulsar experiments and imaging can be conducted at the same time. All tuning and pointing functions including fringe stopping and delay compensation are provided by the array for all of the instruments that will use it. The ATA imager is one of those instruments. It will have two 100 MHz IF ports available to it for a total bandwidth capability of 200 MHz. A modest prototype correlator for only 4 antennas has been developed in order to test various concepts and to develop VHDL code that will be used in the 350 antenna version. It is a 100 MHz correlator in an FX architecture with 1024 frequency channels and it measures all 4 Stokes parameters. The current status of the imaging back end will be discussed.

As I presented at this conference two years ago, the ATA imager relies on an FX correlator architecture. In order to avoid the severe channel to channel sidelobes produced by using the FFT as a filterbank, a polyphase technique is used. The severe problem of distributing the signals from the polyphase filterbank to the correlator is solved by using a corner turner of unique design which converts the 350 streams of 1024 channels into 350 streams of antennas of 3 frequency channels each. Each correlator is presented with a sequential stream of all of the antennas where all 61425 baselines are computed as the data enters one antenna at a time.

There have been some changes to the architecture of the correlator since I last presented it at this conference two years ago. One innovation enables us to replace a significant amount expensive FPGA memory with less expensive off chip memory while preserving the basic idea of a pipeline correlator with low chip to chip wiring and easy expandability. This innovation requires the use of inexpensive memory as a signal buffer to reorder the frequency channel samples as they emerge from the polyphase filter bank. The large memory signal buffer also enables us to gain a great deal of flexibility in our implementation of the switched corner turner. The modifications required to a corner turner as the system is expanded will be discussed.

THE EVLA CORRELATOR

David Fort

National Research Council of Canada, Herzberg Institute of Astrophysics, Dominion Radio Astrophysical Observatory

The main features of the EVLA are its ability to handle 16 GHz of bandwidth from each antenna and continuous frequency coverage from 1 GHz to 50 GHz. To support these features enhanced receivers, a new fiber optic transmission system and a new correlator are necessary. The correlator is being designed, constructed and tested at the Dominion Radio Astrophysical Observatory in Penticton, British Columbia, Canada. An overview of the hardware architecture and features of the correlator will be presented. The system is divided into the station, baseline and phasing sub-systems. In this talk, emphasis will be given to the station sub-system. One of the main features of the correlator is the division of each of the eight 2 GHz basebands into sixteen sub-bands for hardware efficiency and flexibility. The filter chip, which is responsible for forming the sub-bands, will be examined in some detail. This chip allows input sample rates of up to 4096 Msamples/s and output sample rates down to 62.5 Ksamples/s. Also included in the chip is a programmable delay that allows the sub-bands to produce synthesized beams offset from each other, a quantizer with associated calibration measurements and a tone extractor for VLBI phase calibration. The filtering is done by a 4-stage FIR filter with up to 512 taps per stage and allows a decimation of up to 16 per stage. The first stage can deal with 4-bit or 8-bit input samples and can be arranged as a single decimate-by-16 filter or as 16 individual filters for VLBI fractional bit correction.

THE ALMA CORRELATOR

J. C. Webber, R. P. Escoffier, C.M. Broadwell
, J. Greenberg, R. Treacy

National Radio Astronomy Observatory, 520 Edgemont Road,
Charlottesville, VA 22903

The status of the correlator under construction by the NRAO for the Atacama Large Millimeter Array (ALMA) radio astronomy observatory is presented here. The NRAO, in collaboration with other North American and European scientific agencies, is developing the ALMA radio astronomy array, planned to consist of a main array of 64 12-meter diameter antennas and a compact array built by the National Astronomical Observatory of Japan of four 12-m and twelve 7-meter antennas. The instrument is to be used for observing astronomical sources at 31 to 950 GHz at a 5000 meter elevation site in the Atacama desert of Chile. The correlator under development will process the outputs of the 64 antennas that are to comprise the main array of the ALMA observatory using a bandwidth of 16 GHz per antenna. The system, designed using a conventional XF architecture, works at a clock rate of 125 MHz. Antenna-based electronics in the correlator include fiber optic receiver cards to recover digitized samples from the remote telescopes, digital FIR filters for bandwidth selection, delay lines, and signal conditioning logic to packetize the output of the high-speed digitizers in order to drive lower-speed correlator circuits. An application-specific integrated circuit (ASIC) has been designed for use in measuring the cross- and auto-correlation coefficients. Each correlator ASIC has 4096 lags, including 20 bits of integration and 16 bits of secondary storage for the results. Prototype units of this ASIC have been received and tested successfully. Prototype logic cards for both station-based and baseline-based applications in the correlator have been evaluated, including the correlator card with 64 of the 4096-lag ASICs mounted. All cards tested so far have demonstrated acceptable functional and speed characteristics. System testing of a prototype 2-antenna correlator is complete. It is planned to incorporate an enhanced digital filter card with multiple selectable output bands, increasing the spectral resolution at the wider bandwidths and permitting operation as a digital hybrid correlator. The architecture of the selected digital filter will be addressed.

A NEW VERY HIGH RESOLUTION INTERFERENCE METHOD WITH POTENTIAL FOR RADIO ASTRONOMY APPLICATIONS

Minkoff, J

ITT Aerospace Communications Division

A scheme for interference rejection at an array is presented, in which the interference, represented as vectors, is removed by an operation in which none of the physical array characteristics such as beam width and resolution come into play. As a result, observation of signals of interest from weak sources, intact, unaffected by the presence of interfering signals from stronger sources arbitrarily close in angle to the weaker sources, is possible. The essential limit on this capability is determined solely by receiver noise. Rejection of up to $M-1$ interfering sources with an array of M elements is accomplished by a single operation. The method seems especially well suited for radio-astronomy applications.

In this approach the rejection is accomplished by projecting the interference, represented as vectors, into the null-space of a matrix: a null-space transformation (NST). The interference is transformed into the zero vector. The scheme differs fundamentally from conventional beamforming/nulling schemes in that the projection operation is applied directly to the observables, the array outputs, rather than to beam steering vectors. The geometrical relationship between the signal and interference subspaces is irrelevant; the issue of subspace orthogonality does not arise. Beamforming plays no part. None of the limitations associated with physical array characteristics such as beamwidth and resolution come into play, which yields an intrinsic high-resolution interference rejection capability not present in conventional schemes employing beamforming/nulling operations. There is no fundamental limitation on the minimum angular separation between an interfering source that can be rejected and a signal of interest that can be recovered intact, undisturbed by the process. Excluding possible implemental hardware issues, which we do not consider here, the practical limit on the extent to which this property of the scheme can be realized is determined solely by receiver noise. Other desirable properties of the scheme are (2) for N interfering sources an array of only $M = N+1$ elements is necessary; $M \geq N$ is unnecessary. (3) interference rejection is accomplished by a single matrix multiplication independently of the number of interferers. (4) The interfering signals are removed selectively at each array element with signals of interest completely recoverable. As evidence of this, beam patterns after interference rejection, if desired, are identical to what they would be with no interference, and coherent summation over the array of the recovered signals yields the usual $10 \log M$ dB improvement in signal-to-noise ratio. Results of computer experiments are presented validating all aforementioned assertions.

A MULTIPURPOSE SPECTROMETER FOR SETI AND RADIO ASTRONOMY

Parsons, A., Werthimer, D.
UC Berkeley

We describe a low cost spectrometer technology for applications in SETI, FX correlators, pulsar and general radio astronomy.

Each of the new spectrometer boards processes two polarizations, each polarization with up to 150 MHz bandwidth and 64 million channels. The compact pci board utilizes four 200 MHz 8 bit ADC's for analog input, and 176 digital I/O lines for optional digital input and/or fast readout. The signal processing is implemented in a Xilinx Virtex II Field Programmable Gate Array chip, which can be dynamically programmed for various applications. A smaller additional Xilinx FPGA is used as a reconfigurable backend processor which can pass data off to an independent computer.

The spectrometer uses a polyphase filter bank (PFB) to implement a bank of steep cut-off bandpass filters, providing a significant improvement in signal-to-noise and out-of-band-rejection over the common FFT algorithm. The PFB uses a biphase pipelined architecture which allows data to be input and output at the full sample rate, and can do two polarizations simultaneously with no extra cost in hardware or data flow rate. The board will also have the ability to digitally down-convert a single side band signal to provide excellent image rejection.

Spectrometers are currently planned for use at Berkeley, Arecibo, and JPL. The SERENDIP V SETI sky survey will utilize Arecibo Observatory's upcoming seven beam L band feed array and 21 spectrometer boards for a 2.7 billion channel instrument. The JPL SETI sky survey plans to use 200 of these boards to cover 20 GHz band with 25 billion channels. The Allen Telescope Array plans to use the polyphase filter bank design in the FX correlator. We hope others will find these boards or the FPGA based spectrometer designs useful.

WIDEBAND ANALOG LAG CORRELATION SPECTROMETERS FOR RADIO ASTRONOMY

Andrew Harris¹, Stephen Maas², Stephanie Zonak¹

¹Department of Astronomy, University of Maryland, College Park, MD

²Nonlinear Technologies, Long Beach, CA

Increasing mixer and front-end amplifier bandwidths make heterodyne spectrometers with many gigahertz of instantaneous bandwidth possible. The science drivers for such instruments include millimeter-wave spectral searches for distant objects with poorly known redshifts, submillimeter and far-infrared observations of Doppler-broadened spectral lines from galaxies, and observations of pressure-broadened atmospheric lines. Modest spectral resolution is sufficient for these observations.

There are a number of reasonably mature and proven technologies for broadband microwave spectrometers suitable for astronomical spectroscopy (Harris 2003a,b provide brief reviews): acousto-optical spectrometers, digital correlation spectrometers, and analog correlation spectrometers.

Here we summarize our work on analog auto- and cross-correlation spectrometers. Analog correlators obtain their wide bandwidths by a combination of transmission line delays and direct voltage multiplication in transistor or diode mixers. WASP2 is a compact, low-power correlator with approximately 33 MHz resolution over 3.75 GHz bandwidth (Harris & Zmuidzinas 2001). Correlator bandwidth in these spectrometers is limited by the transistor multiplier circuit. We show new results from a custom MMIC Gilbert-cell multiplier circuit that provides bandwidths of more than 20 GHz.

Correlation spectrometers find use both as autocorrelators and cross-correlators. Autocorrelators are useful for single-dish radiometers; cross-correlators are essential for spatial interferometers and multi-channel/continuous-comparison radiometers.

References:

Harris, A.I. & Zmuidzinas, J., "Wideband Lag Correlator for Heterodyne Spectroscopy," *Rev. Sci. Inst.* **72**, 1531-1538 (2001); Harris, A.I., "Heterodyne Spectrometers with very Wide Bandwidths," *Proc. SPIE International Symposium on Astronomical Telescopes and Instrumentation*, ed. T.G. Phillips & J. Zmuidzinas, *Proc. SPIE* **4855**, 279-289 (2003a); Harris, A.I., "Heterodyne Spectrometers," in *Proc. Far-IR, Sub-MM & MM Detector Technology Workshop*, eds. J. Wolf J. Farhoomand, and C.R. McCreight, NASA/CP-211408, in press (2003b)

STATISTICS OF CORRELATION OF QUANTIZED NOISE
LIKE SIGNALSGwinn, C.R.

Physics Dept., UC Santa Barbara, Santa Barbara CA 93106 USA

Radio-astronomical signals are invariably noiselike, with Gaussian statistics. All astrophysical observations seek to determine the variance or covariance of that Gaussian noise, between signals with different spectral, temporal or other domains. For example, the autocorrelation function is an estimate of the covariance of the electric field from a source with some time lag; its Fourier transform is an estimate of the spectrum. Similarly, the Stokes parameters are variances and covariances among electric fields with different polarizations. Because results are usually averaged over many samples, the covariances estimated from such observations are completely characterized by a deterministic part (the mean); and a random part (the standard deviation or noise). At radio frequencies, that covariance is estimated by correlating the underlying noiselike signals. Commonly, the astrophysical signals are quantized before correlation. This quantization describes the signals using just a few levels, characterized by signal thresholds and weights at the correlator.

The underlying covariance of the signals affects the noise of the measured correlation. In combination with effects of quantization, increasing covariance can increase or decrease the noise. I present analytical expressions for the expected noise, as a function of the covariance, and of the thresholds and weights of the quantization scheme. Results match those of Cooper (1970) and others in the limit of small covariance. The results also agree with computer simulations of correlation. I find that the optimal quantization scheme depends on the expected covariance. Interestingly, correlation of quantized noiselike signals can yield higher signal-to-noise ratio than would correlation of the underlying continuous signals. I discuss these effects for auto- and cross-correlation functions, and for estimates of spectra obtained from them.

A VERY WIDEBAND ANALOG AUTOCORRELATION SPECTROMETER

Neal R. Erickson, Robert Goeller, Gopal Narayanan
University of Massachusetts, Amherst

A receiver system is being built which will cover the widest instantaneous bandwidth ever utilized by an astronomical heterodyne receiver. The entire 75-111 GHz band will be covered with a low noise frontend and a backend spectrometer having 30 MHz resolution. The receiver is intended for astronomical use in searching for the highly redshifted spectral lines from galaxies of unknown redshift. The receiver will use InP MMIC based low noise amplifiers operated at 20 K, and will operate with two dual polarization feeds.

The four receivers have a combined IF bandwidth of 144 GHz, and the entire band must be spectrally processed simultaneously. A spectrometer using analog autocorrelation (used by Harris and Zmuidzinis) is being refined to permit much wider bandwidth at significantly lower cost. The basic idea is as follows. A signal is split two ways and sent in both ends of a long tapped delay line. The taps sample a small amount of each signal, and the tapped signals are then multiplied. The set of multiplied tapped signals forms the autocorrelation function, which is then Fourier transformed to generate the spectrum.

In this new design the delay lines cover a frequency range of 0-8 GHz, a considerable increase over the 4 GHz previous bandwidth. One improvement that makes this possible is the use of tap resistors on quartz substrates with much lower parasitic capacitance than ceramic substrates. No analog multipliers are used, but instead the taps are simply summed and detected with biased silicon diodes. A square law detector is an excellent multiplier, but it also produces total power terms. If the two tap signals are A and B, the detector output is: $A^2 + B^2 + 2 AB$, and the only part that is desired is AB. The unwanted parts are readily eliminated by phase switching the signal to one delay line by 180 degrees, which causes the sign of only the AB term to change. AC processing of the signal captures only the desired part. Biased silicon diodes make excellent square law detectors, with a very wide dynamic range. After amplification, the signal is directly digitized, before any further signal processing, using a low cost 18 bit sigma-delta converter.

The delay lines themselves and the A/D converters all will be assembled into a single multilayer, double sided circuit board, with 64 lags in each sub-unit (one tapped line) and 256 lags on a complete circuit board. Each board will include an FPGA to multiplex the A/D converter outputs, and minimize the interconnection complexity. Considerable signal processing, including synchronous detection of the phase switch modulation and beam switching, and some averaging, will be done in the FPGA.

Session B/K1, 13:40-Monday

**BIOLOGICAL EFFECTS AND
MEDICAL APPLICATIONS OF
ELECTROMAGNETIC FIELDS AND
WAVES**

Chairpersons: Susan C. Hagness and Gianluca Lazzi

B/K1

COMPUTATIONAL MODELING EVIDENCE OF A NON-THERMAL ELECTROMAGNETIC INTERACTION MECHANISM WITH LIVING CELLS: MICROWAVE NONLINEARITY IN THE CELLULAR SODIUM ION CHANNEL

Stoykov, N.¹, Jerome, J.², Taffove, A.³, Pierce, L.⁴

¹Rehabilitation Institute of Chicago, Chicago, IL

²Department of Mathematics, Northwestern University, Evanston, IL

³Department of Electrical and Computer Engineering, Northwestern University, Evanston, IL

⁴Honors Program in Medical Education, Northwestern University, Evanston, IL

This paper reports the results of a detailed, one-dimensional computational study of the response of the cellular sodium ion channel to an amplitude-modulated microwave electric field excitation. We have extended and applied a hydrodynamic model that integrates a system of four coupled partial differential equations which includes the Poisson-Nernst-Planck equations as a limiting case. The simulation code for our model is adapted from that created by C.-W. Shu of Brown University, and is used with permission. We believe this to be the initial application of such modeling technology to the electromagnetic bioeffects problem.

Our computational model is based upon the dynamic conservation law formulation. The spatial dimensions of the model are in the order of nanometers in length, and the temporal events analyzed occupy time scales ranging from subpicoseconds to tens of nanoseconds. Because this is much less than the duration of channel gating pulses (which are typically in the millisecond range), we are thus examining the open channel. By applying the previously developed, essentially non-oscillatory (ENO) shock-capturing scheme, our model can accurately treat a variety of complex, nonlinear fluid behavior including the formation of propagating shock waves.

Our model indicates that the cellular sodium ion channel exhibits an electrical nonlinearity at microwave frequencies which generates an intermodulation spectrum when excited by an amplitude-modulated electric field. Intermodulation products having frequencies in the biologically meaningful low-frequency range below 1,000 Hz appear possible. This is a new nonthermal microwave interaction mechanism with living tissues. There exist potential impacts in commercial and defense technology areas.

EFFECTS OF CELLULAR PHONES RADIATION EXPOSURE
ON HUMAN IMMUNE SYSTEM WHITE BLOOD CELLS IN
VITRO

Aly, A. and Barnes, F.

University of Colorado at Boulder

Effects of Cellular Phones Radiation Exposure on Human Immune System White Blood Cells in Vitro.

Ashraf Aly, and Frank S. Barnes. Department of Electrical Engineering, University of Colorado, Boulder, Colorado, USA

ABSTRACT The rapid worldwide growth in the use of mobile phones has raised the concerns about the public exposure to mobile phones radiation and the possible interaction between the radio frequency electromagnetic radiation and the biological effects on human tissues, particularly the brain and the human immune system. Our goal is to help the public users to find answers to their concerns, and also help the communication companies to create a new generation of mobile phones with reduced risks to humans. Evidence has been reported about the possible health effects such as; brain tumor, blood-brain barrier (BBB) permeability function, sleep problems, cognitive function, DNA damage, immunity system function, stress reaction, and increased incidence rate of traffic accidents due to using mobile phone during driving. The aim of this paper is to study the effects of mobile phones radio frequency radiation on the immune system by investigate the activity and behavior of human leukocytes (white blood cells) upon exposure to radiofrequency fields in vitro. This is done by investigating the ability of leukocytes to track the cyclic-Amp concentration gradient, and study the cells behavior. We used blood from healthy Adults donors, and observed the effects of applying radio frequency electromagnetic fields (for 15 min each time) on leukocyte cells from digital NOKIA cellular phone (model 3390b) which operate at frequency range from 1850 MHz to 1910 MHz. Our observations to date of the chemotactic response shows no change in the leukocytes velocity, but we observed an effect on the movement direction. The chemotactic direction is vertical, which is parallel with mobile phone position. Significant change in leukocytes behavior, include changing shape much faster than the normal case (without applying RF radiation). The cells were shrinking, expanding, and rolling.

Key words: mobile phones; radiofrequency; chemotactic effect; human leukocytes.

INITIAL INVESTIGATIONS WITH A BROADBAND CROSS-POLARIZED ANTENNA FOR BREAST CANCER DETECTION

Yun, X., Johnston, R.H., Fear, E.C.
University of Calgary

The limitations of current breast imaging technologies encourage investigation of complementary approaches to assist in early tumor detection and cancer diagnosis (*Mammography and beyond*, S.J. Nass et al, eds., National Academy Press, Washington, 2001). One such approach is microwave imaging, which detects tumors using the significant difference in electrical properties of malignant tumors and fatty breast tissues. Confocal microwave imaging (CMI) was introduced by Hagness et al (S.C. Hagness et al, *IEEE Trans. Biomed. Eng.*, **45**, 1470-1479, 1998). CMI involves illuminating the breast with a pulse of microwaves by an antenna, and recording reflections at the same antenna. Significant reflections are expected from malignant tumors. To avoid the large reflections expected from the chest wall, cross-polarized reflected waves may be observed (S.C. Hagness et al, *IEEE Trans. Antennas Propag.*, **47**, 783-791, 1999). As a test of this approach, we designed a broadband bowtie antenna and investigated the application of this antenna to tumor detection.

The antenna consists of a pair of crossed bowtie metal planar antennas embedded in a dielectric, which is similar to fatty tissue. The antenna is 1.66 cm in length, 1.66 cm in width, and 1mm in depth. The computer simulations of this antenna and simple breast models are performed with the WIPL-D program (B.M. Kolundzija et al, *WIPL-D Electromagnetic modeling of composite metallic and dielectric structures*, Artech House, Boston, 2000). The breast model consists of a homogeneous half-space of fat ($\epsilon_r=9$, $\sigma=0.4$ S/m). The space above the antenna is also filled with a lossy substance representing fat. Prolate ellipsoidal or spherical tumors ($\epsilon_r=50$, $\sigma=7$ S/m) are placed below the antenna.

The antenna embedded in fatty tissue (without a tumor present) is simulated, and antenna characteristics S11 and S12 indicate that the antenna operates reasonably well from 2 to 4.25 GHz. We also examine the changes in frequency responses with different tumor shapes, sizes, locations and depths. As an ellipsoid tumor moves from the centre of the antenna, the magnitude of the response decreases. For spherical and ellipsoidal tumors in approximately the same location, different frequency responses are observed. It appears feasible to detect a 4.8 mm long and 1.6 mm wide ellipsoidal tumor at a depth of 5 cm. Finally the effects of changing tumor orientation are examined. Response increases as the tumor rotates from 0 to 45 degrees relative to the xy axes of the antenna and decreases as the tumor rotates in the xz plane from 0 to 90 degrees. Initial experimental verification of the antenna performance has been performed, and testing with simple breast phantoms is ongoing.

MAGNETIC RESONANCE IMAGING AT LOW AND HIGH FIELDS: AN ELECTROMAGNETIC PERSPECTIVE

Ibrahim, T.S.

The University of Oklahoma

Magnetic resonance imaging (MRI) is a powerful medical diagnostic technique, which is based on the nuclear magnetic resonance (NMR) phenomenon. In the medical diagnostic field, NMR is the absorption of radiofrequency (RF) energy by the nuclei of the human body's atoms, which are in the presence of an external static magnetic field. The advantages of MRI among other medical diagnostic techniques are its non-invasive nature, versatility, excellent tissue contrast and sensitivity to flow and diffusion. As a result of its unprecedented power, MRI scanners now permeate the nation's hospitals. Indeed, it can be argued that MRI is the premier diagnostic imaging technique, not only for its past achievements, but also for its unparalleled research potential.

The advancement of MRI as a radiological instrument has been associated with a constant drive towards higher magnetic field strengths resulting in higher operational frequencies. More powerful magnets bring the promise of enhanced signal to noise ratio (D. I. Hoult and R. E. Richards, *J. Magn. Reson.*, 24, 7185, 1976), exquisite resolution (R. Gruetter, S. A. Weisdorf et al, *J. Magn. Reson.*, 135, 260264, 1998), and reduced scan times. At the same time however, MRI at higher frequencies adds significant engineering complexities to the MRI experiment, most notably in designing safe, versatile, and high-performance RF coils.

In this work, computational and theoretical electromagnetic analysis of several RF coils used in MRI are presented at Larmor frequencies for operation up to 11 Tesla. The electromagnetic interactions with phantoms and anatomically detailed head models are studied at different field strengths. The electromagnetic computational tool of choice in this work was the finite difference time domain (FDTD) method. Combined with measurements using an 8 Tesla MRI system, currently the most powerful clinical magnet in the world and a 1.5 Tesla system, the FDTD method is utilized to study, analyze, and eventually design RF coils. The combination of FDTD modeling, experiments, and infrared imaging gives a new perspective onto the electromagnetics associated with low and high field clinical imaging. Ultra high field (8 Tesla) human MRI images will be presented, which outline a new vision for this imaging modality. Experimental and theoretical approaches centered on the application of FDTD method will demonstrate the need for solid engineering approaches if MRI is to continue its meteoric ascent in human medicine.

LOW FREQUENCY AC AND DC MAGNETIC FIELD EFFECTS ON WHITE BLOOD CELL MOBILITY

Zhou, Rong¹, Rathnabharathi, Kalani², Aly, Ashraf³
, Barnes, Frank⁴

¹University of Colorado at Boulder, ECE Dept, Room ECEE 121, Boulder, CO, USA

²University of Colorado at Boulder, ECE Dept, Room ECEE 121, Boulder, CO, USA

³University of Colorado at Boulder, ECE Dept, Room ECEE 121, Boulder, CO, USA

⁴University of Colorado at Boulder, Engineering Center, OT 250, Boulder, CO, USA

Electric power is used all over the world. But the generation, transmission, and use of electric energy is associated with the production of weak electric and magnetic field (EMF), which are emitted by power distribution lines, transformers, service wires, and electrical panels as well as by home appliances. Although there are lots of papers to study the biological effects of electromagnetic fields, the possible relationship between human exposure to ELF magnetic field and adverse health effects such as cancers and leukemia is still a subject of considerable contemporary interest and debate. This paper is focused to explore the possibility that low frequency AC and DC magnetic field can affect the ability of white blood cells to track a concentration gradient of chemoattractants such as cyclic-AMP, which is known to control various cellular processes such as proliferation and gene expression. We adopt a quantitative method for measuring the concentration gradients that could cause white blood cells or leucocytes to move across a microscope slide in a relatively straight line along the concentration gradient of the second messenger chemoattractant. In order to avoid the adverse influence of temperature, we always keep the slides temperature within 37°C. Through high resolution microscope and monitor system, weve observed random movement of white blood cells in the very beginning without DC magnetic field, and directional movement with DC magnetic field, which direction depends on the polarity of DC magnetic field. For the low frequency AC magnetic field, white blood cells move more randomly compared with DC magnetic field. Higher the AC frequency is, more randomly white blood cells move.

LOW FREQUENCY AC AND DC ELECTRIC FIELD EFFECTS ON WHITE BLOOD CELL MOBILITY

Rathnabharathi K.N., Aly A., Zhou R. , Barnes F.S.
University of Colorado, Boulder, USA

This is an experimental study on the mobility of human white blood cells (mainly polymorphonuclear leucocytes) when exposed to external electric fields. Using the Stripe Source Diffusion Technique and Cyclic-AMP (Adenosine3, 5-monophosphate) as the chemoattractant, well-defined chemotactic fields are created on microscope slides. This is done by placing a stripe of the chemo-attractant on one side of the microscope slide and then slowly sliding the cover slip over it. Observations are made based on the polarity, intensity, and distribution of the applied electric fields at temperatures ranging from 36C to 39C. Initially we performed some experiments on the mobility of the leucocytes due to changes in temperature and observed that the optimal performance of the leucocytes were in the temperature range of 36C to 39C. So far in our experiments with the electric fields we have observed that leukocyte motion changes according to the direction of the applied fields. In most of our experiments the leucocytes showed positive and negative chemotaxis based on the polarity of the electric field when the field distribution was parallel to the concentration gradient. When the electric field was in the same direction of the concentration gradient we got positive chemotaxis and vice versa. Also the velocity of the leucocytes changes with the applied fields; in most cases we observed a decrease in the velocities of the white blood cells once the fields were applied. The cells which were initially moving with some velocity would start reducing its speed when exposed to these fields. Our experiments are still in the preliminary stage and more experiments are expected to be performed before definite conclusions can be reached.

MODELING OF INTERFACE FIELDS AND OPTIMIZATION
OF BOLUS AND INTER-ELEMENT SPACING OF ARRAYS
FOR COHERENT AND INCOHERENT HYPERTHERMIA

Lumori, M.L.D.

University of San Diego, 5998 Alcala Park, San Diego, CA 92110

In a cancer treatment set-up, a water-bolus is placed between the aperture antennas (applicators) and the body for matching and cooling during hyperthermia. Reliable field simulations are possible if the entire system is modeled using experimental field data from a liquid muscle-like phantom and applying a Gaussian Beam Model (GBM) to the data to prescribe practical aperture and incident fields, thus improving numerical simulations of SAR (specific absorption rates) [1]. Equation (1) represents the GBM where $a = a_1 + ja_2$ and $b = b_1 + jb_2$ are source parameters in the principal E- and H-planes and E_0 a constant.

$$E(x, y, z) = E_0 \cdot \exp(-jkz) / \sqrt{[(z-a)(z-b)]} \cdot \exp(-jx^2) / [2(z-a)] \cdot \exp(-jy^2) / [2(z-b)] \quad (1)$$

Preclusion of the aperture-bolus-air-fat-muscle interface fields can cause erroneous simulations. An optimal incident field in the muscle can be attained by optimizing the water-bolus thickness for both coherent and incoherent hyperthermia, but optimal inter-element spacing of arrays is only necessary for incoherent hyperthermia [2].

GBM simulations of field distributions or SAR from multi-element array applicators for use in superficial hyperthermia have been reported [3, 4]. These predictions, supported by experimental data, have demonstrated that arrays of current sheet applicators (CSAs) can achieve a much larger effective field size (EFS) than a single applicator and that the penetration associated with coherent arrays may be increased over that achieved for incoherent operation. Practical implementation of such arrays involves inter-element spacing and the use of a water-bolus, both of which must be optimized prior to routine use in the clinic for cancer therapy. To this end this paper presents GBM simulations of applicator array performance in layered media (bolus-air-fat-muscle) to achieve contiguous and optimal EFS and improved penetration of cancerous muscle tissues, such as breast cancer.

References: [1] (M. L. D. Lumori, *IEEE Trans. MTT*, **48**, 1522-1530, 2000), [2] (M. Prior, M. L. D. Lumori, J. W. Hand, *IEEE Trans. Biomed. Engr.*, **42**, 694-698, 1995), [3] (M. L. D. Lumori, et al., *Phys. in Med. and Biol.*, **35**, 387-397, 1990), [4] (M.L.D. Lumori, et al., *IEEE Trans. MTT*, **38**, 1623-1630, 1990).

OPTIMIZATION
OF ELECTROMAGNETIC PHASED-ARRAYS FOR HYPER-
THERMIA

Marc E. Kowalski¹ , Jian-Ming Jin²

¹Advanced Computations Department, Stanford Linear Accelerator Center, Menlo Park, CA, USA

²Department of Electrical and Computer Engineering, University of Illinois, Urbana, IL, USA

Electromagnetic hyperthermia is a promising treatment for a variety of types of cancer, especially when used in combination with chemical and radiation treatment modalities. However, in the past, two major obstacles have hampered repeatable demonstrations and, thus, clinical acceptance of this technology. First, at the frequencies typically employed, the human body behaves as an inhomogeneous and dispersive medium, making the prediction and control of the electromagnetic power deposition pattern difficult. Second, the lack of a reliable noninvasive temperature monitoring technique has hampered clinicians ability to prevent undesired heating of healthy tissue, at the same time failing to provide a method to judge the success of meeting temperature-based treatment goals. The combination of these difficulties has lead to an uneven trail of successes, spanning almost two decades.

In this talk, two recently developed approaches to overcoming the aforementioned difficulties are described. In the first approach, a patient-specific computational model is built as part of a pretreatment planning process. Then, this computational model is used to optimize the hyperthermia applicator and provide some idea of the feasibility of the treatment. Novel approaches for computationally efficient optimization, even in the face of underlying nonlinear dynamics, are emphasized. In the second, complimentary approach, non-invasive temperature measurements, acquired via magnetic resonance imaging (MRI), are employed to continually re-optimize the hyperthermia applicator as treatment progresses. In this way, the negative impact of both modeling errors in pretreatment planning and physiological changes on treatment efficacy can be minimized. Throughout the talk, the novel features of our approach will be highlighted, and the feasibility of the system will be demonstrated with simulation and experimental results.

NUMERICAL INVESTIGATION OF A NON-INVASIVE ULTRA-WIDEBAND MICROWAVE HYPERTHERMIA MODALITY FOR BREAST CANCER TREATMENT

Converse, M.C., Bond, E.J., Hagness, S.C. , Van Veen, B.D.

Department of Electrical and Computer Engineering, University of Wisconsin, Madison, WI 53706

It is well known that the effect of radiation therapy and chemotherapy for breast cancer treatment can be enhanced using microwave hyperthermia. The persisting challenge, however, is to preferentially heat the cancerous tissue without harming superficial and surrounding healthy breast tissue. Sophisticated adaptive focusing algorithms have been developed for use in narrowband phased-array hyperthermia treatment, but they rely upon invasive feedback probes located within the breast.

In this talk, we propose a new non-invasive ultrawideband (UWB) microwave hyperthermia approach for breast cancer treatment. This approach uses a recently developed UWB space-time microwave imaging method, rather than feedback probes, to ensure that the transmitted energy is focused on the lesion. The tumor is localized by sequentially transmitting low-power UWB pulses from antennas located near the surface of the breast. The received backscattered signals are passed through a space-time beamformer that is designed to image backscattered signal energy as a function of location. The microwave backscatter signals obtained during this scan of the breast inherently contain the information needed to tightly focus high-power pulses at the site of the tumor. Thus, by utilizing similar focusing techniques and launching high-power signals from all antennas simultaneously, energy can be optimally focused in the breast.

We present a numerical investigation of the feasibility of focusing energy to specific locations in the breast using space-time filtering prior to transmitting the signals across the antenna array. The initial feasibility study is done using 2D computational models of the breast. The evaluation is done in two steps. First, the transmit focusing procedure is simulated and the deposited electromagnetic energy (SAR) distributions within the breast are calculated using an FDTD solution to Maxwells equations. The FDTD model includes the dispersive properties of biological tissue, as well as the heterogeneity of the breast derived from MRI data. Second, the SAR distributions are used in an FDTD solution of the bioheat equation to calculate temperature distributions in the breast. Focusing efficacy is measured using both SAR and temperature distributions. The results of the initial study show extremely good focusing of both SAR and temperature for various target locations within the breast. This indicates that use of this approach for hyperthermia treatment of breast cancer is promising and should be further investigated.

AN INVESTIGATION OF THE ELECTROMAGNETIC AND THERMAL EFFECTS ASSOCIATED WITH OPERATION OF THE WIRELESS TELEMETRY LINK AND IMPLANTED CHIP IN A RETINAL PROSTHESIS

Keyoor Gosalia, Gianluca Lazzi

Department of Electrical and Computer Engineering, NC State University, Raleigh, NC

Communication between the extra ocular and intraocular units of a dual-unit prosthesis takes place via a wireless telemetry link (inductive power transfer and microwave data communication). In this work, the data telemetry link is established at two frequencies of 1.45 GHz and 2.45 GHz by designing appropriately sized extraocular (25×25 mm) and intraocular (6×6 mm) patch antennas using the Finite Difference Time Domain (FDTD) method. Coupling measurements were performed between these antennas at a separation of 25 mm both in free space and with the intraocular antenna embedded in an eye phantom. As compared to coupling in free space, when the intraocular antenna is immersed in the eye phantom, an improvement in coupling is observed (4–6 dB at 1.45 GHz and 1–2 dB at 2.45 GHz) both numerically and experimentally. These results indicate that the eye ball acts as a dielectric lens and improves the coupling performance of the wireless link. The power deposited in the head and eye tissues due to operation of the data telemetry link is computationally evaluated in terms of the specific absorption rate (SAR) at both the frequencies for a maximum transmitted power of 50 mW. Computed peak 1-g SAR at 1.45 GHz is 0.985 W/kg and at 2.45 GHz is 1.158 W/kg and hence are within the IEEE stipulated limit of 1.6 W/kg.

Also, to determine the increase in the natural steady state temperature in the head-eye tissues due to the operation of an implanted chip, several 3-dimensional thermal simulations have been performed by discretizing and numerically implementing the Bio-Heat equation. The thermal simulations account for variation in the location, size and power dissipation level of the implanted chip. For a constant power dissipated of 12.4 mW, it was observed that when the chip was placed between the ciliary muscles of the eye, the temperature increase in the vitreous cavity and on retina was less by 0.1°C and 0.07°C respectively as compared to the case when the chip was located in the center of the vitreous cavity. Also, a larger chip dissipating the same amount of power reduced the temperature increase on the vitreous cavity and retina by 0.11°C and 0.02°C respectively. Detailed results characterizing the microwave data telemetry link and thermal elevation incurred in the head model will be presented.

INDEX

A

Abdu, M. 194, 281
 ACT Collaboration, The
 349
 Ade, P. 344
 Aguirre, J. 344
 Allen, C. 345
 Alu, A. 17
 Aly, A. 396, 399, 400
 Amatucci, W. 269, 312,
 326, 327
 Anagnostou, D. 112
 Anderson, D. 191, 222, 227
 Anderson, K. 174
 Anderson, P. 232
 Andersson, L. H4-10 303,
 304
 Anghel, A. 191, 226, 227
 Annaratone, B. 265
 Antar Y. 88
 Araujo-Pradere, E. 226
 Asher, W. 149
 Ashour-Abdalla, M. 300
 Atchley, W. 3
 Atkinson, L. 44
 Axelrad, P. 153
 Aziz, M. 150

B

Babu, S. 345
 Bach, J. 9
 Baedke, W. 129
 Bagenal, F. 299
 Bahar, E. 20, 21, 22, 154
 Baktur, R. 32, 105
 Ballato, J. 32, 105
 Balsler, D. 331, 338
 Bao, J. 144
 Barnes, F. 106, 396, 399,
 400
 Bartram, B. 153
 Batista, I. 281
 Baum, C.E. 6, 41, 121, 123
 Baum, C.W. 124
 Bell, T. 289, 314, 315
 Benard, A. 30
 Benford, D. 343
 Bennert, E. 200
 Benson, R. 276
 Berkey, F. 210
 Bernhard, J. 78, 114

Bernhardt, P. 44, 203, 215,
 277

Bharadwaj, N. 87
 Bharadwaj, V. 76
 Bigelow, S. 3
 Billinger, R. 138
 Biloiu, C. 323
 Birn, J. 295
 Boardsen, S. 287, 310
 Bock, J. 344, 358
 Boling, R. 125
 Bond, E. 403
 Bopp, C. 28, 29
 Bortnik, J. 314
 Bounds, S. 321
 Bowen, L. 3, 122
 Bowers, K. 128
 Braatz, J. 335
 Briczinski, S. 253
 Bright, V. 100
 Brisken, W. 378
 Broadwell, C. 386
 Brown, G. 178
 Brown, P. 258
 Brown, W. 143
 Brugman, B. 322
 Brunkow, D. 85
 Buehrer, R. 76
 Burgess, E. 167
 Burk, S. 166
 Burnside, W. 115
 Burton, J. 44
 Bushyager, N. 96
 Bust, G. 202, 203, 204
 Butler, C. 27, 28, 29, 67, 68

C

Cai, Y. 113
 Caloz, C. 118
 Camilo, F. 333
 CAPMAP Collaboration,
 The 353, 377
 Carlson, C. 285
 Carter, T. 322
 Cen, R. 366
 Cetiner, B. 99, 111
 Chamberlin, K. 169
 Chandrasekar, V. 83, 85, 87
 Chau, J. 195, 227, 255
 Chen, A. 240
 Chen, C. 264
 Chen, M. 221

Chen, S. 55
 Chen, T. 37
 Chevalier, M. 315
 Chevalier, T. 289
 Chiao, J. 113
 Childers, J. 375
 Chilson, P. 141
 Chin, G. 380
 Ching, K. 107
 Chiu, C. 37
 Cho, H. 348
 Cho, Y. 85
 Christensen, A. 199, 201
 Christodoulou, C. 9, 111
 Chu, Y. 221
 Church, S. 356
 Chuss, D. 345
 Clarke, J. 348
 Cline, D. 151
 Close, S. 254, 258
 Codrescu, M. 222, 224
 Cohn, S. 143
 Coker, C. 200
 Collins, R. 263
 Colom, J. 83
 Comberiate, J. 201
 Condon, J. 338
 Constantikes, K. 338
 Converse, M. 403
 Convery, P. 300
 Cooke, D. 290
 Coster, A. 234, 256, 258
 Cousins, M. 214
 Cox, A. 138
 Crittenden, P. 20, 21
 Crowley G. 201, 232
 Cruz-Pol, S. 83
 Cummer, S. 239, 248

D

Davidson, K. 165
 Davis, W. 5, 10
 Day, P. 358
 De Flavii, F. 99, 111
 DeGroot, D. 11
 Deiker, S. 346
 Delamere, P. 299
 DeMajistre, R. 199, 201
 DeMinco, N. 39
 Denardini, C. 194
 DeNatale, J. 97
 Dimant, Y. 283

Index

Dobbs, M. 348, 357
Domer, F. 44
Donlan, B. 76
Dorey, S. 52
Doriase, W. 346
Dorland, W. 322
Doss-Hammel, S. 173
Dotson, J. 345
Doviak, R. 142, 143
Dowell, D. 345
Drayton, R. 101
Drew, K. 258
Droegemeier, K. 83
Duel-Hallen, A. 75
Duncan, W. 347
Durand, D. 256, 258
Duric, N. 370
Dymond, K. 200
Dyrud, L. 254, 258

E

Eaton F. 173
Ebersbach, H. 40
Eccles, J. 192
Edgington, S. 344
Engargiola, G. 357
Engheta, N. 17
Erentok, A. 16
Ergun, R. 303, 304
Erickson, N. 376, 391
Erickson, P. 215, 217, 218,
256, 277
Erickson, R. 376
Erricolo, D. 64, 65, 66
Ersoy, O. 91
Escoffier, R. 386

F

Farr, E. 3, 122
Fast, S. 80, 168
Fath, V. 376
Fathy, A. 116
Fear, E. 397
Fedder, J. 296
Fedotov, I. 23
Feerst, A. 44
Feldner, L. 112
Feng, J. 114
Ferencz, O. 247
Feria, A. 42
Fish, C. 285, 326
Fitzgerald, T.J. 231
Ford, C. 175
Fort, D. 385
Fortov, V. 265

Foster, J. 215
Frank, L. 296
Fraser, B. 282
Frasier, S. 83, 141
Frazier, K. 256
Frederickson, P. 165
Fukao, S. 203
Fuller-Rowell, T. 222, 224
Fung, A. 161
Fung, S. H5-4 287, 310
Furlanetto, S. 369

G

Gaier, T. 379
Gaiser, P. 149
Ganguli, G. 268, 312
Garcia, L. 287, 310
Gardner, R. 126
Garner, T. 202
Gasiewski, A. 133, 134,
137, 144, 146, 151, 153
Gatling, G. 269, 312
Gaussiran, T. 202
Gekelman, W. 321
Gelinias, L. 263, 274, 327
Gerken, E. 244
Gerstoft, P. 181, 182, 183
Ghigo, F. 331
Ghodsian, B. 99, 111
Gilbreath, C. 173
Glenn, J. 344, 372
Gnedin, N. 363
Goeller, R. 391
Goldin, A. 344, 358
Goldman, M. 304
Golish, D. 380
Golka, R. 246
Golwala, S. 344
Gosalia, K. 404
Goyal, A. 4
Grau, A. 111
Green, J. 276, 287, 310, 311
Greenberg, J. 386
Greenhill, L. 335
Groppi, C. 380
Grosslein, R. 376
Grydeland, T. 217
Guerrieri, J. 145
Gupta, A. 70
Gupta, K. 100
Gwinn, C. 390

H

Haack, T. 166
Hacihaliloglu, I. 90

Hagness, S. 403
Hahn, J. 236
Haig, J. 344
Haiman, Z. 365
Hairston, M. 222
Hajj, G. 223, 225, 232
Hallen, H. 75
Hand, G. 175
Harper, D. 345
Harris, A. 389
Havrilla, M. 52
Hawkins, D. 383
Hawley, M. 30, 31
Hayes, P. 57
Hedden, A. 380
Hedman, M. 377
Heelis, R. 222
Heiles, C. 336, 337
Heinselman, C. 214, 257
Henkel, C. 335
Hensley, S. 159
Hernandez-Pajares, M. 235
Hesse, M. 295
Hill, R. 146
Hilton, G. 346
Hinshaw, G. 360
Hodgkiss, W. 181
Hollansworth, J. 124
Hollweg, J. 291
Holt, J. 217, 218
Holzapfel, W. 348, 357
Hoppe, D. 42
Horanyi, M. 261, 262, 266,
324
Howe, B. 222
Hoyle, V. 234
Hsu, R. 240
Huang, C. 221
Huang, E. 161
Huang, X. 311
Hubbert, J. 87
Huff, G. 114
Hunt, C. 358
Hunt, S. 258
Hysell, D. 193, 205

I

Ibrahim, T. 398
Imbriale, W. 42
Inan, U. 243, 244, 289, 307,
314, 315
Irisov, V. 134
Irwin, K. 346
Itoh, T. 118
Iturbide-Sanchez, F. 136

Index

Ivanov, A. 265
Ivlev, A. 265

J

Jablecki, M. 182, 183
Jackson, D. 63
Jackson, J.D. 325
Jackson, R. 136
Jacobson, A. 231
Janches, D. 255
Jargon, J. 11
Jerome, J. 395
Jewell, P. 331
Jhabvala, M. 345
Ji, C. 33, 34
Jin, J. 402
Johnson, W. 63
Johnston, R. 397
Jordan, C. 257
Jorgensen, J. 257
Joshi, S. 4
Jung, C. 99

K

Kartal, M. 90
Katehi, L. 98
Katzberg, S. 153
Keating, B. 350
Keen, J. 68
Kelley, M. 189, 263, 274,
327
Kelly, J. 214
Kelly, R. 151
Kempel, L. 30, 31
Kermish, Z. 357
Khayat, M. 50, 51, 63
Khazanov, G. 288
Khazanov, I. 302
Khmyrov, G. 275
Kil, H. 201
Kim, E. 108
Kintner, P. 189
Klein, M. 134, 137, 144,
151
Kletzing, C. 321
Klumov, B. 265
Knapmiller, S. 324
Knapp, E. 150
Knudson, R. 9
Ko, K. 56
Kogut, A. 364
Kohlberg, I. 125
Kollman, R. 58
Komjathy, A. 233, 235
Konopka, U. 265

Kooi, J. 380
Kowalski, M. 56, 402
Krauss, C. 266
Kretschmer, M. 265
Krolik, J. 89, 182, 183
Kudeki, E. 195
Kulesa, C. 380
Kurose, J. 83

L

L. Garcia, L. 287
LaBelle, J. 286
Lang, R. 157, 160
Lange, A. 344, 358, 359
Langston, G. 331
Lanney, M. 3
Lanting, T. 348, 357
Larsen, M. 205
Larsen, T. 66
Latess, J. 128
Laurent, G. 344
Laurin, C. 234
Lawrence, C. 379
Lawry, D. 122
Lazzi, G. 70, 404
Leckenby, M. 40
LeDuc, H. 358
Ledvina, B. 189
Lee, A. 348, 357
Lee, J. 71
Lee, L. 56
Lee, L. 240
Lee, M. 212
Lee, S. 71, 100
Lee, Y. 100
Lehnert, K. 346
Lembege, B. 301
Lemon, C. 295
Leong, M.S. 15
Lertsirimit C. 63
Leuiski, V. 134, 137, 144
Levy, A. 375
Li, C. 55
Li, H. 113
Li, Z. 56
Lichtenberger, A. 380
Licul, S. 5
Liepa, V. 69
Lim, S. 118, 236
Lin, L. 113
Lin, X. 45
Lind, F. 215, 217, 218, 277
Lipaev, A. 265
Liu, C. 55
Liu, N. 245

Lockard, M. 27, 67
Lockman, F. 332
Lopez-Dekker, P. 141
Lubin, P. 375
Luebbers, R. 176
Luebbes, R.J. 80
Lueker, M. 348
Lumori, M. 401
Lynch, K. 263, 327
Lyon, J. 296
Lyons, W. 239, 248

M

Maas, S. 389
Mac Reynolds, K. 145
Mack, K. 368
Macnae, J. 152
Maddalena, R. 331
Maheshwari, S. 4
Main, D. 303
Makela, J. 189
Maloney, P. 344
Mandell, M. 290
Mandrake, L. 223
Mannucci, A. 233
Margot, J. 334
Markovskii, S. 291
Marshall, R. 167, 170, 243
Marvil, J. 375
Mason, B. 339
Masters, D. 153
Mathews, J. 251, 253, 255
Mattioli, V. 135
Mauskopf, P. 344
Mazin, B. 358
McGeehan, B. 323
McGraw, J. 204
McKenzie, D. 199
McLaughlin, D. 83
Meinhold, P. 375
Meisel, D. 255
Menk, F. 282
Meyer, M. 213
Mihailovich, R. 97
Minkoff, J. 387
Minter, A. 331
Minter, C. 222, 224
Mishin, E. 274
Molotkov, V. 265
Moore, M. 44
Morabito, A. 213
Moran, J. 335
Morfill, G. 265
Morrison, D. 199, 201
Moseley, H. 343

Index

Moseley, S. 345
 Moys, A. 165
 Mukai, T. 296
 Murakami, B. 107
 Muschiatti, L. 301
 Muschinski, A. 141
 Muthitacharoen, A. 106
 Myers, M. 357

N

Narayanan, G. 380, 391
 Narayanan, R. 84, 86
 Nefedov, A. 265
 Newman, D. 304
 Ng, C. 56
 Nguyen, H. 344
 Nikoular, R. 216
 Nolan, M. 255

O

O'brient, R. 357
 Oh, E. 173
 Oh, S.P. 368
 Ohta, A. 107
 O'Neil, K. 331
 O'Neill, H. 375
 O'Neill, P. 160
 Ooi, L. 15
 Oppenheim, M. 254, 258,
 283
 Otto, A. 242
 Oughstun, K. 18

P

Pace, S. 124
 Padmanabhan, S. 136, 149
 Page, L. 355
 Pajic, S. 102
 Papadopoulos, K. 308
 Papapolymerou, J. 102
 Papila, I. 91
 Parsons, A. 388
 Pasko, V. 245
 Patel, C. 77
 Paxton, L. 199, 201
 Paznukhov, V. 275
 Pearson, L. 32, 105, 124
 Pelhe, A. 169
 Peroulis, D. 98
 Petrov, O. 265
 Pi, X. 223, 225
 Pierce, L. 395
 Pincinti, J. 49
 Pogorzelski, R. 38

Ponchak, G. 95
 Pongratz, M. 231
 Ponomarenko, P. 282
 Popovic, Z. 102
 Porter, C. 42
 Pratt, T. 77
 Prestage, R. 338
 Pribyl, P. 322
 Prober, D. 380

Q

Quataert, E. 322

R

Ramadoss, R. 100
 Ramakrishnan, D. 89
 Randa, J. 138
 Rathnabharathi, K. 399,
 400
 Reinisch, B. 275, 276, 277,
 281, 287, 310, 311
 Reising, S. 136, 149, 150
 Rengarajan, S. 43
 Richards, P. 348, 357
 Richmond, A. 221
 Ricklin, J. 173
 Riddolls, R. 212
 Rideout, W. 217, 218
 Robertson, S. 261, 262,
 266, 324
 Robishaw, T. 336, 337
 Rodriguez, E. 159
 Rogers, L.T. 181, 182, 183
 Ropiak, C. 127
 Rose, L. 149
 Rosen, G. 225
 Rosen, I. 223
 Rosenberg, M. 270
 Rossinot, P., 344
 Rothermel, H. 265
 Rottier, J. 167
 Rubin-Zuzic, M. 265
 Rudakov, L. 268
 Rudbeck, J. 27
 Ruhl, J. 354
 Ryan, F. 204, 211

S

Saatchi, S. 158
 Sahr, J. 213
 Sales, G. 275, 281, 316
 Samara, M. 286
 Sammoura, F. 113
 Sancheti, S. 4
 Santalla del Rio V. 88
 São Sabbas, F. 242
 Sarabandi, K. 79
 Sayers, J. 344
 Scales, W. 264
 Scherliess, L. 222
 Schmidt, S. 70
 Schriver, D. 300
 Schulz, M. 309
 Schunk, R. 222
 Schuster, J. 80, 176
 Scime, E. 269, 323
 SCUBA-2 Collaboration,
 The 347
 Seetharam, V. 124
 Seiffert, M. 379
 Sekelsky, S. 83
 Seker, S. 160
 Selcher, C. 203
 Sentman, D. 242
 Sessions, W. 129
 Seyler, C. 298
 Sgriccia, N. 30
 Shapiro, P. 367
 Sheehan, R. 190
 Shiroma, W. 107
 Siah, E. 69
 Sibeck, D. 296
 Sieftring, C. 44, 203
 Sievenpiper, D. 117
 Sikdar, P. 210
 Silver, J. 267
 Silverberg, R. 345
 Simoneau, J. 124
 Singh, N. 302
 Siqueira, P. 159
 Skiff, F. 321
 Skone, S. 234
 Sletten, M. 177
 Slinker, S. 296
 Small, B. 316
 Smiley, B. 261, 262
 Smith, A. 80
 Smith, E. 187
 Sobral, J. 194
 Sojka, J. 222
 Song, P. 275, 311
 Sparks, L. 233
 Spieler, H. 348, 357
 Spitsyn, V. 23, 284
 Staggs, S. 349, 353
 Stankov, B. 134, 144, 151
 Stanley, M. 239
 Stapleton, J. 170
 Starks, M. 274, 316, 317
 Stebor, N. 375

Index

Stenbaek-Nielsen, H. 252
Stenzel, R. 313
Sternovsky, Z. 261, 262,
324
Stoudt, D. 126, 128, 129
Stover, P. 344
Stoykov, N. 395
Straus, P. 199, 201, 232
Streltsov, A. 297
Strohmaier, K. 313
Stuber, G. 77
Su, H. 240
Su, Y. 113
Sulzer, M. 215, 216
Sun, R. 30, 31
Sun, X. 323
Suszcynsky, D. 231
Swenson, C. 285, 326

T

Taflove, A. 395
Talaat, E. 201
Tamamoto, M. 107
Tamura, D. 145
Taylor, C. 203
Tentzeris, M. 96
Tesche, F. 28, 68
Theunissen, W. 115
Thiel, D. 19, 40
Thomas, E. 267, 325
Thomas, H. 265
Thompson, D. H6-6 222,
326
Thonnard, S. 200
Toffoletto, F. 295
Toporkov, J. 177
Torrice, S. 157
Tran, H. 357
Tran, T. 3
Treacy, R. 386
Trew, R. ix
Troland, T. 336, 337
Tsegaye, T. 160
Tsintikidis, D. 173
Tsoy, Y. 23
Tsunoda, R. 188
Tu, T. 37

U

Ullom, J. 346
Urrutia, J.M. 313
Urry, W. 384
Uslenghi, P. 49, 64, 65, 66
Utku, C., 160

V

Vale, R.L. 346
Valente, M. 246
Valentine, C. 168
Valladares, C. 190
Van Veen, B. 403
Varaljay, N. 95
Vayonakis, A. 358
Veliz, O. 227
Vincena, S. 321
Voellmer, G. 345
Volakis, J. 69
Voronovich, A. 144, 146
Vouvakis, M. 71

W

Walker, C. 380
Walker, D. 138, 269, 312
Wallace, E. 325
Walter, F. 371
Wang, C. 223, 225
Wang, F. 79
Wang, G. 33, 34
Wang, J. 264
Wang, L. 45
Wang, Y. 15
Ward, J. 285
Washington, G. 115
Waters, C. 282
Webb, P. 276
Webber, J. 386
Weber, B. 134, 151
Weber, R. 144, 146
Wei, L. 108
Weinreb, S. 376, 380
Werner, K. 376
Werthimer, D. 388
Westwater, E. 135, 137
Whalen, B. 44
Wick, G. -3 134, 151
Wielgus, J. 376
Wilkens, M. 203
Williams, B. 375
Williams, E. 246
Williams, J. 267
Wilson, A. 335
Wilson, B. 223, 225
Wilson, G. 19, 344
Wilton, D. 50, 51, 63
Wnag, C. 223
Wollack, E. 345
Wong, A. 273
Wood, W. 52
Woodman, R. 255

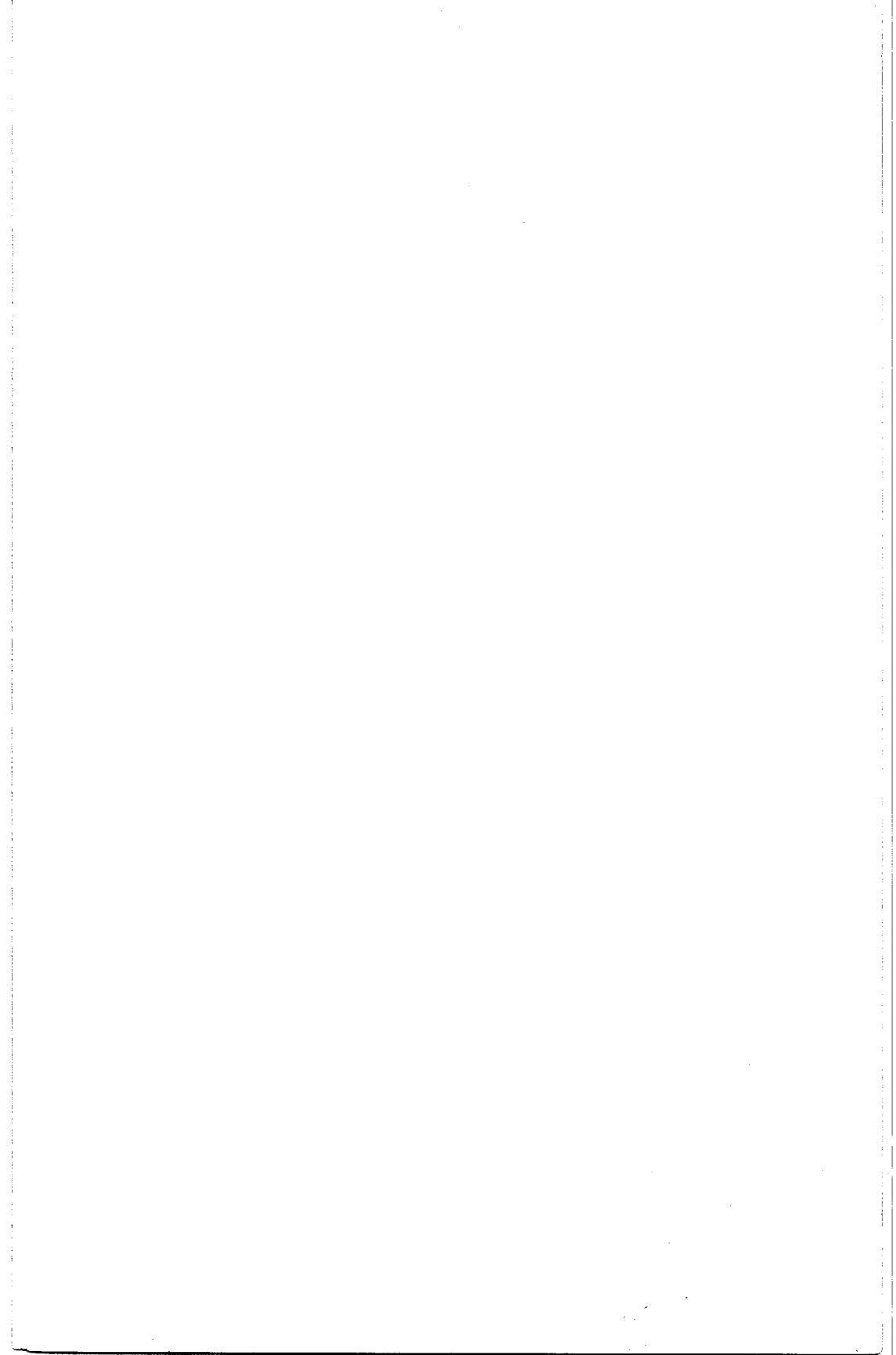
Wright, J. 209
Wu, K. 176, 298

Y

Yamamoto, M. 203
Yang, H. 58
Yang, T. 75
Yaroshenko, V. 265
Yildirim, O. 59
Yilmaz, A. 59
Yoo, H. 111
Yoon, H. 115
Yu, T. 142
Yuan, P. 34
Yun, M. 358
Yun, X. 397

Z

Zabotin, N. 209
Zamora, R. 153
Zavorotny, V. 133, 153
Zhang, G. 142, 143
Zhang, S. 114
Zhang, Y. 33, 34, 84, 86
Zheng, E. 102
Zhou, R. 399, 400
Zhou, S. 30, 31
Ziolkowski, R. 16
Zmuidzinas, x, 358
Zonak, S. 389
Zong, L. 30



Dev Palmer - ARO